REPORT NO.
UCB/EERC-83/23
OCTOBER 1983

EARTHQUAKE ENGINEERING RESEARCH CENTER

LOCAL BOND STRESS-SLIP RELATIONSHIPS OF DEFORMED BARS UNDER GENERALIZED EXCITATIONS

by

ROLF ELIGEHAUSEN
EGOR P. POPOV
VITELMO V. BERTERO

Report to the National Science Foundation

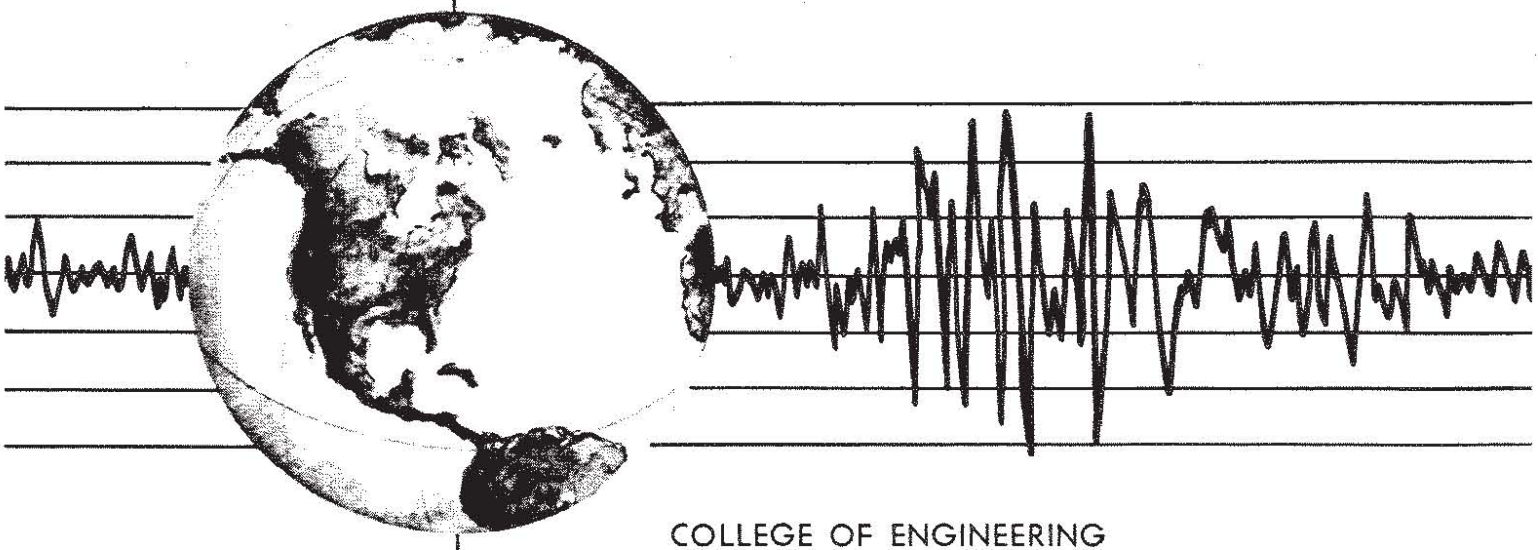

COLLEGE OF ENGINEERING
UNIVERSITY OF CALIFORNIA · Berkeley, California

LOCAL BOND STRESS-SLIP RELATIONSHIPS OF DEFORMED BARS UNDER GENERALIZED EXCITATIONS

Experimental Results and Analytical Model

by

Rolf Eligehausen

Visiting Scholar from the University of Stuttgart,
Federal Republic of Germany

Egor P. Popov

Professor of Civil Engineering
University of California, Berkeley

Vitelmo V. Bertero

Professor of Civil Engineering
University of California, Berkeley

A report on research sponsored by the
National Science Foundation.

Report No. UCB/EERC-83/23
Earthquake Engineering Research Center
College of Engineering
University of California
Berkeley, California

October 1983

ABSTRACT

This report covers integrated experimental and analytical investigations that permit predicting analytically the local bond stress-slip relationship of deformed reinforcing bars subjected to generalized excitations, such as may occur during the response of reinforced concrete (R/C) structures to severe earthquake ground motions.

Some 125 pull-out specimens were tested. Each one of these specimens simulated the confined region of a beam-column joint. Only a short length (five times the bar diameter) of a Grade 60 deformed reinforcing bar was embedded in confined concrete. The tests were run under displacement control by subjecting one bar end to the required force needed to induce the desired slip which was measured at the unloaded bar end. The influence of the following parameters on the bond stress-slip relationship was studied: (1) loading history, (2) confining reinforcement, (3) bar diameter and deformation pattern, (4) concrete compressive strength, (5) clear bar spacing, (6) transverse pressure, and (7) loading rate.

The detailed experimental results are presented and compared with results given in the literature. Based on the experimental results obtained, a relatively simple analytical model for the local bond stress-slip relationship of deformed bars embedded in confined concrete is developed. The model takes into account the significant parameters that appear to control the behavior observed in the experiments. The main assumption is that bond deterioration during generalized excitations depends on the damage experienced by the concrete which, in turn, is a function of the total dissipated energy. This assumption appears to apply only in the range of low cycle fatigue; that is, when a small number of cycles at relatively large slip values is applied.

The proposed analytical model for the local bond stress-slip relationship exhibits satisfactory agreement with experimental results under various slip histories and for various bond conditions.

The concrete in R/C joints of ductile moment resisting frames outside of stirrup-ties is unconfined. Therefore, based on the evaluation of test data given in literature, the analtyical

model is modified to include such regions. Furthermore, rules are formulated to extend the validity of the model to conditions different from those present in the tests.

The results of the investigation reported herein are used to offer some conclusions regarding the behavior of bond of deformed bars under monotonic and cyclic loading, and recommendations for further work are indicated.

ACKNOWLEDGEMENTS

The authors are grateful for the financial support provided for this investigation by the National Science Foundation under Grant PFR79-08984 to the University of California, Berkeley. The support of Dr. R. Eligehausen by the Deutsche Forschungs-gemeinschaft are gratefully acknowledged. The project was under general supervision of Professors E. P. Popov and V. V. Bertero.

F. C. Filippou assisted with the preparation of the report for publication. Gail Feazell made the drawings and prepared them for publication, and Linda Calvin did the typing of the final manuscript. The authors would like to thank them for their help.

TABLE OF CONTENTS

Table of Contents (cont'd) Page

Table of Contents (cont'd)

Page

TABLE OF CONVERSION FACTORS

To convert	To	Multiply by
inches (in.)	millimeters (mm)	25.4
feet (ft)	meters (m)	0.305
yards (yd)	meters (m)	0.914
square inches (sq in.)	square millimeters (mm^2)	645
cubic inches (cu in.)	cubic millimeters (mm^3)	16.4×10^3
cubic feet (cu ft)	cubic meters (m^3)	0.028
pounds mass (lbm)	kilograms (kg)	0.453
tons (ton) mass	kilograms (kg)	907
pound force (lbf)	newtons (N)	4.45
kilograms force (kgf)	newtons (N)	9.81
pounds force per square inch (psi)	kilopascals (kPa)	6.89

LIST OF TABLES

LIST OF FIGURES

List of Figures (cont'd) Page

List of Figures (cont'd) Page

List of Figures (cont'd) Page

List of Figures (cont'd) Page

List of Figures (cont'd) Page

LOCAL BOND STRESS-SLIP RELATIONSHIPS OF DEFORMED BARS UNDER GENERALIZED EXCITATIONS

Experimental Results and Analytical Model

I. INTRODUCTION

1.1 General

In earthquake resistant design of structures, economical requirements usually lead to the need for large seismic energy input absorption and dissipation through large but controllable inelastic deformations of the structure. The need for controlling the inelastic deformations follows from the recommendations of the Structural Engineer's Association of California [1] that buildings be designed to resist major earthquakes such that structural and nonstructural damages incurred from an earthquake do not lead to collapse of the structure or to the endangerment of human life. Therefore, to meet the above requirements, the sources of potential structural brittle failure must be eliminated and degradation of stiffness and strength under repeated loadings must be minimized or delayed long enough to allow sufficient energy to dissipate through stable hysteretic behavior.

In reinforced concrete (R/C), one of the sources of brittle failure is the sudden loss of bond between reinforcing bars and concrete in anchorage zones, which has been the cause of severe local damage to, and even collapse of, many structures during recent strong earthquakes. Present bond seismic code provisions [2] appear to be inadequate. These provisions are based on results obtained under monotonic loading, which are inadequate for gauging the actual structural behavior during severe seismic shaking [3].

Even if no anchorage failures occur, the hysteretic behavior of reinforced concrete structures, subjected to severe seismic excitations, is highly dependent on the interaction between steel and concrete (bond stress-slip relationship) [4]. Tests show that developing displacement ductility ratios of four or more, fixed end rotations caused by slip of the main steel bars along their embedment length in beam-column joints, may contribute up to 50 percent of the total

beam deflections [5-7]. These effects must be included in the analyses. However, this is not possible at present because, in spite of recent integrated experimental and analytical studies [8] devoted to finding such a relationship, no simple reliable bond stress-slip laws for generalized excitations are available [9].

1.2 Objectives and Scope

The ultimate objectives of the work reported herein were to conduct all the necessary integrated experimental and analytical investigations that will permit to predict analytically the local bond stress-slip relationship of deformed reinforcing bars subjected to generalized excitations; for instance, as expected during the response of R/C structures to severe earthquake ground motions.

To achieve these objectives, some 125 pull-out specimens were tested. Each one of the specimens tested represented the confined region of a beam-column joint. Only a short length (5 times the bar diameter d_b) of a Grade 60 deformed reinforcing bar was embedded in confined concrete. Each specimen was installed in a specially designed testing frame and was loaded by a hydraulic servo-controlled universal testing machine. The tests were run under displacement control by subjecting one bar end to the required force needed to induce the desired slip, which was measured at the unloaded bar end.

The influence of the following parameters on the bond stress-slip relationship was studied.

(1) Loading history. The main parameters were: the peak value of slip (0.1 mm $\leqslant$ s $\leqslant$ 15 mm), the difference Δs between the peak values of slip between which the specimen was cyclically loaded (Δs = 0.05 mm, 1 s_{max}, and 2 s_{max}), and the number of cycles (1 to 30).

(2) Confining Reinforcement (none to 3% of concrete volume).

(3) Bar Diameter (#6, #8 and #10 bars ($d_b \approx$ 19, 25, 32 mm)).

(4) Concrete Compressive Strength (f_c' = 30 N/mm^2 (4350 psi) and f_c' = 55 N/mm^2 (8000 psi)).

(5) Clear Bar Spacing (s = 1 d_b to 6 d_b).

(6) Transverse Pressure (p = 0 to 13.5 N/mm^2 (1960 psi)).

(7) Loading Rate (increase of slip 170 mm/min., 1.7 mm/min., and 0.034 mm/min. (6.7 in/min., 0.067 in/min., and 0.0013 in/min.)).

Based on the results obtained, an analytical model for the local bond stress-slip relationship was developed. It takes into account the significant parameters that control the behavior observed in the experiments. By evaluating test data given in literature, rules were formulated to extend the validity of the model to conditions different from those present in the tests.

II. LITERATURE REVIEW

2.1 Experimental Studies on Local Bond Stress-Slip Relationship

2.1.1 General Description

The interaction of deformed bars with concrete depends mainly on the mechanical interlocking between lugs and concrete; adhesion and friction between the rough bar surface and concrete adds only a little to the bond resistance [10,11]. The bond characteristic of bars can best be described by a relationship between local bond stress, τ, and pertinent local slip, s, of the bar [10]. In this report slip is defined as the relative displacement of the bar with respect to concrete. This relationship is also needed for analytical models for predicting the behavior of anchored bars. Therefore, the influence of the different parameters on the local bond stress-slip relationship will be described in the following.

Fig. 2.1 shows a bond stress-slip relationship (valid for a slip controlled test) for monotonic and cyclic loading. The graph is based on the results given in [8,9,10,12], with some modifications based on the test results reported herein. The curves are simplified to better distinguish the different regions.

When loading a specimen the first time, a bond stress-slip relationship is followed which is called herein "monotonic envelope" (paths OABCDEF or $OA_1B_1C_1D_1E_1F_1$). Imposing a slip reversal at point G, a stiff "unloading branch" is followed up to the point where the frictional bond resistance (τ_f^-) is reached (path GHI). Further slippage in the negative direction takes place along the "friction branch" without significant increase in τ (path IJ). When the bar is almost back in the position before loading ($s \approx 0$), it picks up load again, but the values of τ might be reduced compared to the values corresponding to the monotonic envelope, as illustrated by path $JB'_1C'_1K$. The curve $OA'_1B'_1C'_1D'_1E'_1F'_1$ is called herein "reduced envelope". When reversing the slip again at K, first the stiff unloading branch and then the friction branch with $\tau = \tau_f^+$ are followed (path KLM). Well before reaching s_{max} (from which unloading started), the bond stresses increase again ("reloading branch", path MG'). For $s = s_{max}$, the

corresponding τ is much lower than at first loading. Increasing the slip further, a curve similar to the monotonic curve is followed, but with τ values that might be reduced (path G'D'E'F'). This curve is also called herein "reduced envelope". In the following, the different branches of the local bond stress-slip relationship and the main parameters influencing them will be discussed in more detail.

2.1.2 Monotonic Loading

The monotonic envelope can be described by the characteristic points OABCDEF.

When loading an anchored bar, relative movements between steel and concrete (slip) will occur. The slip is caused mainly by crushing of the concrete in front of the lugs. At first, the bond resistance is made up by adhesion up to point A. Further loading will mobilize the mechanical interlocking of cement paste on the microscopic irregularities of the bar surface as well as the mechanical interlocking between the lugs and concrete. The high pressure on the concrete in front of the lugs causes tensile stresses in the concrete around the bar, which, in turn, create internal inclined cracks, called herein "bond" cracks, say at point B. These bond cracks were shown by Goto [14] experimentally (Fig. 2.2) and by several researchers [7,8,11,13,15] analytically, using the method of finite elements.

The bond cracks modify the response of concrete to loading. Its stiffness will be diminished and, therefore, larger slip increments will be needed for further τ-increments than before cracking. After the occurrence of bond cracks, the stress transfer from steel to the surrounding concrete is achieved by inclined compressive forces spreading from the lugs into concrete at an angle α (Fig. 2.2c). The components of these forces parallel to the bar axis are proportional to the bond stress τ. The radial component, with respect to the bar axis, loads the concrete like an internal pressure and induces tensile hoop stresses which cause splitting cracks. When these cracks reach the concrete surface, say at a τ illustrated by point C in Fig. 2.1, and none or only a small amount of confining reinforcement is provided, the bond resistance will drop to zero (path CP).

However, if the concrete is well confined, the load can be increased further. When approaching the maximum bond resistance (point D), shear cracks in a part of the concrete keys between ribs are initiated [10,16] (Fig. 2.3). With increasing slip with respect to $s_{\tau_{max}}$, an increasing area of concrete between lugs is affected by this shear failure and, consequently, the bond resistance is reduced. At point E, the concrete between lugs is completely sheared off, and the only mechanism left is frictional resistance between rough concrete at the cylindrical surface where shear failure occurred. On the contrary to [10,16], Tassios [9] assumes that the maximum bond resistance is controlled by a compression failure of the compression struts spreading out from the lugs into the concrete.

The ascending branch of the bond stress-slip curve (path OABCD in Fig. 2.1) has been studied extensively. However, not much is known about the descending branch (path DEF), which can only be measured in a deformation controlled test.

The bond resistance offered by adhesion is rather small ($\tau_A \approx$ 0.5 to 1.0 N/mm^2 (~ 72 to 145 psi) [9]). The bond stress at occurrence of internal bond cracks can be roughly estimated to $\tau_B \approx$ 2 to 3 N/mm^2 (290 to 435 psi) for a concrete with $f_c' = 30$ N/mm^2 (4350 psi) [7,9]. Analysis of these values reveals that under service load adhesion is overcome and internal bond cracks will occur.

Splitting of concrete due to bond has been thoroughly studied in [17-19]. According to this work, the splitting resistance depends mainly on the concrete tensile strength, concrete cover, bar spacing, amount of transverse reinforcement and transverse pressure. The bond stress τ_c at splitting may be as low as 2 N/mm^2 (290 psi) or as high as 7 N/mm^2 (1015 psi) for a concrete having a $f_c' = 30$ N/mm^2 (4350 psi) and with no transverse pressure applied, depending on the actual values for concrete cover, bar spacing, and confining reinforcement.

The maximum bond resistance τ_{max} is mainly influenced by the concrete strength, bar deformations, and the position of the bar during casting. The influence of the bar diameter is relatively small if all dimensions (height and distance of bar lugs and concrete dimensions) are kept constant as multiples of the bar diameter [13]. The bond strength might also be

influenced by confining reinforcement and transverse pressure, but their influence is not sufficiently studied yet.

The τ_{max} increases with increasing concrete strength. It amounts to $\tau_{max} \approx$ 10 to 15 N/mm^2 (1450 to 2175 psi) for $f_c' = 30$ N/mm^2 (4350 psi) and bars with normal deformation patterns cast horizontally. The given values are average τ_{max} over a certain bond length (usually 3 d_b to 5 d_b). Locally τ_{max} might be larger. Rehm [10] and Martin [13] assume that τ_{max} is proportional to f_c', but other authors [20,21] normalize the results for different concrete strengths with $\sqrt{f_c'}$. The influence of the deformation pattern can best be described by the so-called "related rib area", α_{sR} [10] (Eqn. 2.1); that is, the relation between bearing area (area of the lugs perpendicular to the bar axis) to the shearing area (perimeter times lug spacing).

$$\alpha_{sR} = \frac{k \cdot F_R \cdot \sin\beta}{\pi \cdot d_b \cdot c} \tag{2.1}$$

where

k = number of transverse lugs around perimeter;
F_R = area of one transverse lug;
$\sin\beta$ = angle between lug and longitudinal axis of bar;
c = center to center distance between transverse lugs.

For bars cold worked by twisting, a second term is added [10] which is not given here. Figure 2.4 shows the influence of the related rib area and of the position of the bar during casting on the local bond stress-slip relationship. It can be seen that bond strength and bond stiffness increase with increasing values α_{sR}. Reinforcing bars commonly used in the U.S. have values α_{sR} between approximately 0.05 and 0.08.

The frictional bond resistance τ_E has been barely investigated yet. For a concrete with f_c' = 30 N/mm^2 (4350 psi), values for τ_D of about 0.4 N/mm^2 (58 psi) to 10 N/mm^2 (1450) are given [8,9,22].

The bond resistance at given slip values scatters considerably. Extensive studies [23] show that the average standard deviation for the bond resistance in the slip range s = 0.01 mm (0.0004 in.) to $s_{\tau_{max}}$ is about 1.3 N/mm^2 (189 psi) for ideal test conditions (e.g., pull-out tests

of identical bars with short embedment length and specimens cast from the same concrete batch). A much higher scatter is to be expected for less ideal conditions. This partially explains the scatter of the data given in the literature for characteristic τ-values (e.g., τ_{max}).

The bond stiffness given in the literature scatter even more. This is demonstrated by Fig. 2.5, which shows local bond stress-slip relationships for small slip values after different authors. The local bond stress-slip relationships were derived from the results of tests with different test specimens. They are valid for bond regions well away from a concrete face. According to [24], the large scatter of available data is mainly due to difficulties in measuring slip between steel and concrete correctly and to the use of different test specimens with different stress conditions in the concrete surrounding the bar. Furthermore, the scatter may have been caused by the use of bars with different diameter and different deformation pattern. According to [10], the bond stiffness decreases for constant bar diameter with increasing relation between lug distance c and lug height a and for constant values c/a with increasing bar diameter. Also, the number of tests was not always sufficient to produce reliable local bond laws.

The shape of the local bond law is significantly influenced by the position of the bar during casting (Fig. 2.4). The largest bond stiffness is reached for bars cast vertically and loaded against the setting direction of fresh concrete. Bars cast horizontally show a much smaller stiffness and a lower bond strength. Bars cast in the vertical position but loaded in the setting direction of the concrete may perform even poorer than bars cast horizontally [10]. The same is true for bars cast in a horizontal position when the depth of concrete beneath the bar is increased [20].

The local bond law for loading in tension or compression is almost identical [10]. Observed differences in tests (e.g. in [12]) can mainly be attributed to loading the bar in different directions with respect to the setting direction of the fresh concrete.

The local bond stress-slip relationship may vary along the embedment length. According to [25-28], bond stiffness and bond strength are 2-3 times larger in the interior of a specimen with tension forces acting on both ends of the embedded bar than towards the ends. However,

no significant influence of the location on the local bond law was observed in the comparable tests [29]. In [8] three different regions with very different bond stress-slip behaviors were identified in a beam-column joint: unconfined concrete in tension, confined concrete and unconfined concrete in compression (Fig. 2.6). A similar influence of the location on the local bond law was found in [22].

2.1.3 Cyclic Loading

The influence of repeated (not reversed) loading with constant peak loads has been studied in [30-32]. According to [31], repeated load has a similar influence on the slip and the bond strength of deformed bars as on the deformation and failure behavior of unreinforced concrete loaded in compression. The bond strength decreases with increasing number of cycles between constant bond stresses (fatigue strength of bond, Fig. 2.7). The slip under peak load and the residual slip increase considerably as the number of cycles increases (Fig. 2.8). If no fatigue failure of bond occurs during cycling and the load is increased afterwards, the monotonic envelope is reached again and followed thereafter. That means, provided the peak load is smaller than the load corresponding to the fatigue strength of bond, a preapplied repeated load influences the behavior of bond under service load but does not adversely affect the bond behavior near failure compared to a monotonic loading.

Although many factors related to early concrete damage (microcracking and microcrushing due to high local stresses at the lugs) may be involved in this bond behavior during repeated loads, the main cause of the slip increase under constant peak bond stresses is creep of concrete between lugs [31].

The influence of reversed loading on the local bond stress-slip relationship has not been studied extensively. In [12] the following characteristic behavior was found:

(a) After loading in one direction, the bond stress-slip relationship for loading in the reversed direction is almost identical with the monotonic envelope in that direction.

(b) Once a peak slip value is reached, a considerable reduction in bond resistance is produced at lower slip values in the subsequent load history.

(c) The peak bond stress under cyclic loading between constant slip values deteriorates moderately and is not significantly influenced by the loading history.

(d) A small number of cycles between limited slip values do not give a significant effect on the bond stress-slip behavior for slip values larger than the peak slip in the previous cycles.

This behavior was also found in the earlier studies [33,34]. However, it must be remembered that in all these tests cycling was performed between rather small slip values with corresponding bond stresses well below the monotonic τ_{max} or the fatigue strength of bond (compare Fig. 2.7).

In [8] specimens representing a beam-column interior joint were cycled between different increasing s_{max}. Figure 2.9 shows a typical local bond stress-slip relationship, which was deduced from the measured steel strains along the anchorage length and the measured slip at the bar ends. These results indicate that cycles between constant slip values equal to or larger than the slip $s_{\tau_{max}}$ ($s_{\tau_{max}}$ = slip value corresponding to the monotonic τ_{max}) do produce a pronounced deterioration of the bond resistance at peak slip and may have a significant effect on the bond stress-slip behavior at slip values larger than the peak slip in the previous cycles. The deterioration of bond strength and bond stiffness is much more pronounced for full reversed cycles ($|s_{min}| = |s_{max}|$) than for half cycles ($s_{min} = 0$) [3,6].

According to [9,12] the frictional bond stress τ_f after first unloading from a bond stress $\tau < \tau_{max}$ seems to be a constant multiple of τ ($\tau_f = \alpha \cdot \tau$, with $\alpha \approx 0.18\text{-}0.25$). On the contrary, in [8] it is assumed that τ_f is independent of the bond stress from which the unloading is started, and the given value ($\tau_f \approx 0.4$ N/mm^2 (60 psi)) is rather low. The frictional bond resistance deteriorates during subsequent cycles between fixed slip values. A rough estimate of the deterioration rate is given in [9].

2.2 Analytical Models for Cyclic Loading

The first analytical model of the local bond stress-slip relationship for cyclic loading was

proposed by Morita/Kaku [12]. It is shown in Fig. 2.10.

The monotonic envelopes, which are different for loading in tension or compression and for confined or unconfined concrete, are given by two successive straight lines which follow closely the experimentally measured curve. The assumed bond stress-slip relationship for the first cycle coincides relatively well with the behavior observed in experiments. However, the observed deterioration of the bond resistance at peak slip and of the frictional bond resistance with increasing number of cycles is not taken into account. After cycling between arbitrary slip values, it is assumed that the monotonic envelope is reached again at slip values larger than the peak value in the previous cycle and followed thereafter.

The model is sufficiently accurate for a small number of cycles between relatively small slip values with corresponding bond stresses smaller than about 80 percent of the monotonic τ_{max}. However, it is inaccurate for several load cycles, and it is not valid for slip values larger than the one corresponding to 0.8 τ_{max}. In [35] a simplified version of this model was used for the analytical investigation of a concrete panel under load cycles with some success.

Figure 2.11 shows the bond model proposed by Tassios [9]. The monotonic envelope consists of six successive straight lines. The coordinates of the controlling points A to E, which have the same physical meaning as described in Section 2.1.2, are theoretically evaluated and given as a function of the relevant influencing parameters. The same bond stress-slip relationship is assumed regardless of whether the bar is pulled or pushed. After loading to a slip value $s > s_B$, the values of τ of the bond stress-slip relationship for loading in the reversed direction are reduced by 1/3 compared to the monotonic envelope. The bond stress-slip relationship for reloading and for subsequent cycles between fixed slip values is somewhat simplified compared to the real behavior. However, the deterioration of the bond resistance at peak slip and of the frictional bond resistance is taken into account. When increasing the slip beyond the cyclic peak value ($s > s_G$ in Fig. 2.11), it is assumed that the monotonic envelope is reached again and, therefore, no deterioration of the monotonic envelope is taken into account.

Tassios' model is an improvement compared to the older one of Morita/Kaku insofar as

the descending branch of the local bond stress-slip relationship is given and the influence of load cycles on bond deterioration for slip values smaller than or equal to the peak slip value in the previous cycle is taken into account. However, the assumption that for slip values larger than the peak value in the previous cycle the monotonic envelope is reached again and followed thereafter, while the bond stresses in the reversed direction are reduced by 1/3 compared to the monotonic envelope, is not sufficiently accurate. For monotonic loading, the model is useful for the total slip range. However, for cyclic loading it is valid for slip values $s << s_{\tau_{max}}$ only.

Recently, another proposal for a local bond stress-slip law was published in [8] (Fig. 2.12). The model's main characteristics are as follows:

(a) A four stage piecewise linear approximation is used as monotonic envelope. The physical meaning of the controlling points are the same as described in Section 2.1.2. However, points B and C (occurrence of internal bond cracks and splitting cracks) are omitted. Different monotonic envelopes are assumed for unconfined concrete in tension, confined concrete and unconfined concrete in compression, which simulate the behavior observed in the experiments (compare Fig. 2.6).

(b) Cycling between points A and A_1 or unloading and reloading only (paths GIG or KLK) do not deteriorate the envelope.

(c) Unloading from a point beyond A or A_1 and following the friction path for an arbitrary small slip value produces reduced envelopes (OAD'E'F' and $OA_1D'_1E'_1F'_1$) by reducing the characteristic bond stresses $\tau_D, \tau_{D1}, \tau_E, \tau_{E1}$ and the slip values s_E, s_{E1} by a reduction factor. The latter depends on the cumulative slip having magnitudes larger than those of the previous cycle. Therefore, no further reduction of the envelope is assumed for subsequent cycles between slip values smaller than or equal to the previous peak slips.

As an example, Eqn. 2.2 gives the reduction of τ_D. Similar equations exist for the reduction of the other characteristic values which describe the model.

$$\tau'_D = \alpha_D \cdot \tau_D = \left(1 - \alpha_{\tau_D} \frac{\sum s_i / s_D}{p_D} \cdot \xi_{\tau_D} - \beta_{\tau_D} \frac{\sum s_{i1} / s_D}{p_D} \cdot \xi_{\tau_D}\right) \tau_D \qquad (2.2)$$

where

$\sum s_i, \sum s_{i1}$: sum of the peak slip values having a magnitude larger than in the previous cycles for loading in tension or compression, respectively;

s_D: slip at point D;

$\alpha_{\tau_D}, \beta_{\tau_D}, \xi_{\tau_D}, p_D$: constants, evaluated from test results.

(d) The frictional bond resistance is assumed to be equal to τ_E of the monotonic envelope and independent of the number of cycles.

(e) The bond stress-slip relationships for the reloading branch (path MRN) and for additional cycles between fixed slip limits are very similar to those proposed in [12].

The above model is a major improvement, because it takes several features observed in experiments into account and it is approximately valid for cycling between arbitrary slip values. However, in spite of being rather complicated, it is not general. Some 20 parameters are needed to describe the bond stress-slip relationship for cyclic loading, which have no clear physical meaning and must be evaluated from test results. Furthermore, the assumptions on which the calculation of the reduced envelope is based need improvement. For example, an arbitrary number of cycles ($\geqslant 1$) in well-confined concrete between $s_{max} = 2s_D$ and $s_{min} = -2s_D$ reduces τ_D independent of the number of cycles by 13 percent. On the contrary to that τ_D is reduced to zero after eight cycles between almost the same peak slip values if only the value of s_{max} is increased arbitrarily small in each cycle.

2.3 Summary of Chapter 2

To date several thousand experiments have been carried out to study the ascending branch of the local bond stress-slip relationship for monotonic loading. By contrast, its descending branch, which can only be measured in a deformation controlled test, has hardly been investigated. While the bond behavior for repeated (not reversed) loadings with peak bond stresses well below the monotonic bond strength under monotonic loading is fairly well known, the knowledge about this behavior for reversed loadings between relatively large peak slip

values is rather limited.

Bond between reinforcing bars and concrete does scatter significantly, even under nearly ideal laboratory conditions. This has to be taken into account when evaluating results from bond tests, planning new test series, or estimating the influence of bond on the overall behavior of reinforced concrete elements or structures.

While the characteristic bond resistances of the ascending branch of the monotonic envelope can be fairly well estimated, the prediction of the corresponding slip values is very difficult and a large scatter must be expected. The shape of its descending branch and the ultimate frictional bond resistance are hardly known yet.

The bond behavior for reversed loadings between rather small slip values ($s << s_{\tau_{max}}$) can be predicted with sufficient accuracy. However, the knowledge about the influence of cycles between larger slip values ($s \geq s_{\tau_{max}}$) on the local bond stress-slip relationship is still in its infancy.

The analytical models for a local bond stress-slip relationship for cyclic loadings proposed so far reflect this inadequate knowledge and cannot be accepted for general excitations. Therefore, the present study concentrates on the local bond law for relatively large slip values for monotonic and cyclic loadings. The results of an extensive experimental investigation and an analytical model for prediction of such laws is presented herein.

III. EXPERIMENTAL PROGRAM

3.1 Test Specimen

The test specimens should represent as closely as possible the conditions found in a beam-column joint. Therefore, these conditions and the considerations to model them appropriately in a test specimen are described in the following.

Figure 3.1 (after [36]) shows the hysteretic behavior of an interior joint when loaded by a lateral force H, which simulates the effect of an earthquake loading. First, as H increases from O to B, cracks develop on both sides of the column, Fig. 3.1(b). After unloading and applying H in the opposite direction (path BCD), diametrically opposed cracks develop on either side of the column, Fig. 3.1(c). If the load reversals applied in both directions are sufficiently severe to cause permanent strain in beam bars, cracks through the entire beam cross section are formed, as shown in Fig. 3.1(d). The bars that run through the column are simultaneously pulled and pushed from opposite sides under cyclic loading. The critical condition develops when a bar is subjected to full reversals of tensile and compressive forces developing high bond stresses along the bar embedment length within the column. This may lead to a severe stiffness degradation of the joint caused by bond failure of the beam bars within the column.

In Fig. 3.2 (taken from [37]), an interior joint after testing is shown. If the column is less strong than in this experiment, bending and shear cracks will develop in the column as well (Fig. 3.3, taken from [38]), which can change the bond stress-slip relationship. Even if no bending and shear cracks occur in the joint, the bond conditions vary along the embedment length (Fig. 2.6), depending on the state of stress and strain in the concrete around the bar.

The unconfined concrete at the tensioned bar end offers the least bond resistance because of the early formation of radial splitting cracks caused by high tensile hoop stresses. Bond failure is caused by the separation of a concrete cone (Fig. 3.4) from the concrete block due to bond forces acting on the concrete in front of the lugs. Much better bond conditions are found in the concrete core between confining reinforcement. Splitting cracks in the plane between

bars may develop, but their growth will be controlled by the confining reinforcement, and bond failure is probably due to a shear failure in the concrete between lugs. The best bond is offered by the unconfined concrete at the compressed bar end, because at this end the concrete lateral to the bar is under high compressive stresses caused by the column normal force and the moment acting on the joint and caused by the expansion of the bar due to the Poisson effect. The bond is not only influenced by the above mentioned parameters, but it might also be different for top and bottom bars (top bar effect), edge and interior bars (different confinement) and may vary with such parameters as bar diameter, concrete strength, bar distance, degree of confinement, etc.

To simulate the simultaneous push-pull condition of a beam bar in an interior joint, a simplified model was used in [8,22]. Single bars were cast in well-confined concrete blocks, their width being up to 25 times the bar diameter, and subjected to monotonic or cyclic loadings (see Fig. 2.6). Extensive data (applied forces, steel strains along embedment length, displacements of bar ends relative to the middle of the concrete block and cracks) were taken during the tests. The results gave a very good insight in the overall behavior of an anchored bar. Some local bond stress-slip relationships were deduced from the data. However, the evaluation of such relationships was complex, and their accuracy is somewhat questionable. Local bond stresses and local slip were calculated from the difference of the measured steel strains at adjacent points along a bar and converting them into local slip and steel stresses. Since the strain measurements have considerable scatter, particularly so for cyclic loading after a bar yields, the calculated results tend to be inaccurate. Furthermore, these tests are expensive and time consuming, which prohibits a thorough study of relevant parameters. Therefore, a different approach was used in this study.

The specimen (Fig. 3.5) should represent the confined region of a beam-column joint. Therefore, the concrete was confined by secondary reinforcement representing the column reinforcement. To ensure a good anchorage of the vertical bars, they were rigidly connected with the top and bottom stirrups by arc welding.

Only a short length of a Grade 60 deformed bar was embedded in concrete. During the test, the force acting on the loaded bar end and the slip, measured at the unloaded bar end, were recorded. *Assuming that the bond stresses are evenly distributed along the bonded length,* they can easily be calculated from the measured forces. Furthermore, because the steel behaves elastically and the embedment length is short, the slip values at the unloaded and loaded bar ends do not differ significantly from each other. Therefore, the measured slip represents the local slip in the middle of the embedment length with sufficient accuracy. *Note that strictly speaking the so obtained relationship is not a local bond stress-slip relationship but an average one.* However, the embedment length was chosen to 5 d_b. This embedment length is short enough so that the basic assumptions (see above) are still valid with sufficient accuracy but long enough to reduce the scatter of test results usually observed in tests with a very short bonded length.

The bonded length was positioned in the middle of the specimen, and a bond free length of 5 d_b at either side was employed. By this arrangement and by placing teflon between the specimen and the bearing plates (see Fig. 3.6 and Section 3.5), the influence of a possible restraint of concrete lateral strains by friction at the bearing plates was reduced as much as possible.

The bond free length was obtained by placing a thin metal tube concentrically around the bar and sealing the ends with mastic to prevent concrete from flowing in. The inner diameter of the tubes was about 4 mm (0.16 in.) larger than the outer diameter of the bars, including lugs. The tubes neither restrained the slip of the bar nor significantly affected the transfer of bar forces to the concrete. Some preliminary tests showed that the bond stress-slip relationship was not influenced by tubes with slightly different inner diameters or wall thicknesses.

Because splitting cracks might influence the bond stress-slip behavior, the resistance against splitting was simulated as closely as possible to that which might exist in a real structure. For this purpose, thin plastic sheets were placed in the plane of the longitudinal axis of the bar (Fig. 3.5), which limited the concrete splitting area to the desired value. The length of the splitting area was 1.5 d_b larger than the bond length because of the higher relation between

splitting and bond forces in tests with short embedment length compared to the middle of a long anchorage [19,39]. The width of the splitting area was equal to the assumed clear bar distance, which was varied between 1 d_b and 6 d_b. This method of simulating various bar distances was chosen because the outer dimensions of the specimen and the confining reinforcement could be kept constant, which simplified the production of the specimens.

The bars were placed in the middle of the specimens (height 12 inches $\approx$ 300 mm) and cast in a horizontal position. Therefore, the bond could be expected to be somewhat superior or inferior to top or bottom bars, respectively.

3.2 Test Program

A summary of the test program is given in Table 3.1. The tests are subdivided into 7 series, depending on the parameter studied. Only one parameter was varied in a test series, while all other parameters were kept constant. The "normal" or standard set of parameters was:

Tested Bar:	#8 (d_b = 25.4 mm)
Confining Reinforcement:	made out of #4 bars (d_b = 12.7 mm)
Concrete Strength:	f_c' = 30 N/mm^2 ($\approx$ 4350 psi)
Transverse Pressure:	None
Loading Rate:	1.7 mm (0.067 in.) slip/minute

Main Test Series 2 (Table 3.1a) was used to investigate the influence of various slip histories on the local bond stress-slip relationship. The main parameters were:

- Monotonic loading in tension and compression (Series 2.1, 2.2, and 2.16).
- Cyclic loading between full reversals of slip (full cycles) at different peak slip values covering the whole range of the bond stress-slip law (Series 2.3 to 2.11 - Fig. 3.7).
- Cyclic loading between slip s=0 and a selected peak slip value (half cycles) (Series 2.12 to 2.15).

- Cyclic loadings with a difference in slip $\Delta s = 0.05$ mm at selected peak slip values (Series 2.17 and 2.18). In these tests the load dropped from the peak value to almost zero.
- Cyclic loading under different increasing s_{max} (Series 2.19 to 2.22).

In the Test Series 2.3 to 2.18, after the specimens were subjected to either 1 or, alternatively, to 10 cycles up to the selected peak values of slip, the slip was increased monotonically to failure. On the contrary, the bars of Test Series 2.19 to 2.22 were subjected to a series of cycles at different values of slip with 5 cycles at each step.

In the cyclic test, usually the first and final loadings after completing the cycles were done in tension. Only in Test Series 2.6* was the loading started and completed in compression.

In the other six test series (Table 3.1b), the influence of various other parameters on the basic bond behavior under monotonic and cyclic loadings were studied:

Series 1: **Confining reinforcement:** The diameter of the vertical bars were varied from #8 ($d_b \approx 25$ mm) to #2 ($d_b \approx 6.4$ mm) (Series 1.1 to 1.3). In addition, specimens without confining reinforcement were tested (Series 1.4). In Series 1.5, the influence of the stirrups was studied.

Series 3: **Bar diameter:** The bar diameter was varied from #6 ($d_b \approx 19$ mm) to #10 ($d_b \approx 32$ mm), thus covering the range normally used in buildings designed to resist severe earthquakes.

Series 4: **Concrete strength:** While usually the concrete strength was $f_c' \approx 30$ N/mm^2 ($\approx$ 4350 psi), it was increased to $f_c' \approx 55$ N/mm^2 ($\approx$ 7975 psi) in Test Series 4.

Series 5: **Bar spacing:** The clear distance between bars was varied between $c = 1\ d_b$ (minimum value allowed in the code) to $c = 6\ d_b$.

Series 6: **Transverse pressure:** Pressure ranging from 5 N/mm^2 (725 psi) to 13.2 N/mm^2 (1914 psi) was applied in the direction of the column reinforcement to simulate the influence of column compression forces on bond behavior.

The applied maximum pressure was equal to about 45 percent of the concrete compressive strength. For comparison, tests with no transverse pressure were carried out as well.

Series 7: **Loading rate:** The adopted standard rate of pull-out (1.7 mm (0.067 in.) slip per minute) was mainly chosen for practical reasons to terminate a test in a reasonable time. It was about 10 times faster than the loading rate recommended for standardized load-controlled pull-out tests [40]. The chosen slip increase of 1.7 mm (0.067 in.) per minute gave an average increase in steel strain up to the peak load of about 1.5 mm/m per minute. During an earthquake, larger strain rates are reached. Therefore, the rate of pull-out was increased to 170 mm (6.69 in.) slip/min. (100 times faster than the standard value) in Test Series 7.1 and 7.3. In addition, the influence of a 50 times slower rate of pull-out (0.034 mm (0.0013 in.) slip/min.) was studied in Test Series 7.2.

The influence of the above mentioned parameters was studied for monotonically increasing slip and for cyclic loading at a peak slip value s_{max} = 1.65 mm (0.065 in.). In the cyclic tests, after performing 10 cycles between fixed slip values, the slip was increased monotonically to failure.

Usually two or three identical tests were carried out to reduce the effect of inevitable scatter of results. Note that the average values calculated from two or three tests represent no statistically reliable mean value. To determine such a value, more repetitive tests are necessary. However, the objective of this study was not to achieve statistically reliable bond stress-slip relationships for a small number of variables but to investigate the influence of several parameters on the bond behavior, especially under cyclic loading. Altogether 125 specimens were tested; from that 47 specimens were loaded monotonically and 78 specimens loaded cyclically.

3.3 Material Properties

3.3.1 Concrete

The concrete was made from normal weight aggregate. The mixes used are given in Table 3.2. For the medium strength concrete ($f_c' = 30$ N/mm$^2 \approx 4350$ psi), the amount of cement was 356 kg/m^3 (596 lb/cu. yd.), the water-cement ratio was 0.57 and the maximum aggregate size was 9.5 mm (3/8 in.). For the high strength concrete ($f_c' = 55$ N/mm$^2 \approx 7975$ psi), the values were: amount of cement = 505 kg/ m^3 (845 lb/cu. yd.), water-cement ratio = 0.38, and maximum aggregate size = 9.5 mm (3/8 in.). The aggregate grading is shown in Fig. 3.8.

The average slump was 4.75 inches (120.7 mm), with minimum and maximum values of 3.25 and 6.0 inches (82.6 and 157.4 mm), respectively. The concrete was relatively easy to cast and compact, with no apparent segregation of its components.

The measured concrete strengths are summarized in Table 3.3. Twelve standard cylinders were cast from each concrete batch. Nine cylinders were used to measure the concrete compressive strength and three cylinders to test the splitting tensile strength. The compression tests were done usually at the beginning, in the middle, and at the end of the time needed to test all specimens cast from one batch. This time was 3 to 5 days. The splitting tensile strength tests were performed in the middle of that time. The tests started about four weeks after casting. No significant increase in strength was noticed during the time of testing. Therefore, only the average strengths of all tested cylinders are given in Table 3.3.

The average concrete strengths agreed very well with the values aimed at. Note that the small coefficients of variation for the 30 N/mm^2 concrete (3.3 percent for f_c' and 6.9 percent for f_t, respectively) indicate that a very good uniformity of concrete properties was achieved throughout the tests. This was due to the fact that the amount of material needed for all tests was stored at the beginning. In the last column of Table 3.3, the relation between f_t and $f_c'^{2/3}$ is given. The average relationship agrees well with the value given in [41].

3.3.2 Reinforcing Steel

Grade 60 deformed bars were used for the test bars as well as for the bars of reinforcing cages. The test bar deformation pattern is shown in Fig. 3.9, and the geometry of the deformations is given in Table 3.4. The related rib area α_{SR} was calculated using Eqn. 2.1. This particular deformation pattern was selected to be approximately the same as that used in the previous bond tests [8,22].

The test bars were pulled out of the specimens after completing a test and were reused. Therefore, only 55 different #8 test bars were used for Series 1, 2, and 4 to 7, which were made from 10 different rods of one delivery. The geometry of deformations of these test bars varied very little. The related rib area was $\alpha_{SR} = 0.066$.

The test bars for Series 3 (influence of bar diameter) were produced from one rod each. For #8 bars, deformations with more pronounced lugs ($\alpha_{SR} \approx 0.11$) were chosen in order to make them more comparable to those of #6 and #10 bars, respectively.

The maximum steel stress during the tests was well below the yield strength, which was about f_y = 485, 530, and 495 N/mm^2 (66.4, 76.9 and 77.8 ksi) for #6, #8, and #10 bars, respectively.

The mechanical properties of the secondary reinforcement were not measured because these values were insignificant for interpretation of test results.

3.4 Manufacture and Curing of Test Specimens

All test bars were thoroughly cleaned by sandblasting in the region of the embedment length. The specimens were cast in plastic-coated wooden forms, with test bars in a horizontal position. One form accommodated three to four specimens. To ease assembling of specimens, the front and rear sides of the forms were divided in the middle. The fabrication of the specimens went on as follows.

First, the prefabricated reinforcement cage (Fig. 3.5) was installed and held in place by plastic spacers. After putting the test bar with mounted tubes into place, the plastic sheets (Fig.

3.5) were slid into thin slits in the dividers to ensure their exact position and bonded to tubes and formwork. They stayed in place during casting. Then the form was completed by mounting the upper part of the form's front and rear sides. Mastic was placed around the test bar where it penetrated the form to prevent leakage and to give sufficient support (fixity) to the bar to prevent its movement during casting. Figure 3.10 shows a photo of specimens prior to casting, with front and back form sides not in place.

The concrete was poured very carefully to prevent loosening of the plastic sheets, and it was thoroughly compacted internally with a plunger vibrator. The plastic sheets had some small holes to prevent air bubbles in the concrete beneath the plastic. Usually 9 to 12 specimens were cast at one time (see Table 3.3). After casting, the forms were covered with wet burlap and plastic sheets until their removal, which was done one week after casting. From then on, the specimens were stored in the laboratory (temperature about 20 degrees C (68 degrees F), relative humidity about 60 percent).

3.5 Experimental Setup and Testing Procedure

The specimens were installed in a specially designed testing frame and tested in a four-column hydraulic servo-controlled universal testing machine (make MTS) (Fig. 3.11), having a capacity of $\pm$ 300 kips ($\approx$ 1350 kN), which allowed the application of prescribed tension and compression forces, or deformations, to the embedded bars. The tests were run under slip control by subjecting the threaded loading end of the bar to the required force needed to induce the desired slip, which was measured at the unloaded bar end by using two LVDT's.

The testing frame is shown in Fig. 3.6. It consisted of upper and lower heads, connected by four threaded rods and a device to connect the test bar with the testing machine. The upper head of the testing frame and the lower part of the connecting device were screwed into the heads of the testing machine. Then the installation of a specimen proceeded as follows.

The specimen was put onto the lower bearing plate by using a forklift and moved along the slit into the correct position. This position was marked by teflon sheets which were fixed to

the bearing plates and whose size coincided with the outer dimensions of the specimens. To minimize possible eccentricities during testing, the specimen's top and bottom faces had to be parallel to each other at right angles to the test bar and had to be smooth. To fulfill these requirements, in some cases a thin layer of hydrostone was placed on the critical specimen faces before installation. In a monotonic tension test, a small gap was left between the specimen and the upper head of the test setup to reduce friction. In a tension-compression test, the upper head rested on the specimen and the nuts of the connecting rods were tightened to prevent movement of the specimen when changing the sign of the applied force. The specimen and the testing machine were connected by screwing a round plate to the test bar and connecting the latter with a similar plate by four bolts. Afterwards, two L-shaped profiles were screwed to the lower head to make up for the reduction in stiffness caused by the slit. Finally, two linear variable differential transformers (LVDT's) with a maximum displacement of ± 25 mm (1 in.) for measuring the slip at the unloaded bar end were mounted by screwing their holding device onto the sawed bar end. The plungers passed through holes made specially in the bearing plate and rested against the concrete, which was coated in this region with a thin layer of epoxy resin to have a very smooth surface. Figure 3.11 shows a specimen in place ready for a tension test.

Thanks to the specially designed testing frame, installing and aligning of a test specimen was relatively easy, fast (time needed was less than 30 minutes), and accurate, with no noticeable eccentricities. Special care was taken to prevent any operations that might have disturbed the bond between the bar and concrete.

In Test Series 6, transverse pressure was applied to the specimens by two hydraulic jacks, with a capacity of 200 kips ($\approx$ 900 kN) (Fig. 3.12). The reaction forces were taken by two heads, connected by four threaded rods. The jacks pressed against stiff steel plates to ensure a uniform pressure. The specimen and the device for applying transverse pressure were assembled on the arms of a forklift and then lifted into place. Figure 3.13 shows an installed specimen. The desired transverse force was applied before starting a test and held constant during its course.

Usually, the slip was controlled at a rate of 1.7 mm/min. (0.067 in/min.). Thus, monotonic tests lasted for about 15 minutes and cycling tests up to 3 hours, depending on the peak slip and the number of cycles. In Series 7, the rate of slip increase varied between 170 mm/min. and 0.034 max./min. (6.69 in/min. and 0.0013 in/min.). In the latter case, a monotonic test was stopped after about 7.5 hours, reaching a slip of about 15 mm (0.59 in.). During cycling, triangular slip waves were induced.

The applied force, measured by a load cell situated in the testing machine's head, and the average output of the LVDT's were continuously monitored on an XY recorder. Figure 3.14 shows the console with electronics for controlling the MTS and the XY recorder.

IV. EXPERIMENTAL RESULTS

4.1 General

In this chapter the experimental results will be presented and the influence of the different parameters investigated will be discussed in detail. Bond stress-slip diagrams were deduced by taking applied forces at given slip values from the records monitored by the XY recorder and converting them into bond stresses using Eqn. 4.1:

$$\tau = \frac{F}{\pi \cdot d_b \cdot l_e} \tag{4.1}$$

where

F = force [N];

d_b = actual bar diameter [mm] (see Table 3.4);

l_e = embedment length;

= 3.75 inches (95.3 mm) for #6 bars;

= 5.0 inches (127.0 mm) for #8 bars;

= 6.25 inches (158.8 mm) for #10 bars.

The concrete strength differed somewhat from the desired value $f_c' = 30$ N/mm^2. Therefore, the bond stresses plotted were converted to the latter value by Eqn. 4.2:

$$\tau_{(f_c' = 30\ N/mm^2)} = \tau_{(Eqn.\ 4.1)} \cdot \sqrt{30/f_c'} \tag{4.2}$$

where f_c' is the actual concrete compressive strength in N/mm^2.

For plotting bond stress-slip diagrams, the following convention was used:

positive or negative bond stress - bar in tension or compression, respectively

positive or negative slip values - bar pulled out or pushed in, respectively.

4.2 Visual Observations and Failure Mode

In all tests, except those with an applied transverse pressure, a splitting crack developed prior to failure in the plane of the longitudinal axis of the bar. Its development could often be noted from a low bang or could sometimes be detected from the monitored load-slip relationship. The bond stress at splitting was about 4 to 9 N/mm^2 (580 to 1305 psi) for concrete with

$f_c' = 30$ N/mm^2 (4350 psi). After developing this crack, the load dropped rapidly if the concrete was not confined by reinforcement (Series 1.4). However, in the case of confined concrete, the load could be increased further with a gradually decreasing bond stiffness. This can be explained by the fact that the growth of cracks was controlled by the vertical bars crossing the crack plane. The width of these cracks could not be measured exactly because of the plastic sheets used to limit the concrete splitting area (Fig. 3.5), but it is believed that they did not exceed about 0.05 mm (0.002 in.), in general, or 0.1 mm (0.004) (vertical bars #2), respectively.

In all tests conducted on specimens with confined concrete, the failure was caused by pulling out of the bars at steel stresses well below yield strength (max. $\sigma_s \approx 0.4$ to 0.8 f_y). The concrete between lugs was completely sheared off and almost pulverized (Fig. 4.1). By sawing the concrete and the vertical reinforcement of some specimens, it was possible to take the specimen apart and to inspect the surface of the concrete that was in contact with the bar. No signs of failure of the concrete in compression in the direction of inclined bond forces (as assumed by Tassios [9]) could be detected.

The specimens of Series 1.4 (no confining reinforcement) failed by splitting of the concrete in the plane of the longitudinal axis of the bar at about 45 percent of the pull-out load of comparable specimens with confined concrete. The concrete between lugs was intact and no severe damage (shear cracks or crushing) could be detected (Fig. 4.2).

4.3 Monotonic Loading

The test results for monotonic loading are plotted in Figs. 4.3 to 4.20.

4.3.1 General Behavior

Figures 4.3 to 4.9 show the results of all monotonic loading tests of Series 1 and Series 2. For tests with confined concrete, the typical behavior was as follows.

The stiffness of the ascending branch of the bond stress-slip curve decreased gradually from its initial large value to zero when approaching the maximum bond resistance at a slip

value of approximately 1.5 mm (0.06 in.) (Fig. 4.8). After passing τ_{max}, the bond resistance decreased slowly and almost linearly until it leveled off at a slip of $s \approx$ 11 to 12 mm (0.43 to 0.47 in.). This value is almost identical to the clear distance between lugs. For larger slip values, the bond resistance was usually almost constant (Fig. 4.7) or decreased slightly in some cases (Figs. 4.3 to 4.5). Therefore, the bond stress-slip curves of all other tests were drawn only up to 12 mm (0.47 in.) slip.

The scatter of the bond stress-slip curves of specimens cast from the same batch and tested identically was significantly smaller than what could be expected according to [23]. The scatter in Test Series 1.3 and 1.5 corresponded approximately to the lower and upper bounds of the values experienced in all tests. On an average, the standard deviation of the bond resistances for given slip values for all monotonically loaded tests was about 0.65 N/mm^2 (94 psi), with only a small influence of the extent of slip (Table 4.1). Because of the relatively small scatter, normally only two identical tests were carried out in Series 2 to 7. The number of repetitive tests was increased to three when the difference between the first two test results was relatively large.

Figure 4.8 shows the average results of those test series that were monotonically loaded almost up to the frictional resistance. The specimens of the different test series were cast from different concrete batches. In Fig. 4.9 the average bond stress-slip relationship of Test Series 2 as well as the lowest and highest single result are plotted. By comparing Figs. 4.8 and 4.9 with Figs. 4.5 and 4.7, it can be seen that the scatter is much larger when the specimens are cast from different concrete batches.

4.3.2 Influencing Parameters

4.3.2.1 Tension or Compression Loading. Figure 4.10 shows the bond stress-slip relationships for Series 2.1 (tension loading) and Series 2.2 (compression loading), which were cast from the same batch. Bond stresses and slip values for compression loading were multiplied by -1 to facilitate the comparison. In addition, the average curve of Series 2 is plotted.

The bond stress-slip relationship of Series 2.2 (bars pushed) is almost identical to that of Series 2.1 (bars pulled) for slip values $\leqslant 0.1$ mm (0.004 in.) and slightly lower for larger slip values. The results of both test series do not differ much from the average curve of Series 2. If inevitable scatter is taken into account, it is reasonable to assume that the basic bond law for tension and compression loading is almost identical. This result could be expected [10] because the bars were cast in a horizontal position.

Equal bond stress-slip relationships for bars in tension and compression remain valid only for steel stresses below yield, as was the case in the reported tests. After yielding, the diameter of a bar in tension is significantly reduced due to the Poisson effect, which may reduce the bond resistance. The opposite is true for a bar yielding in compression. The influence of the Poisson effect on the bond was not studied in these experiments. Evaluation of results given in [8,22] indicates that the Poisson effect will not change the bond resistance more than about 20 to 30 percent even for steel strains as high as 40 mm/m.

4.3.2.2 Confining Reinforcement. In Fig. 4.11 the average bond stress-slip relationships for Series 1.1 to 1.5 are plotted. Figure 4.11a shows the whole slip range, while in Fig. 4.11b only the ascending branches of the bond stress-slip relationships are drawn.

There is a distinctively different behavior for tests with or without confining reinforcement. Specimens having no confining reinforcement failed by splitting of the concrete at a rather small bond stress $\tau \approx 6.0$ N/mm^2 (870 psi). This value compares favorably with the theoretical one calculated according to Eqn. 4.3 proposed in [19].

$$\tau_{crack} = 1.5 \cdot f_{ct} \cdot \sqrt{c/d_b} \tag{4.3}$$

where

τ_{crack} = bond stress at occurrence of splitting cracks;
c = minimum concrete cover;
f_{ct} = axial tensile strength of concrete.
d_b = diameter of bar.

According to [41] f_{ct} can be taken to about 90% of the splitting tensile strength f_t. With values applicable for the present tests ($f_{ct} = 2.8$ N/mm^2 (406 psi) (see Table 3.3),

$c/d_b = 2.0$), one gets $\tau_{crack} = 5.9$ N/mm^2 (855 psi).

After splitting, the bond resistance dropped rapidly and reached $\tau \approx 1$ N/mm^2 (145 psi) at s = 4 mm (0.16 in.). Without any friction at the bearing plates, the specimens would have fallen apart completely with a consequent dropping of the bond resistance to zero.

Specimens with confined concrete failed by the bars pulling out. Because the splitting crack developed in the plane of the longitudinal axis of the bars, only vertical bars crossing this plane were effective in restraining the concrete, while the influence of stirrups was negligible. This can be seen by comparing results of Series 1.2 with those of Series 1.5.

The influence of the area of vertical bars, $\sum A_{sv}$, was rather small in the varied range of $\sum A_{sv}$. While the initial stiffness of the bond stress-slip curve was almost identical for all test series (Fig. 4.11b), specimens with vertical #2 bars ($d_b = 6.35$ mm) (Series 1.3) had about 10 to 15 percent less bond strength after development of the splitting crack than specimens with #4 ($d_b = 12.7$ mm) (Series 1.2) and #8 ($d_b = 25.4$ mm) (Series 1.1) vertical bars. The bond stress-slip relationships for specimens with #4 ($d_b = 12.7$ mm) and #8 ($d_b = 25.4$ mm) vertical bars were practically identical. This shows that an upper limit for an effective restraining reinforcement exists beyond which the bond behavior cannot be improved further, because the main role of this reinforcement is to prevent opening of splitting cracks. For this reason, all the tests in Series 2 to 7 were carried out with vertical #4 ($d_b = 12.7$ mm) bars.

The bond behavior of specimens with less confining reinforcement than tested will be between those for Series 1.3 and 1.4. This vast region was not explored further, because it was felt that it is not of great practical importance in earthquake resistant design, where large restraining forces could be developed because of the very stringent requirements regarding confinement of concrete. Furthermore, the confinement offered might depend on the location of the vertical bars with respect to the test bar. The influence of this parameter was not studied.

The stress, σ_{sv}, in the vertical reinforcement can be estimated as follows (compare Fig. 2.2):

Splitting force, s', per unit length:

$$s' = \tau \cdot tg\alpha \cdot d_b \tag{4.4}$$

where

$tg\alpha$ = tangent of the angle under which the bond forces spread into the concrete.

For a constant bond stress (as in the present tests), the total splitting force, S, is:

$$S = \tau \cdot tg\alpha \cdot d_b \cdot l_e \tag{4.5}$$

Introducing:

$$S = \sum A_{sv} \cdot \sigma_{sv} \tag{4.6}$$

and

$$\tau = \frac{\sigma_s \cdot A_s}{\pi \cdot d_b \cdot l_e} \tag{4.7}$$

into Eqn. 4.5, and solving for σ_{sv} results in:

$$\sigma_{sv} = \frac{A_s}{\sum A_{sv}} \cdot \frac{tg\alpha}{\pi} \cdot \sigma_s \tag{4.8}$$

where

σ_{sv} = stress in the vertical reinforcement;
σ_s = stress in the tested bar;
A_s = area of tested bar.

The value of $tg\alpha$ is not yet known exactly. According to [19,42], it depends mainly on the slip, s, with respect to $s_{\tau_{max}}$. When reaching $s_{\tau_{max}}$, $tg\alpha$ will be in the order of 1.0 [17,19]. If the latter value is adopted, one gets:

$$\sigma_{sv} \approx 0.3 \cdot \frac{A_s}{\sum A_{sv}} \cdot \sigma_s \tag{4.9}$$

In the tests of Series 1, the test bars were stressed up to $\sigma_s \approx$ 300 N/mm^2 (43500 psi) (Series 1.1 and 1.2) and $\sigma_s \approx$ 250 N/ mm^2 (36250 psi) (Series 1.3), respectively, resulting in a stress in the vertical bars of $\sigma_{sv} \approx$ 90 N/mm^2 (13050 psi) (Series 1.2, #4 bars) and $\sigma_{sv} \approx$ 300 N/mm^2 (43500 psi) (Series 1.3, #2 bars). These stresses being lower than the yield strength of the vertical reinforcement in combination with the good anchorage of these bars

explain the small widths of splitting cracks observed.

Equation 4.9 can also be used to estimate the area of reinforcement required for an effective confinement. This question is discussed in Section 4.5.

4.3.2.3 Bar Diameter. In Fig. 4.12 the results of tests with bars of different diameters are plotted. For comparison the average bond stress-slip curve for all monotonic tests of Series 2 is plotted as well.

The related rib area of the bars used in Series 3 was much larger than those of the bars employed in the other tests ($\alpha_{SR} \approx 0.12$ compared to $\alpha_{SR} \approx 0.066$, see Table 3.4). This resulted in a much stiffer ascending branch of the bond stress-slip relationship because of the larger lug bearing area (reduced pressure) and an increase of bond strength of about 10 percent for #8 (d_b = 25.4 mm) bars. While the peak bond resistance was reached in the tests of Series 3 at a slip of about 0.7 to 0.9 mm (0.028 to 0.035 in.), $s_{\tau_{max}}$ was about 1.5 mm (0.059 in.) in the other tests (Fig. 4.12b). The observed influence of the related rib area on the ascending branch of the local bond law compares favorably with earlier findings [13] (compare Fig. 2.4).

The maximum bond resistance decreased slightly with increasing bar diameter. The relation was 1:0.94:0.85 for #6, #8, and #10 bars ($d_b \approx$ 19, 25, and 32 mm), respectively. If the difference in the values of α_{sR} is taken into account (see Table 3.4), it appears from this limited investigation that τ_{max} decreases by about 5 to 10 percent when using #8 (d_b = 25.4 mm) bars instead of #6 (d_b = 19.0 mm) bars or #10 (d_b = 31.7 mm) bars instead of #8 (d_b = 25.4 mm) bars.

The descending branch of the local bond law leveled off to the frictional resistance at a slip of s $\approx$ 9 to 10 mm (0.35 to 0.39 in.) for #6 (d_b = 19.0 mm) and #10 (d_b = 31.7 mm) bars and a slip s $\approx$ 12 mm (0.47 in.) for #8 (d_b = 25.4 mm) bars. These slip values are again almost identical with the clear distance between lugs.

The frictional bond resistance was not influenced much by the different bar diameter, lug spacings, or values for the related rib area.

4.3.2.4 Concrete Strength. In Fig. 4.13 the results of tests with normal strength (f_c' = 30 N/mm^2 (4350 psi)) and high strength (f_c' = 54.6 N/ mm^2 (7917 psi)) concrete are compared with each other. As can be seen, stiffness of the ascending branch and bond resistance for equal slip values increase with increasing concrete strength. Furthermore, maximum bond resistance is reached at smaller slip values (at approximately 1 mm (0.039 in.) compared to 1.5 mm for normal strength concrete). The latter result agrees with earlier findings [13].

The increase in bond resistance is about 35 percent, which is almost equal to the increase in tensile strength of the high strength concrete compared to the normal strength concrete (see Table 3.3). The measured tensile strengths of these concretes are approximately proportional to $\sqrt{f_c'}$. Therefore, the results of tests with high strength concrete were converted to f_c' = 30 N/mm^2 (4350 psi) by multiplying the bond stresses with the factor $\sqrt{30/f_c'}$. As can be seen, the resultant bond stress-slip curve agrees reasonably well with those of Series 2, with the exception of the initial part of the ascending branch.

4.3.2.5 Bar Spacing. In Fig. 4.14 bond stress-slip relationships for specimens simulating different bar spacings are plotted. The bond behavior improved with increasing bar spacing; however, the influence was relatively small. When increasing the clear bar spacing from the minimum allowable value s = 1 d_b to s = 4 d_b, bond resistance increased by about 20 percent (Fig. 4.15). Further increase of the bar spacing did not effect the bond behavior.

This result can be explained by the fact that in spite of different loads at splitting (compare Eqn. 4.3) the ultimate failure was caused by pulling out, because the growth of splitting cracks was controlled by restraining reinforcement. If less restraining reinforcement is provided so that the ultimate failure will be due to splitting, a more significant influence of bar spacings must be expected.

From the results plotted in Fig. 4.15, it becomes clear that the increase in bar spacing had more influence on the bond resistance of the initial part of the bond stress-slip relationship (τ_{cs} = 0.1mm) than on the maximum bond resistance τ_{max}.

4.3.2.6 Transverse Pressure. Figure 4.16 shows the results of Test Series 6. The specimens were compressed perpendicular to the potential plane of splitting; the pressure applied ranged from p = 0 N/mm^2 (comparison tests) to p = 13.2 N/mm^2 (1914 psi).

As expected, the results of Test Series 6.1 (no transverse pressure) agree well with those of Series 2, within the normal range of scatter. The maximum bond resistance and the ultimate frictional resistance were increased by transverse pressure. The increase amounted to about 25 percent for the maximum pressure applied (Fig. 4.17). The slip at maximum bond resistance shifted to slightly larger values with increasing transverse pressure. The ratio between the added bond resistance and applied pressure decreased significantly with increasing pressure (Fig. 4.18).

4.3.2.7 Rate of Pull-out. The influence of rate of pull-out (or rate of slip) on the local bond law can be seen from Fig. 4.19. While the overall shape of the bond stress-slip relationship was not changed much, bond resistance increased with increasing rate of pull-out. A change of rate of pull-out by a factor of 100 resulted in a change of maximum bond resistance and ultimate frictional bond resistance of about 15 percent (Fig. 4.20). In a semi-logarithmic scale, the test results can be represented by a straight line.

4.3.3 Comparison With Other Results

4.3.3.1 General Behavior. In Fig. 4.21 the results of the present tests with #8 (d_b = 25.4 mm) bars are compared with results given in literature for bars cast in a horizontal position. Figure 4.21a is valid for the initial part of the bond stress-slip relationship. The shaded area represents the range of the bond stress-slip relationship as found by other researchers (compare Fig. 2.5). The results of Test Series 2 (54 tests with #8 (d_b = 25.4 mm) bars) fall into the lower part of that area. The scatter of the measured bond stress-slip curves is considerable. The results of Test Series 3 (4 tests with #8 (d_b = 25.4 mm) bars) fall in the upper part of the shaded area. The bars used in Test Series 3 had higher lugs and a lug bearing area that was about 65% larger than those of the bars employed in Series 2 (see Table 3.4). All other parameters were kept constant. From these data it can be concluded that the large scatter

of the initial bond stiffness found in literature is mainly caused by the inevitable scatter and the use of bars with different rib patterns and/or different bar diameters. Other reasons are the use of different test specimens, difficulties in measuring the slip between steel and concrete when using more sophisticated techniques (measurement of steel and concrete strains) and differences in applied loading and/or slip rates.

Very large displacements may be induced during severe earthquakes. Therefore, bond stress-slip relationships covering the complete range of slip are compared in Fig. 4.21b. Unfortunately, very limited data are available in literature for this range. The curves 1 and 3 were each deduced from strains along the bar and displacements of the bar ends measured in a single pull-out test with an embedment length of 25 d_b [8,22]. In spite of almost identical test conditions and material properties, the deduced local bond laws are rather different. This can partly be attributed to the inevitable scatter of bond tests. However, the main reason can be attributed to the inaccuracies related to deducing the results by this technique. Note that the overall behavior agrees reasonably well with the results reported herein (line 2).

The local bond stress-slip relationship proposed by Martin [13] (line 4) is based on a large number of pull-out tests under load control. The bond law is lower than the one found in the present tests but falls in the observed range of results.

4.3.3.2 Influence of Investigated Parameters.

Restraining Reinforcement: To date the influence of this parameter on the bond behavior was mainly studied in relation to a splitting failure. It was found by previous investigators and substantiated by the present study that a splitting failure can be delayed or avoided altogether by restraining reinforcement. However, no quantitative comparison with the present results is possible because of different test conditions. In previous tests, usually the anchorage lengths of tested bars were large ($>$ 12 to 15 d_b), and concrete cover (bottom and side) was small, resulting in a different type of failure and a much less effective restraining reinforcement than in the experiments reported herein.

The influence of transverse reinforcement on bond strength for a pull-out type of failure has been investigated very little. Usually, it is assumed that once a pull-out failure is reached, either by providing a large concrete area or a sufficiently strong restraining (confining) reinforcement, τ_{max} cannot be increased much further by additional transverse reinforcement. On the contrary, Tassios' proposal [9] results in an increase of τ_{max} of about 5 N/mm^2 (725 psi) or 24 N/mm^2 (3480 psi), respectively, when changing the diameter of the vertical bars in the tests from d_b = 6.35 mm (#2 bars) to d_b = 12.7 mm (#4 bars) or d_b = 25.4 mm (#8 bars), respectively. The present experimental results do not support Tassios' proposal because the bond behavior of specimens with #4 (d_b = 12.7 mm) and #8 (d_b = 25.4 mm) vertical bars as restraining reinforcement was identical and differed only slightly from that of specimens with #2 (d_b = 6.35 mm) bars.

According to ACI 318-77 [43], the basic development length may be reduced by 25% if the anchored bars are enclosed by a spiral reinforcement. This means that 33% higher bond stresses are allowed for bars that are effectively confined by reinforcement compared to bars anchored in unconfined concrete. This increase in bond strength is justified in the case of a splitting failure which will occur when the minimum values for concrete cover and bar spacing allowing by the code are applied.

Bar Diameter: A slight influence of the bar diameter, which was varied between 19 and 32 mm, on the maximum bond resistance was found in the present limited investigation. According to [44], the influence of bar diameter is insignificant in the range d_b = 8 to 32 mm. The latter result is based on an evaluation of the results of a large number of pull-out tests and may be more reliable. According to ACI 318-77 [43], the allowable bond stress varies with $1/d_b$. When the concrete dimensions are assumed as a constant multiple of the bar diameter, this provision is neither supported by the present test results nor by earlier tests [17-19] with bond failures caused by splitting.

Concrete Compressive Strength: While Rehm [10] and Martin [13,44] assume a linear relationship between bond resistance and concrete compressive strength, f_c', other researchers

propose a proportionality between bond resistance and $\sqrt{f_c'}$. The present results confirm the latter assumption. In addition, one has to take into account that $s_{\tau_{max}}$ decreases with increasing concrete strength. ACI 318-77 [43] also assumes τ to vary with $\sqrt{f_c'}$.

Bar Spacing: To date the influence of this parameter on bond behavior has only been studied in connection with splitting failures, where it is of decisive importance. In this respect it is correctly taken into account in ACI 318 [43]. On the contrary, in the present study, bar spacing was of little influence because the growth of splitting cracks was controlled by a very effective restraining reinforcement and bars were pulled out.

Transverse Pressure: In Fig. 4.22 the increase of bond resistance as a function of the transverse pressure used in the tests reported herein is compared with the results of other investigations. The reported increase in bond strength (Fig. 4.22a) for a transverse pressure of 10 N/mm^2 (1450 psi) varies between about 2.5 N/mm^2 and 8.5 N/mm^2 (362 and 1232 psi, respectively). However, when the different test conditions are considered, the differences are reduced.

In the tests of Untrauer/Henry [45] (line 4 in Fig. 4.22a), failure of comparison specimens without normal pressure was caused by splitting of the concrete, and the concrete between lugs was fully intact. On the contrary, specimens compressed by a sufficiently high normal pressure failed by pulling out of the bars, and the concrete between lugs was sheared off. If failure had been caused in all tests by pull-out, the influence of transverse pressure on τ_{max} would have been much smaller than shown in Fig. 4.22a.

In the tests of Viwathanatepe et al [8] and Cowell [22], a transverse pressure of about 10 N/mm^2 (1450 psi) was induced by a bending moment, and the bar was also yielding in compression. Therefore, the observed increase in maximum bond resistance reflects the influence of external pressure and of internal pressure due to expansion of the bar (Poisson's effect). If one estimates that about half of the total increase of τ_{max} was caused by the latter effect, the increase caused by transverse pressure alone compares fairly well with the value measured in the present tests. The increase of τ_{max} observed by Doerr [28] for a pressure of

15 N/mm^2 (2175 psi) seems unrealistically high in comparison to the values measured for a pressure of 5 N/mm^2 and 10 N/mm^2 (125 psi and 1450 psi) and is in contradiction to the general trend found in the other investigations.

The increase of frictional bond resistance caused by transverse pressure found in different experimental investigations scatters considerably (Fig. 4.22b) even if all special circumstances are properly taken into account. The proposal of Tassios [9] is based on theoretical considerations. According to the available experimental results, this proposal significantly overestimates the influence of transverse pressure on the ultimate frictional bond resistance.

Additional tests are necessary in which the influence of external pressure and internal pressure due to Poisson's effect should be investigated separately.

The influence of transverse pressure on the bond behavior is not taken into account in ACI 318-77 [43].

Rate of Slip Increase: Figure 4.23 shows the influence of rate of slip increase on bond resistance. While the present tests were run under deformation (slip) control, the comparable investigations were run under load control. Therefore, an average loading rate for a slip of 0.5 mm (0.02 in.) was taken as relative value. Considering the different test procedures, the results of all investigations agree fairly well. A change of the rate of pull-out by a factor of 100 results in a change of the bond strength of about 15% to 20%.

The influence of the loading rate on the bond behavior is neglected in present codes (e.g. [43]).

4.4 Cyclic Loading

The results of the cyclic loading tests are plotted in Figs. 4.24 to 4.42. In the bond stress-slip diagrams, only a limited number of cycles are drawn for reasons of clarity. In all diagrams, the corresponding bond stress-slip relationship for monotonic loadings are shown, which were obtained from specimens made from the same concrete batch.

While most of the specimens were cycled one or ten times, respectively, at fixed values of

peak slip s_{max} and s_{min}, the specimens of Series 2.19 to 2.22 were first subjected to five cycles at certain values of peak slip (s_{max1}, s_{min1}), then the s_{max} was changed and the specimens were again cycled at (s_{max2}, s_{min2}) and so on. The results of the latter tests are plotted in Fig. 4.39a to Fig. 4.42a for cycles at (s_{max1}, s_{min1}), in Fig. 4.39b to Fig. 4.42b for cycles at (s_{max2}, s_{min2}) and so on.

4.4.1 General Behavior

In general, the behavior during cyclic loading agreed fairly well with the description given in Section 2.1.1. The coefficients of variation for bond resistance during cyclic loading calculated from the results of 2 to 3 repetitive tests are summarized in Table 4.2. These coefficients were calculated for characteristic values of the bond resistance during cyclic loading (τ_{unl} = bond resistance at peak slip s_{max} and τ_f = frictional bond resistance) and of the reduced envelope after cycling (τ_{max} = maximum bond resistance and τ_3 = ultimate frictional bond resistance). They were almost independent of the value s_{max} at which the specimens were cycled and remained practically constant as the number of cycles increased. On the average, they amounted to about 6% for τ_{unl} and to about 10% for τ_f, τ_{max}, and τ_3. A somewhat larger scatter has to be expected if specimens for repetitive tests are cast from different concrete batches.

A comparison of results of Test Series 2 (Figs. 4.24-4.42) leads to the following general observations.

i) If the peak bond stress during cycling did not exceed 70-80% of the monotonic bond strength τ_{max}, the ensuing bond stress-slip relationship at first loading in the reverse direction and at slip values larger than the one at which the specimen was cycled was not significantly affected by up to 10 repeated cycles (see Figs. 4.24, 4.25, 4.33, 4.39a, and 4.42a). The bond resistance at peak slip deteriorated moderately with increasing number of cycles. These results agree well with earlier findings [12,31,33,34]. An explanation for this behavior is given in Section 2.1.3.

(b) When the bar was loaded monotonically to an arbitrary slip value and then cycled up to 10 times between this slip value and a slip value corresponding to a load equal to approximately zero, the monotonic envelope was, for all practical purposes, reached again (Figs. 4.37 and 4.38). From then on the behavior was the same as that obtained in a monotonic test. This agrees well with earlier results [10,12,31]. The reasons for this behavior are that during unloading the small fraction of the total slip that is caused by elastic deformation of the concrete is recovered and the concrete is not much more damaged by a limited number of reloadings.

(c) Loading to slip values inducing a τ larger than 80% of the monotonically obtained τ_{max} in either direction led to a degradation in the bond stress-slip behavior in the reverse direction (Figs. 4.26-4.32). The bond stress-slip relationship at slip values larger than the peak value during previous cycles was significantly different from the virgin monotonic envelope. There always was a significant deterioration of the bond resistance which increased with increasing peak slip s_{max} (Figs. 4.26-4.32), increasing numbers of cycles (Figs. 4.26-4.30), and was larger for full reversals of slip than for half cycles (compare Figs. 4.27a with Fig. 4.34, Fig. 4.29 with Fig. 4.35, and Fig. 4.37 with Fig. 4.36).

Furthermore, the cycles produced a pronounced deterioration of the bond stiffness and bond resistance at slip values smaller than or equal to the peak slip value. These results agree qualitatively with those reported in [8,22]. However, a quantitative comparison is not possible because of different test conditions.

The observed behavior can be explained by assuming that in a well-confined concrete the maximum bond resistance is controlled by local crushing and the initiation of a shear failure in a part of the concrete between the lugs of the bar. The larger the value of slip with respect to $s_{\tau max}$ (i.e. slip at τ_{max}), the larger is the area of concrete between the lugs affected by the crushing and shear failure and the smaller is the bond resistance. If the bar is cycled between constant peak values of s_{max} and s_{min}, the main damage is done in the first cycle. During successive cycles, the concrete at the cylindrical surface, where

failure occurred, is mainly ground off, decreasing its interlocking and frictional resistance. A more detailed explanation will be given in Section 5.2.2.

(d) The frictional bond resistance, τ_f, during cycling was dependent upon the value of the peak slip s_{max} and the number of cycles (see Figs. 4.24-4.32). With repeated cycles, τ_f deteriorated rapidly.

(e) Cycling a specimen at different increasing slip values had a cumulative effect on the deterioration of bond stiffness and bond resistance (compare Figs. 4.39c, 4.40d, and 4.41e with Fig. 4.29). On the other hand, some additional cycles between smaller slip values than the peak value in the previous cycle did not much influence the bond behavior at the larger peak value (compare Fig. 4.41b with Fig. 4.41c).

In the following, the influence of cyclic loading on the different branches of the bond stress-slip relationship as defined in Section 2.1.1 will be discussed in detail.

4.4.2 Unloading Branch

The bond stress-slip relationship for unloading is slightly nonlinear with the flattest slope near zero load (see Fig. 4.24). However, it seems reasonable to linearize the actual behavior. The average slope between the point from which unloading started and the point with zero bond stress is plotted in Fig. 4.43 as a function of the number of unloadings. The slope at first unloading was practically independent of the peak slip value s_{max} and, on the average, amounted to about 200 N/mm^3 (737 kips/in^3) for a concrete with $f_c' = 30$ N/mm^2 (4350 psi). It was approximately equal to the average slope of the monotonic envelope for very small slip values ($\leqslant$ 0.01 mm (0.0004 in.)). During 20 consecutive unloadings, the slope decreased by about 30%. The scatter of the test results was considerable.

For comparison, the average slope of the unloading branch for the tests with high strength concrete ($f_c' = 55$ N/mm^2 (7975 psi)) is plotted as well. On the average, the slope was about 50% larger than that for a medium strength concrete ($f_c' = 30$ N/mm^2 (4350 psi)).

The average slopes of the unloading branch measured in the present tests compare favor-

ably with the values given in [9]. According to [12], the unloading branch is stiffer than found here, which can be explained by the fact that in [12] the bar was pulled out against the setting direction of the concrete.

4.4.3 Frictional Branch

In Fig. 4.44 the frictional bond resistance, τ_f, is plotted as a function of the peak slip value, s_{max}, at which the specimens were cycled. The number of cycles is chosen as a parameter. In the first cycle, τ_f was strongly dependent upon s_{max} and reached its peak value of about 2.9 N/mm^2 (420 psi) at $s_{max} \approx$ 4 to 10 mm (0.16 to 0.4 in.). τ_f was reduced to about 0.2 N/mm^2 to 0.5 N/mm^2 (29 psi to 72.5 psi) by 10 load cycles, the largest deterioration occurring in the first cycle. The rate of decrease of τ_f was larger for larger values of s_{max}. Therefore, after 10 cycles the influence of s_{max} on τ_f was rather small. No clear influence of the slip difference $\Delta s = s_{max} - s_{min}$ ($\Delta s = s_{max}$ for half cycles and $\Delta s = 2s_{max}$ for full cycles) on the deterioration of the frictional bond resistance could be detected.

Figure 4.45 shows the relation between the frictional bond resistance during cycling, τ_f, and the bond stress τ_{unl} at peak slip s_{max} from which unloading started. While this relation was clearly dependent on the peak slip value, s_{max}, it was almost independent of the number of cycles. This observation means that τ_f deteriorated almost at the same rate as the bond resistance at peak slip, τ_{unl}.

According to [9] and [12], the frictional bond resistance amounts to 0.25 or 0.18 times the bond resistance at peak slip, τ_{unl}, respectively. As can be seen from Fig. 4.45, these assumptions are very crude approximations because the relation τ_f/τ_{unl} varies approximately from 0.05 for $s_{max} \approx 0$ mm to 0.4 for $s_{max} \geqslant 9$ mm (0.35 in.). In [8] a constant value $\tau_f \approx$ 0.4 N/mm^2 (58 psi) is assumed, which is rather small and only valid after several load cycles (see Fig. 4.44). In [22] a frictional bond resistance $\tau_f \approx$ 1 N/mm^2 to 3.5 N/ mm^2 (145 psi to 507 psi) was found, which compares favorably with the present tests.

4.4.4 Reloading Branch

When reloading the specimen after a cycle between slip values s_{max} and s_{min} with $|s_{min}| = s_{max}$ for full cycles and $s_{min} = 0$ for half cycles, the bond resistance increased well before reaching s_{max} (Figs. 4.24-4.36). On the average, τ started to increase significantly at a slip value equal to about 45% of s_{max}. While the value was not much influenced by any of the investigated parameters, its scatter was rather large.

On reloading, the bond resistance at peak slip, τ_{unl}, never reached its initial value at first loading (N=1). This can be seen from Fig. 4.46, which shows the bond ratio τ_{unl} (N)/τ_{unl} (N=1) as a function of the number of cycles, N, for different values of the peak slip, s_{max}, at which the specimen was cycled. In Fig. 4.46a the results of tests with full reversals of slip and in Fig. 4.46b the corresponding results for tests with half cycles are plotted. After one cycle, the bond resistance at peak slip, τ_{unl}, was reduced to about 25% to 85% of its original value, depending on the specific conditions. After 10 cycles, these values were down to 7% and 60%. The major part of the total deterioration observed after 10 cycles was produced in the first cycle. Under comparable conditions (s_{max} = const. N = const.), τ_{unl} was significantly more deteriorated for cycles between full reversals of slip than for half cycles (compare Fig. 4.46a with Fig. 4.46b).

The bond deterioration ratios shown in Fig. 4.46a are plotted in Fig. 4.47 in a double logarithmic scale. As can be seen, only the results for cycles between rather small slip values can be approximated by a straight line. On the other hand, the ratios for cycles with s_{max} near or beyond $s_{\tau max}$ (slip value at the monotonic τ_{max}) can only be approximated by two straight lines with a breaking point at about cycle 2. It is well known that the results of creep tests on concrete under cyclic compression, plotted in a double logarithmic scale, can be approximated by a straight line [47]. The same is true for relaxation tests on concrete under cyclic compression. Therefore, if the bond resistance deterioration would only be caused by a process similar to relaxation of concrete, the test results would follow a straight line when plotted in a double logarithmic scale. Following this argument, it can be concluded that the deterioration of bond

resistance was caused by a process similar to relaxation when the specimens were cycled between small peak slip values ($<\approx$ 0.4 mm (0.016 in.)). On the other hand, the bond resistance deterioration during the first cycle between larger peak slip values was caused by damaging the concrete between lugs (local crushing and initiation of shear cracks), while in subsequent cycles it was caused by gradual grinding off of the concrete at the cylindrical surface where shear failure and local crushing occurred.

Figure 4.48 shows the bond deterioration ratio at peak slip s_{max} for tests with full reversal of slip (full cycles) and for half cycles ($s_{min} = 0$) as a function of s_{max}. The influence of s_{max} on the bond deterioration ratio is pronounced. While for small values of s_{max} half and full cycles reduced the bond resistance at peak slip almost by the same amount, the bond resistance was significantly more deteriorated by full cycles than by half cycles when the peak slip values increased. The differences become much smaller if the test results for half cycles are plotted at $s_{max}/2$. That means that cycles between $s = \pm s_{max}/2$ caused as much damage in the bond resistance at peak slip as an equal number of cycles between $s = 0$ and $s = s_{max}$, provided s_{max} was larger than about 0.4 mm.

The bond deterioration ratios found for cycles between small peak values of slip ($\leqslant$ 0.5 mm) agree fairly well with those reported in [12]. A comparison for larger slip values is not possible because of lack of comparable results in literature.

4.4.5 Reduced Envelope

In Fig. 4.49, reloading curves for similar specimens subjected to different loading histories are plotted. The lines denoted by "a" represent the behavior of specimens cycled once or ten times, respectively, between the peak slip values corresponding to point "a". It can be seen by comparing the lines denoted by the letters "a" to "e" with the monotonic loading curve that cycling between sufficiently large slip values reduced the maximum bond resistance τ_{max} as well as the frictional bond resistance τ_3. In order to get a proper estimate of the bond deterioration rate, the test results were idealized as shown in Fig. 4.50 and then the reductions of τ_1 (approximately equal to bond strength τ_{max}) and τ_3 (frictional bond resistance) were calculated. The

results are plotted in Figs. 4.51 and 4.52 as a function of the peak slip value s_{max} during cycling.

According to these graphs, the monotonic envelope was reached again after up to 10 cycles between rather small slip values in the order of $s_{max} < 0.4$ mm (0.016 in.). With increasing values of s_{max} and increasing numbers of cycles, the envelope was increasingly deteriorated. The main reduction was caused by the first cycle. Frictional bond resistance deteriorated less than bond strength.

Figure 4.52 shows that one-sided cycles with $s_{max} \geq 0.5$ mm (0.02 in.) generally produced less deterioration of the envelope than an equal number of cycles with full reversals of slip. The test results of these cycles fit fairly well the lines valid for full cycles if they were plotted at $s_{max}/2$. This means that cycles between s=0 and s=s_{max} produced about the same deterioration of the monotonic envelope than an equal number of cycles between $s = \pm s_{max}/2$, provided s_{max} was larger than about 0.4 mm (0.016 in.).

The present test results agree qualitatively with those published in [8,22]. However, a quantitative comparison is not possible because of completely different test conditions. Roughly speaking, the deterioration of the envelope found in [8] and [22] seems to be smaller or larger, respectively, than observed in the present investigation.

4.4.6 Influencing Parameters

While in Sections 4.4.1 to 4.4.5 the results of cyclic tests of Series 2 were discussed, in this section the results of the cyclic tests done in Series 1 and Series 3 to 7 will be discussed. In these tests the specimens were cycled at a peak slip value $s_{max} = 1.65$ mm (0.065 in.), which almost coincided with the value of slip at the maximum bond resistance under monotonic loading. The influence of the following parameters on the bond behavior under cyclic loading was studied.

- Diameter of vertical bars of transverse reinforcement ($d_b = 6.4$ mm (#2 bar)), Series 1.6 and 1.7.
- Direction of loading. First loading in compression (Series 2.6*) as compared to loading in

tension (Series 2.6).

- Diameter of test bar (d_b = 19 mm to 32 mm (#6 bars to #10 bars)), Series 3.4 to 3.6.
- Concrete strength (f_c' = 54.6 N/mm^2 (7917 psi)), Series 4.2 and 4.3.
- Clear spacing of bars (1 d_b to 6 d_b), Series 5.4 to 5.6.
- Transverse pressure p (5 N/mm^2 (725 psi) and 10 N/mm^2 (1450 psi)), Series 6.5 and 6.6.
- Rate of slip increase ($\dot{s}$ = 170 mm/sec. (6.7 in./sec.)), Series 7.3.

The results of these tests are plotted in Figs. 4.27b and 4.53 to 4.65. The results of the comparable "standard" tests (Series 2.6 (full cycles) and Series 2.13 (one-sided cycles)) are shown in Figs. 4.27a and 4.34, respectively. The influence of a certain investigated parameter on the cyclic bond behavior can be studied by comparing Figs. 4.54 and 4.59 with Fig. 4.34 and Figs. 4.53, 4.55 to 4.58 and 4.60 to 4.65 with Fig. 4.27a. It can be seen that the overall cyclic bond behavior was not much influenced by the above mentioned investigated parameters.

A more detailed elaboration is given by Figs. 4.66 and 4.67. In Fig. 4.66 the deterioration of the bond resistance measured in Test Series 2.6 (Standard Test) is compared with those observed in Series 1.6, 2.6*, 4.2, 5.4 to 5.6, 6.5, 6.6 and 7.3 (Specific Test). A comparison of the deterioration behavior of Test Series 2.13 with those of Test Series 1.7 and 4.3 is also included in the figure. In Fig. 4.67 a similar comparison is done for Series 3.4 to 3.6 (influence of bar diameter). The following values were chosen to characterize the deterioration of the bond resistance during cyclic loading.

(a) Relation of bond resistance at peak slip, τ_{unl}, after cycling to the corresponding bond resistance for monotonic loading.

(b) Relation between frictional bond resistance, τ_f, during cycling and the bond resistance at peak slip, τ_{unl}.

(c) Relation between τ_1 (approximately equal to maximum bond resistance) and τ_3 (ultimate frictional bond resistance) of the reduced envelope to the corresponding values of the monotonic envelope.

In (a) and (b) above the defined relationships were calculated for Cycles 1 to 10 and then averaged. The relationship (c) was evaluated as average value for the first slip reversal at τ_1 (for cycles between s = ± 1.65 mm (0.065 in.)) and after 10 cycles at τ_1 and τ_3.

In Figs. 4.66 and 4.67 values greater than unity for the ratio bond deterioration standard test (Series 2.6 or 2.13, respectively) to bond deterioration specific test (e.g. Series 1.6) means that in the standard test τ_{unl} as well as τ_1 and τ_3 of the envelope were reduced less by the load cycles and the relation τ_f/τ_{unl} was lower than in the specific test. The dashed lines represent the acceptable scatter that can be expected for identical test specimens but made from different concrete batches. The investigated parameters significantly influence the cyclic bond behavior only if the calculated ratios fall outside the range given by the dashed lines.

According to Fig. 4.66, the cyclic bond behavior was approximately the same when the test bars were first loaded in tension (Series 2.6) or compression (Series 2.6*). This behavior was expected because of the similarity of the monotonic envelopes. Substituting #2 bars (d_b = 6.35 mm) (Series 1.6 and 1.7) for #4 bars (d_b = 12.7 mm) as transverse (restraining) reinforcement had no significant effect on the cyclic bond behavior. This is also true for specimens made out of high strength concrete (Series 4.2 and 4.3) instead of medium strength concrete. While the cyclic bond behavior of specimens simulating a clear bar spacing of 1 d_b and 6 d_b (Series 5.4 and 5.6) was not much different from those of the specimen with a clear spacing of 4 d_b (Series 2.6), the specimens with a clear spacing of 2 d_b (Series 5.5) experienced more bond deterioration than the specimens of Series 2.6. This result can be attributed to excessive scatter because it does not fit in the general trend and cannot be rationalized. Transverse pressure in the investigated range (5 N/mm^2 and 10 N/mm^2 (725 psi and 1450 psi)) (Series 6.5 and 6.6) and a 100 times faster loading rate (Series 7.3) did not change the cyclic bond behavior very much.

On the contrary, the specimens of Series 3 experienced significantly more bond deterioration than the specimens of Series 2.6 (left part of Fig. 4.67). The specimens of Series 3 and of Series 2.6 were cycled at the same peak slip value s_{max} = 1.65 mm (0.065 in.). The bars used

in Series 3 had a much larger related rib area than the standard bars used in Series 2.6 (see Table 3.4). This resulted in a steeper ascending branch of the bond stress-slip relationship. The maximum bond resistance was reached at a slip value of $s_{\tau_{max}}$ of about 0.7 mm to 0.9 mm (0.028 in. to 0.035 in.) (Fig. 4.12) compared to about 1.6 mm (0.062 in.) in Series 2.6 (Fig. 4.27a). Therefore, the specimens of Series 3 were cycled at about 2 times the slip value $s_{\tau_{max}}$, while the specimens of Series 2.6 were cycled approximately at $s_{\tau_{max}}$. If the results of Series 3 are compared with those of the test specimens of Series 2.7 which were cycled at $s_{max} \approx 1.6$ $s_{\tau_{max}}$, the influence of the bar diameter and the deformation pattern on the cyclic bond behavior is not significant (see right part of Fig. 4.67).

Note that specimens with the small bar (#6, d_b = 19 mm) developed a somewhat larger maximum bond resistance than those with larger bars during monotonic loading (Fig. 4.12) but experienced more bond deterioration during cyclic loading (Fig. 4.67). Therefore, the bond resistance was almost independent of the bar size after some load cycles (see Figs. 4.55-4.57).

The results of Test Series 3 indicate that the bond deterioration during cycling does not only depend on the absolute value of the peak slip, as shown in Figs. 4.48 and 4.52, but on its relation to characteristic slip values ($s_{\tau_{max}}$ or s_3) of the monotonic envelope. However, more tests with bars of different diameters and deformation patterns are needed to deduce more clearly bond deterioration as a function of either the ratio $s_{max}/s_{\tau_{max}}$ or s_{max}/s_3.

Summarizing, it can be stated that the behavior of bond during cyclic loading is not significantly affected by the various parameters investigated if the deterioration of bond resistance is related to the pertinent monotonic envelope. However, the influence of bar diameter and deformation pattern on the cyclic bond behavior should be studied more thoroughly in the future.

4.5 Required Restraining Reinforcement

Equation 4.9 can be used to estimate the required area of reinforcement to effectively restrain concrete in the joint so that a pull-out failure and not a splitting bond failure will occur.

Let us first consider an interior joint with one beam passing through it. In the extreme case, approximately equal forces of same sense are acting on each side of the anchored beam bars. The worst bond conditions are found at the tension side of the beam bars because the vertical column bars there are also in tension. At the compressed bar end, sufficient confinement is provided by compressed column bars and by compression column forces acting on the joint. Therefore, the required area of restraining reinforcement needs to be calculated for one side of the beam only, but this reinforcement must be provided at both sides of the joint because the external excitation might change the direction of loading. Furthermore, in each layer several beam bars are passing through the joint, in which case the splitting forces of all bars in one layer must be added. Solving Eqn. 4.9 for $\sum A_{sv}$ one obtains:

$$\sum A_{sv} = 0.3 \cdot n \cdot A_s \frac{\sigma_s}{\sigma_{sv}} \tag{4.10}$$

where

$\sum A_{sv}$ = required area of reinforcement for restraining the concrete at one column side;

n = number of beam bars in one layer passing through the joint;

A_s = area of one beam bar in a layer, for bars with different bar diameters the average area may be taken;

σ_s = stress in beam bar at the column face;

σ_{sv} = allowable stress in the vertical column reinforcement.

The allowable stress σ_{sv} is not well known yet. In tests with sufficient restraining reinforcement, it reached about 300 N/mm^2 (43.5 ksi). However, it should be noted that restraining vertical bars were well anchored and were placed close to the test bar. Bars less well anchored, or in a larger distance from the origin of splitting forces, will offer less restraint at equal steel stresses. Therefore, it is proposed that σ_{sv} should neither exceed the yield stress nor a value of 300 N/mm^2 (43.5 ksi).

Often at interior joints, beams from four directions are joining together. In this case, the restraining reinforcement according to Eqn. 4.10 must be provided in the joint at each side of

the column. Eqn. 4.10 is also valid for external joints, where it gives the area of the restraining reinforcement at that side of the column that faces the beam. Preferably, stirrups enclosing the top and bottom layers of beam bars should be used as restraining reinforcement. The column reinforcement can also be used as restraining reinforcement if it can take up the additional splitting forces without exceeding the yield stress. However, in the latter case, one should use a larger number of small diameter column bars instead of a small number of large diameter bars to ensure a good anchorage of the bars.

It should be noted that the above proposal for the area of restraining reinforcement in the joint (Eqn. 4.10) is based on the following assumptions:

-Ratio between bond forces and splitting forces, as explained in Section 4.3.2.2, has been set equal to unity.

-Allowable steel stress for restraining reinforcement ($\sigma_{sv} \leqslant$ 300 N/mm^2 (43.5 ksi) and $\leqslant f_y$ has been proposed).

-Superposition of splitting forces and forces caused by external excitations (under the combined actions, σ_{sv} may not exceed f_y).

The validity of the above assumptions should be checked by additional experimental and theoretical studies.

V. ANALYTICAL MODEL OF LOCAL BOND STRESS-SLIP RELATIONSHIP

5.1 General

The fixed end rotation of an interior or exterior joint can be an important source of stiffness degradation in the lateral load-deformation relationship of moment-resisting frames. This fixed-end rotation must either be minimized by a sufficient anchorage of the beam bar or its effect must be considered in the design and, therefore, it should be included in the analysis of building response to obtain realistic behavior of a frame under severe cyclic loadings.

The fixed-end rotations of beams can be calculated when the the slip of the beam top and bottom bars with respect to the column faces are known. This slip can analytically be predicted if the following items are available:

(a) Analytical procedure to solve the differential equation of bond.

(b) Analytical model for local bond stress-slip relationship.

(c) Analytical model for the stress-strain relationship of bars.

In this report, only point (b) will be described. Points (a) and (c) will be described in detail in a companion report [49].

5.2 Theory of Bond Resistance Mechanism

A theory of bond resistance mechanism for monotonic and cyclic loading will be presented because it can form a rational basis for developing hysteretic rules for bond behavior under generalized loading. Furthermore, it helps to understand the results of the present tests (Chapter 4) more clearly. The theory is valid for well-confined concrete, where the propagation and particularly the width of possible splitting cracks are kept small so that the ultimate failure is caused by bar pull-out. A theory of bond resistance mechanism for unconfined concrete near the bar end loaded in tension, where failure is caused by breakout of a concrete cone, has been presented in [8].

5.2.1 Monotonic Loading

Inclined cracks initiate at relatively low bond stresses at the point of contact between steel and concrete [14] as shown in Fig. 2.2 and Fig. 5.1a. The length and width of these cracks are arrested by the restraint offered by secondary reinforcement (indicated in Fig. 5.1 by normal stresses at the top of the element). With increasing induced slip, the concrete in front of the lugs will be crushed. The bond forces which transfer the steel force into the concrete are inclined with respect to the longitudinal bar axis; at this relatively low loading stage the angle is relatively small ($\approx$ 30 degrees [13,19,39]). Under otherwise constant conditions, the slope of the initial part of the bond stress-slip curve depends on the lug bearing area α_{sR} (Eqn. 2.1).

Increasing the stress in the bar further more slip occurs because more local crushing takes place and later shear cracks (see Fig. 2.3) in the concrete keys between lugs are initiated. According to Rehm [10], this happens when the slope of the bond stress-slip curve decreases rapidly (approximately at Point B in the diagram of Fig. 5.1b). At maximum bond resistance (Point C), a part of, or the total, concrete key between the lugs has been sheared off, depending on the ratio of clear lug distance, c_1, to average lug height, a. For normal ratios ($c_1/a > 6$), only a part of the key will be sheared off (see Fig. 2.3). The length of the shear crack is given by Rehm [10] as 6 times the lug height and by Lutz/Gergely [17] as 2 to 3 times the lug height. Therefore, an average value of approximately 4 times the lug height is assumed as shear crack length. At this loading stage, the bond forces will spread into the concrete under an increased angle of about 45 degrees, because of the wedging action of sheared off concrete.

The bars used in the main tests had a ratio clear lug spacing to lug height of about 9 and the maximum bond resistance was reached at a slip $s_{\tau max}$ equal to about 1.2 times the lug height. Therefore, it is estimated that about 50% of the key's length was sheared off when the maximum resistance was reached (Fig. 5.1b).

When more slip is induced, an increasingly larger part of the concrete is sheared off without much drop in bond resistance. In the reported tests, the resistance at a slip equal to approximately 3 times the value $s_{\tau max}$ was about 85% of the maximum bond resistance. The

shear cracks might have reached the base of the concrete key at the adjacent lug at a slip of about 0.5 times the clear lug distance (Point D in the diagram of Fig. 5.1c). Increasingly less force is needed to shear off the remaining bits of the concrete keys and to smooth out the surface of the shear crack. When the slip is equal to the clear lug distance, that means the lugs have traveled into the position of the neighboring rib before loading (Point E) only frictional resistance is left, which will be practically independent of the deformation pattern or the related rib area. Because of the shear cracks, it is likely that inclined bond cracks will not grow much wider than those that developed at Point C and that new inclined cracks might develop (shown by dashed lines in Fig. 5.1c) due to the still high compression forces on the concrete in front of the lugs.

It should be noted that the gradual shearing off of the concrete keys is only possible in well restrained (confined) concrete. If the confinement offered by transverse reinforcement cannot prevent the excessive growth of eventually developing splitting cracks, the bars will be pulled-out before the concrete keys will be totally or partially sheared off.

With the exception of Series 3, all reported experiments were carried out with bars with an almost identical rib pattern. The frictional bond resistance was always reached at a slip value of about 11 mm to 12 mm (0.43 in. to 0.47 in.), which is a little more than the clear distance between lugs measured at their midheight of approximately 10.5 mm (0.41 in.). This supports the proposed theory. The bars used in Series 3 had a much larger related rib area (bearing area), which explains the steeper ascending branch and the smaller value of the slip at maximum bond resistance, $s_{\tau_{max}}$, compared to the tests of Series 2. In spite of that, in the tests of Series 3.2 with #8 bars ($d_b \approx$ 25 mm), which had almost the same clear lug distance than the #8 bars used in the tests of Series 2, the frictional bond resistance was also reached at a slip value of approximately 12 mm (0.47 in.) (Fig. 4.12a). On the contrary, the clear lug distance of the #6 bars (d_b = 19 mm) and #10 bars (d_b = 31.7 mm) used in Test Series 3.1 and 3.3 was only about 7 and 8.5 mm, respectively. In these tests the descending branch of the bond stress-slip curve leveled off at a slip of about 8 to 9 mm (Fig. 4.12a). The ultimate frictional

bond resistance in the tests of Series 2 and 3 was almost the same, which shows that it was not influenced much by different values of the related rib area. These observations are in accordance with the proposed theory.

5.2.2 Cyclic Loading

In Fig. 5.2a it is assumed that the slip is reversed before shear cracks develop in the concrete keys. For the loading cycle OA, the response is exactly the same as described in Section 5.2.1. After unloading (path AF), a gap remains open with a width equal to the slip at point F between the left side of the lug and the surrounding concrete (compare Fig. 5.1a), because only the small fraction of slip that is caused by elastic concrete deformations is recovered during unloading.

As soon as additional slip in the reverse direction is imposed, some frictional resistance is built up. This resistance is rather small because the surface of the concrete surrounding the bar is relatively smooth. At H the lug is again in contact with the concrete, but a gap has opened at the lug's right side. Due to the concrete blocking any further movement of the bar lug, a sharp rise in stiffness of the hysteretic curve (path HI) occurs. The increase in resistance might as well start a little before H due to the load transfer by some pieces of broken concrete that might have been produced during loading from O to A. With increasing load, the old cracks close, allowing the transfer of compressive stresses across the crack with no noticeable reduction in stiffness. Inclined cracks perpendicular to the old cracks will open if the negative bond stress continues to rise and the old and new cracks may even join. However, since the concrete is well confined, the broken pieces of concrete cannot move. Therefore, the bond stress-slip relationship for loading in the opposite direction follows very closely the monotonic envelope. At I a gap with a width equal to s_{FI}, that is the difference between slip of points F and I has opened (Fig. 5.2a). When again reversing the slip at I, the bond mechanism for the loading path IKL is similar to that of path AFH described earlier. However, the bond resistance starts only to increase again at L, when the lug starts to press broken pieces of concrete against the previous bearing face. With further movement, stresses are built up to close the crack previ-

ously opened and open those previously closed. At M lug and concrete are fully in contact again. If more slip in the same direction is imposed, the monotonic envelope is reached again and followed thereafter for the same reasons as given for path HI.

A different behavior is followed if the slip is reversed after the initiation of shear cracks in the concrete keys (path OABC in diagram of Fig. 5.2b). Therefore, the bond resistance is reduced compared to the monotonic envelope. When loading in the reverse direction (path CFGHI), the lug presses against a key whose resistance is lowered by shear cracks over a part of its length induced by the first half cycle. Furthermore, the old relatively wide inclined cracks will probably close at higher loads than in the cycle considered in Fig. 5.2a, thus complicating the transfer of inclined bond forces into the surrounding concrete. Therefore, shear cracks in the hitherto undamaged side of the concrete key might be initiated at lower loads and might join the old shear cracks (Fig. 5.2b). Therefore, the bond resistance is reduced compared to the monotonic envelope. When reversing the slip again (path IKLMN), only the remaining intact parts of the concrete between lugs must be sheared off, resulting in an even lower maximum resistance than at point I.

In the next example it is assumed that a large slip is imposed during the first half cycle (path OABCD in diagram of Fig. 5.2c), resulting in the shearing off of almost the total concrete key (compare Fig. 5.1c). When moving the bar back, a higher frictional resistance must be overcome than in the cases described previously because the concrete surface is rough along the entire width of the lugs. At H the lugs are again in contact with the remaining "intact" part of the keys (Fig. 5.2c) which do not offer much resistance. Therefore, the maximum resistance during the second half cycle is almost the same as the ultimate frictional resistance during monotonic loading. During reloading (path JKLMNO), an even lower resistance is offered because the concrete at the cylindrical surface where shear failure occurred has been smoothed already during the first cycle.

From the above considerations it follows that if the bar is cycled between constant peak values of s_{max} and s_{min}, the main damage is done during the first cycle. During successive

cycles, the concrete at the cylindrical surface were shear failure occurred is mainly ground off, decreasing its interlocking and frictional resistance. This explains the observed decrease in maximum resistance during reloading (path LMN in Figs. 5.2b and 5.2c) with increasing number of cycles (see Figs. 4.46 to 4.48 and Fig. 4.51).

According to the above theory, under otherwise constant conditions, bars with smaller ratios clear lug spacing, c_1, to lug height, a, will produce more bond deterioration than bars with larger ratios c_1/a when cycled between the same values of peak slip, s_{max} and s_{min}. This is shown by the results of Series 3 in comparison to those of Series 2 (see Fig. 4.67). However, additional tests are needed for further proof and quantification of the influence of deformation pattern on cyclic behavior of bond.

5.3 Analytical Model for Confined Concrete

The assumed bond model which was first presented in [48] is illustrated in Fig. 5.3. Although it simplifies the real behavior, it takes into account the significant parameters that appear to control the behavior observed in the experiments. This model, in spite of being simpler than the ones proposed hitherto (see Section 2.2), is believed to be more general because it can be easily applied to any bond condition. The model's main characteristics, illustrated by following a typical cycle (Fig. 5.3b), are described below.

When loading the first time, the assumed bond stress-slip relationship follows a curve valid for monotonically increasing slip, which is called herein "monotonic envelope" (paths $OABCD$ or $OA_1B_1C_1D_1$). Imposing a slip reversal at an arbitrary slip value, a stiff "unloading branch" is followed up to the point where the frictional bond resistance τ_f if reached (path EFG). Further slippage in the negative direction takes place without an increase in τ up to the intersection of the "friction branch" with the curve OA'_1 (path GHI). If more slip in the negative direction is imposed, a bond stress-slip relationship similar to the virgin monotonic curve is followed, but with values of τ reduced as illustrated by paths IA'_1J. This curve ($O\ A'_1\ B'_1\ C'_1\ D'_1$) is called the "reduced envelope". When reversing the slip again at J, first the unloading branch and then the frictional branch with $\tau = \tau_f^+$ are followed up to point N,

which lies on the unloading branch EFG (path JLN). At N the "reloading branch" (same stiffness as the unloading branch) is followed up to the intersection with the reduced envelope $O\,A'B'C'D'$ (path NE'), which is followed thereafter (path $E'B'S$). If instead of increasing the slip beyond point N, more cycles between the slip values corresponding to points N and K are imposed, the bond stress-slip relationship is like that of a rigid plastic model, the only difference being that frictional bond resistance decreases with increasing number of cycles. A similar behavior as described is followed if the slip is reversed again at point S (path STU) or negative slip values are imposed first. To complete the illustration of the model, details for the different branches referred to in the above overall description

(illustrated in Fig. 5.3a) are given in the following section. The given numerical values for the different parameters are deduced from the results of Test Series 2. The influence of bond conditions different from those in Test Series 2 on these parameters will be discussed in Section 5.3.5.

5.3.1 Monotonic Envelope

The simplified monotonic envelope simulates the experimentally obtained curve under monotonically increasing slip. It consists of an initial nonlinear relationship $\tau = \tau_1 \, (s/s_1)^\alpha$ valid for $s \leqslant s_1$, followed by a plateau $\tau = \tau_1$ for $s_1 \leqslant s \leqslant s_2$ (Fig. 5.3b). For $s \geqslant s_2$, τ decreases linearly to the value of the ultimate frictional bond resistance τ_3 at a slip value of s_3. This value s_3 is assumed to be equal to the clear distance between the lugs of the deformed bars. The reason for this assumption is given in Section 5.2. The same bond stress-slip relationship is assumed regardless of whether the bar is pulled or pushed.

With the values:

$s_1 = 1.0$ mm
$s_2 = 3.0$ mm
$s_3 = 10.5$ mm
$\tau_1 = 13.5$ N/mm^2
$\tau_3 = 5.0$ N/mm^2
$\alpha = 0.40$

the analytically obtained bond stress-slip relationship agrees well with the average curve obtained in Test Series 2 (Fig. 5.4). However, it must be observed that bond between deformed bars and concrete inevitably scatters (see Fig. 4.9). Therefore, the values for τ_1, τ_3, and α may vary between $\tau_1 \approx$ 15.5 N/mm^2, $\tau_3 \approx$ 6 N/mm^2, $\alpha \approx 0.33$, and $\tau_1 \approx$ 11.5 N/mm^2, $\tau_3 \approx$ 4.2 ˆ N/mm^2, $\alpha \approx 0.45$. Furthermore, the values of s_1 and s_2 might scatter as well.

5.3.2 Reduced Envelopes

Reduced envelopes are obtained from the monotonic envelopes by reducing the characteristic bond stresses τ_1 and τ_3 through reduction factors, which are formulated as a function of one parameter, called the "damage factor", d. For no damage, d=0, the reloading branch reaches the monotonic envelope. For full damage, d=1, bond is completely destroyed (τ=0).

The rationale for this assumption is given by Fig. 4.49, which shows that reloading curves for similar specimens subjected to different loading histories appear to form a parametric family of curves and that almost the same reduced envelope is followed after a small number of cycles between large peak slip values or after a larger number of cycles between smaller peak values of slip. Furthermore, it can be seen that the maximum bond resistance, τ_1, deteriorates faster than the ultimate frictional resistance, τ_3. However, there is a strong correlation between the deterioration rate of the maximum and frictional bond resistance. This can be seen from Fig. 5.5, which illustrates the reduction of τ_3 as a function of the damage parameter d, deduced from the reduction of τ_1. Considering the inevitable scatter, the simple analytical function shown in Fig. 5.5 seems to be adequate.

The deterioration of the monotonic envelope seems to depend on the damage experienced by the concrete, particularly the length of the concrete keys between the lugs of the bar that has been sheared off. This, in turn, is a function of the magnitude of the slip induced in the bar in both directions; the larger the s_{max} and the difference between peak slip values, the larger the damage. Another influencing factor is the number of cycles. These parameters can be related to the energy dissipated during the loading and unloading processes. Therefore, it

was assumed that the damage parameter d is a function of the total dissipated energy only. However, it has also been assumed that only a fraction of the energy dissipated during repeated cycles between fixed peak slip values appears to cause damage, while the other part appears to be used to overcome the frictional resistance and is transformed into heat.

Figure 5.6 illustrates the correlation between the measured damage factor, d, as a function of the computed dimensionless dissipated energy factor, E/E_o. The proposed function for d is shown in the figure. Because of the reason given above, in the computation of E, only 50% of the energy dissipated by friction is taken into account. The normalizing energy, E_o, corresponds to the absorbed energy under monotonically increasing slip up to the value s_3. Although there is some scatter, the agreement between the analytical and experimental results seems acceptable.

While two results for specimens, which were subjected to one-sided cycles between s=0 and $s=s_{max}$, fit the proposed analytical function nicely; two others, however, indicate much less damage than predicted. This discrepancy cannot be explained in a fully satisfactory manner. It could be excessive scatter or it could suggest that the influence of the difference between the peak values of slip ($s_{max} - s_{min}$) is not accurately taken into account by the proposed approach. Therefore, another assumption for d, expressed as:

$$d = c_1 \cdot c_2 \tag{5.1}$$

where

$c_1 \leqslant 1.0$ is a function of $(s_{max} - s_{min})/s_3$ and takes the influence of the maximum excursion in both directions into account, and

$c_2 \leqslant 1.0$ is a function of (E/E_o) and represents the influence of the number of cycles only

was tried. However, the scatter was much the same; therefore, the above described simple assumption was adopted.

No reduction of the current envelope (monotonic or reduced) is assumed for unloading or reloading only (e.g. path EFE, Fig. 5.3b). In the tests, cycles were always carried out between

fixed peak values of slip. However, during generalized excitations, it may happen that a cycle is not completed to the current values of s_{max} or s_{min} (e.g. path GHM in Fig. 5.3b). In this case, the damage parameter is interpolated between the values valid for the last slip reversal and for the completed cycle (point E and point P in this example) using Eqn. 5.2:

$$d = d_L + (d_C - d_L) \frac{s_L - s}{s_L - s_C} \tag{5.2}$$

where

d = damage factor of current inversion point(point H in example)
d_L = damage factor of last inversion point (point E in example)
d_C = damage factor for the completed cycle (point P in example)
s_L = slip value of last inversion point (slip of point E in example)
s_C = slip value of completed cycle (slip of point P in example)
s = slip value of current inversion point (slip of point H in example)

Because of the absence of any test results concerning this problem, the assumed linear relation would seem to be appropriate.

If unloading is done from a larger slip value than the peak slip in the previous cycle (e.g. path STU in Fig. 5.3b), the new reduced envelope is calculated as a function of the total dissipated energy using the analytical expression shown in Fig. 5.6.

It should be observed that the proposal for calculating the damage parameter as a function of the total dissipated energy is theoretically correct only in the range of the low cycle fatigue. That is, when a small number of cycles at relatively large slip values is carried out. In fact, if a high number of cycles at small slip values is performed, the energy dissipated can be relatively large, but no significant damage is produced and the reloading branch reaches the monotonic envelope again [12,31]. On the other hand, when limiting our attention to a small number of cycles (<30), as in the present study, the energy dissipated for cycles between small slip values is rather small and the calculated damage, as a consequence, is insignificant.

5.3.3 Frictional Resistance

The frictional bond resistance, τ_f, depends upon the peak value of slip, s_{max}, reached in

either direction, and is related to the bond stress, from which unloading started (Fig. 4.45). However, the reduction of bond resistance at peak slip is only very roughly taken into account in the proposed model insofar as the bond resistance at peak slip is limited by the reduced envelope (see Fig. 5.3b). Therefore, the frictional bond resistance (τ_f in Fig. 5.3b) was related to the value of the ultimate frictional bond resistance of the corresponding reduced envelope (τ_3 in Fig. 5.3b), because this value is calculated in the current model (see Section 5.3.2). The relationship between τ_f and τ_3 as a function of the ratio s_{max}/s_3 deduced from the tests is shown in Fig. 5.7. For the first slip reversal, the ratio τ_f/τ_3 depends significantly on the value s_{max}/s_3 (line a,b,c in Fig. 5.7). However, when cycling between fixed values of slip (e.g. between s_{max} and s_{min} in Fig. 5.3b), τ_f is reduced more rapidly than the ultimate τ_3 of the corresponding reduced envelope. After 10 cycles, the ratio τ_f/τ_3 is almost independent of s_{max}/s_3 (see Fig. 5.7). Therefore, the analytical function abc in Fig. 5.7 is used only for the calculation of the frictional resistance for the first slip reversal (τ_f in Fig. 5.3b). For subsequent cycles, τ_f (e.g., τ_f^+ in Fig. 5.3b) is deduced from this initial value by multiplying it with an additional reduction factor d_f. It seemed reasonable to assume that the latter depends on the energy dissipated by friction alone.

Figure 5.8 illustrates the correlation between the measured reduction factor d_f as a function of the computed dimensionless dissipated energy factor E_f/E_{of}, as well as the proposed function for d_f. E_f is the energy dissipated by friction alone and the normalizing energy E_{of} is equal to the product $\tau_3 \cdot s_3$ and is, therefore, related to the monotonic envelope. A relatively large scatter for the damage factor d_f can be expected because of the large scatter of τ_f (see Table 4.2). If one neglects tests which had small values of s_{max}, all results cluster around the proposed analytical function with no apparent influence of the varied parameters. Although only a small amount of frictional energy was dissipated during cycles between small values of peak slip, the deterioration of the frictional bond resistance was rather large. However, it should be remembered that the absolute value of τ_f is very small in this case (see Fig. 4.44).

If unloading is done from a larger slip value than the peak slip in the previous cycle (e.g.

path STU in Fig. 5.3b), the new frictional bond resistance, τ_{fu}, is interpolated between two values (Fig. 5.9): the first value is related to τ_3 of the corresponding new reduced envelope using the analytical function given in Fig. 5.7 and the second value is the τ_f reached in the last cycle ($\tau_f(1)$ in Fig. 5.9). This interpolation is done in order to have a smooth transition in the values of τ_f. In subsequent cycles between newly established peak slip values, the calculated new initial value ($\tau_{fo}(2)$ in Fig. 5.9) is deteriorated again as a function of the energy E_f dissipated by friction alone using the analytical relationship given in Fig. 5.8. In the calculation of E_f, the friction energy dissipated in the previous cycles is neglected because it is taken into account in the calculation of $\tau_{fo}(2)$.

5.3.4 Unloading and Reloading Branch

The slope of any unloading branch (paths EFG or JKL in Fig. 5.3b) is taken as K = 180 N/mm^3. The relatively small influence of the number of cycles on the stiffness of the unloading branch is neglected. The same slope is assumed for any reloading branch (e.g. path NE' in Fig. 5.3b).

5.3.5 Effects of Variation of Different Parameters on the Analytical Model

The analytical model described above and illustrated in Fig. 5.3 has been deduced from standard tests conducted on standard specimens which had the following main characteristics:

bar diameter: d_b = 25 mm (#8 bars)

deformation pattern: see Table 3.4, α_{sR} = 0.065

concrete strength: $f_c' \approx$ 30 N/mm^2 (4350 psi)

clear spacing between bars: 4 d_b

restraining reinforcement: about 4 times the minimum value given in Section 4.5

external pressure: none

increase of slip: 1.7 mm/min.

Position of bars during casting: The bars were cast horizontally with a depth of concrete of $\approx$ 150 mm ($\approx$ 6 in.) below the bar.

In what follows, the effects of variations of these main parameters on the analytical model are discussed.

5.3.5.1 Effects on Monotonic Envelope. If no specific test results are available which provide accurate data on the bond stress-slip relationship in a specific case, the following procedure may be used to modify the monotonic envelope defined in Section 5.3.1.

(a) Bar Diameter

In the present tests a slight decrease of maximum bond resistance was observed with increasing bar diameter for equal values of the related rib area, although in the more extensive investigations, no influence of d_b was found [44]. Based on the present work, it is proposed to increase τ_1 by up to 10% if #6 bars (d_b = 19 mm) are used instead of #8 bars (d_b = 25 mm) and to decrease τ_1 by 10% if #10 bars (d_b = 32 mm) are used.

(b) Deformation Pattern

The related rib area, α_{SR}, affects mainly the ascending branch of the bond law. If the actual value of α_{SR} differs much from the value α_{SR} = 0.065, its influence should be taken into account by modifying s_1, τ_1, and α using the data given in Fig. 2.4. For $\alpha_{SR} \approx 0.11$, τ_1 should be increased by about 10% whereas s_1 and α should be decreased by about 0.7 mm and 0.33 mm, respectively.

The clear spacing, c_1, between lugs has a significant effect on the local bond stress-slip relationship since, with increasing values of c_1, the values of slip at maximum bond resistance and at leveling off to the frictional bond resistance increase. The bond deterioration during cyclic loading decreases with increasing clear lug spacing c_1. However, more tests are needed to quantify the influence of the bar deformation pattern on slip more accurately. In the reported tests, the clear distance between lugs of the standard bars was 10.5 mm and the corresponding one for #6 bars was about 7 mm. It is proposed to modify the values for s_1, s_2, and s_3 given in Section 5.3.1 with the factor $c_1/10.5$ (c_1 in mm), but because of lack of data the modification should not exceed $\pm 30\%$.

(c) Concrete Strength

The influence of this parameter can easily be taken into account by multiplying τ_1 and τ_3 with the factor $(f_c'/30)^{\beta}$, where $\beta \approx$ 1/2 to 2/3 and f_c' is the concrete compressive strength in N/mm^2. Furthermore, the value of s_1 should be changed approximately in proportion to $\sqrt{f_c'}$ to take into account the variation of $s_{\tau_{max}}$ with concrete strength.

(d) Clear Spacing

If the clear spacing between bars is smaller than 4 d_b, τ_1 and τ_3 should be reduced using the information given in Fig. 4.15.

(e) Restraining Reinforcement

If the minimum restraining reinforcement as given in Section 4.5 is provided, a pull-out type of failure can be expected. The maximum and frictional bond resistances will not be much lower (<15%) than the cited values, which are applicable for cases having a 4 times heavier transverse reinforcement than required in Section 4.5. However, if less restrainment (confinement) than required in Section 4.5 is provided, a splitting type of failure may occur. In this case, the bond stress-slip relationship may differ much from that for a well-confined concrete (see Fig. 4.11). However, not enough data are available to reliably cover this case.

(f) External Pressure

The influence of external transverse pressure p (for example, by column compressive forces) can be taken into account by increasing τ_1 and τ_3 according to Fig. 4.17.

(g) Loading Rate

If the loading rate differs significantly from that used for testing standard specimens (1.7 mm slip per minute), the values of τ_1 and τ_3 should be modified according to Fig. 4.20.

(h) Position of Bars During Casting

The proposed bond law is valid for bars positioned horizontally in mid-height of a 300 mm (12 in.) high specimen and surrounded by well compacted concrete. The bond stress-slip relationship may be significantly different for different bond conditions, e.g. more or less fresh

concrete beneath the bars or concrete less well compacted. However, no quantification of these influence factors is given because of lack of data. For possible modification of the monotonic envelope, see Section 2.1.1.

5.3.5.2 Effects on Cyclic Parameters. According to Section 4.4.6, several parameters investigated do not influence significantly the cyclic bond behavior if the deterioration of bond resistance is related to the pertinent monotonic envelope and calculated for equal ratios of s_{max}/s_3. In the proposed model, bond resistance during cyclic loading is related to the monotonic envelope, and the influence of s_3 is taken into account by calculating the reduced envelope and the frictional resistance during cycling through the normalizing energy E_o and E_{of}, respectively. Therefore, it is assumed that the cyclic parameters given in Sections 5.3.2 and 5.3.3 are also valid for different test conditions than those on which they have been determined (see above). The influence of the different parameters on the stiffness of the unloading and reloading branch can be taken into account by modifying its slope ($K \approx 180\ N/mm^3$, Section 5.3.4) in the same way as the values τ_1 (see Section 5.3.5.1). It is believed that this approximation is sufficiently accurate for practical purposes because the slope of the unloading branch only slightly influences the overall behavior of a long anchorage [49].

5.3.6 Comparison of Analytical Predictions of Local Bond Stress-Slip Relationships with Experimental Results

The local bond stress-slip relationships predicted using the model described above are compared in Figs. 5.10 to 5.22 with the results obtained in some of the present tests. For making the calculations, a computer program was written which is described in a companion report [49]. To take the inevitable scatter into account, the parameters which describe the monotonic envelope were varied in the given range (Section 5.3.5.1) to match the experimental results. As can be seen, except for the reloading curves starting from $s \approx 0$ and reaching the values of the peak slip between which the specimen was cycled, the agreement is quite good. This is also true for the results of Test Series 1 and 3 to 7, in which the influence of several parameters on the bond behavior was studied. In general, the model was successful in reproducing the experi-

mental results with sufficient accuracy.

5.4 Analytical Model for Unconfined Concrete in Tension and Compression

The bond conditions in a joint vary along the embedment length as described in Sections 2.1.2 and 3.1 (see also Fig. 2.6). In the following, the implications on the bond stress-slip relationship during monotonic and cyclic loading are discussed.

5.4.1 Monotonic Envelope

Figure 5.23 shows the different regions in an interior joint as identified in [8] and typical bond stress-slip relationships for monotonic loading in both directions. Loading 1 (tension force applied at the left bar end, compression force at the right bar end) results in a rather inferior bond behavior at the left unconfined end of the concrete block compared to the middle confined region due to the early formation of a concrete cone which separates from the main concrete block (Fig. 3.4). The opposite is true for the right unconfined end of the block because of the column compressive force transverse compressive stresses are acting on the bar. For a monotonic loading in the opposite direction (loading 2), the bond behavior of the two end regions reverses. The length of the end regions with different bond behavior and the pertinent bond laws are not well known yet.

According to [8] the length of the concrete cone that eventually breaks out is influenced by the thickness of the (unconfined) cover, the amount and particular arrangement (spacing) of the stirrups and the arrangement of the longitudinal bars (see Fig. 3.4). In the experiments performed in [8] this length amounted to about 3-4 d_b. From the results given in [22], this length can be estimated to about 5 d_b. The bond strength in this zone will not be uniform, but will vary from a relatively low value at the column face to almost the value applicable for confined concrete at the tip of the cone because some concrete at the column face will break out first. Approximately the same length as given above is assumed for the zone with very good bond at the other end of the block.

The bond strength of the unconfined tensioned region close to the column face may drop

down as low as about 5 N/mm^2 (725 psi) for a concrete strength $f'_c = 30$ N/mm^2 (4350 psi) [8,22]. After the formation of a cone, the bond resistance will decrease rapidly to about zero.

The maximum bond resistance in the compressed region near the column face depends on the transverse pressure which acts on the bar. A pressure of 10 N/mm^2 (1450 psi), which was approximately present in the tests [8,22] at maximum load, will increase τ_{max} by about 20%. Furthermore, compression stresses due to the Poisson effect (bar yielding in compression) are acting on the bar, which might increase τ_{max} by an additional 20%. The same percentage increase can be expected for the ultimate frictional bond resistance. The characteristic slip values are not likely to change much.

With due consideration of the above mentioned data, the following monotonic envelopes are suggested as being valid for a concrete strength $f'_c = 30$ N/mm^2 (4350 psi).

Unconfined region at column face:

Tension Side:	Compression Side:
$\tau_1 = 5$ N/mm^2 (725 psi)	$\tau_1 = 20$ N/mm^2 (1900 psi)
$\tau_3 = 0$	$\tau_3 = 7.5$ N/mm^2 (1087 psi)
$s_1 = s_2 = 0.3$ mm (0.012 in.)	$s_1 = 1$ mm (0.04 in.), $s_2 = 3$ mm (0.12 in.)
$s_3 = 1$ mm (0.04 in.)	$s_3 = 10.5$ mm (0.41 in.)
$\alpha = 0.4$	$\alpha = 0.4$

The influence of a different concrete strength can be taken into account as proposed in Section 5.3.5.1. If the maximum transverse pressure is less than 10 N/mm^2 (1450 psi) or the bar does not yield in compression, the values for the maximum and frictional bond resistance of the unconfined region in compression should be modified accordingly.

For conditions as present in the tests [8,22], the following distribution of the characteristic bond stresses and slip values is proposed (Fig. 5.24):

(a) $x=0$ to $x=2\ d_b$ and $x=l_e$ to $x=l_e-2\,d_b$	Characteristic bond stresses and slip values of the unconfined concrete in tension and compression, as given above.
(b) $x=0.25\ l_e \leq 5\ d_b$ to $x=0.75\ l_e \geq l_e-5\ d_b$	Characteristic bond stresses and slip values of the confined region, see Section 5.3.

(c)	Embedment length between regions (a) and (b).	Linear interpolation of the characteristic bond stresses and slip values between regions (a) and (b).

It should be noted that the above proposals are highly speculative, which has to be taken into account when using them. Additional tests are needed to reliably quantify the bond in the various zones along a bar.

5.4.2 Cyclic Parameters

Figure 5.23a (bottom left) shows typical monotonic bond laws for the left unconfined region 1. If first a slip in the negative direction is imposed (bar is pushed in), relatively good bond is developed and "normal" damage in the concrete surrounding the bar is induced. On the contrary, if one imposes first slip in the positive direction (bar is pulled out), the concrete is prone to early cone formation. Therefore, much more damage than "normal" is produced when loaded to equal slip values. It is reasonable to assume that not much bond resistance is left after the formation of a cone. Therefore, the following modifications to the analytical bond model for cyclic loading are proposed.

The normalizing cyclic parameters (E_o, E_{of}, and s_3) are related to the monotonic envelope for push-in loading (inducing slip in the negative direction for region 1 or in the positive direction for region 2 in Fig. 5.23). To take the more severe damage into account which is caused by bar pull-out (inducing slip in the opposite direction than described above), the pertinent total dissipated energy, E, and energy dissipated by friction alone, E_f, are multiplied by an amplification factor δ. It is proposed to take this amplification factor as twice the ratio between the value E_o for push-in loading and the value E_o for pull-out loading. This definition of the amplification factor results in a reduced envelope for push-in loading with characteristic bond stresses of about 10% of the values of the monotonic envelope, when the bar is first pulled out up to a slip value $s = s_3$ and then the direction of loading is reversed.

Note that the above proposal is rather crude because the deterioration of bond caused by pull-out to very small slip values ($< s_1$) is probably overestimated. However, a more

sophisticated approach seems not to be justified in the light of the current limited knowledge. The validity of the above described assumptions was shown in a companion report [49] by a good agreement between predicted and measured behavior of deformed bars with an anchorage length of 25 d_b.

VI. CONCLUSIONS AND RECOMMENDATIONS FOR FUTURE RESEARCH

6.1 Summary and Conclusions

From the results obtained in this study, the following main observations can be made for the local bond behavior under monotonic and cyclic loading.

6.1.1 Monotonic Loading

(1) The local bond stress-slip relationship of bars embedded in well-confined concrete and failing by pull-out has a characteristic shape. The stiffness of the ascending branch decreases gradually from its initial large value to zero when approaching the maximum bond resistance, τ_{max}. After passing τ_{max}, the bond resistance decreases almost linearly to the ultimate frictional bond resistance, τ_3 at a slip, s_3, which is approximately equal to the clear distance between lugs, and remains almost constant thereafter.

(2) If the bond failure is caused by splitting, the bond resistance drops rapidly to zero after the occurrence of splitting cracks.

(3) The scatter of the bond resistance at constant slip values is almost independent of the value of the slip. The standard deviation amounts to about 1 to 1.3 N/mm^2 (145 to 190 psi) for specimens tested under identical conditions but cast from different concrete batches.

(4) To ensure that the bond failure is caused by pull-out, normally a restraining reinforcement must be provided. The minimum area for this reinforcement is given in Section 4.5. Providing a restraining reinforcement with an area larger than the minimum value does not result in a significant improvement of the bond behavior.

(5) The following statements are valid for a pull-out failure.

   (a) The influence of the bar diameter on the local bond stress-slip relationship was rather small in the tested range (d_b = 19 mm to 32 mm) (#6 to #10 bars).

   (b) The bond resistance increased approximately proportional to $\sqrt{f_c'}$. However, the slip value corresponding to the maximum bond resistance decreased almost

proportional to $1/\sqrt{f_c'}$.

(c) Increasing the clear bar spacing from the minimum value s = 1 d_b to s = 4 d_b resulted in an increase of the bond resistance by about 20%.

(d) The bond behavior was improved by applying transverse pressure to the test specimens. The maximum bond resistance was increased by about 25% for a pressure of 13.5 N/mm^2 (1914 psi). The concrete compressive strength was f_c' = 30 N/mm^2 (4350 psi).

(e) The bond resistance was increased (decreased) by an increase (decrease) of the loading rate. A change of the rate of pull-out by a factor of 100 resulted in a change of the bond resistance by about 15%.

6.1.2 Cyclic Loading

(1) During cyclic loading the degradation of bond strength and bond stiffness depends primarily on the maximum value of peak slip in both directions reached previously. Other significant parameters are the number of cycles and the difference between the peak values of slip between which the bar is cyclically loaded, i.e. $\Delta s = s_{max} - s_{min}$. The bond deterioration is larger for full reversals of slip than for half cycles.

(2) Cycling up to 10 times between slip values corresponding to bond stresses smaller than about 80 percent of the maximum bond resistance, τ_{max}, attained under monotonically increasing slip reduces moderately the bond resistance at the peak slip values as the number of cycles increase but does not significantly affect the bond stress-slip behavior at larger slip values.

(3) Cycling between slip limits larger than the values corresponding to a bond stress of 80 percent of τ_{max} produces a pronounced deterioration of bond strength and bond stiffness at slip values smaller than the peak slip value and has a distinct effect on the bond stress-slip behavior at larger slip values.

(4) The various parameters investigated do not influence significantly the cyclic bond behavior if the deterioration of bond resistance is related to the pertinent monotonic envelope and is calculated for equal ratios of peak slip s_{max} to slip s_3, where s_3 is the slip value of the monotonic envelope at which the descending branch levels off to the frictional resistance.

6.1.3 Analytical Bond Model

(1) The proposed analytical model for the local bond stress-slip relationship of deformed bars embedded in well-confined concrete for generalized excitations is very simple compared with the real behavior but provides a satisfactory agreement with experimental results under various slip histories and for various bond conditions.

6.2 Recommendations for Future Research

While the studies reported herein have clarified some aspects of the bond between deformed bars and well confined concrete under monotonic and cyclic loadings, some areas should be the subject of future research:

(1) More experiments are needed to study the influence of deformation patterns, especially the distance between and height of lugs on the bond behavior under monotonic and cyclic loading. The results of these tests can be used to reconsider and eventually modify the proposed theory for the mechanism of bond resistance.

(2) The effect of the strain of the bar, especially beyond yield strain, on the local bond stress-slip relationship should be investigated.

(3) The relation between bond forces and splitting forces is not well known yet and should be studied in appropriate tests. The results are useful to reliably estimate the necessary amount of restraining reinforcement to ensure a pull-out type of failure. If these restraining bars are resisting any other actions, this simultaneous effect should be studied.

(4) The bond behavior in the unconfined end regions of beam-column joints is rarely known yet and should be studied in appropriate tests.

(5) If the concrete is not well confined, the bond failure may be caused by splitting. The pertinent bond behavior under monotonic and cyclic loading is very little known yet.

REFERENCES

1. Seismology Committee, "Recommended Lateral Force Requirements and Commentary," Structural Engineers Association of California, 1969.

2. International Conference of Building Officials, Uniform Building Code, 1970 Edition, Vol. 1, Pasadena, California.

3. Bertero, V. V., "Seismic Behavior of Structural Concrete Linear Elements (Beams, Columns) and Their Connections," Comité Euro-International due Béton, Bulletin D'Information No. 131, Paris, April 1979.

4. Popov, E. P., "Mechanical Characteristics and Bond of Reinforcing Steel Under Seismic Loading," Workshop on Earthquake Resistant Reinforced Concrete Building Construction, University of California, Berkeley, 1977.

5. Takeda, T., Sozen, M. A., and Nielsen, N. N., "Reinforced Concrete Response to Simulated Earthquakes," *Journal of the Structural Division,* ASCE, Vol. 96, No. ST-12, December 1970.

6. Ismail, M. and Jirsa, J., "Behavior of Anchored Bars Under Low Cycle Overloads Producing Inelastic Strains," *ACI Journal,* July 1972.

7. Ma, S. M., Bertero, V. V. and Popov. E. P., "Experimental and Analytical Studies on the Hysteretic Behavior of Reinforced Concrete Rectangular and T-Beams," Earthquake Engineering Research Center, *Report No. EERC 76-2,* University of California, Berkeley, May 1976.

8. Viwathanatepa, S., Popov, E. P., and Bertero, V. V., "Effects of Generalized Loadings on Bond of Reinforcing Bars Embedded in Confined Concrete Blocks," Earthquake Engineering Research Center, *Report No. UCB/EERC-79/22,* University of California, Berkeley, August 1979.

9. Tassios, T. P., "Properties of Bond Between Concrete and Steel Under Load Cycles Idealizing Seismic Actions," Comité Euro-International Du Béton, Bulletin No. 131, Paris, April 1979.

10. Rehm, G., "Ueber die Grundlagen des Verbundes zwischen Stahl und Beton (On the Basic Laws of Bond Between Steel and Concrete)," Schriftenreihe des Deutschen Ausschusses fuer Stahlbeton, Heft 138, Berlin, 1961 (in German).

11. Lutz, L. A., "Analysis of Stresses in Concrete near a Reinforcing Bar Due to Bond and Transverse Cracking," *ACI Journal,* Vol. 67, No. 10, p. 778, October 1970.

12. Morita, S. and Kaku, T., "Local Bond Stress-Slip Relationship and Repeated Loading," Proceedings, IABSE Symposium on "Resistance and Ultimate Deformability of Structures Acted on by Well Defined Repeated Loads," Lisboa, 1973.

13. Martin, H., "Zusammenhang zwischen Oberflaechen-Beschaffenheit, Verbund und Sprengwirkung von Bewehrungsstaehlen unter Kurzzeitbelastung (Relationship Between Deformation Pattern, Bond and Splitting of Reinforcing Bars Under Short Time Loading)," Schriftenreihe des Deutschen Ausschusses fuer Stahlbeton, Heft 228, Berlin, 1973 (in German).

14. Goto, Y., "Cracks Formed in Concrete Around Tension Bars," *ACI Journal, Proceedings,* Vol. 68, No. 4, April 1971.

15. Yannopoulos, P., "Fatigue, Bond and Cracking Characteristics of Reinforced Concrete Tension Members," Ph.D. Thesis, Imperial College, London, January 1976.

16. Lutz, L. A. and Gergely, P., "Mechanics of Bond and Slip of Deformed Bars in Concrete," *ACI Journal,* Vol. 64, No. 11, pp. 711-721, November 1967.

17. Tepfers, R., "A Theory of Bond Applied to Overlapped Tensile Reinforcement Splices for Deformed Bars," University of Technology, Division of Concrete Structures, Goteborg, Publication 73.2, 1973.

18. Orangun, C. O., Jirsa, J. O. and Breen, J. E., "A Re-Evaluation of Test Data on Development Length and Splices," *ACI Journal,* March 1977.

19. Eligehausen, R., "Ubergreifungsstoesse zugbeanspruchter Rippenstaebe mit geraden Stabenden, (Lapped Splices of Tensioned Deformed Bars With Straight Ends)," Schriftenreihe des Deutschen Ausschusses fur Stahlbeton, Berlin, 1979 (in German).

20. Menzel, G. A., "A Proposed Standard Deformed Bar for Reinforced Concrete," presented at the 17th Semi-Annual Meeting, Concrete Reinforcing Steel Institute, Colorado Springs, Colorado, September 1941.

21. ACI Committee 408, "Bond Stress - The State-of-the-Art," *ACI Journal,* Vol. 63, No. 11, pp. 1161-1188, November 1966.

22. Cowell, A. D., Bertero, V. V., and Popov, E. P., "An Investigation of Local Bond Slip Under Variation of Specimen Parameters," Earthquake Engineering Research Center, Report No. UCB/EERC 82/23, University of California, Berkeley, 1982.

23. Sortz, S., "Verbund zwischen Stahleinlagen und Beton als Pruef-und Verwendungs eigenschaft (Bond Between Steel and Concrete as Test and User Property)," Zement und Beton, Heft 75, June/July 1974 (in German).

24. Eibl, J. and Ivanyi, G., "Studie zum Trag-und Verformungsverhalten von Stahlbeton (Study on the Bearing and Deformation Behavior of Reinforced Concrete)," Schriftenreihe des Deutschen Ausschusses fuer Stahlbeton, Heft 260, Berlin, 1976 (in German).

25. Nilson, A. H., "Internal Measurement of Bond Slip," *ACI Journal,* Vol. 63, No. 7, July 1972.

26. Tanner, G. H., "An Experimental Investigation of Bond Slip in Reinforced Concrete," M.S. Thesis, Cornell University, November 1971.

27. Wahla, M. I., "Direct Measurement of Bond Slip in Reinforced Concrete," Ph.D. Thesis, Cornell University, January 1970.

28. Dörr, K., "Bond Behavior of Ribbed Reinforcement Under Transverse Pressure," IASS Symposium on Nonlinear Behavior of Reinforced Concrete Spatial Structures, Volume 1, Preliminary Report, Werner Verlag, Dusseldorf, 1978.

29. Mirza, S. M. and Houde, G., "Study of Bond Stress-Slip Relationships in Reinforced Concrete," *ACI Journal,* January 1979.

30. Perry, E. S. and Jundi, N., "Pullout Bond Stress Distribution Under Static and Dynamic Repeated Loadings," *ACI Journal,* Proceedings, Vol. 66, No. 5, May 1969.

31. Rehm, G. and Eligehausen, R., "Einfluss einer nicht ruhenden Belastung auf das Verbundverhalten von Rippenstaeben (Influence of Repeated Loads on the Bond Behavior of Deformed Bars)," Betonwerk-Fertigteil-Technik, Heft 6, 1977 (in German).

32. Edwards, A. D. and Yannopoulos, P. J., "Local Bond-Stress-Slip Relationship Under Repeated Loading," *Magazine of Concrete Research,* Vol. 30, No. 103, June 1978.

33. Bertero, V. V. and Bresler, B., "Behavior of Reinforced Concrete Under Repeated Loads," *Journal of the Structural Division,* ASCE, June 1968.

34. Ismail, M. and Jirsa, J., "Bond Deterioration in Reinforced Concrete Subjected to Low Cycle Loads," *ACI Journal, Proceedings,* Vol. 69, No. 6, June 1972.

35. Shipman, G. M. and Gerstle, K. H., "Bond Deterioration in Concrete Panels Under Load Cycles," *ACI Journal,* Vol. 76, No. 2, February 1979.

36. Bertero, V. V. and Popov, E. P., "Seismic Behavior of Ductile Moment-Resisting Reinforced Concrete Frames," ACI Special Publication SP-53, pp. 247-292, Detroit, 1977.

37. Viwathanatepa, S., Popov, E. P., and Bertero, V. V., "Seismic Behavior of Reinforced Concrete Interior Beam-Column Joints," Earthquake Engineering Research Center, Report No. UCB/EERC 79/14, University of California, Berkeley, 1979.

38. Pauley, T., Park, R., and Priestley, M.J.N., "Reinforced Concrete Beam-Column Joints Under Seismic Actions," ACI Journal, Proceedings, November 1978.

39. Rehm, G., Eligehausen, R., and Schelling, G., "Hoehe und Verteilung der Querzugspannungen im Bereich von Stabverankerungen in Beton (Distribution of Tensile Hook Stresses in Concrete in the Region of Anchorages of Ribbed Bars)," Report of the Lehrstuhl fuer Werkstoffe im Bauwesen, Universitaet Stuttgart, 1978 (in German).

40. RILEM Document RC6, "Bond Test Reinforcing Steel, 2. Pull-Out Test," RILEM Bulletin, Paris, 1976.

41. Heilmann, H. G., "Beziehungen zwischen Zug und Druckfestigkeit des Betons (Relationships Between Tensile and Compressive Strength of Concrete)," Beton, Heft 2, 1969 (in German).

42. Losberg, A. and Olsson, P. A., "Bond Failure of Deformed Reinforcing Bars Based on the Longitudinal Splitting Effect of the Bars," *ACI Journal,* January 1979.

43. ACI 318-77, "Building Code Requirements for Reinforced Concrete," American Concrete Institute, Detroit, 1977.

44. Martin, H. and Noakowski, P., "Verbundverhalten von Rippenstaeben, Auswertung von Ausziehversuchen (Bond Behavior of Ribbed Bars, Evaluation of Pull-out Tests)," Schriftenreihe des Deutschen Ausschusses fuer Stahlbeton, Heft 319, Berlin, 1981 (in German).

45. Untrauer, R. E. and Henry, R. L., "Influence of Normal Pressure on Bond Strength," *ACI Journal,* Proceedings, Vol. 62, No. 5, May 1965.

46. Hjorth, O., "Ein Beitrag zur Frage der Festigkeit und des Verbundverhaltens von Stahl und Beton bei hohen Beanspruchungsgeschwindigkeiten," Schriftenreihe of the Institut fuer Baustoffkunde und Stahlbetonbau der Technischen Universitaet Braunschweig, Heft 32, Mai 1976 (in German).

47. Whaley, C. P. and Neville, A. M., "Non-elastic Deformation of Concrete Under Cyclic Compression," Magazine of Concrete Research, V. 25, No. 84, Sept. 1973.

48. Ciampi, V., Eligehausen, R., Bertero, V. V. and Popov, E. P., "Analytical Model for Deformed Bar Bond Under Generalized Excitations," Proceedings, IABSE Collogium on "Advanced Mechanics in Reinforced Concrete," Delft, 1981.

49. Ciampi, V., Eligehausen, R., Bertero, V. V., and Popov, E. P., "Analytical Model for Deformed Bar Bond Under Generalized Excitations," Earthquake Engineering Research Center, Report No. UCB/EERC-82/23, University of California, Berkeley, 1982.

Series	Row	Investigated Parameter	Confining Reinforcement[1] Vertical	Confining Reinforcement[1] Stirrups	Loading History		Number of Cycles	Bar Diameter[1]	Concrete Strength f'_c N/mm²	Clear Bar Distance s/d_b	Transverse Pressure N/mm²	Slip Rate mm/min	Number of Specimens	Actual Concrete Strength, f'_c N/mm²
2	1	Loading History	#4	#4	Monotonic in Tension		0	#8	30	4	0	1.7	2	29.6
	2				Monotonic in Compression		0						3	29.6
	3				Cyclic between s (mm)	± 0.107	10						3	29.7
	4					± 0.44	10						3	29.6
	5					± 1.02	1 10						2 2	30.7
	6					± 1.65	1 10						2 2	29.7
	6*					± 1.65 (starting in compression)	10						2	30.7
	7					± 2.54	1 10						2 2	30.7
	8					± 4.57	10						2	30.7
	9					± 6.86	1 10						2 2	29.6
	10					± 9.2	10						2	30.7
	11					± 15.2	1 10						1 2	29.6
	12					0 and 0.44	10						2	30.7
	13					0 and 1.65	10						2	30.7
	14					0 and 4.57	10						2	30.7
	15					0 and 9.2	10						3	30.7
	16				Monotonic in Tension		0						2	28.5
	17				Cyclic	Δs = 0.05 mm at s = 1.65 mm, 2.54 mm	10 each						2	28.5
	18					Δs = 0.05 mm at s = 1.02 mm, 1.65 mm, 4.57 mm	10 each						2	28.5
	19				Cyclic between s (mm)	±0.44,±1.65,±4.57,±9.2	5 each						2	30.7
	20					±1.02,±1.65,±2.54, ±4.57,±9.2	5 each						2	30.7
	21					±1.02,±2.45,±1.65,±2.54, ±4.6,±1.65,±9.2	5 each						2	29.7
	22					0-0.44, 0-1.65, 0-4.57, 1-9.2	5 each						2	29.7

[1] #4: d_b = 12.7 mm; #8: d_b = 25.4 mm

TABLE 3.1a TEST PROGRAM

Series	Row	Investigated Parameter	Confining Reinforcement[1] Vertical	Confining Reinforcement[1] Stirrup	Loading History	Number of Cycles	Bar Diameter[1]	Concrete Strength f'_c N/mm²	Clear Bar Distance s/d_b	Transverse Pressure N/mm²	Slip Rate mm/min	Number of Specimens	Actual Concrete Strength, f'_c N/mm²
1	1	Confining Reinforcement	#8	#4	Monotonic in Tension	0	#8	30	4	0	1.7	3	29.4
	2		#4	#4								3	30.5
	3		#2	#2								3	30.5
	4		--	--								2	30.7
	5		#4	#2								3	30.5
	6		#2	#4	Cyclic s = ±1.65 mm	10						2	30.7
	7		#2	#4	Cyclic s = 0 to 1.65 mm							2	30.7
3	1	Bar Diameter	#4	#4	Monotonic in Tension	0	#6	30	4	0	1.7	2	31.6
	2						#8					2	
	3						#10					2	
	4				Cyclic between s = ±1.65 mm	10	#6					2	
	5						#8					2	
	6						#10					2	
4	1	Concrete Strength	#4	#4	Monotonic in tension	0	#8	55	4	0	1.7	2	54.6
	2				Cyclic, s = ±1.65 mm	10						2	
	3				Cyclic, s = 0 and s = 1.65 mm	10						2	
5	1	Bar Distance	#4	#4	Monotonic in Tension	0	#8	30	1	0	1.7	2	28.2
	2								2			2	
	3								6			2	
	4				Cyclic between s = ±1.65 mm	10			1			2	
	5								2			2	
	6								6			2	
6	1	Transverse Pressure	#4	#4	Monotonic in Tension	0	#8	30	4	0	1.7	2	31.0
	2									5		2	
	3									10		2	
	4									13.2		2	
	5				Cyclic between s = ±1.65 mm	10				5.0		2	
	6									10.0		2	
7	1	Rate of Pull-out	#4	#4	Monotonic in Tension	0	#8	30	4	0	170.	2	29.7
	2										0.034	2	
	3				Cyclic, s = ±1.65 mm	10					170.	2	

[1] #2: d_b = 6.35 mm; #4: d_b = 12.7 mm; #6: d_b = 19.0 mm, #8: d_b = 25.4 mm; #10: d_b = 31.8 mm

TABLE 3.1b TEST PROGRAM

Material	f'_c = 30 N/mm^2		f'_c = 55 N/mm^2	
	Parts by Weight	Weight* kg/m^3	Parts by Weight	Weight* kg/m^3
Cement, Type I-II, Lone Star Brand	1.00	356	1.00	505
Water	0.57	203	0.38	191
Fine Sand	0.43	152	0.36	181
Coarse Sand	2.43	864	1.43	725
Fine Gravel	2.10	746	1.50	760
TOTAL	6.53	2321	4.67	2362

* 1 kg/m^3 = 1.67 lbs/cubic yard

TABLE 3.2 MIX OF CONCRETE

BATCH	NUMBER OF SPECIMENS CAST	SERIES	f'_c [1] N/mm^2	f_t [1] N/mm^2	$\frac{f_t}{\sqrt[3]{f'^2_c}}$
1	3	1	29.4	3.04	0.319
2	9	1	30.5	2.98	0.305
3	6	1	30.7	3.24	0.330
4	11	2	29.6	3.16	0.330
5	11	2	29.7	2.68	0.279
6	11	2	30.7	2.83	0.288
7	9	2	30.7	2.89	0.294
8	11	2	29.7	3.18	0.324
9	11	2 & 7	28.2	3.33	0.345
10	12	5	31.0	3.04	0.328
11	12	6	31.0	3.14	0.318
12	12	3	31.6	2.90	0.290
13	6	2	28.5	2.66	0.284
	124 [2]	$\bar{x}$ v%	30.1 3.3	3.11 6.9	0.310 6.9
14	6	4	54.6	4.03	0.280

[1] $1N/mm^2$ = 145 psi

[2] Five specimens did not yield reliable results because of malprogramming or malfunctioning of testing machine.

TABLE 3.3 CONCRETE COMPRESSIVE AND TENSILE STRENGTHS

Series	Bar	Diameter Nominal (mm)	Diameter Actual[1] (mm)	Transversal Lugs Height (mm) a_1	a_2	a_3	a_4	a_5	a_6	a_7	Width (mm) b_H	b_F	Distance c (mm)	Angle β (0)	Longitudinal Lugs a_L (mm)	b_L (mm)	Related Rib Area α_{SR}
3	#6[2]	19.05	18.78	1.16	1.22	1.44	1.07	1.22	0.86	0.69	2.2	3.8	9.7	74	1.2	3.5	0.10
	#8[2]	25.4	25.11	1.75	1.90	1.70	1.52	1.85	1.73	1.57	2.5	4.2	13.4	75	2.0	4.0	0.11
	#10	31.75	31.82	2.54	2.82	2.86	2.06	2.41	2.13	2.18	3.0	7.0	13.5	72	3.2	3.8	0.16
Other	#8[3]	25.4	24.70	0.34	0.88	1.10	1.23	1.26	1.26	0.57	2.4	4.4	14.0	71	0.7	3.9	0.066

[1] $d_b = 1.274 \sqrt{G/l}$; G = weight in grams, l = length in mm.

[2] Values given for geometry of lugs are averaged from 10 measurements taken at 1 sample.

[3] Values given for geometry of lugs are averaged from 30 measurements taken at 3 samples from 3 different rods.

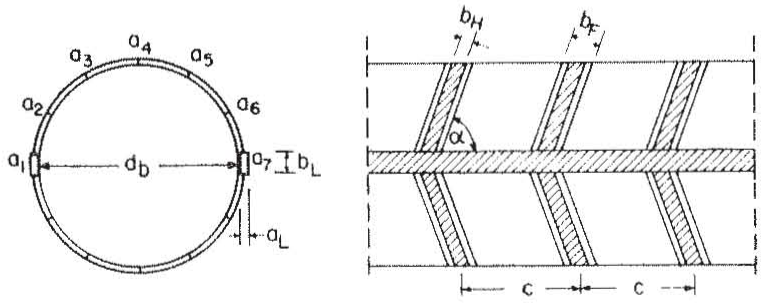

TABLE 3.4 GEOMETRY OF BAR DEFORMATIONS

Standard Deviation of Bond Resistance (N/mm^2)	Slip (mm)				
	0.1	1.0	1.5	5.0	11.5
Average	0.73	0.70	0.65	0.61	0.50
Minimum	0.10	0.07	0.10	0.06	0.06
Maximum	1.50	1.73	1.77	1.55	1.27

TABLE 4.1 STANDARD DEVIATION OF BOND RESISTANCE AT GIVEN SLIP VALUES FOR ALL TESTS MONOTONICALLY LOADED (SERIES 1-7, n = 21 ROWS)

Coefficient of Variation %	τ_{unl} at s_{max}			τ_f during cycling			Reduced Envelope After 10 Cycles	
	N=1	N-2	N=10	N=1	N=2	N=10	τ_{max}	τ_3
Average	5	4	7	17	21	21	10	11
Minimum	2	2	2	11	5	11	2	2
Maximum	8	8	12	24	36	42	18	20

τ_{unl} = Bond resistance

τ_f = Frictional bond resistance during cyclic loading.

τ_{max} = Maximum bond resistance.

τ_3 = Ultimate frictional bond resistance.

N = Number of cycles.

TABLE 4.2 COEFFICIENT OF VARIATION OF BOND RESISTANCE FOR CYCLIC LOADING TESTS (SERIES 2.3-2.15)

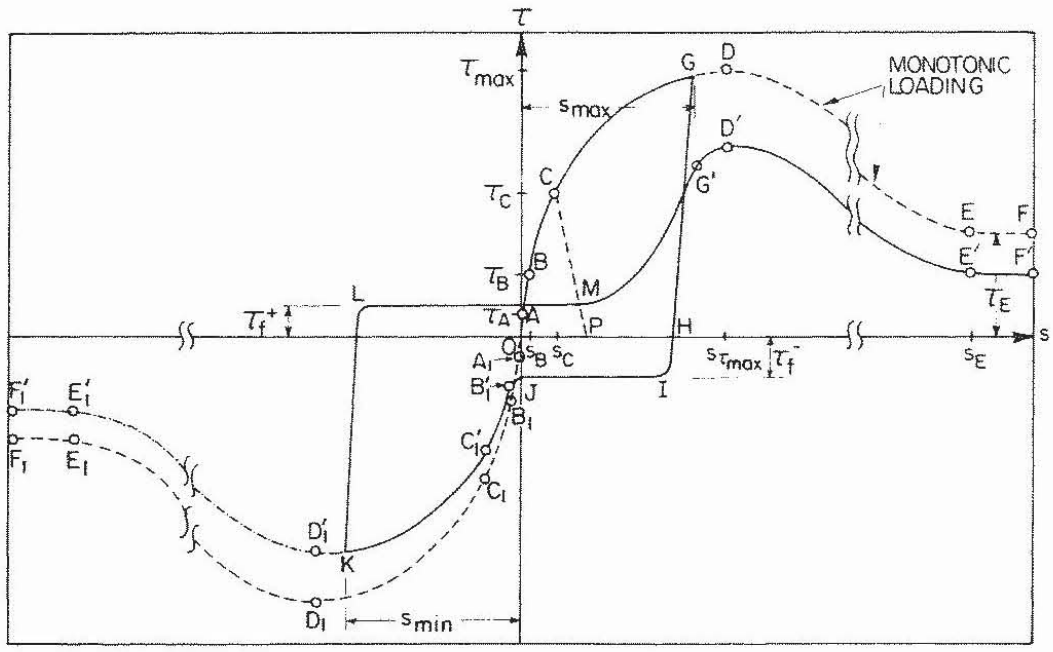

FIG. 2.1 - TYPICAL RELATIONSHIP BETWEEN BOND STRESS τ AND SLIP s FOR MONOTONIC AND CYCLIC LOADING

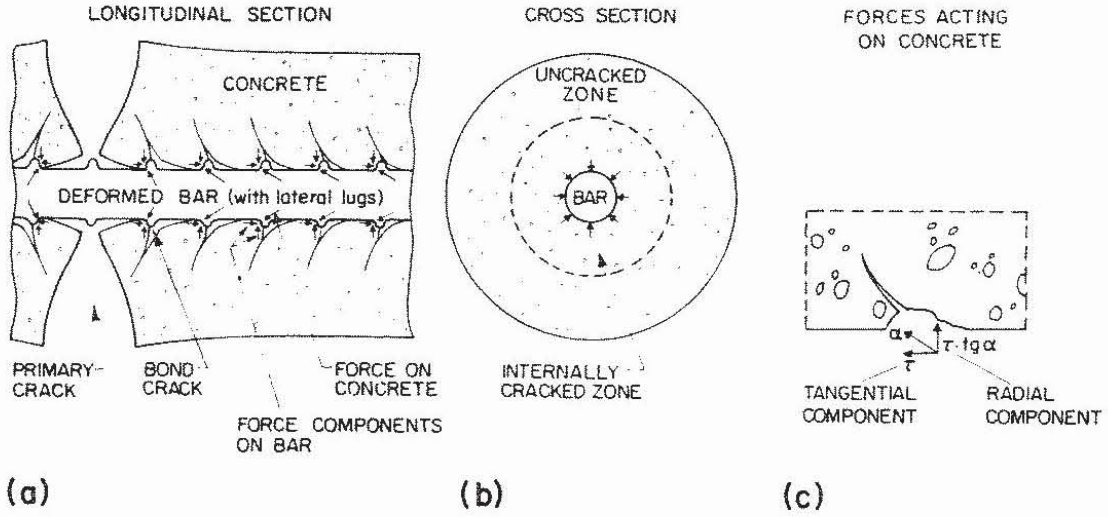

FIG. 2.2 - INTERNAL BOND CRACKS AND FORCES ACTING ON CONCRETE (AFTER [14])

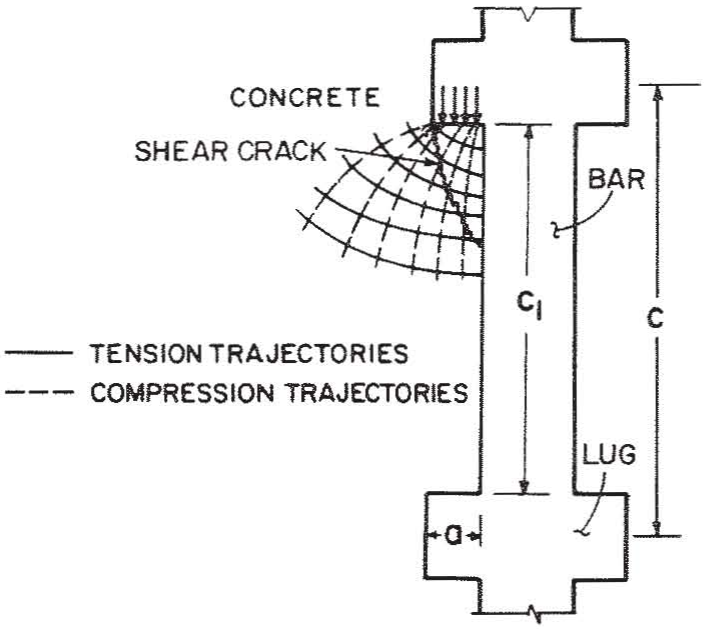

FIG. 2.3 SHEAR CRACKS IN THE CONCRETE KEYS BETWEEN LUGS (AFTER [10]).

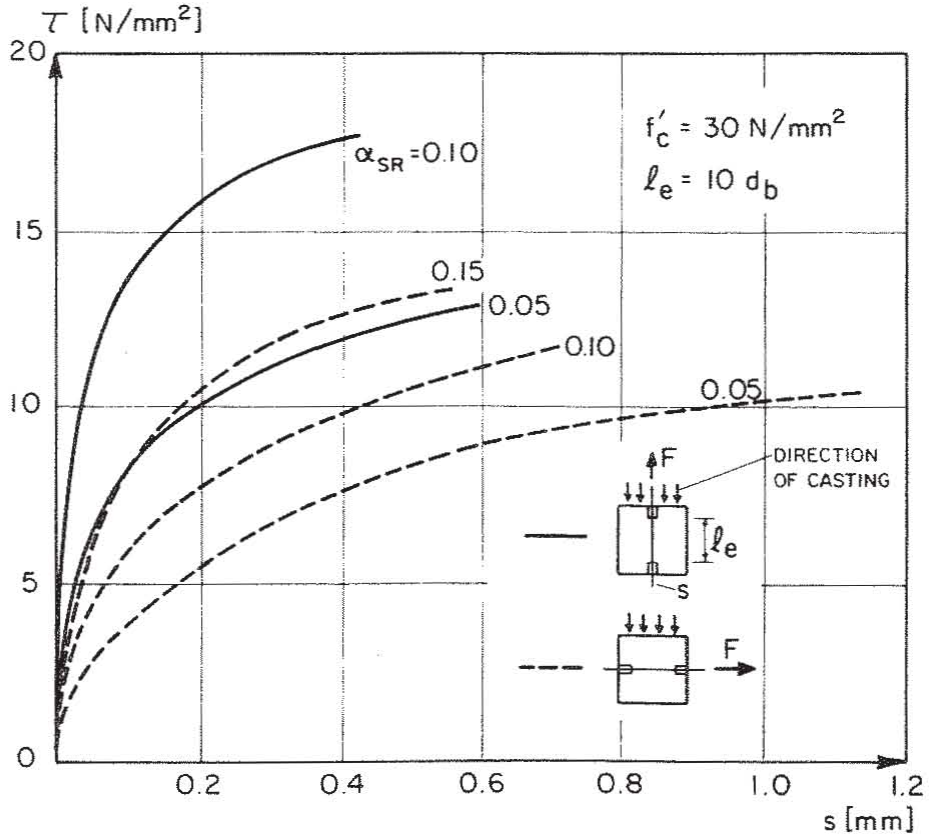

FIG. 2.4 INFLUENCE OF THE RELATED RIB AREA α_{SR} AND DIRECTION OF CASTING ON BOND STRESS-SLIP RELATIONSHIP FOR MONOTONIC LOADING (AFTER [13]).

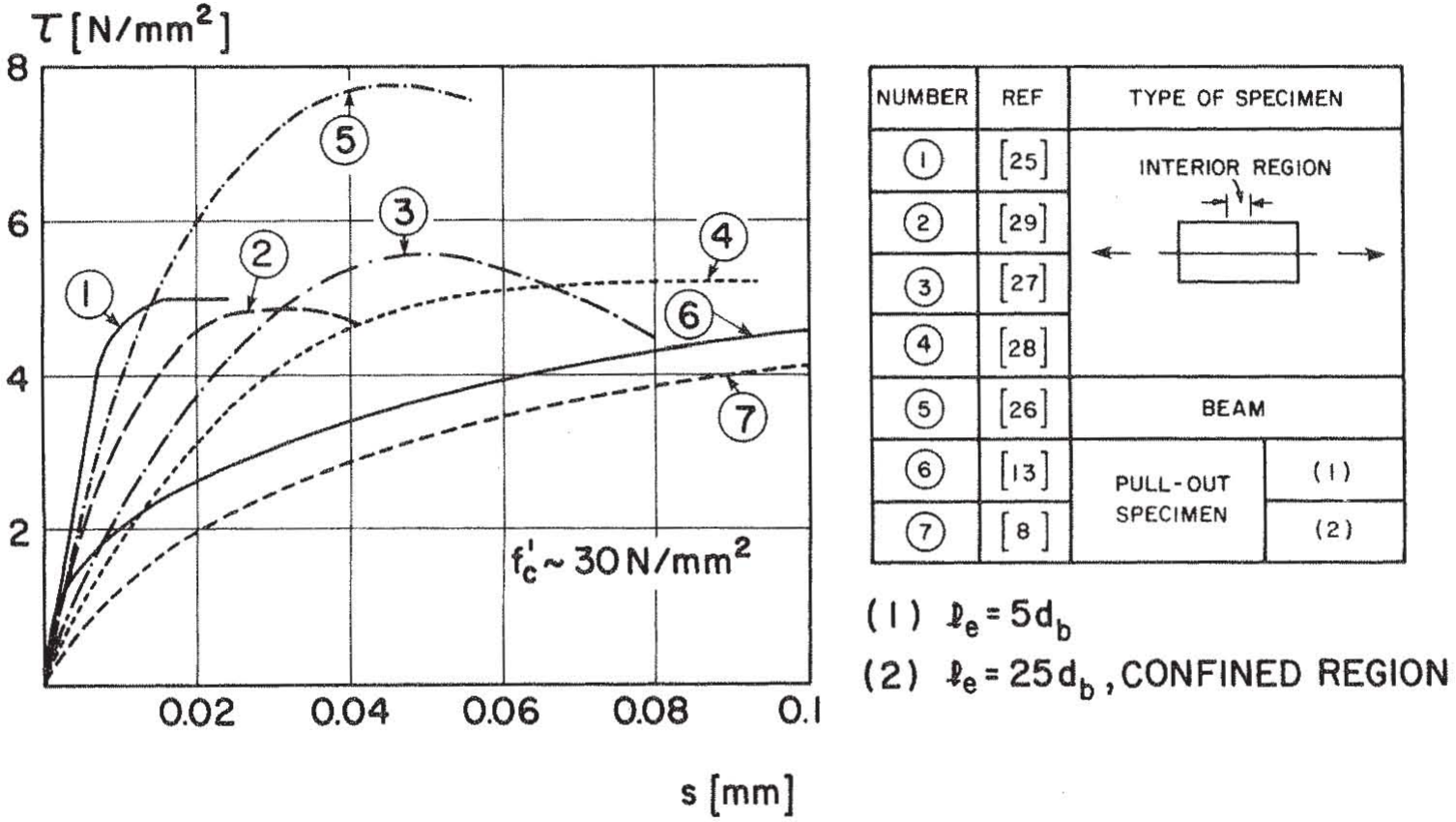

NUMBER	REF	TYPE OF SPECIMEN	
1	[25]	INTERIOR REGION	
2	[29]		
3	[27]		
4	[28]		
5	[26]	BEAM	
6	[13]	PULL-OUT SPECIMEN	(1)
7	[8]		(2)

(1) $\ell_e = 5 d_b$

(2) $\ell_e = 25 d_b$, CONFINED REGION

FIG. 2.5 LOCAL BOND STRESS-SLIP RELATIONSHIPS FOR SMALL SLIP VALUES AFTER DIFFERENT RESEARCHERS.

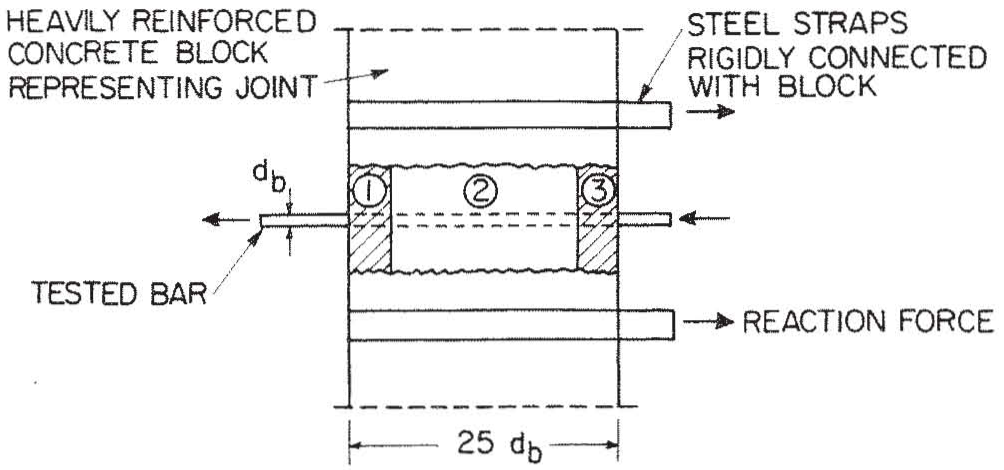

a) SPECIMEN AND TEST SET-UP (SCHEMATIC)

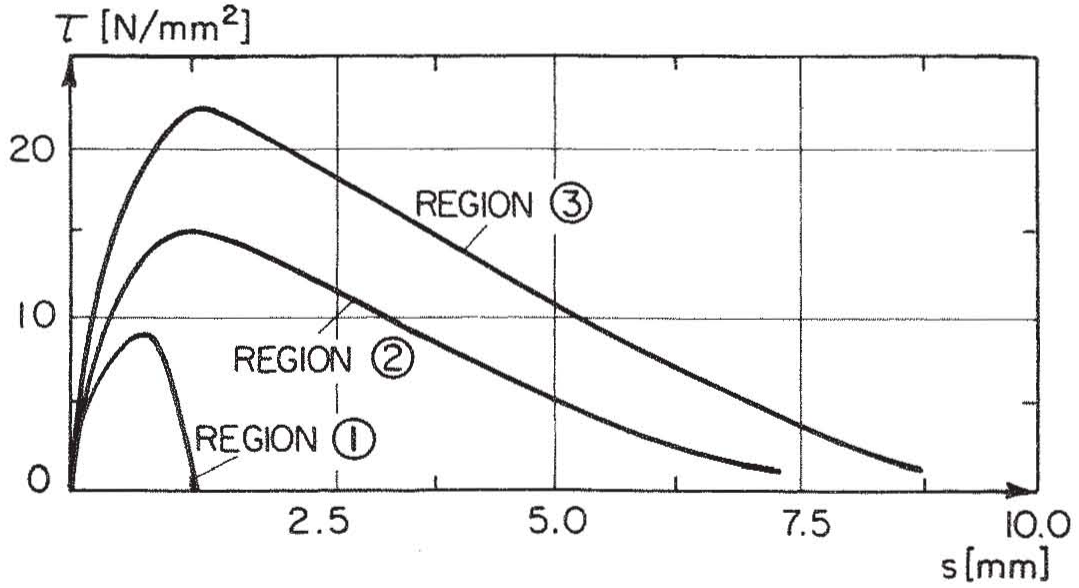

b) LOCAL BOND STRESS-SLIP RELATIONSHIP

FIG. 2.6 BOND STRESS-SLIP RELATIONSHIP FOR MONOTONIC LOADING FOR DIFFERENT REGIONS IN A JOINT (AFTER [8])

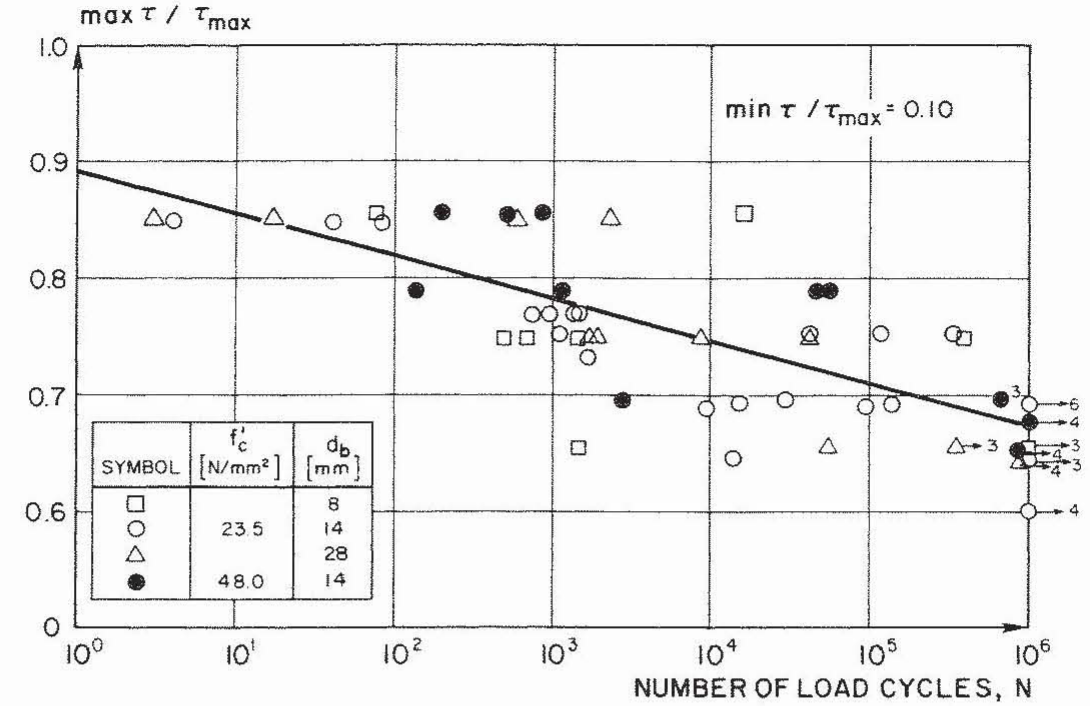

FIG. 2.7 INFLUENCE OF THE RATIO BOND STRESS UNDER UPPER LOAD, MAX τ, TO STATIC BOND STRENGTH, τ_{MAX}, ON THE NUMBER OF CYCLES UNTIL BOND FAILURE (AFTER [31]).

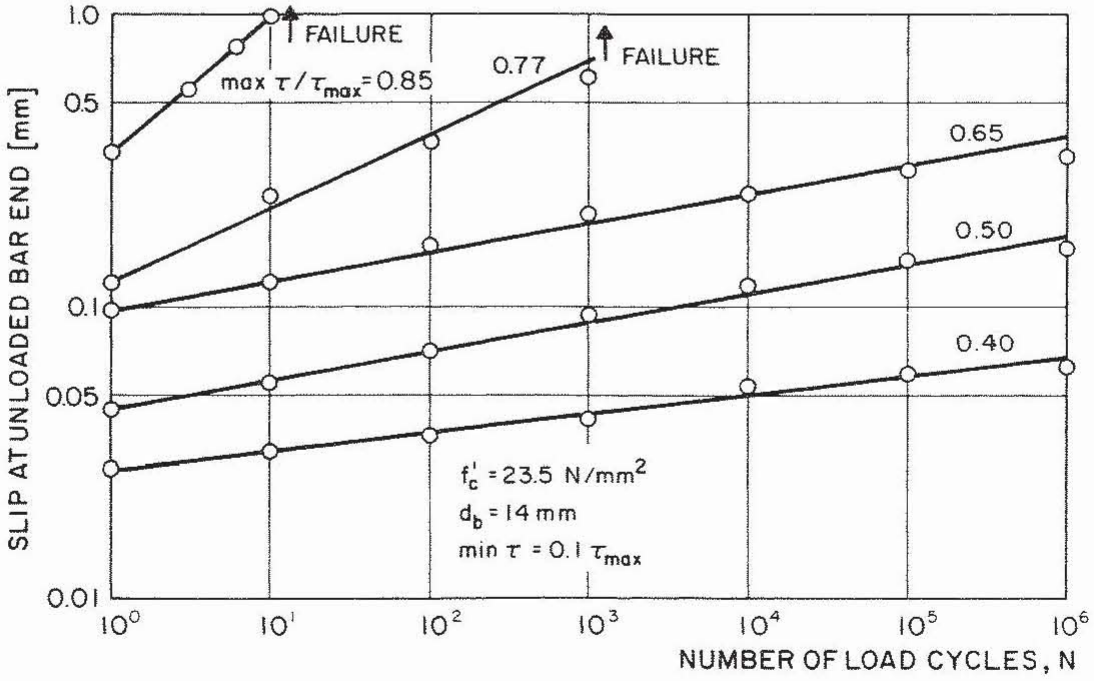

FIG. 2.8 INCREASE OF SLIP AT THE UNLOADED BAR END UNDER PEAK LOAD DURING CYCLIC LOADING AS A FUNCTION OF THE NUMBER OF LOAD REPETITIONS (AFTER [31]).

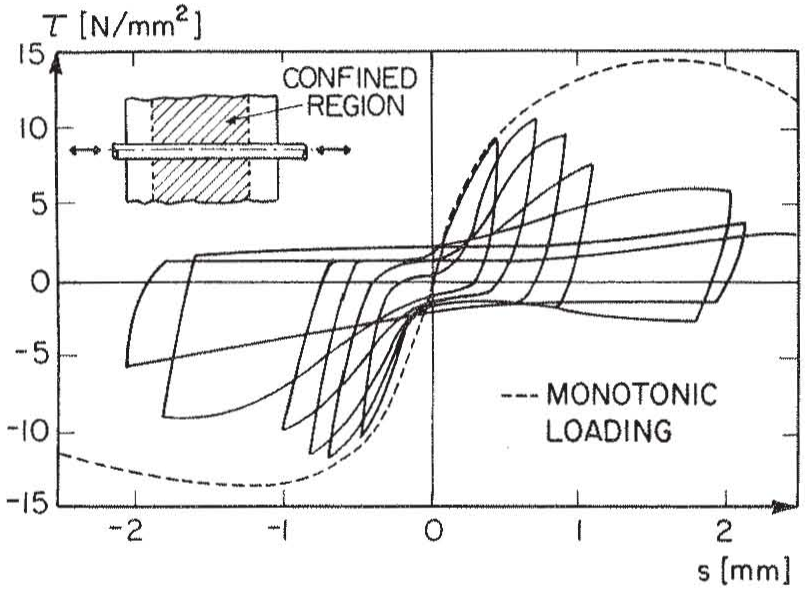

FIG. 2.9 LOCAL BOND STRESS-SLIP RELATIONSHIP FOR CONFINED CONCRETE UNDER CYCLIC LOADING (AFTER [8]).

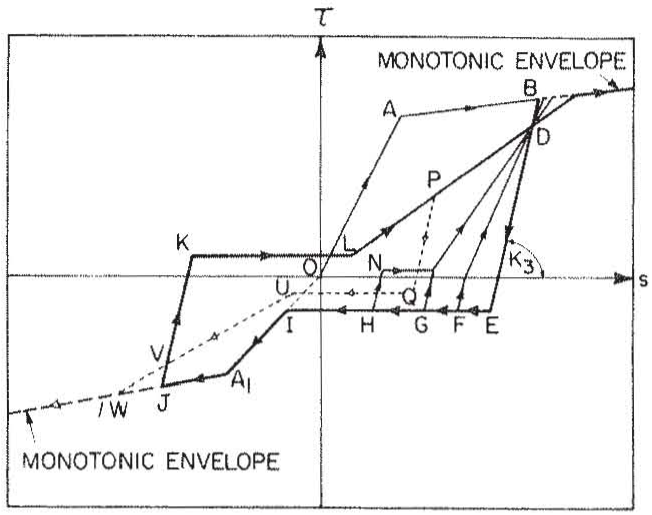

$\tau_D = \beta \cdot \tau_B$ $\tau_K = \alpha \cdot \tau_J$ $s_L = (s_B + s_J)/2$

$\tau_V = \beta \cdot \tau_J$ $\tau_N = \alpha \cdot \tau_H$ $s_U = (s_J + s_P)/2$

$\tau_E = \alpha \cdot \tau_B$ $\tau_Q = \alpha \cdot \tau_P$ $s_G = s_B/2$

$K_3 = 400\ N/mm^3$

$\alpha = 0.18$

$\beta = 0.9$ $s \leq 0.05$ mm

$\beta = 0.9 - 0.44\,(s - 0.05)$ $0.05 \leq s \leq 0.5$ mm

FIG. 2.10 ANALYTICAL MODEL FOR LOCAL BOND STRESS-SLIP RELATIONSHIP PROPOSED BY MORITA/KAKU [12]

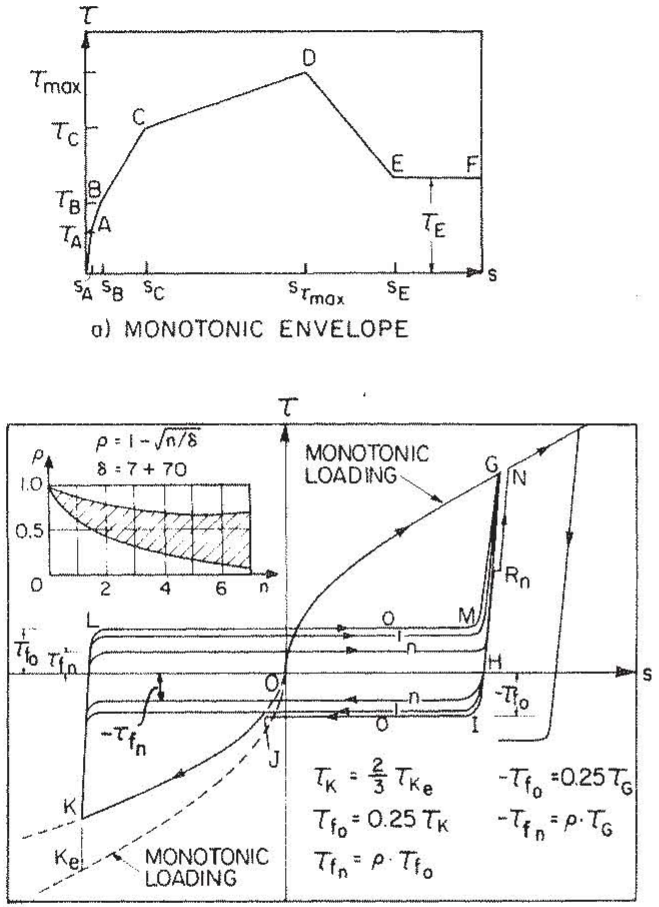

FIG. 2.11 ANALYTICAL MODEL FOR LOCAL BOND STRESS-SLIP RELATIONSHIP PROPOSED BY TASSIOS [9]

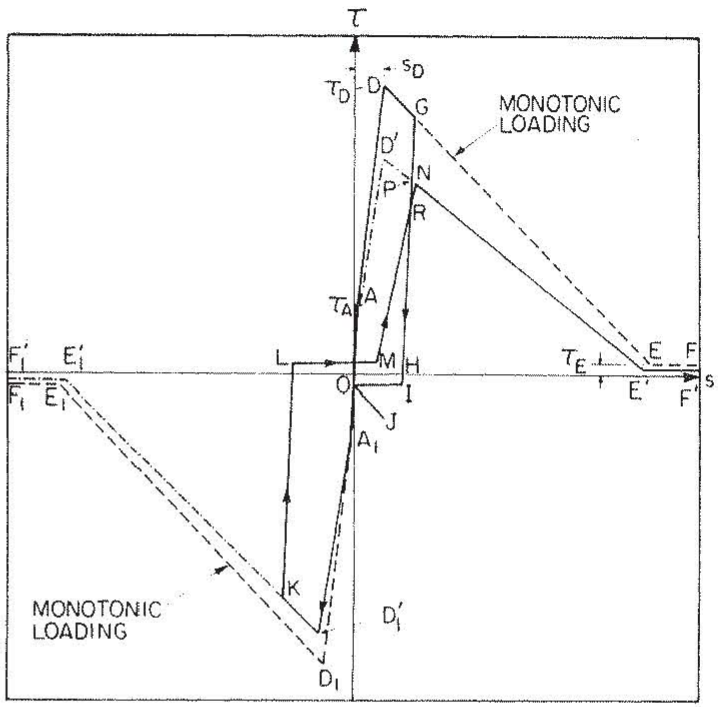

FIG. 2.12 ANALYTICAL MODEL FOR LOCAL BOND STRESS-SLIP RELATIONSHIP PROPOSED BY VIWATHANATEPA/ POPOV/BERTERO [8]

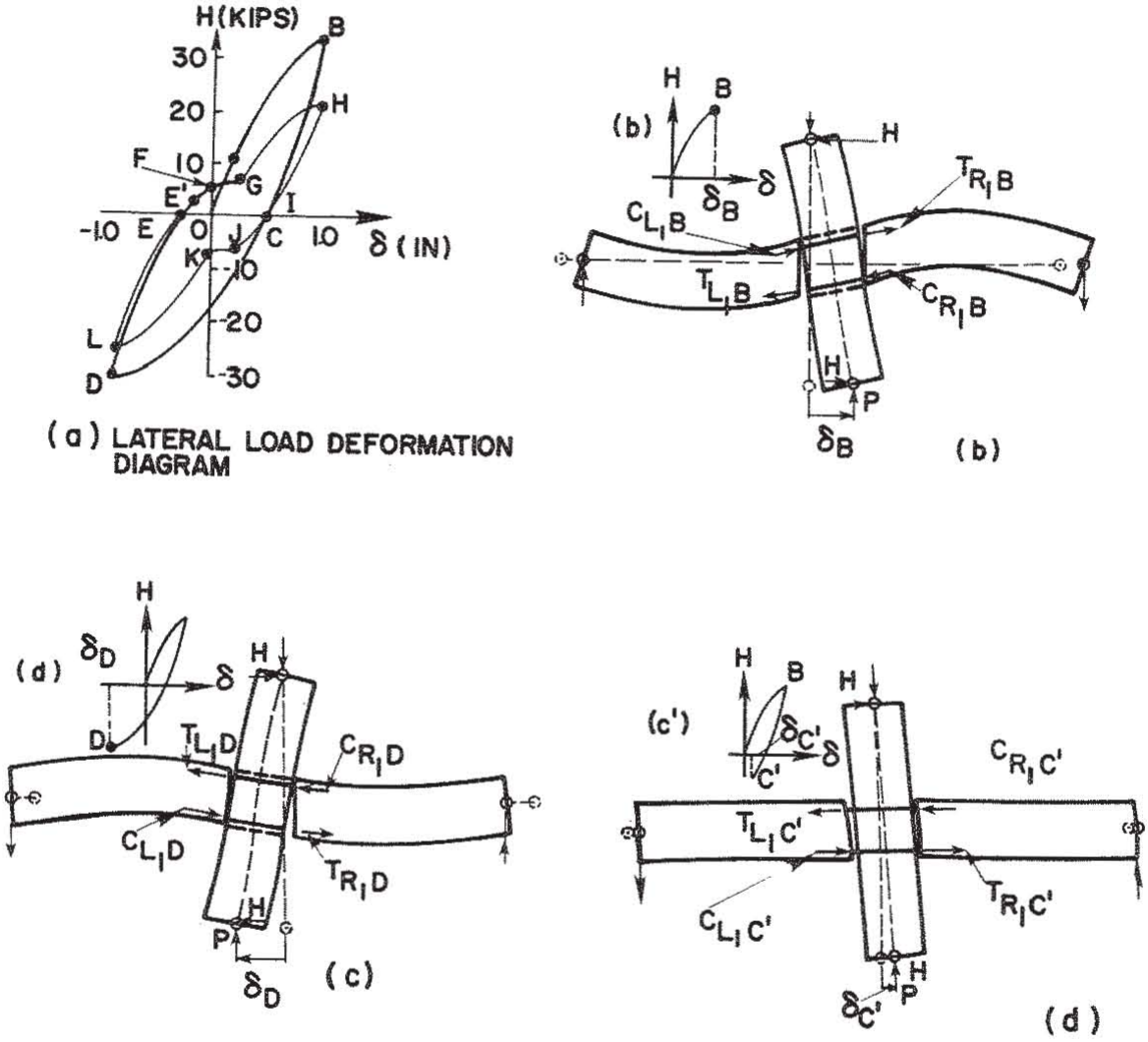

FIG. 3.1 MECHANISM OF DEGRADATION OF STIFFNESS AND STRENGTH OF AN INTERIOR JOINT (AFTER [36])

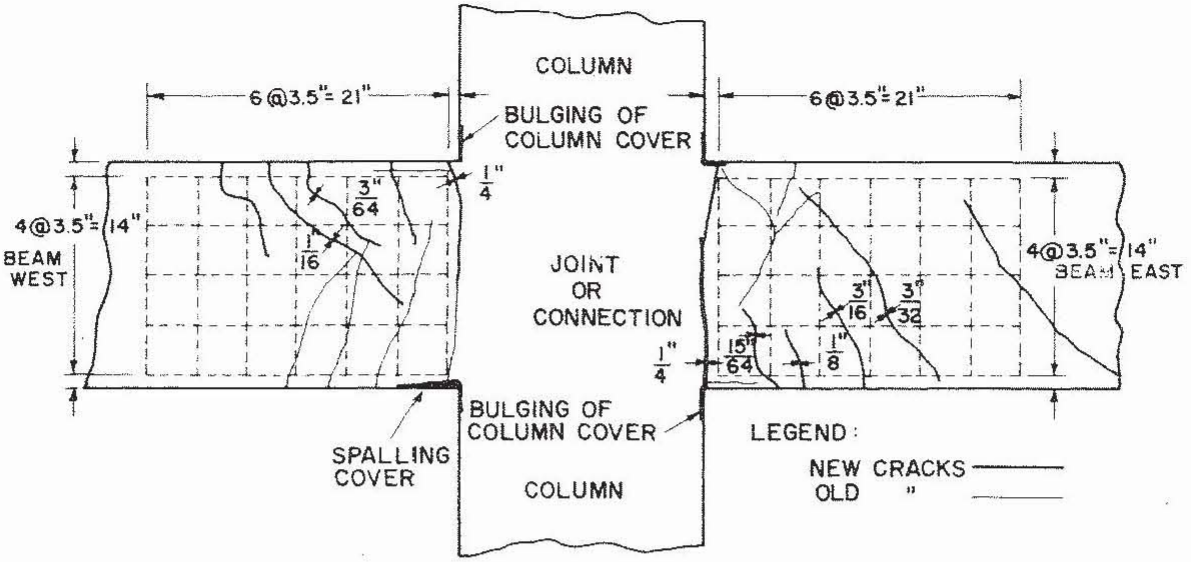

FIG. 3.2 MAJOR CRACKS IN SUBASSEMBLAGE BCU NEAR FAILURE (TAKEN FROM [37]).

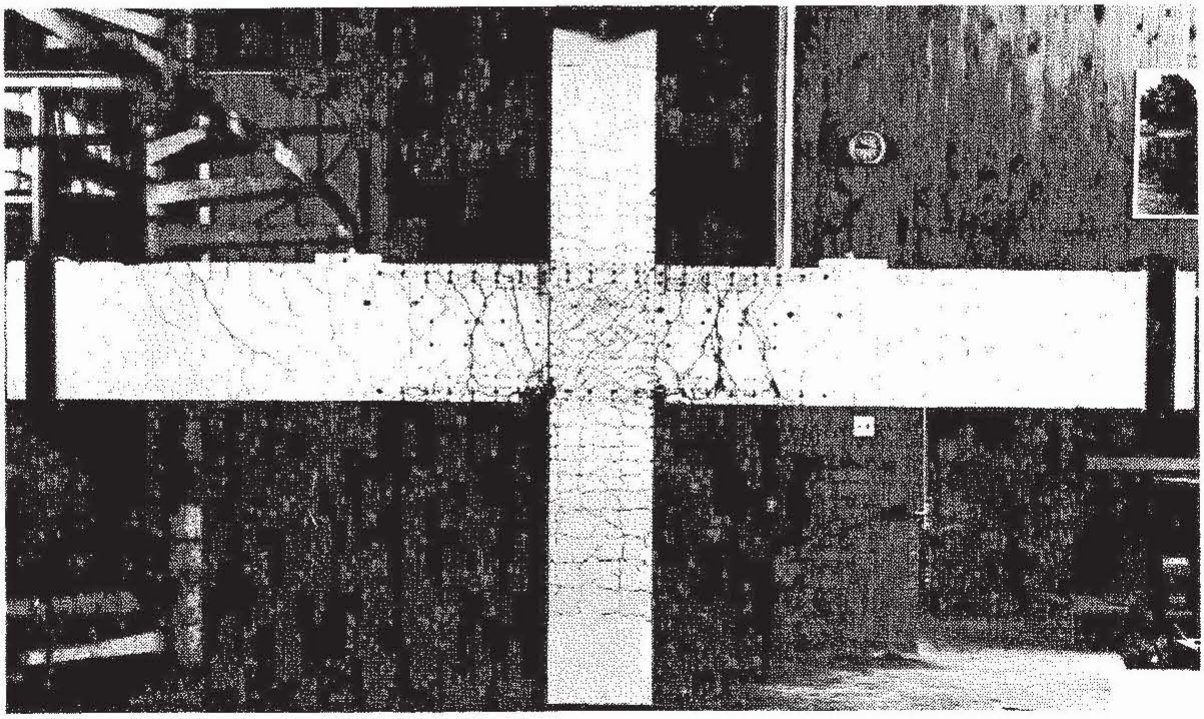

FIG. 3.3 AN INTERIOR BEAM-COLUMN JOINT AFTER SEVERAL INCREASING CYCLES OF REVERSED LOADING (Courtesy of Professor T. Paulay)

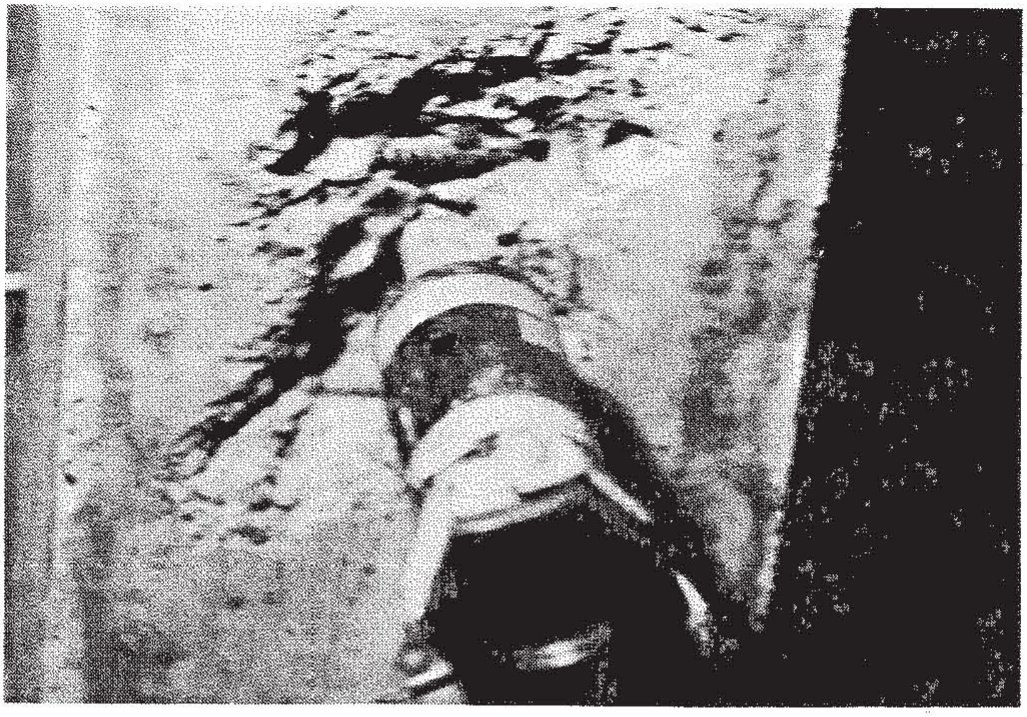

(a) PHOTO OF SPECIMEN AFTER BREAK OUT OF CONCRETE CONE.

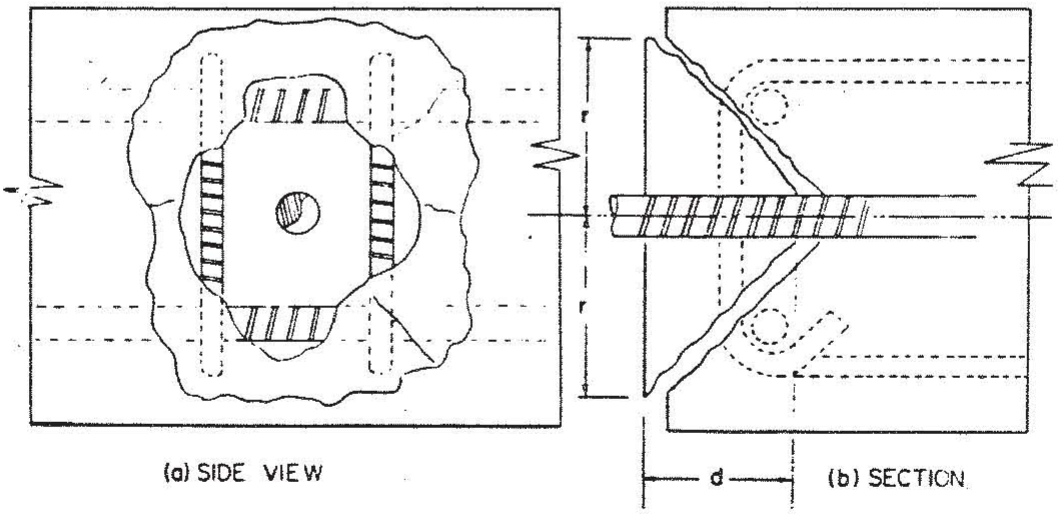

(b) GEOMETRY OF CONCRETE CONE

FIG. 3.4 FORMATION OF CONCRETE CONE IN PULLOUT SPECIMEN (TAKEN FROM [8]).

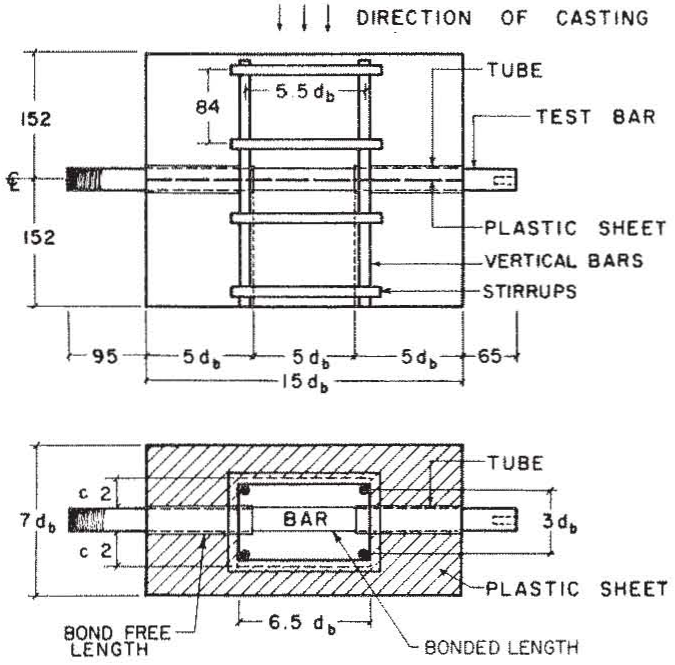

FIG. 3.5 TEST SPECIMEN

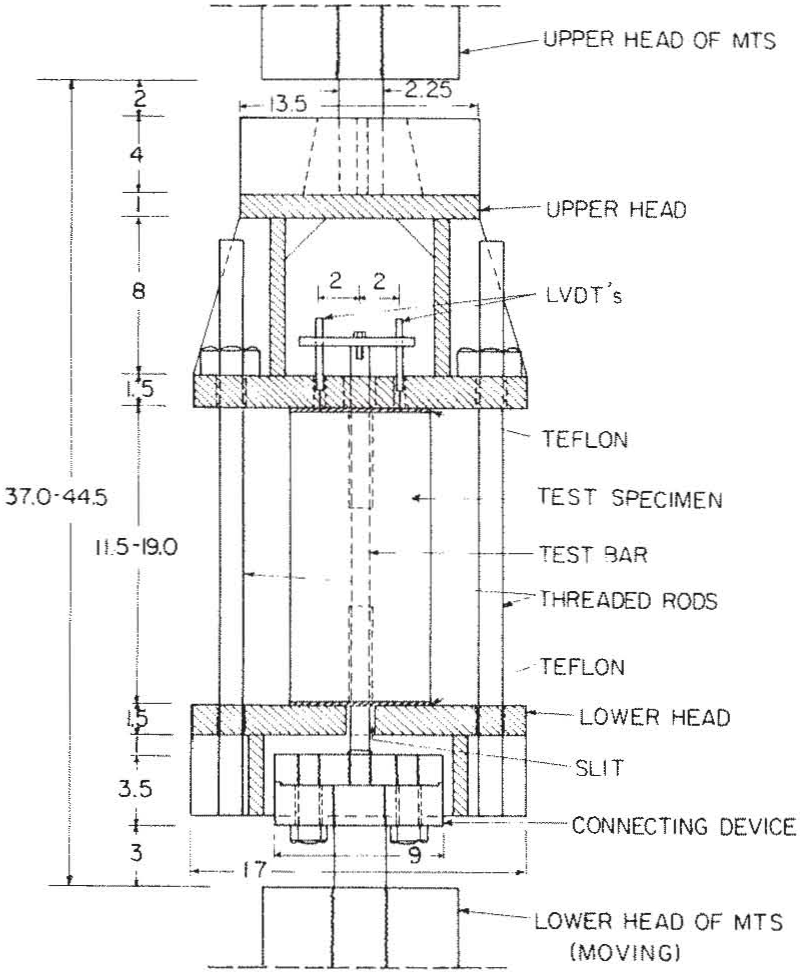

MEASUREMENTS IN INCHES

FIG. 3.6 TEST SETUP

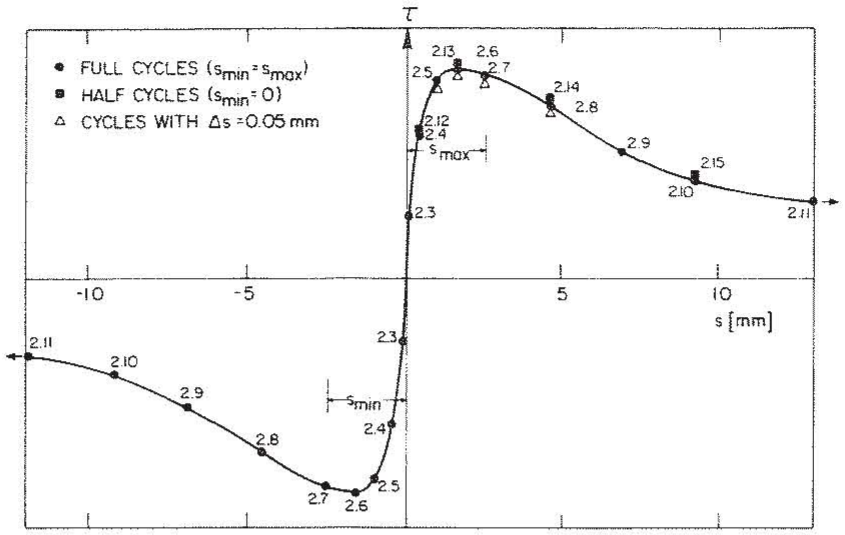

FIG. 3.7 HISTORIES OF SLIP FOR CYCLIC TESTS (SERIES 2)

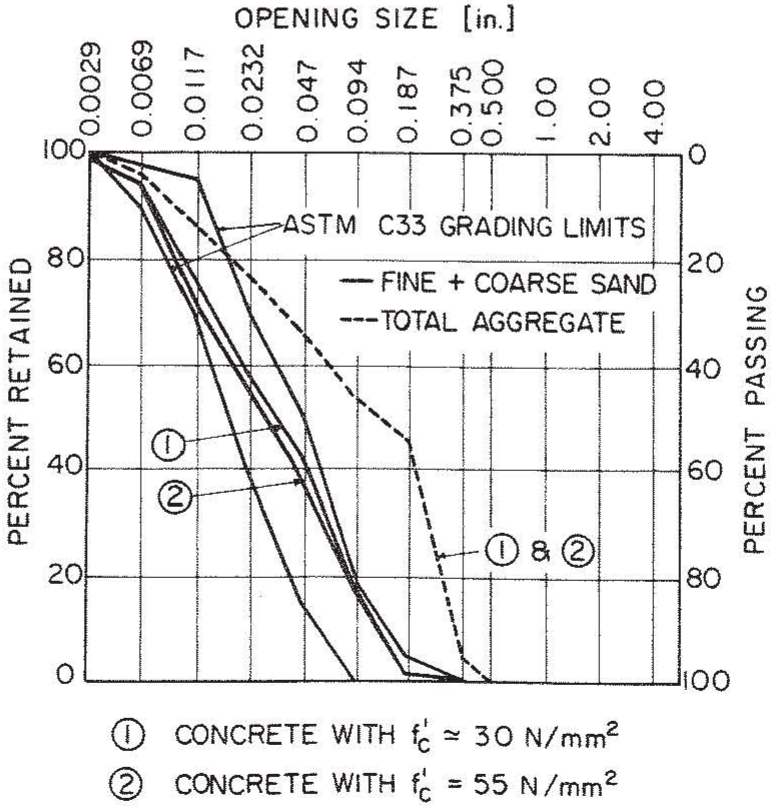

FIG. 3.8 AGGREGATE GRADING

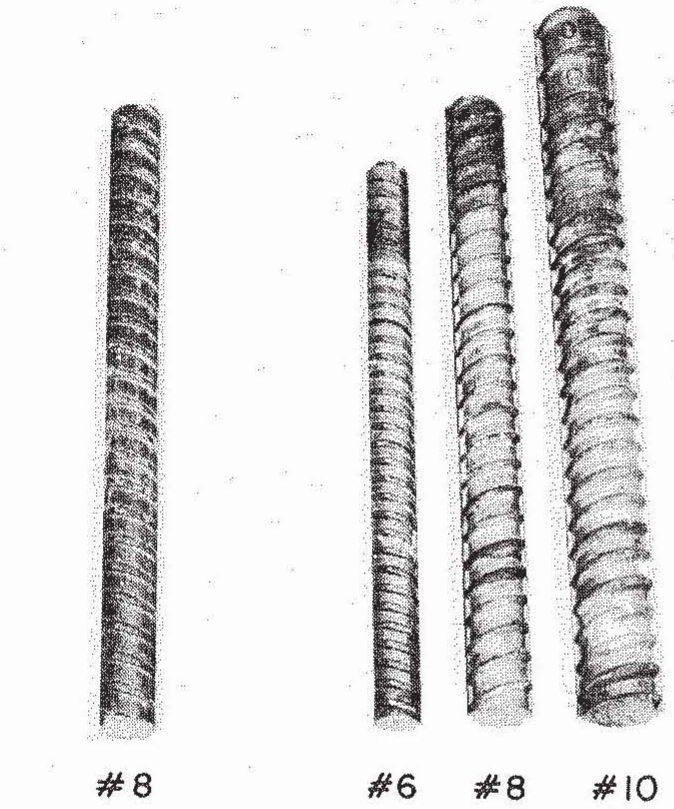

FIG. 3.9 PHOTO OF TEST BARS.

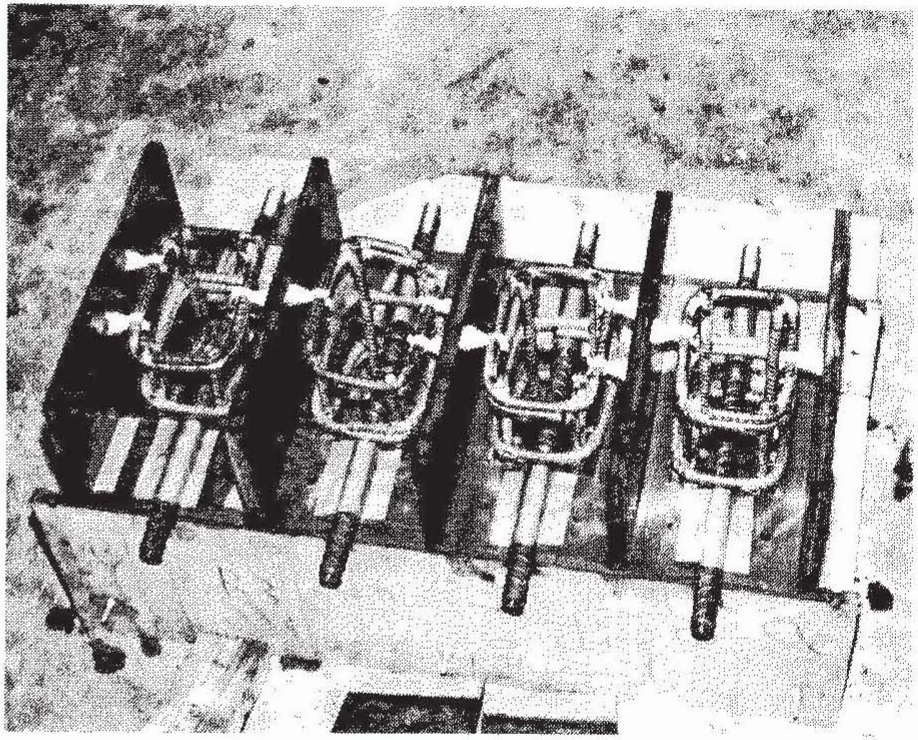

FIG. 3.10 PHOTO OF SPECIMENS PRIOR TO CASTING (FRONT AND BACK SIDES OF FORMS NOT IN PLACE).

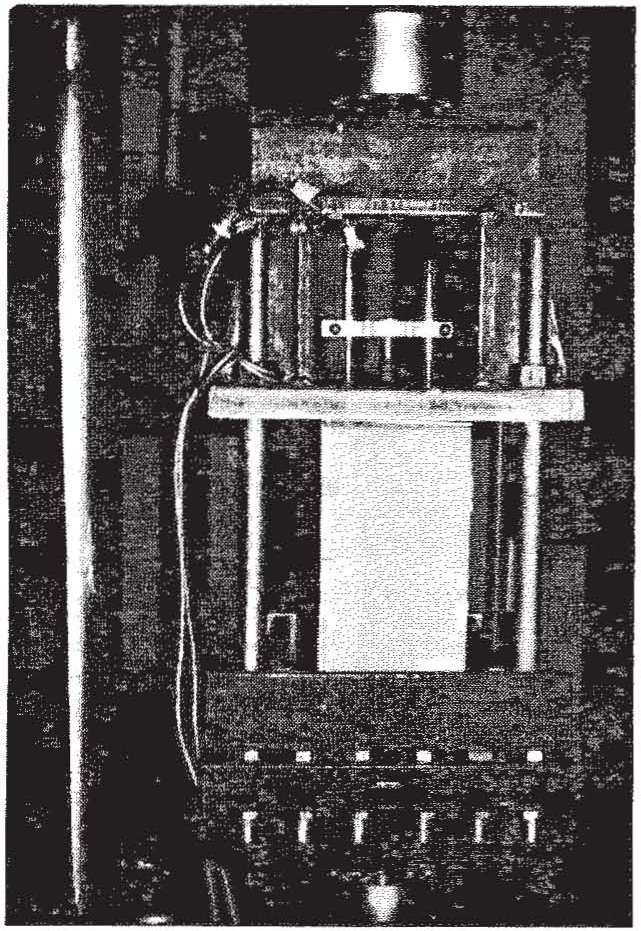

FIG. 3.11 PHOTO OF TEST SPECIMEN PREPARED FOR A TENSION TEST.

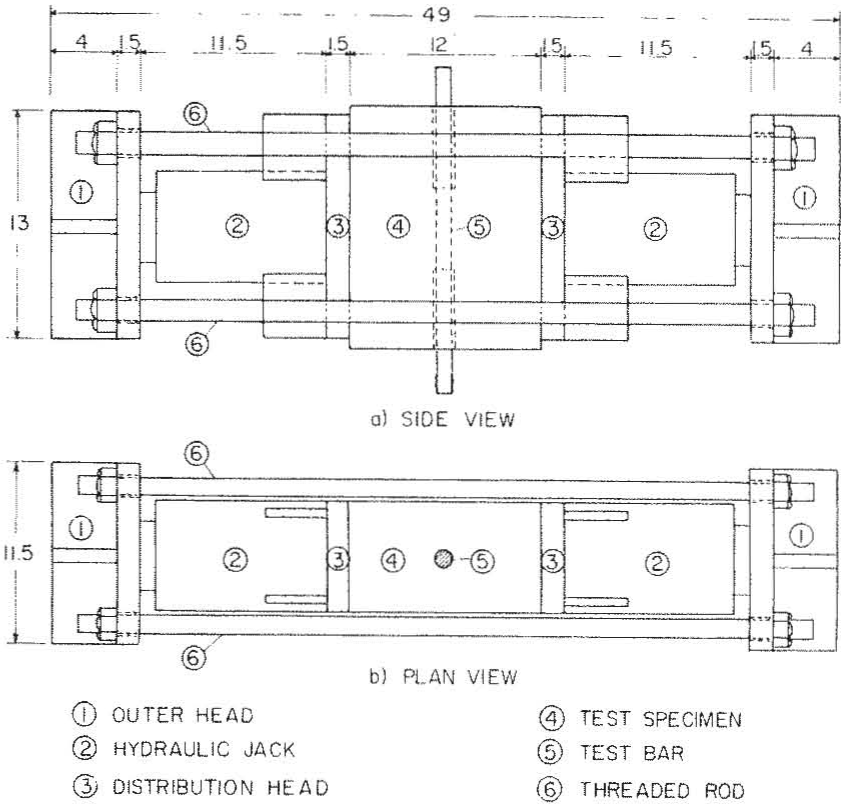

FIG. 3.12 DEVICE FOR APPLYING TRANSVERSE PRESSURE

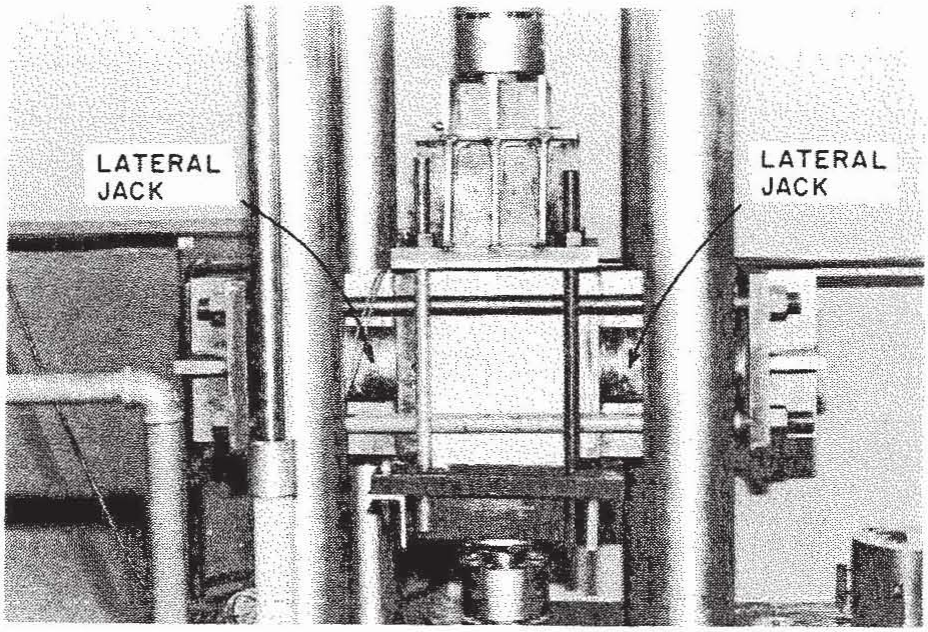

FIG. 3.13 PHOTO OF TEST SPECIMEN IN MACHINE WITH TRANSVERSE PRESSURE APPLIED.

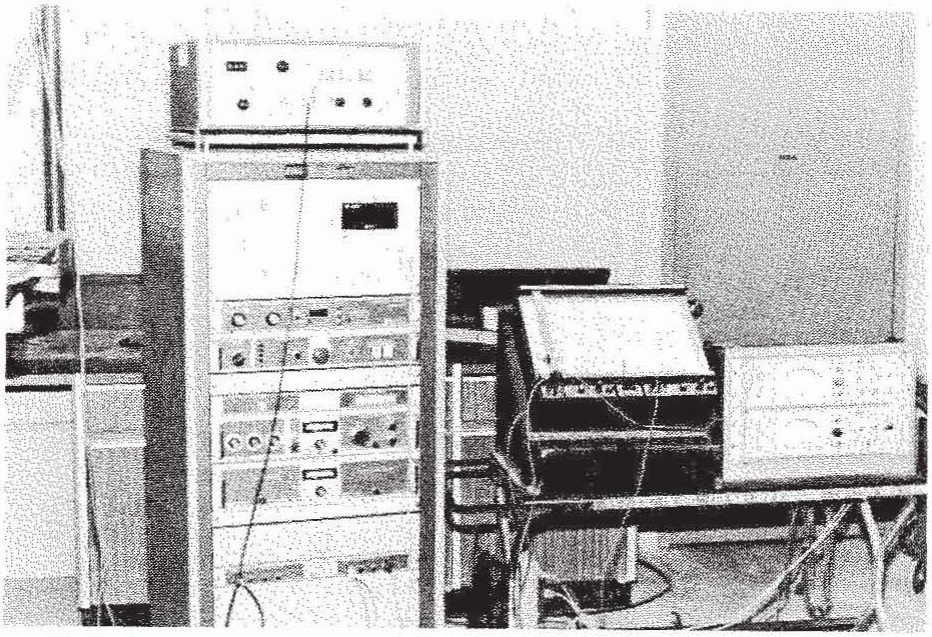

FIG. 3.14 PHOTO OF CONSOLE AND RECORDING DEVICES.

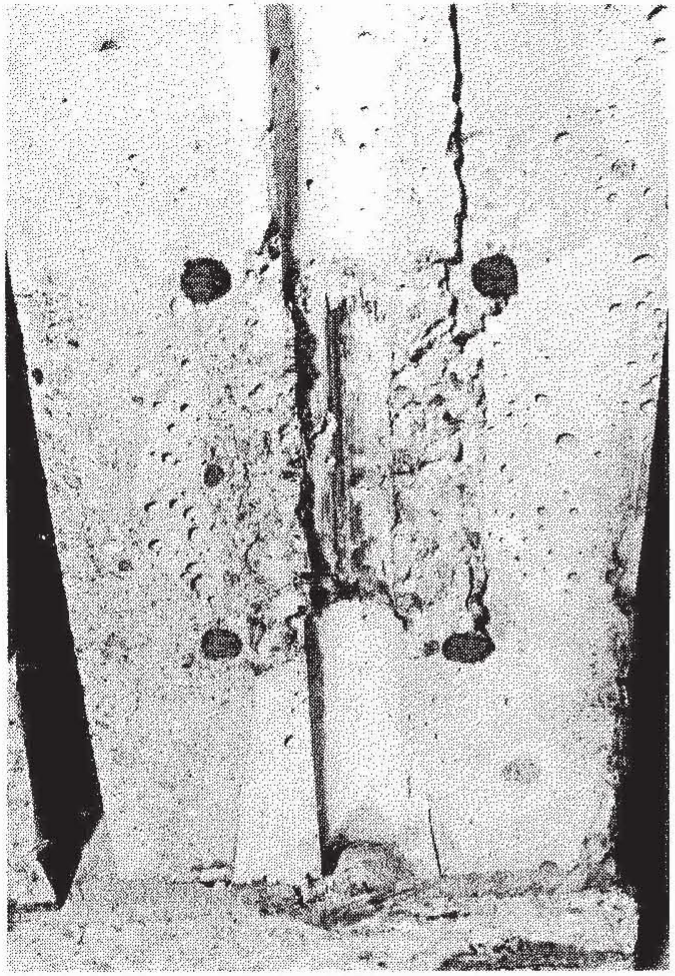

FIG. 4.1 PHOTO OF SAWN SPECIMEN AFTER TESTING. FAILURE BY PULLOUT.

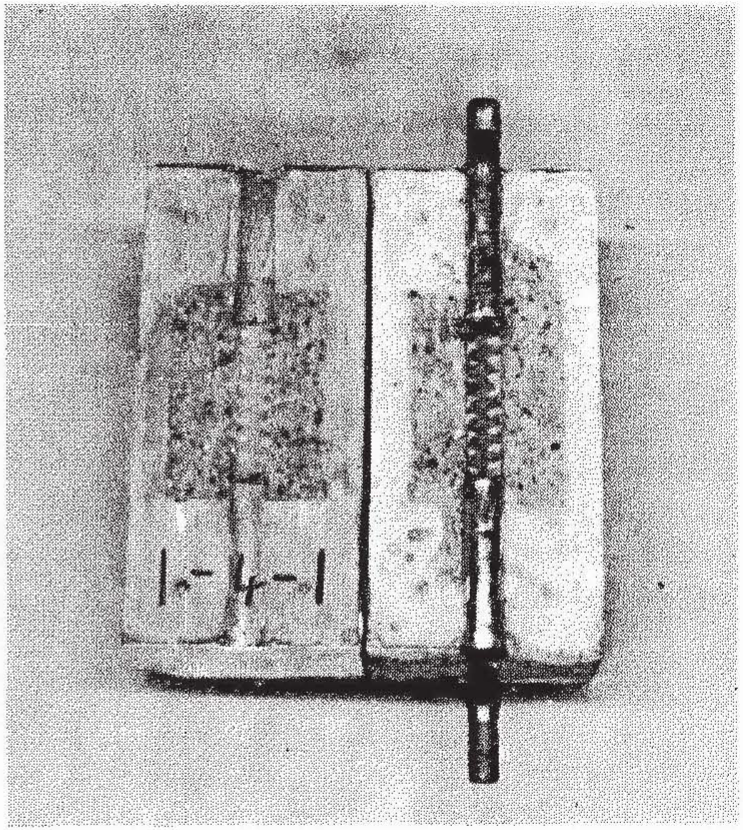

FIG. 4.2 PHOTO OF A SPECIMEN FROM SERIES 1.4. FAILURE BY SPLITTING.

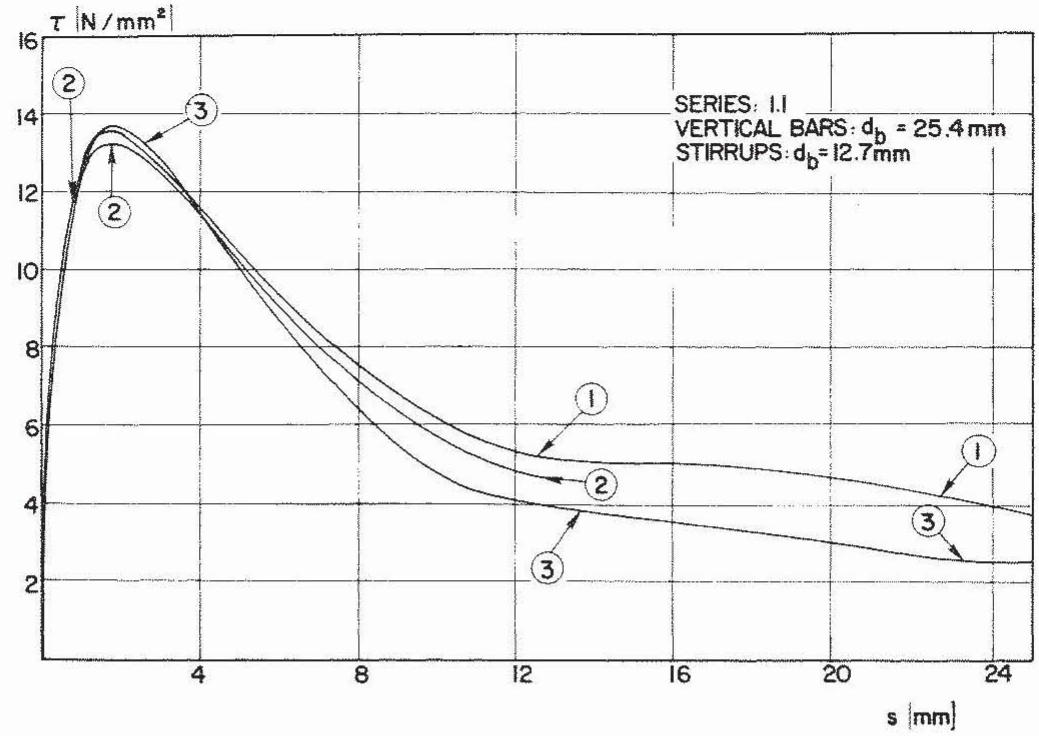

FIG. 4.3 BOND STRESS-SLIP RELATIONSHIP FOR TEST SERIES 1.1

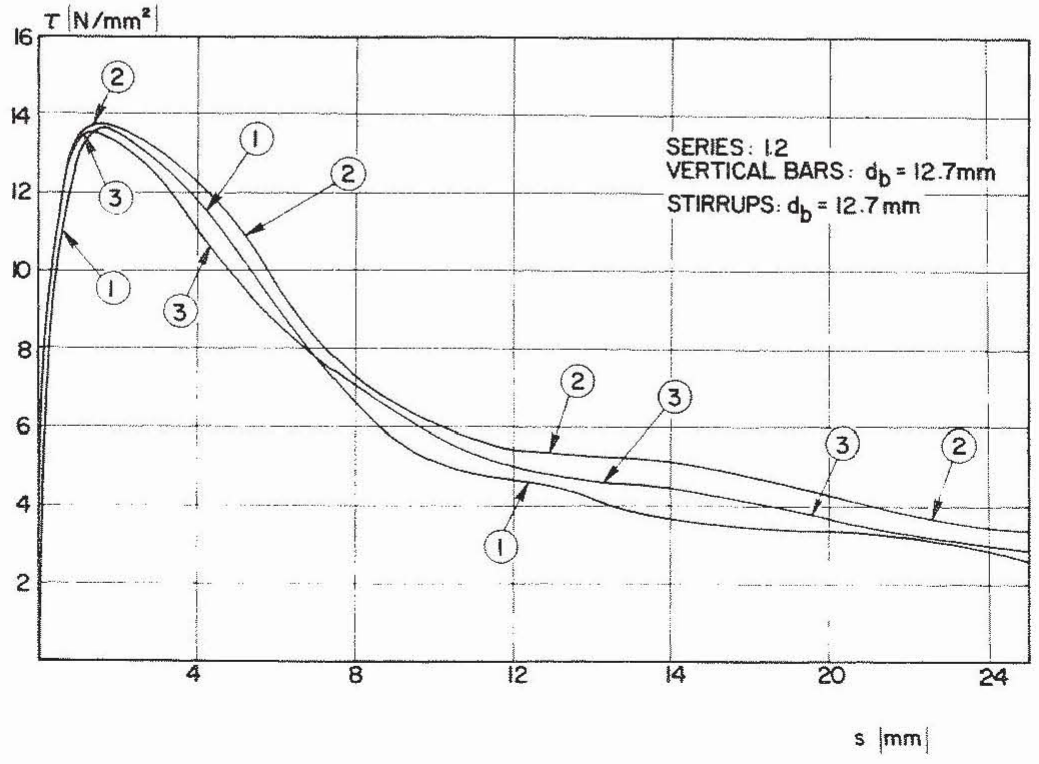

FIG. 4.4 BOND STRESS-SLIP RELATIONSHIP FOR TEST SERIES 1.2

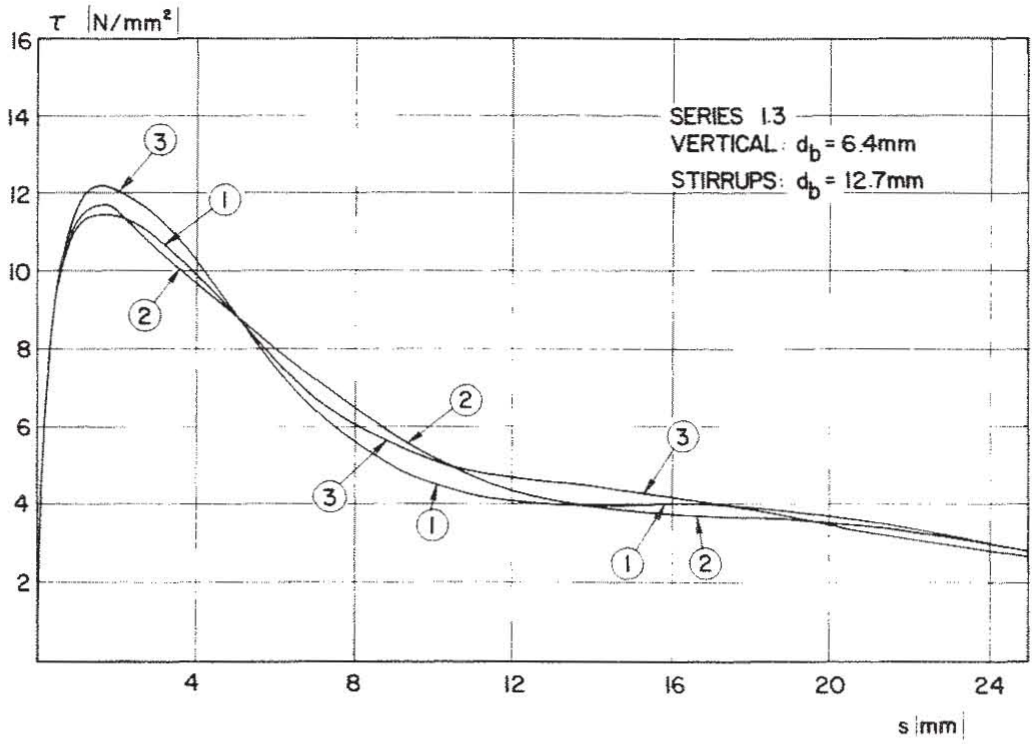

FIG. 4.5 BOND STRESS-SLIP RELATIONSHIP FOR TEST SERIES 1.3

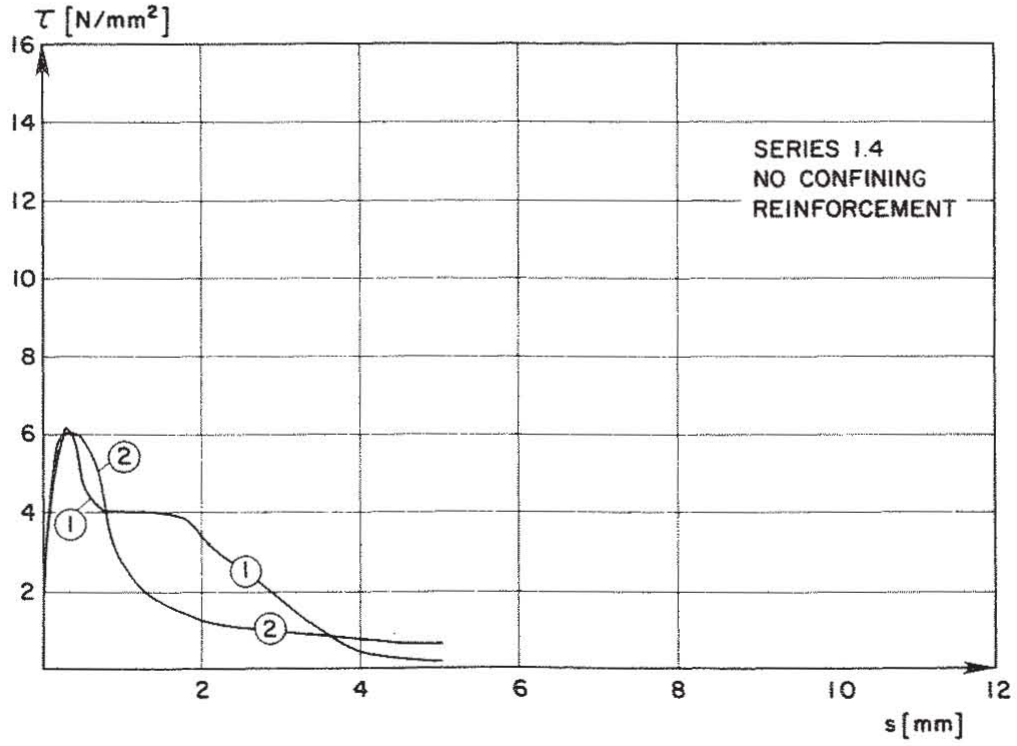

FIG. 4.6 BOND STRESS-SLIP RELATIONSHIP FOR TEST SERIES 1.4

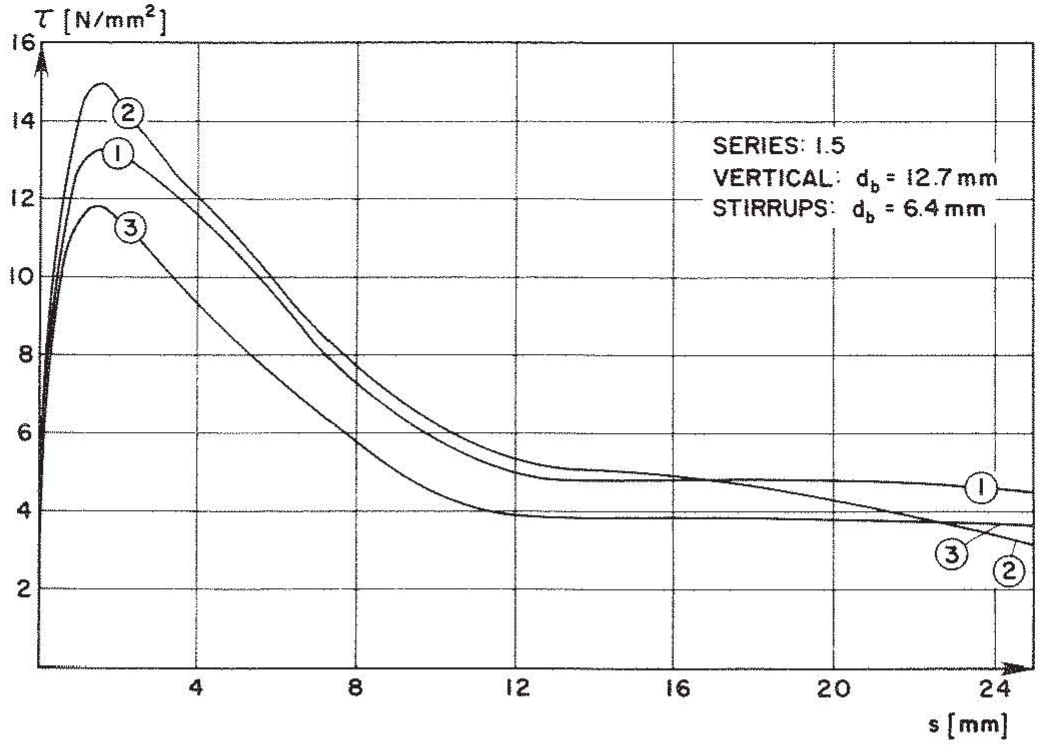

FIG. 4.7 BOND STRESS-SLIP RELATIONSHIP FOR TEST SERIES 1.5

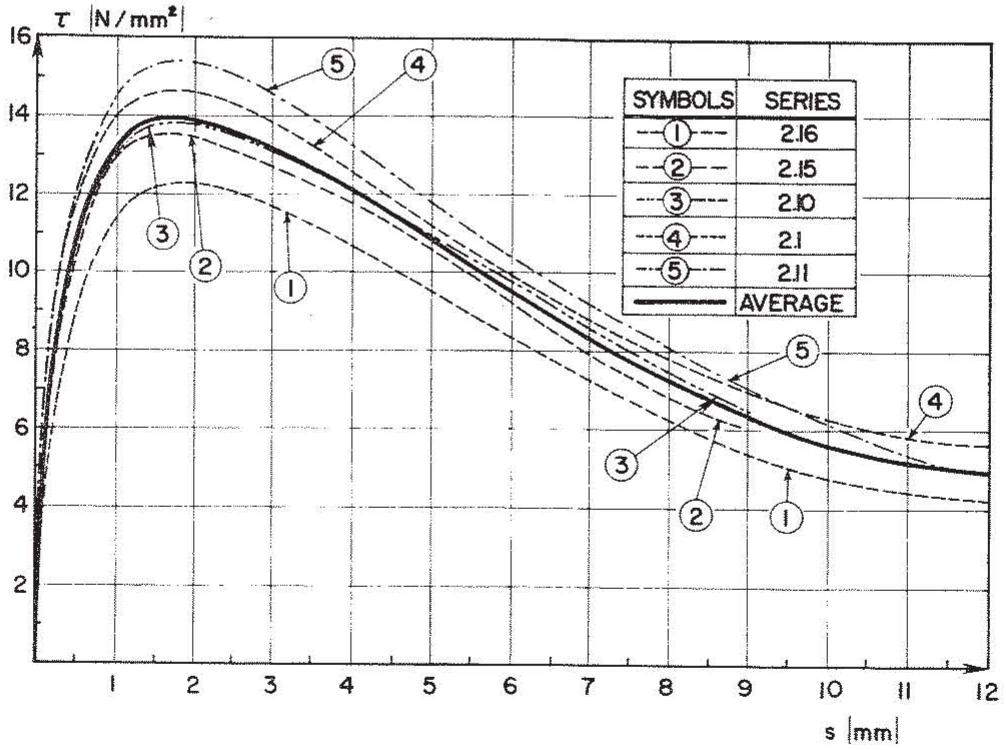

FIG. 4.8 BOND STRESS-SLIP RELATIONSHIP FOR ALL MONOTONIC TESTS OF SERIES 2

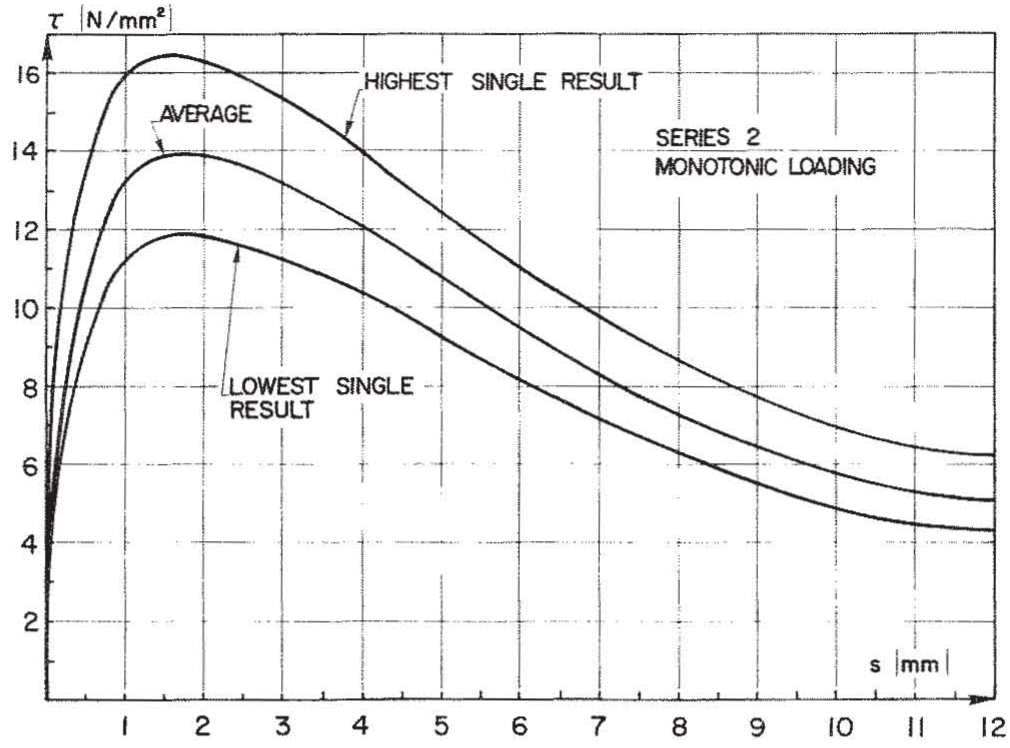

FIG. 4.9 SCATTER OF MEASURED BOND STRESS-SLIP RELATIONSHIPS OF TEST SERIES 2

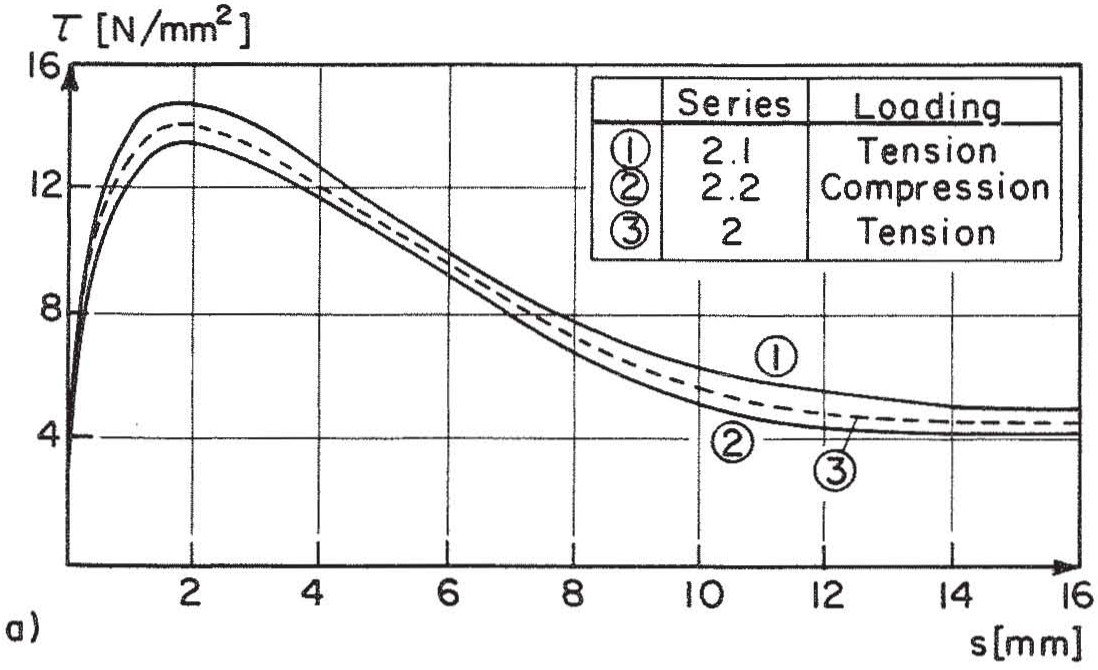

(a) FULL RANGE OF SLIP

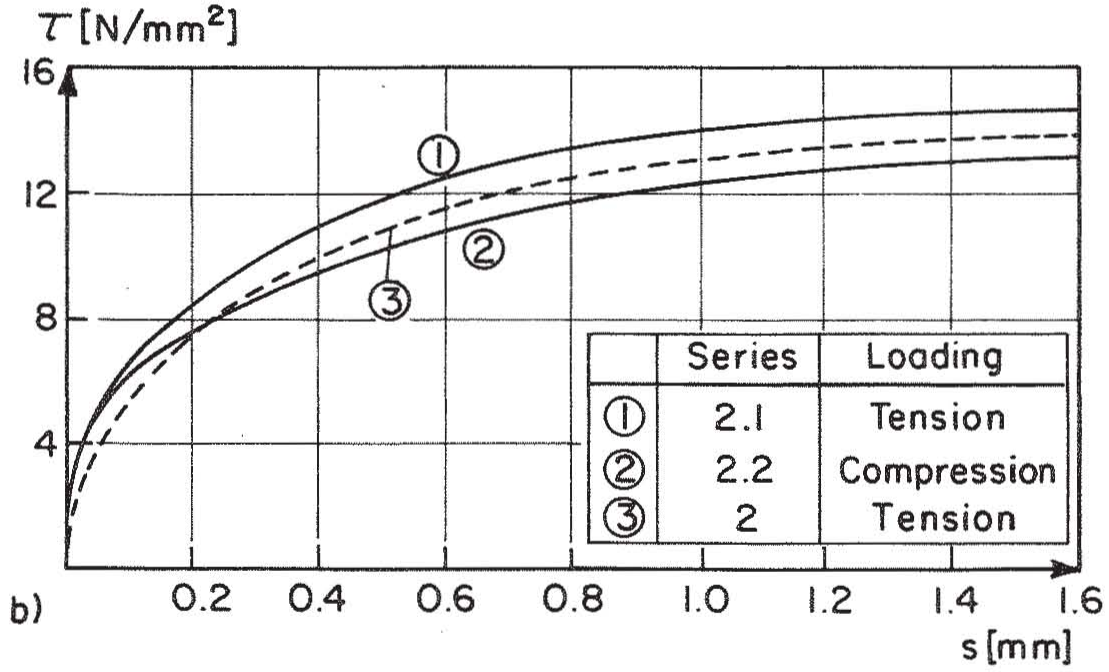

(b) ASCENDING BRANCH OF BOND STRESS-SLIP RELATIONSHIP

FIG. 4.10 INFLUENCE OF DIRECTION OF LOADING (TENSION OR COMPRESSION) ON BOND STRESS-SLIP RELATIONSHIP

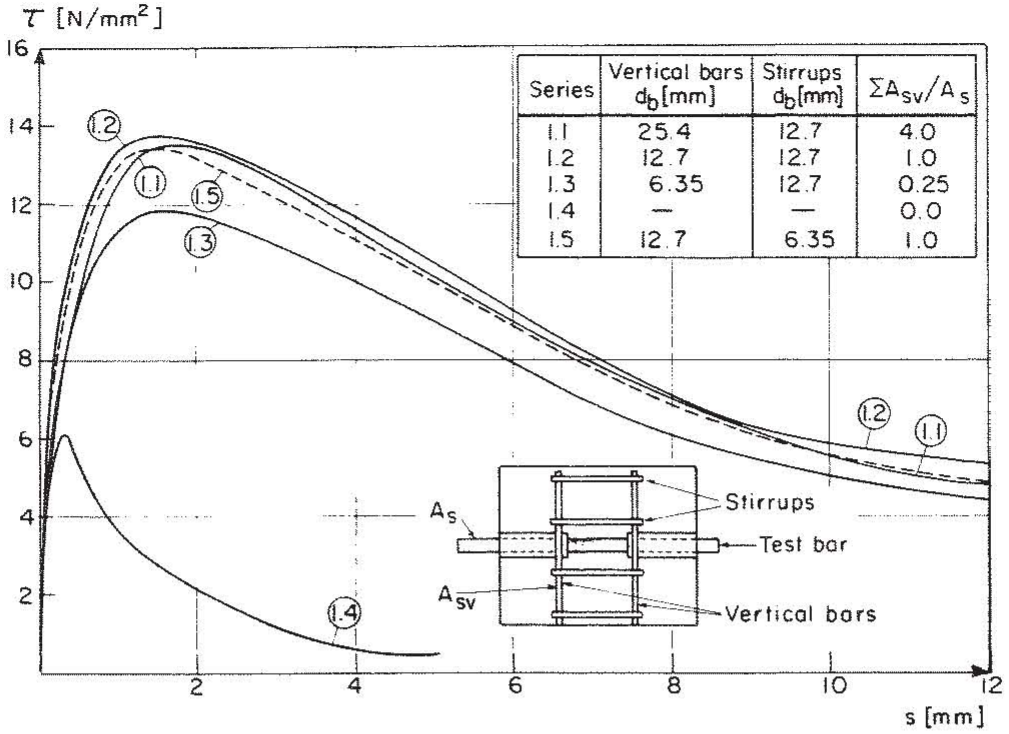

(a) FULL RANGE OF SLIP

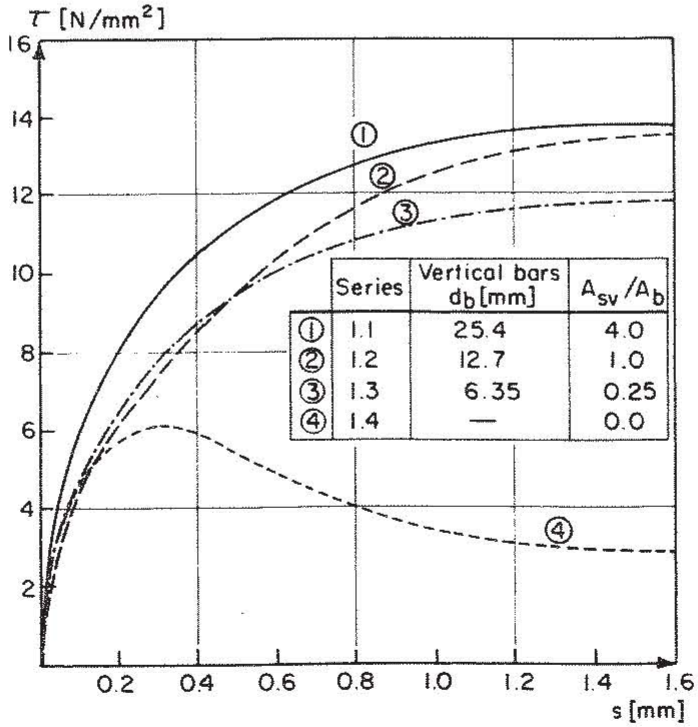

(b) ASCENDING BRANCH OF BOND STRESS-SLIP RELATIONSHIP

FIG. 4.11 INFLUENCE OF TRANSVERSE REINFORCEMENT ON BOND STRESS-SLIP RELATIONSHIP

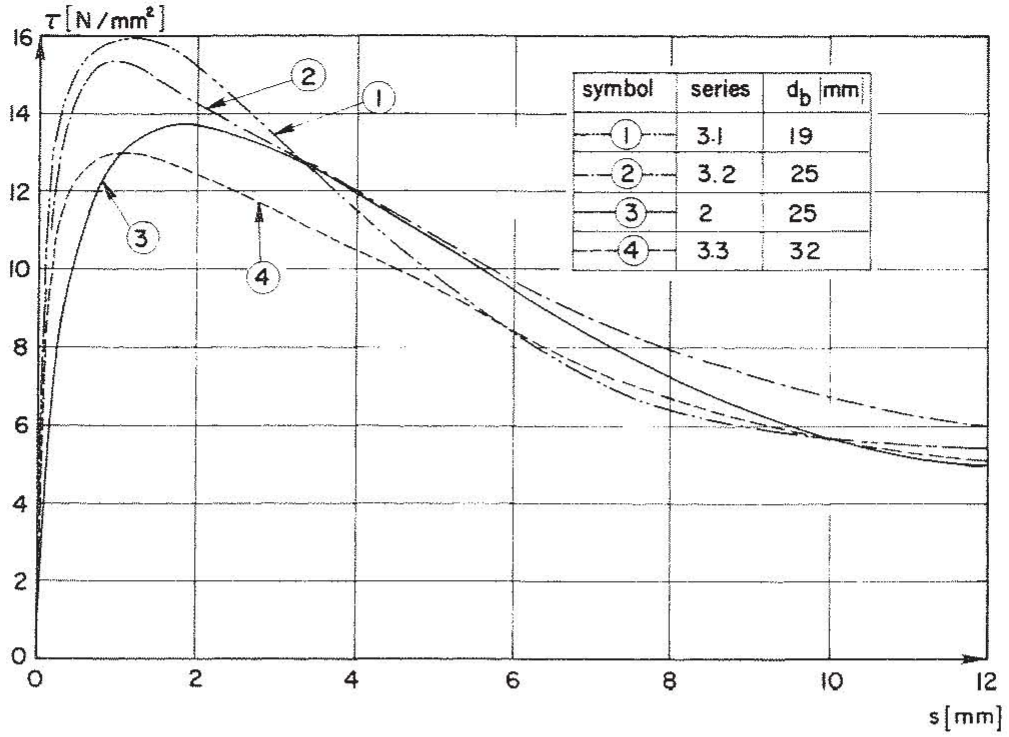

(a) FULL RANGE OF SLIP

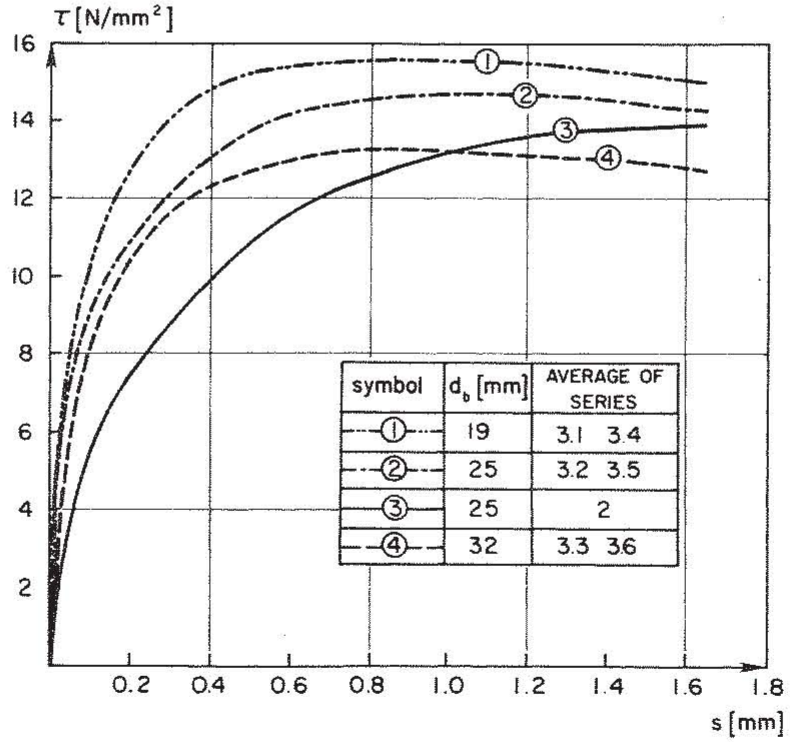

(b) ASCENDING BRANCH OF BOND STRESS-SLIP RELATIONSHIP

FIG. 4.12 INFLUENCE OF BAR DIAMETER AND DEFORMATION PATTERN ON BOND STRESS-SLIP RELATIONSHIP

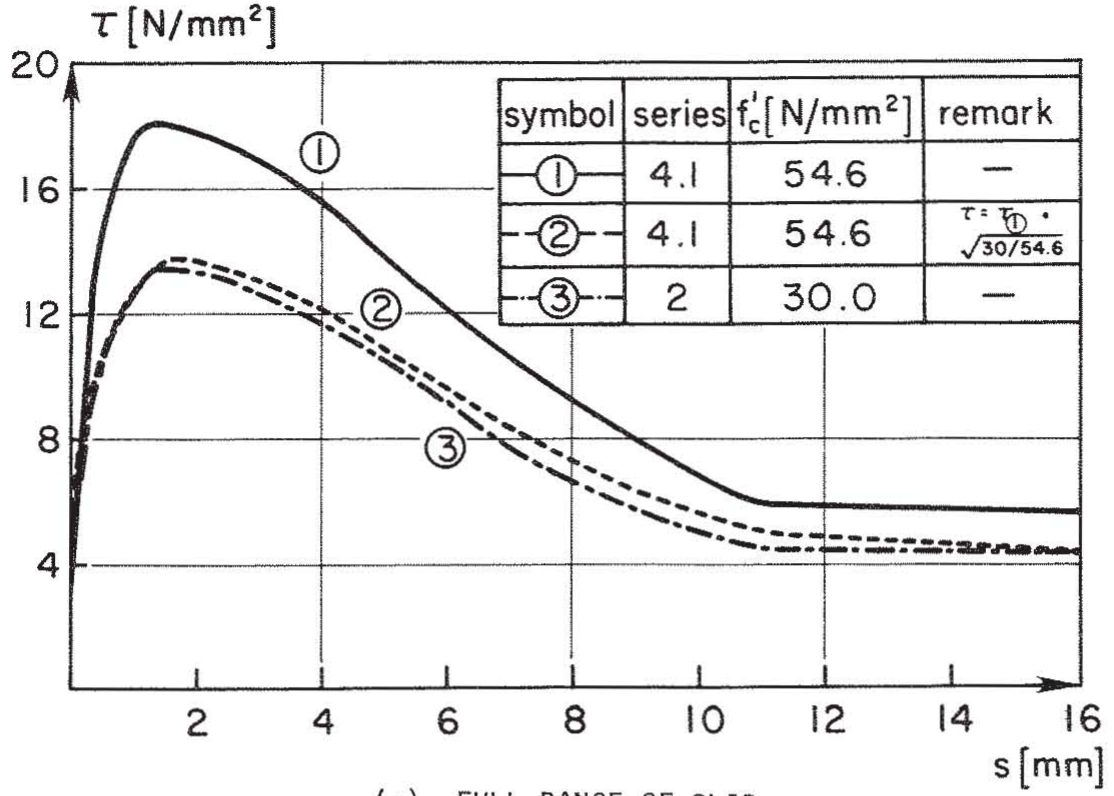

(a) FULL RANGE OF SLIP

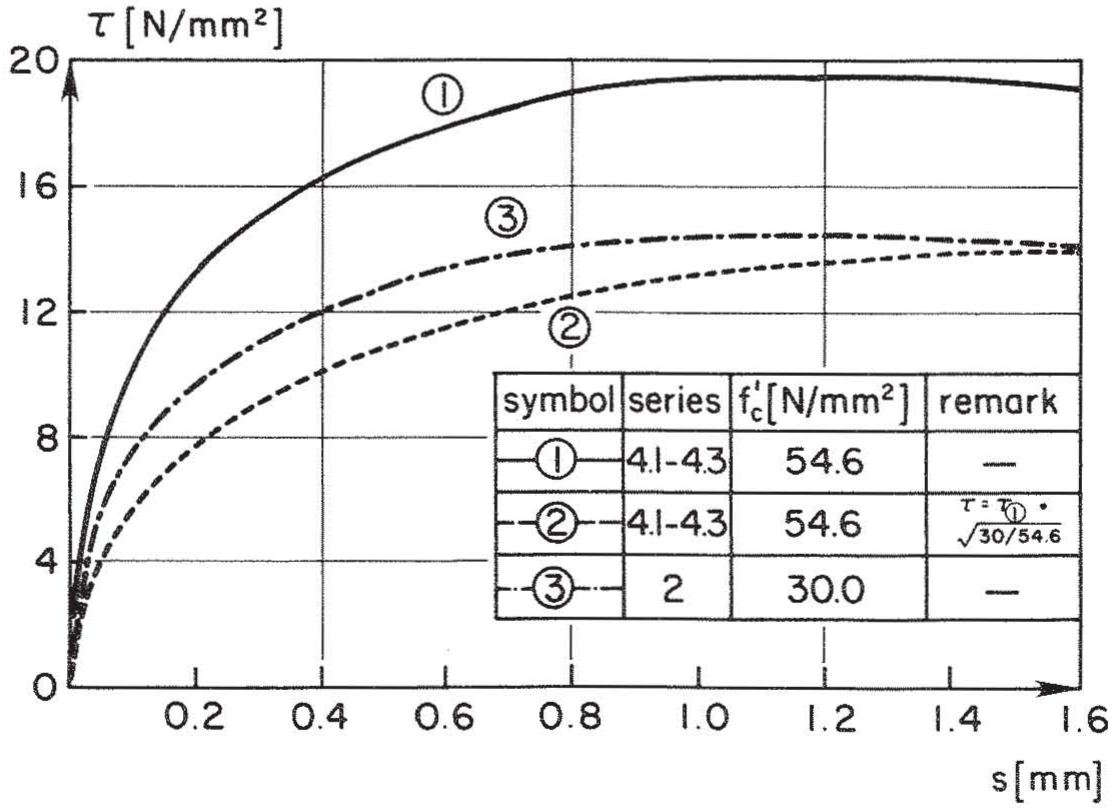

(b) ASCENDING BRANCH OF BOND STRESS-SLIP RELATIONSHIP

FIG. 4.13 INFLUENCE OF CONCRETE STRENGTH ON BOND STRESS-SLIP RELATIONSHIP

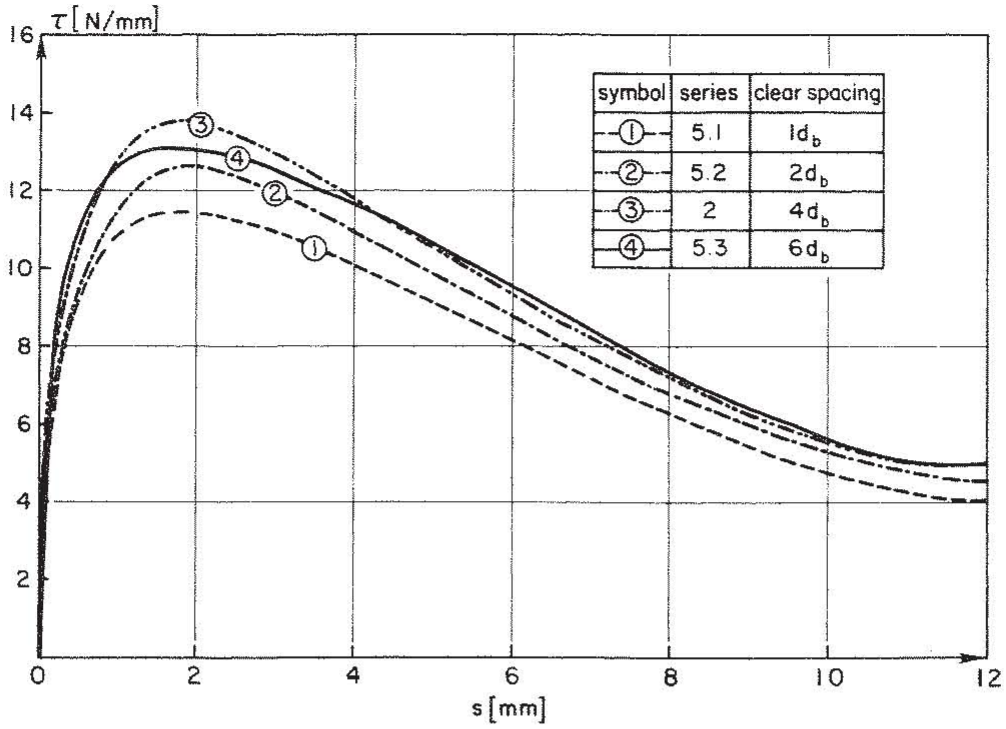

(a) FULL RANGE OF SLIP

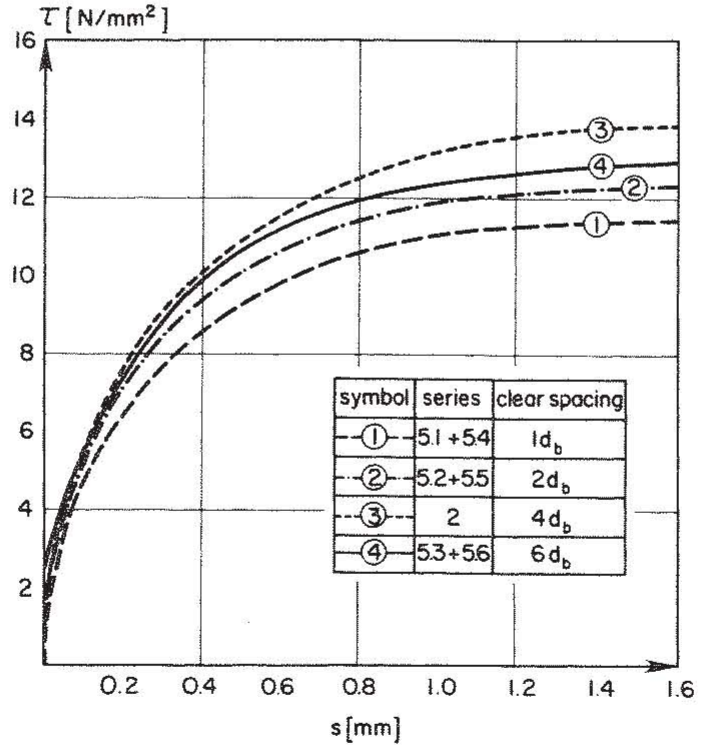

(b) ASCENDING BRANCH OF BOND STRESS-SLIP RELATIONSHIP

FIG. 4.14 INFLUENCE OF CLEAR DISTANCE BETWEEN BARS ON BOND STRESS-SLIP RELATIONSHIP

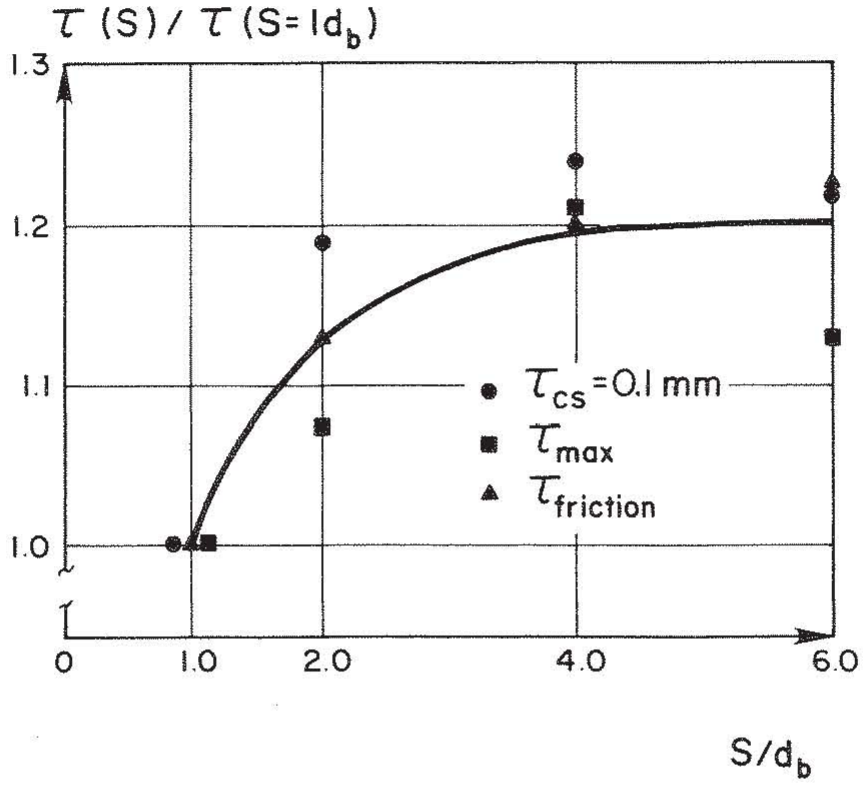

FIG. 4.15 INFLUENCE OF CLEAR BAR SPACING S/d_b ON BOND RESISTANCE

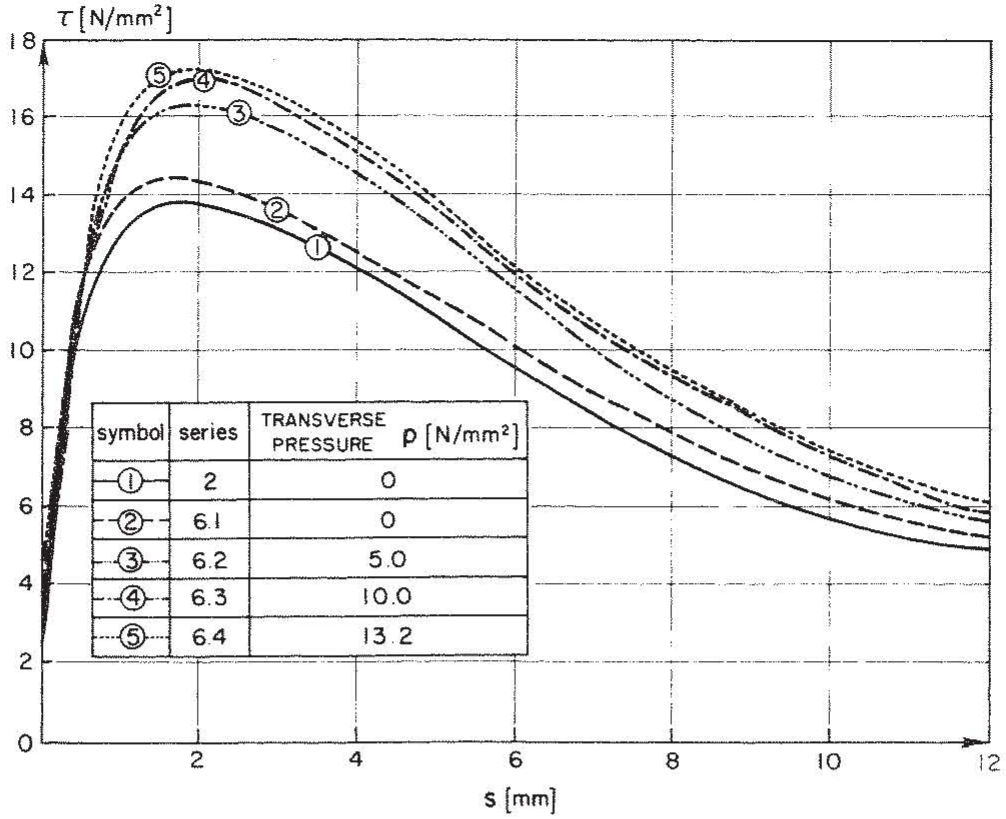

(a) FULL RANGE OF SLIP

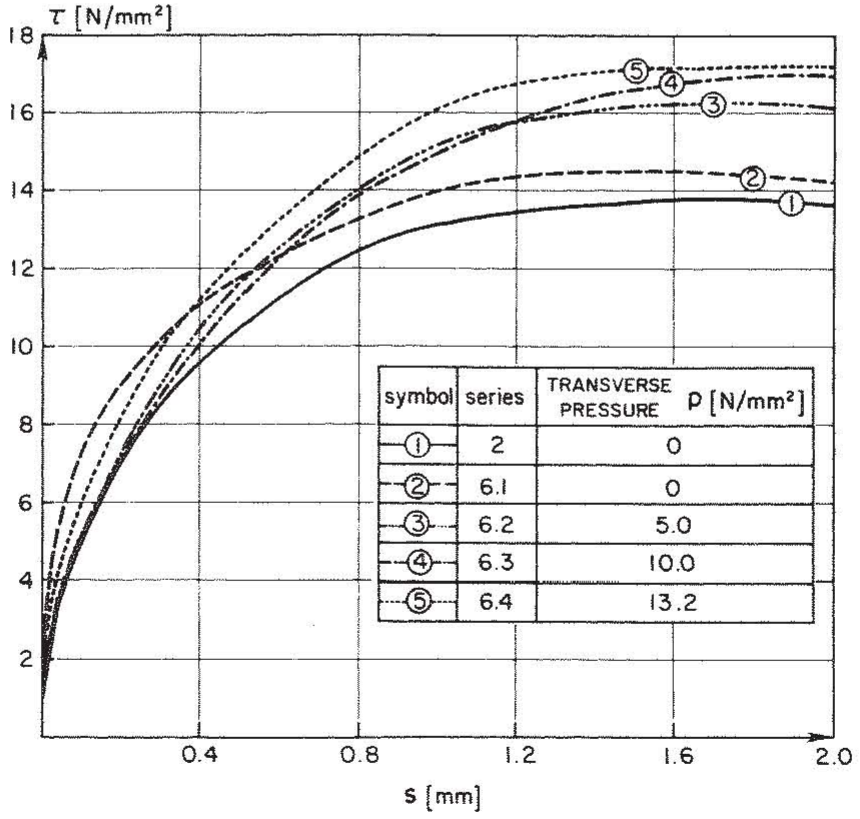

(b) ASCENDING BRANCH OF BOND STRESS-SLIP RELATIONSHIP

FIG. 4.16 INFLUENCE OF TRANSVERSE PRESSURE P ON BOND STRESS-SLIP RELATIONSHIP

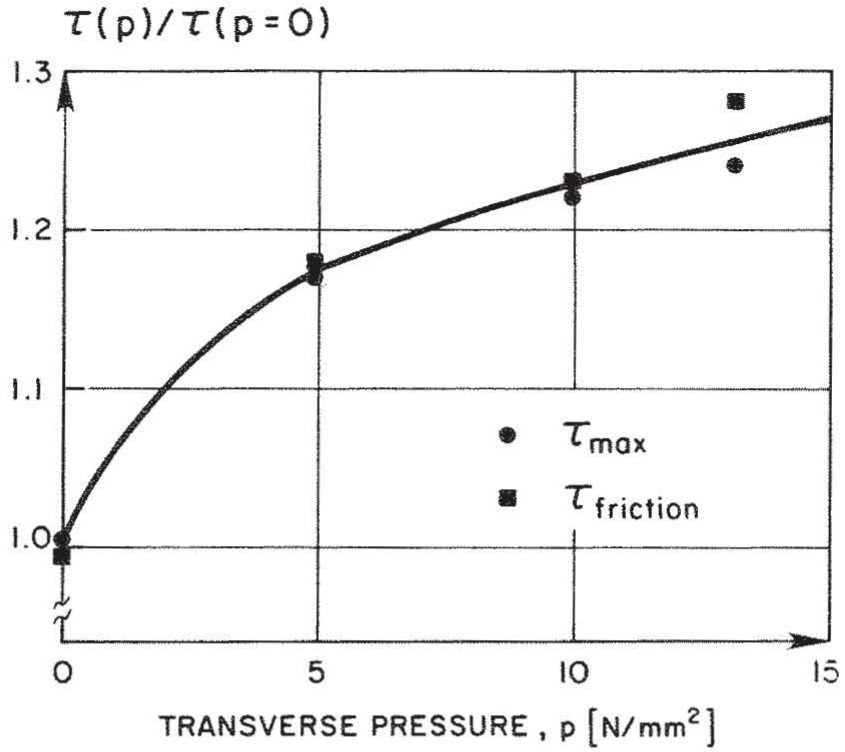

FIG. 4.17 INFLUENCE OF TRANSVERSE PRESSURE P ON BOND RESISTANCE

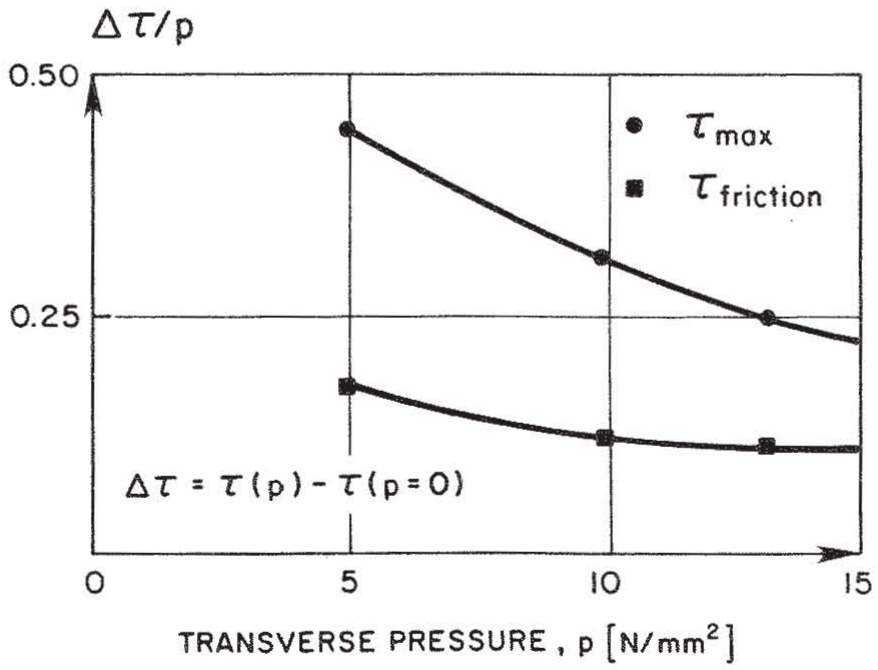

FIG. 4.18 INFLUENCE OF TRANSVERSE PRESSURE P ON COEFFICIENT $\Delta\tau/p$

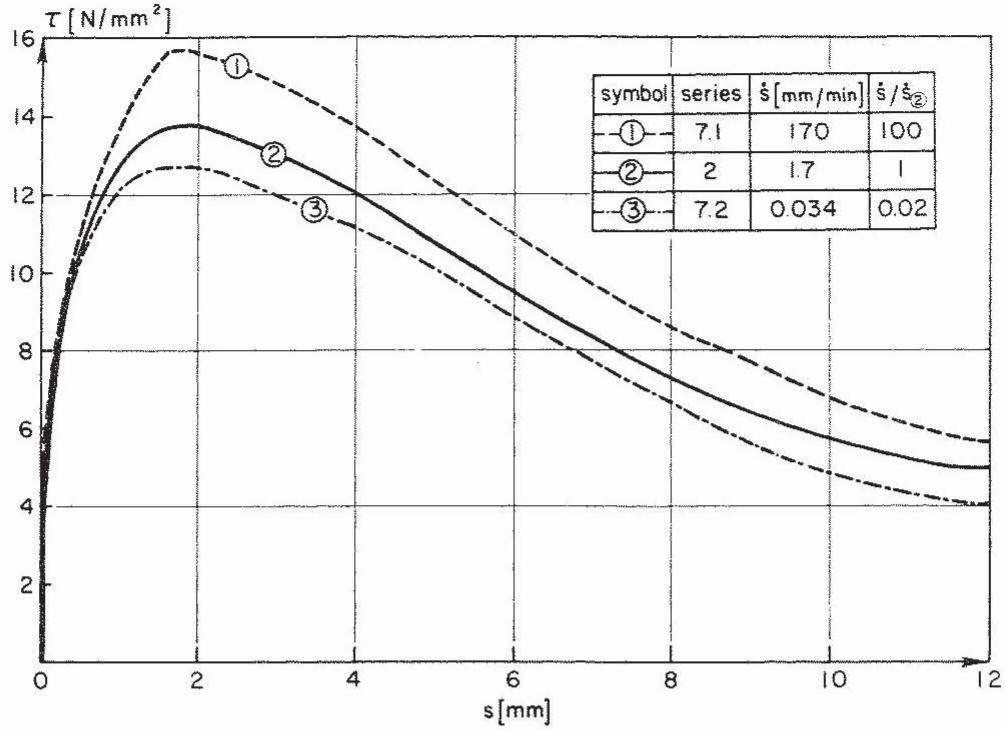

FIG. 4.19 INFLUENCE OF RATE OF PULL-OUT ON BOND STRESS-SLIP RELATIONSHIP

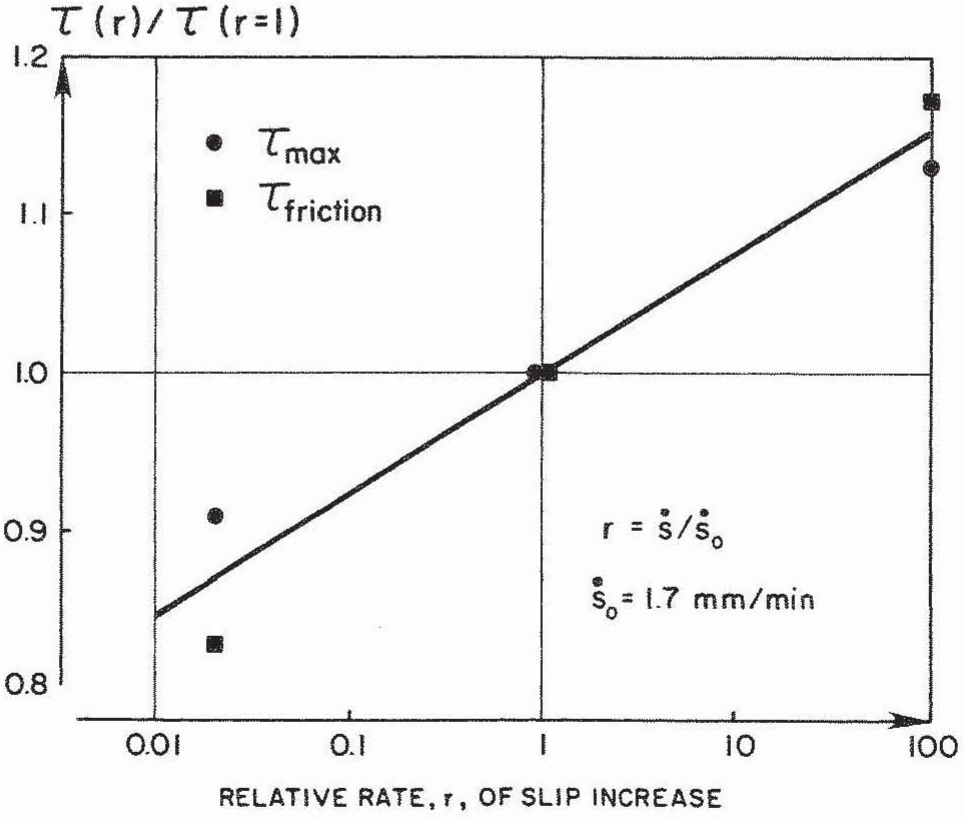

FIG. 4.20 INFLUENCE OF RELATIVE RATE, τ, OF SLIP INCREASE ON BOND RESISTANCE

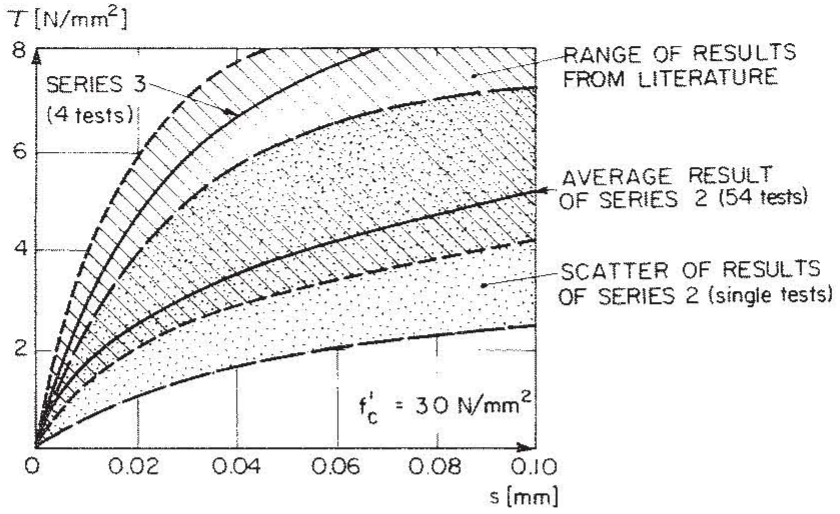

(a) FOR SMALL SLIP VALUES

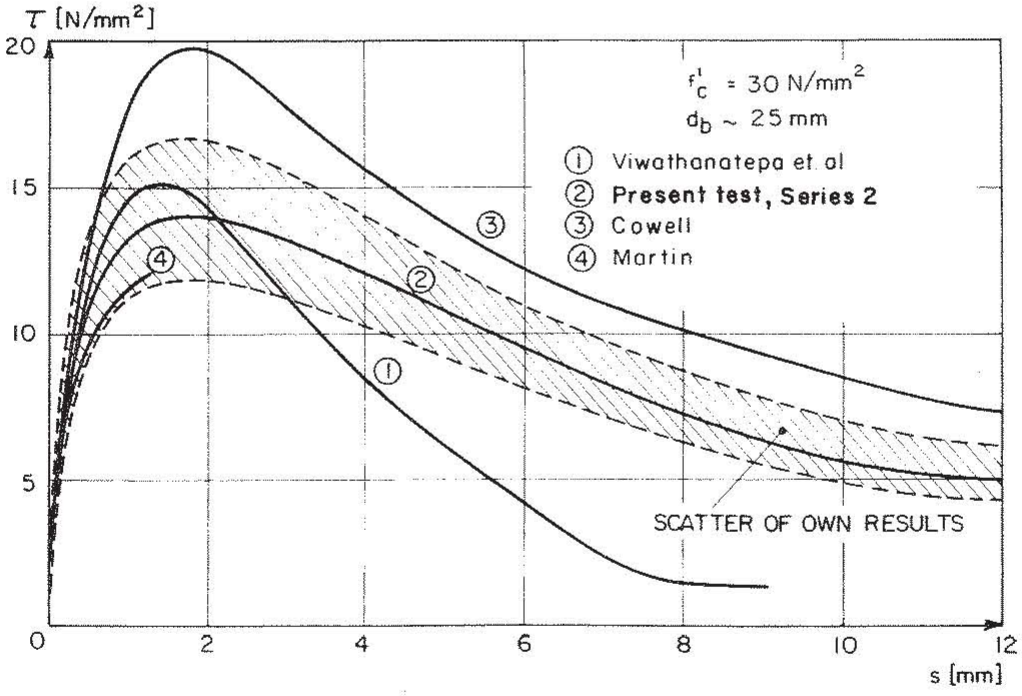

(b) FOR FULL RANGE OF SLIP

FIG. 4.21 COMPARISON OF BOND STRESS-SLIP RELATIONSHIP MEASURED IN PRESENT TESTS WITH DATA GIVEN IN LITERATURE

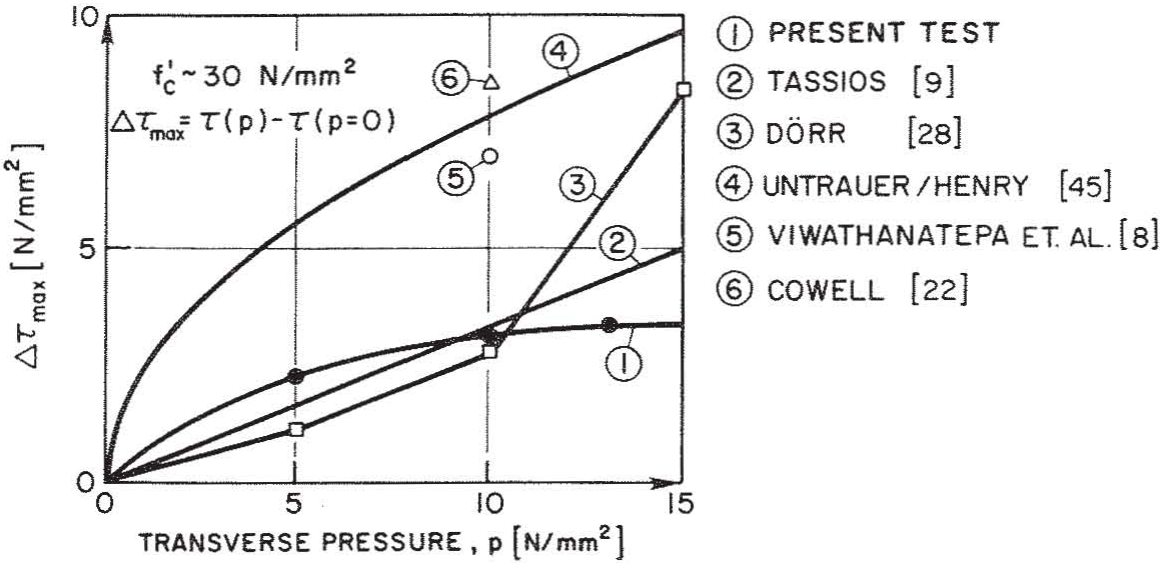

(a) MAXIMUM BOND RESISTANCE

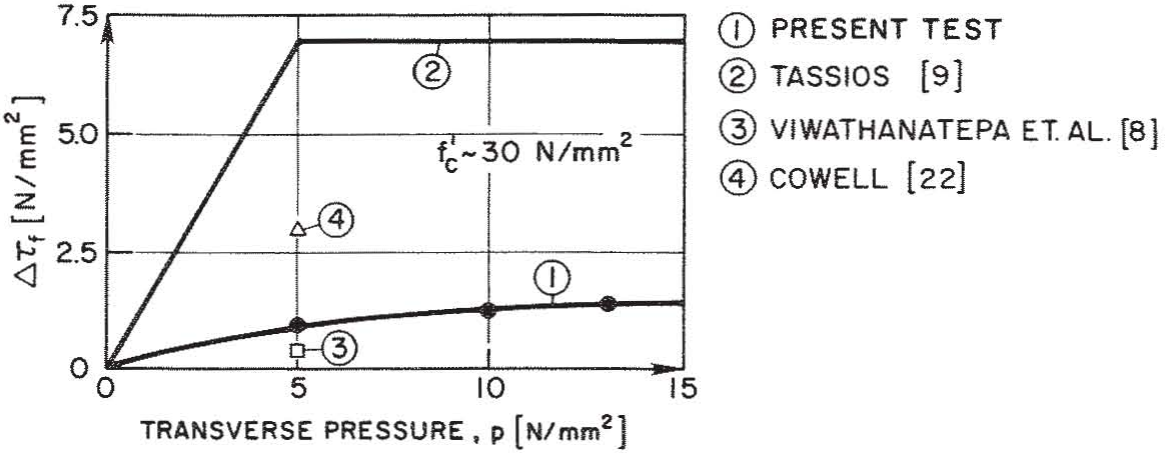

(b) ULTIMATE FRICTIONAL BOND RESISTANCE

FIG. 4.22 INCREASE OF BOND RESISTANCE AS A FUNCTION OF TRANSVERSE PRESSURE P - COMPARISON BETWEEN RESULTS OF PRESENT TESTS AND THOSE GIVEN IN LITERATURE.

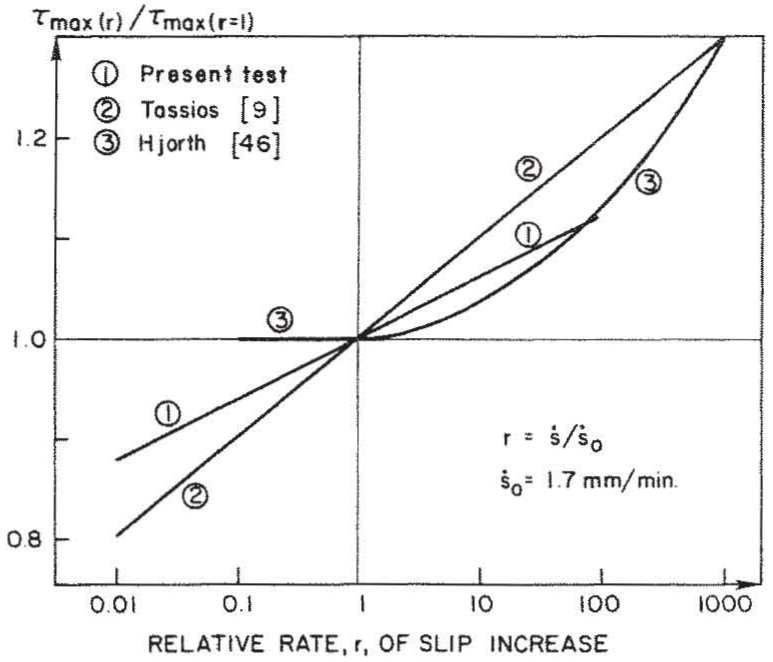

FIG. 4.23 INFLUENCE OF RATE OF PULLOUT ON BOND RESISTANCE. COMPARISON OF RESULTS OF PRESENT TESTS WITH THOSE GIVEN IN LITERATURE.

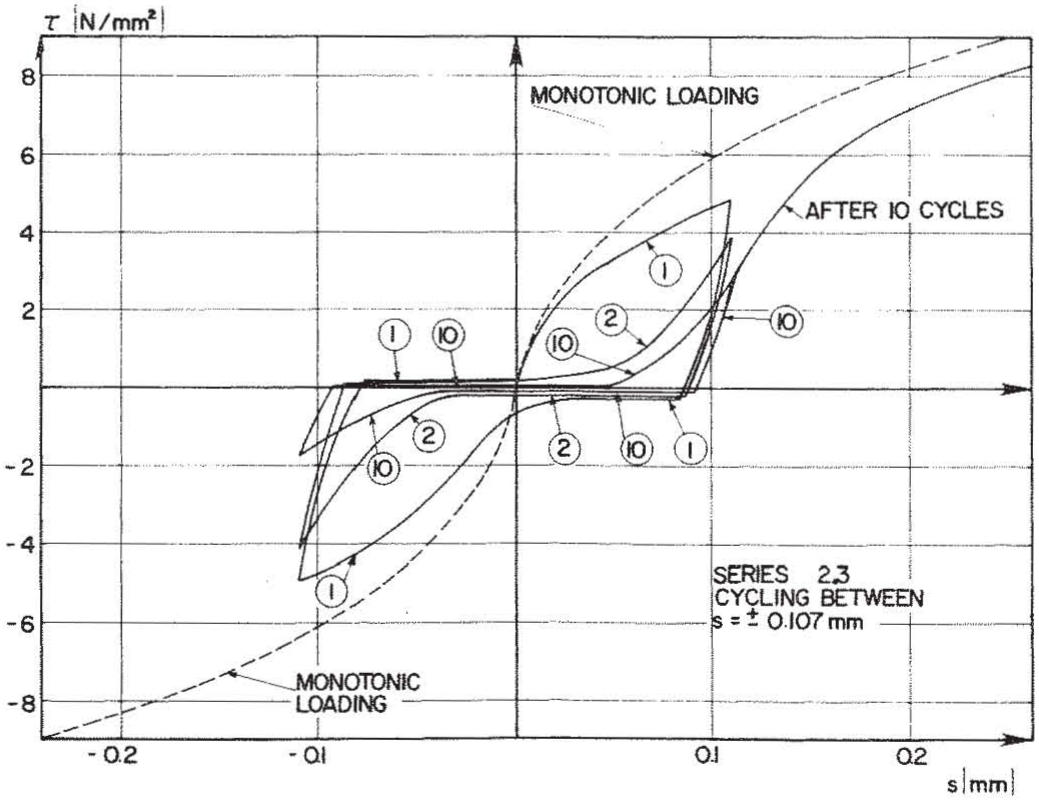

FIG. 4.24 BOND STRESS-SLIP RELATIONSHIP FOR CYCLIC LOADING, SERIES 2.3

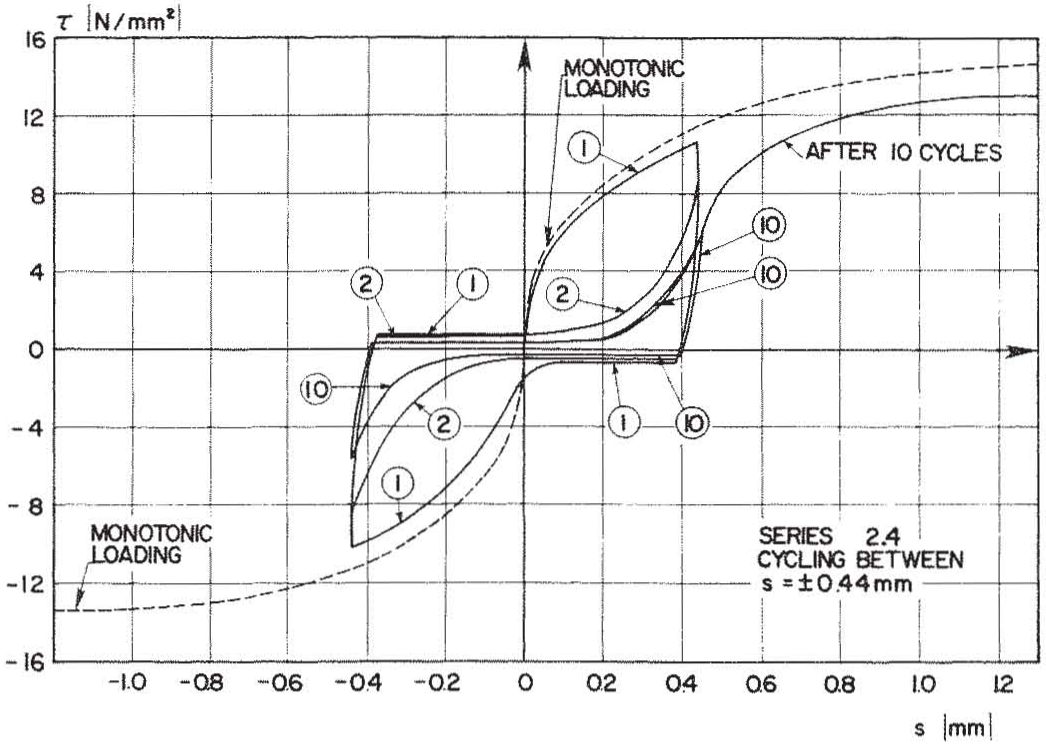

(a)

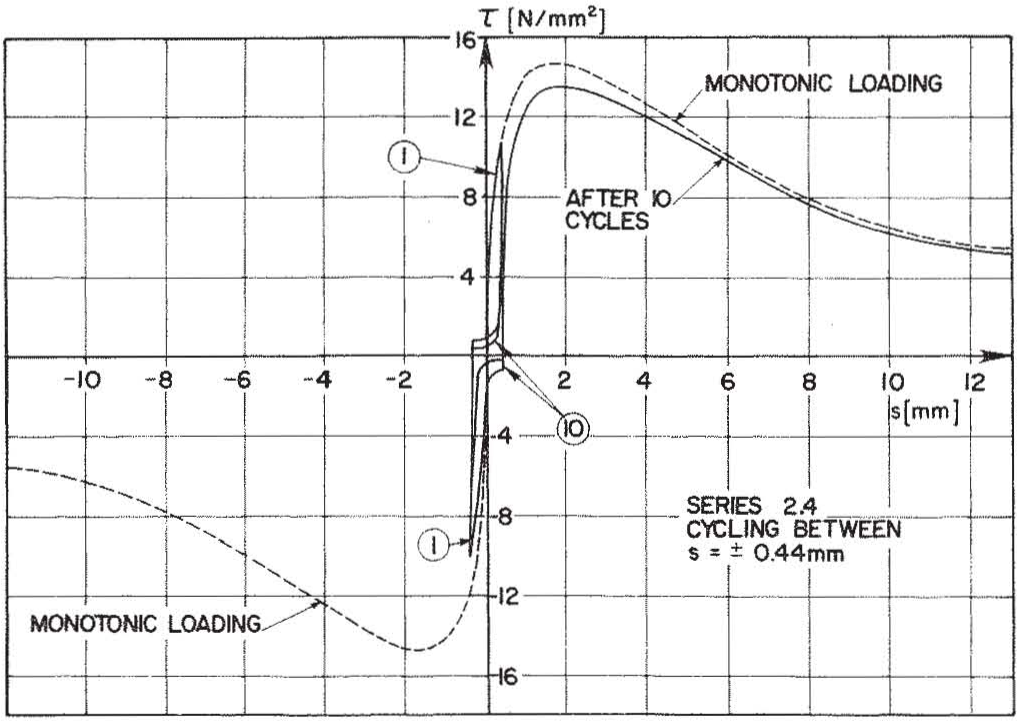

(b)

FIG. 4.25 BOND STRESS-SLIP RELATIONSHIP FOR CYCLIC LOADING, SERIES 2.4

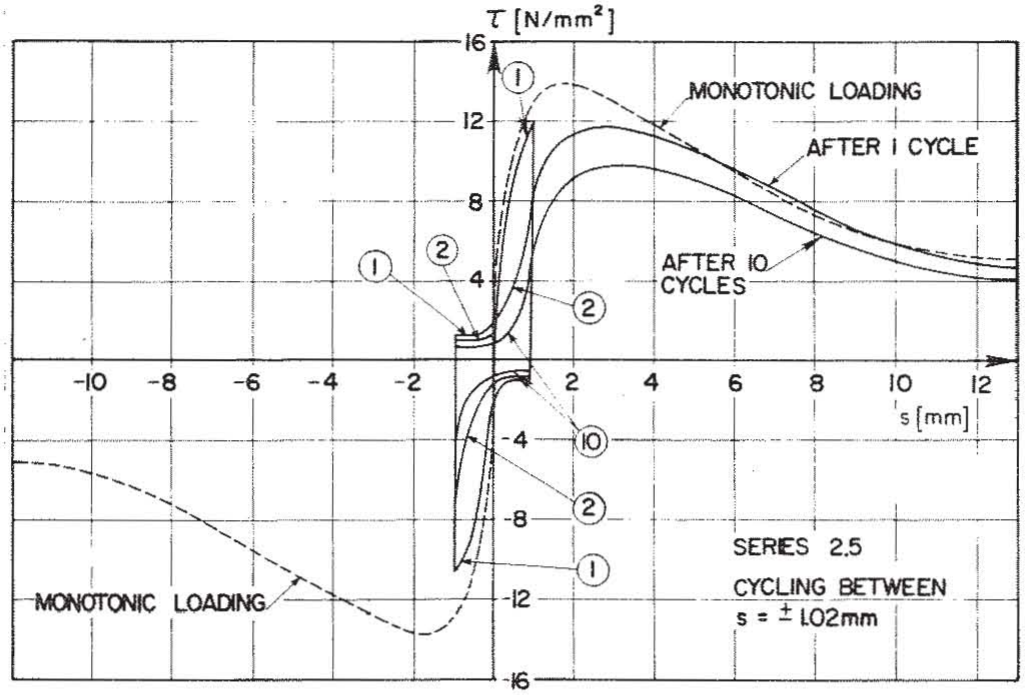

FIG. 4.26 BOND STRESS-SLIP RELATIONSHIP FOR CYCLIC LOADING, SERIES 2.5

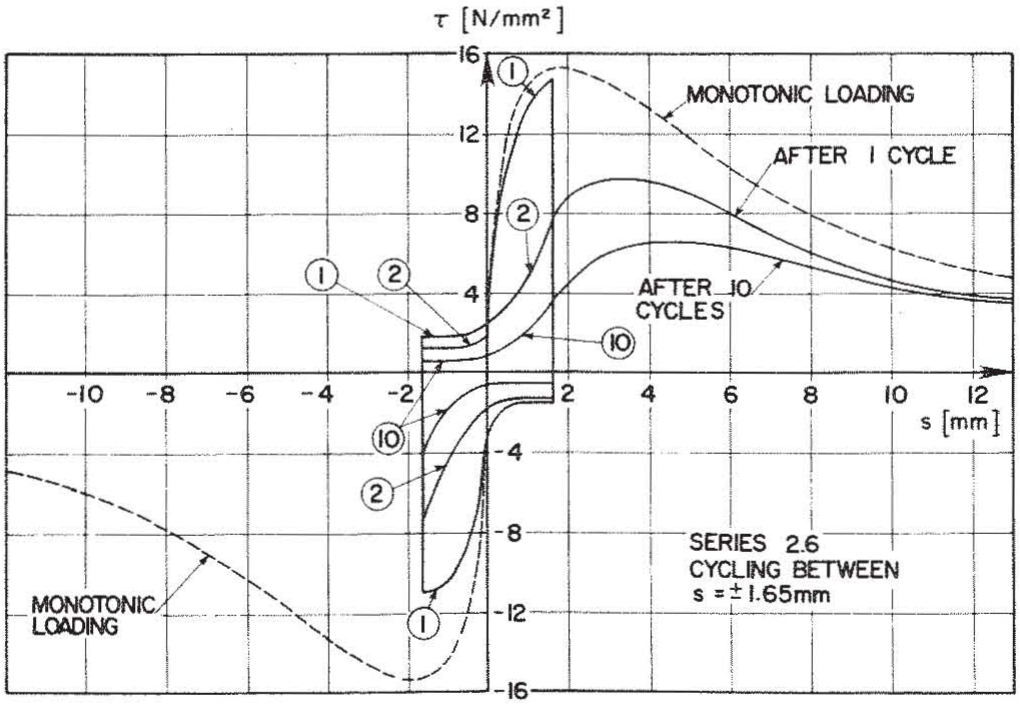

(a)

FIG. 4.27a BOND STRESS-SLIP RELATIONSHIP FOR CYCLIC LOADING, SERIES 2.6

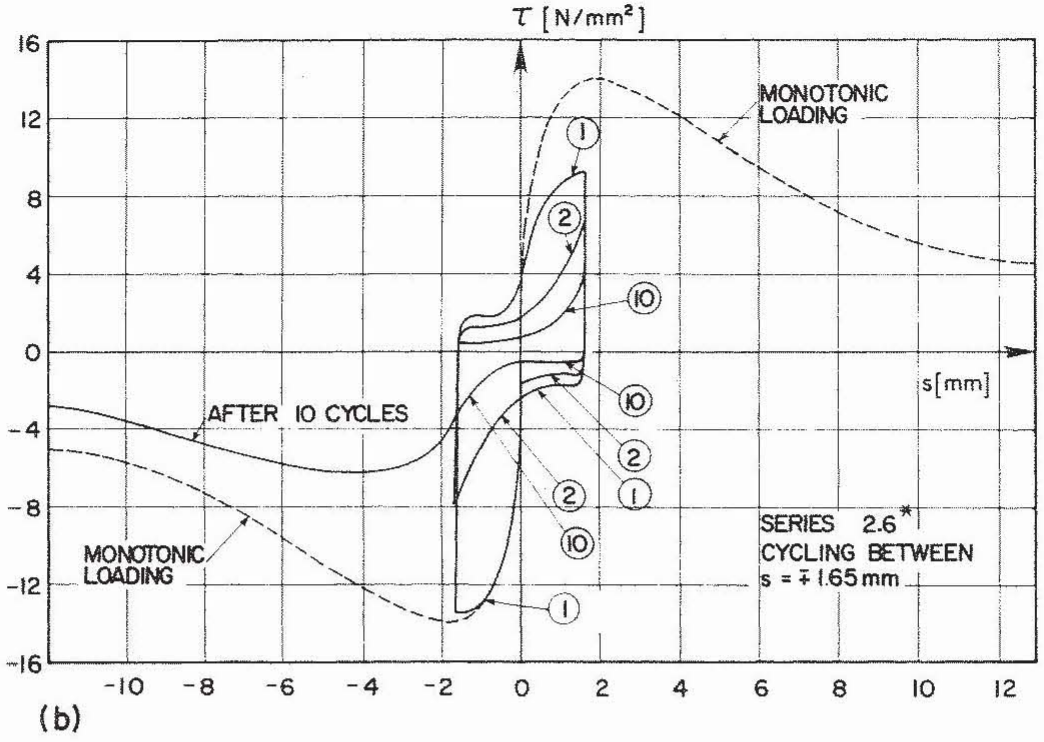

FIG. 4.27b BOND STRESS-SLIP RELATIONSHIP FOR CYCLIC LOADING, SERIES 2.6*

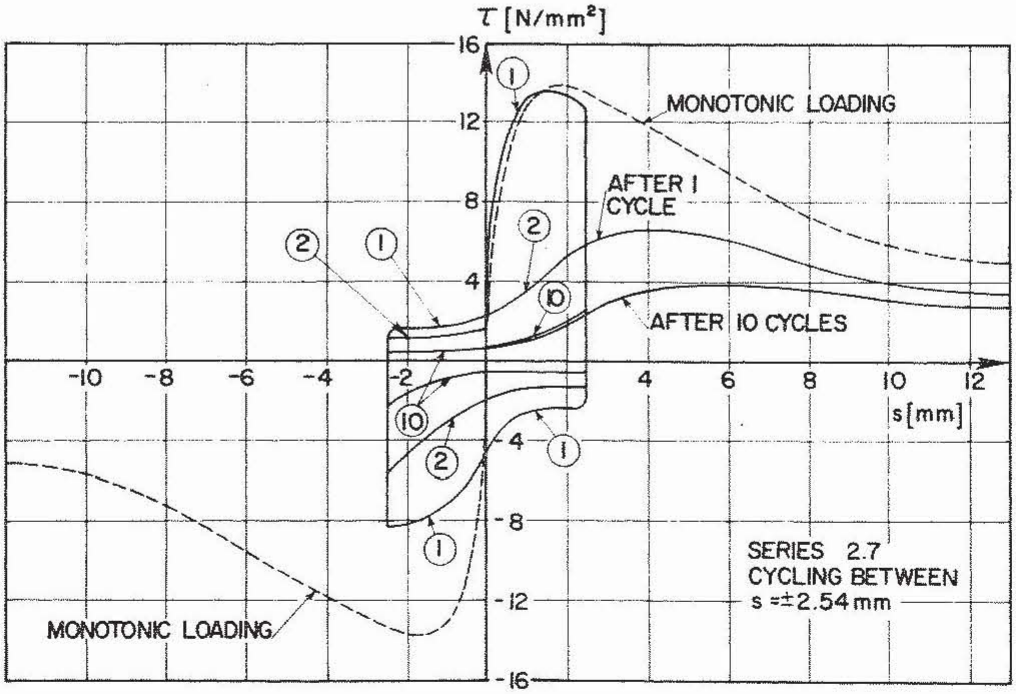

FIG. 4.28 BOND STRESS-SLIP RELATIONSHIP FOR CYCLIC LOADING, SERIES 2.7

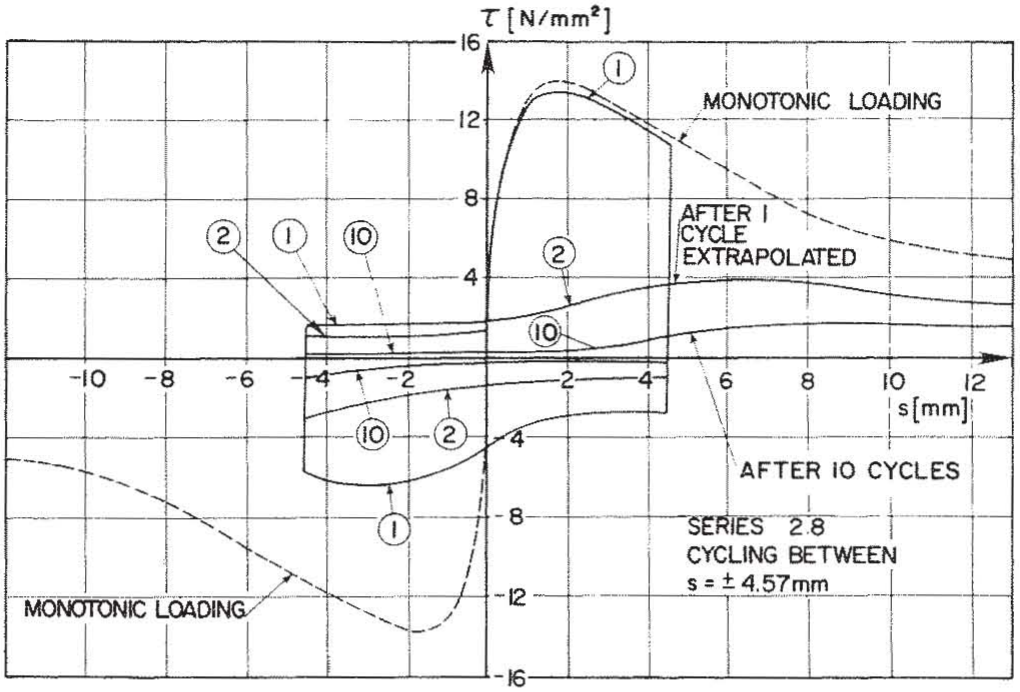

FIG. 4.29 BOND STRESS-SLIP RELATIONSHIP FOR CYCLIC LOADING, SERIES 2.8

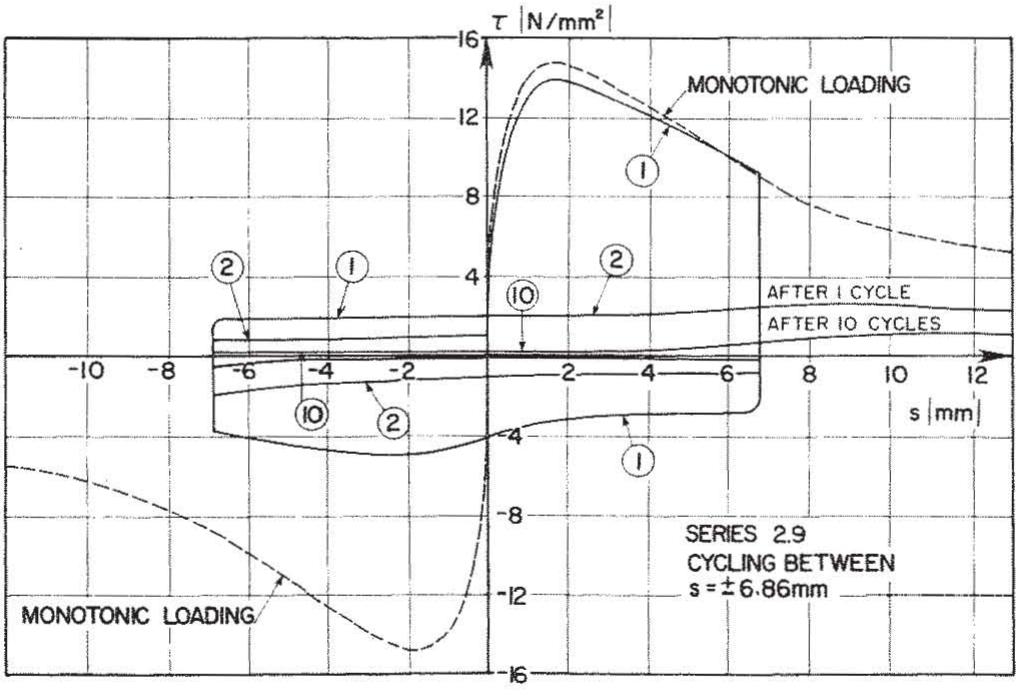

FIG. 4.30 BOND STRESS-SLIP RELATIONSHIP FOR CYCLIC LOADING, SERIES 2.9

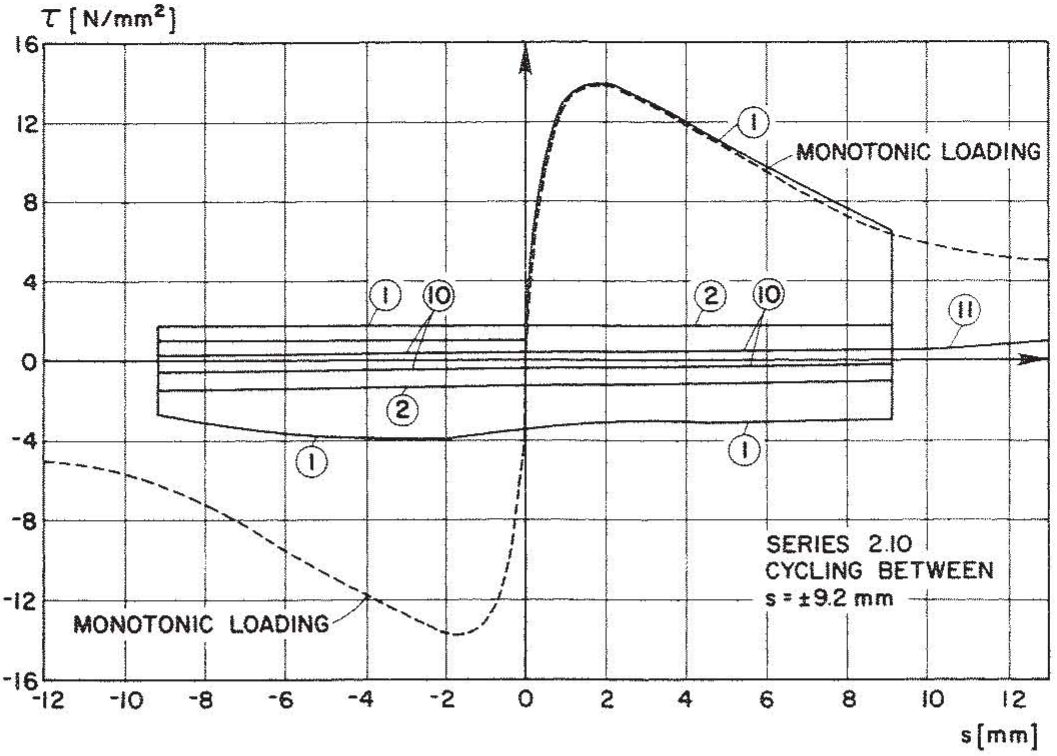

FIG. 4.31 BOND STRESS-SLIP RELATIONSHIP FOR CYCLIC LOADING, SERIES 2.10

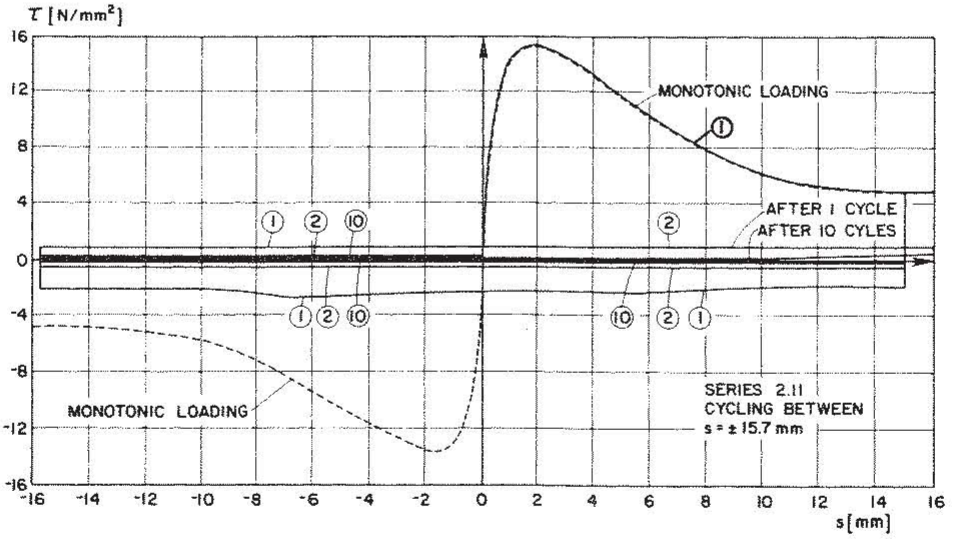

FIG. 4.32 BOND STRESS-SLIP RELATIONSHIP FOR CYCLIC LOADING, SERIES 2.11

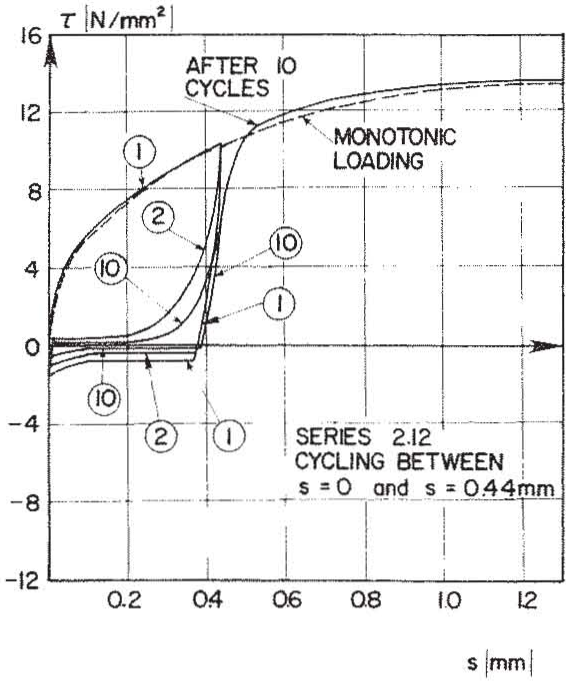

FIG. 4.33 BOND STRESS-SLIP RELATIONSHIP FOR CYCLIC LOADING, SERIES 2.12

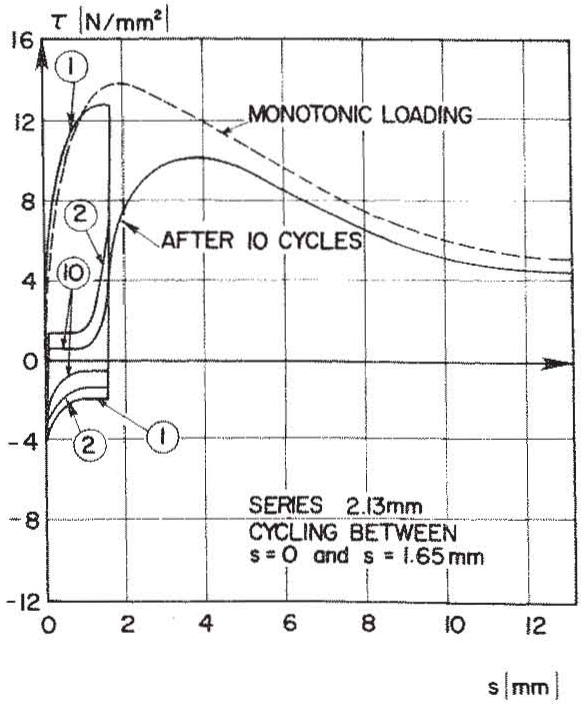

FIG. 4.34 BOND STRESS-SLIP RELATIONSHIP FOR CYCLIC LOADING, SERIES 2.13

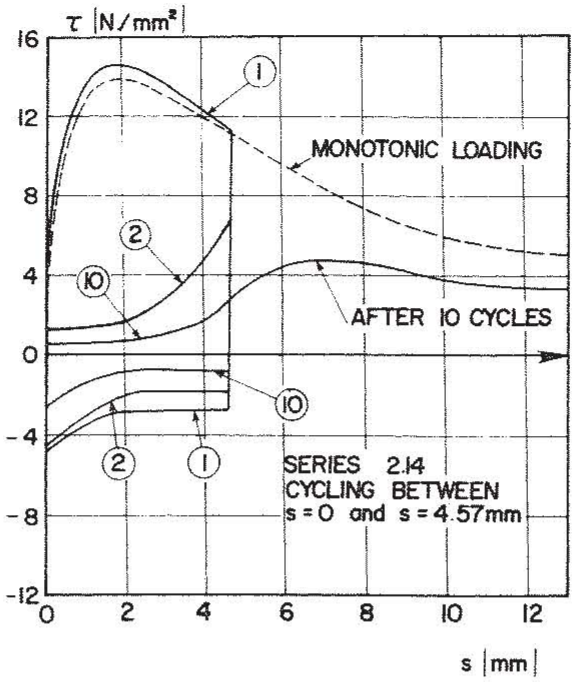

FIG. 4.35 BOND STRESS-SLIP RELATIONSHIP FOR CYCLIC LOADING, SERIES 2.14

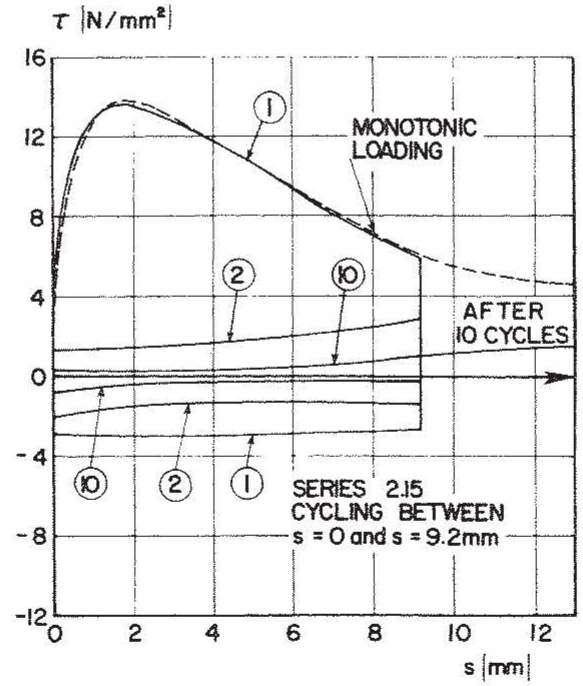

FIG. 4.36 BOND STRESS-SLIP RELATIONSHIP FOR CYCLIC LOADING, SERIES 2.15

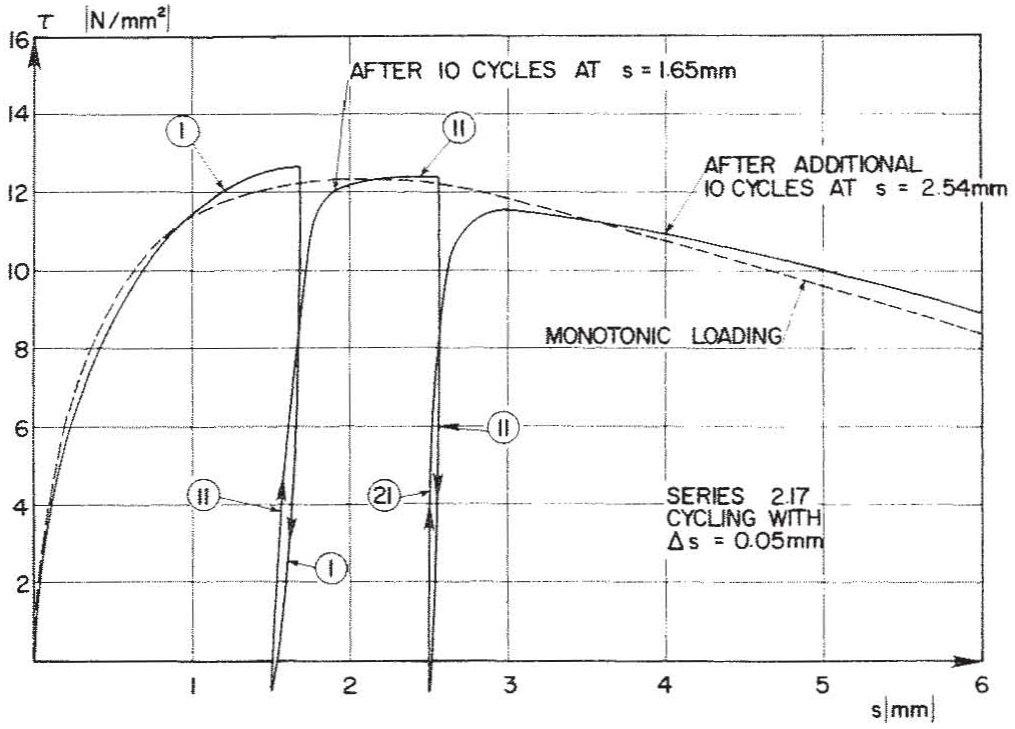

FIG. 4.37 BOND STRESS-SLIP RELATIONSHIP FOR CYCLIC LOADING, SERIES 2.17

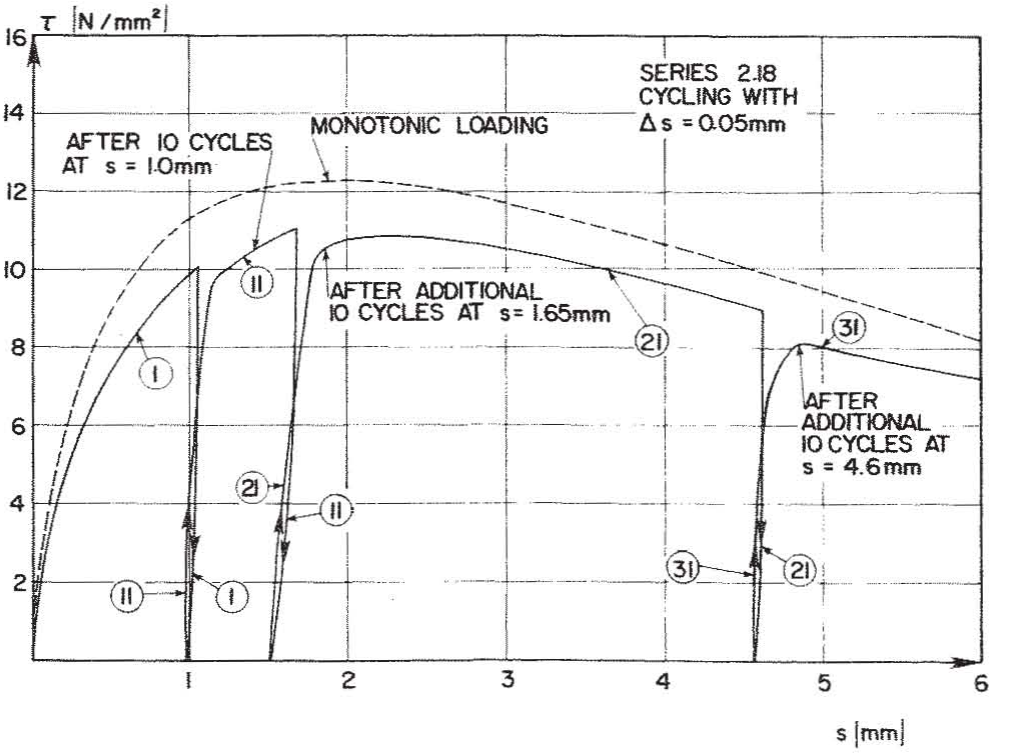

FIG. 4.38 BOND STRESS-SLIP RELATIONSHIP FOR CYCLIC LOADING, SERIES 2.18

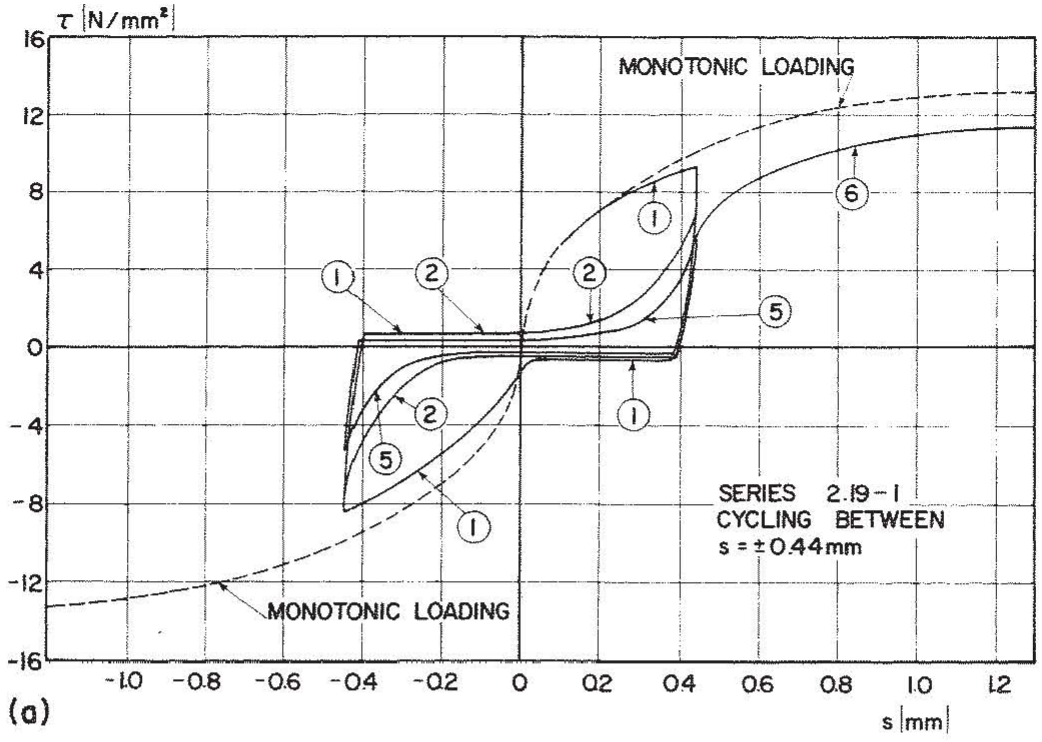

FIG. 4.39a BOND STRESS-SLIP RELATIONSHIP FOR CYCLIC LOADING, SERIES 2.19-1

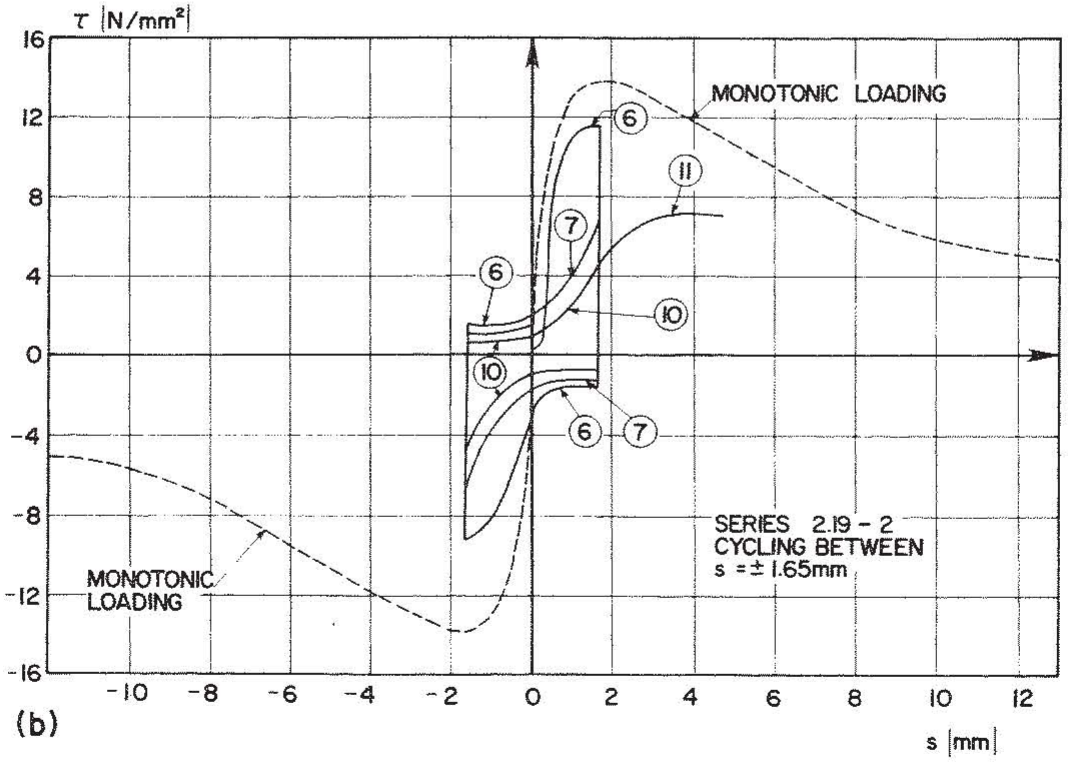

FIG. 4.39b BOND STRESS-SLIP RELATIONSHIP FOR CYCLIC LOADING, SERIES 2.19-2

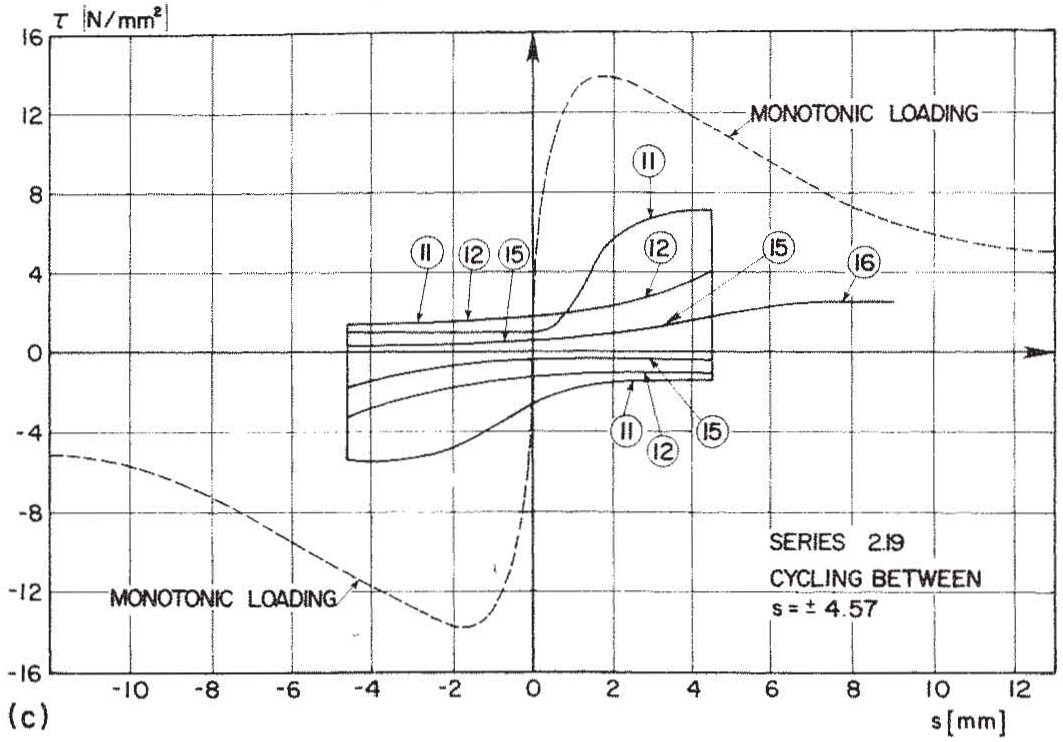

FIG. 4.39c BOND STRESS-SLIP RELATIONSHIP FOR CYCLIC LOADING, SERIES 2.19-3

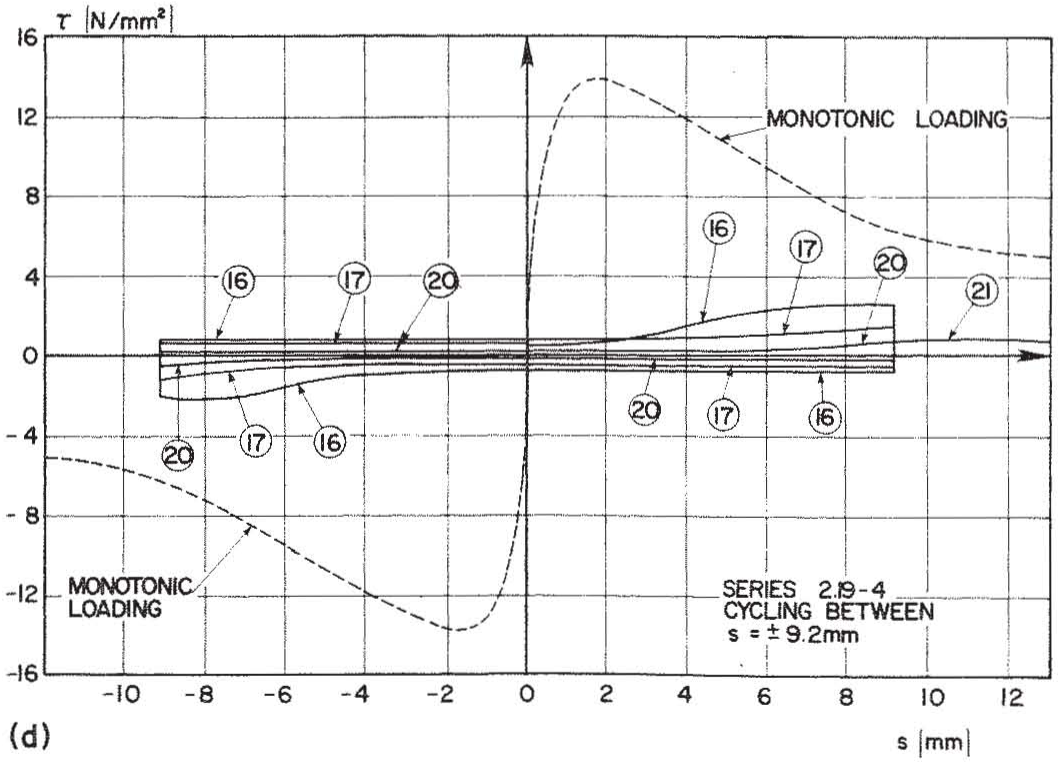

FIG. 4.39d BOND STRESS-SLIP RELATIONSHIP FOR CYCLIC LOADING, SERIES 2.19-4

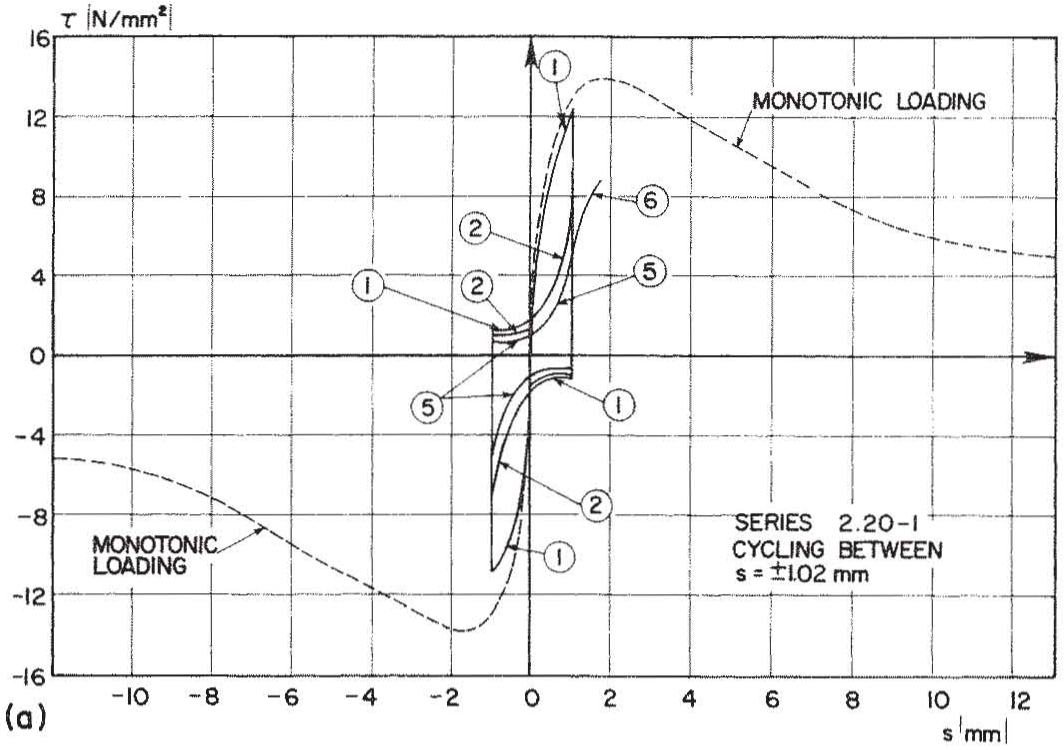

FIG. 4.40a BOND STRESS-SLIP RELATIONSHIP FOR CYCLIC LOADING, SERIES 2.20

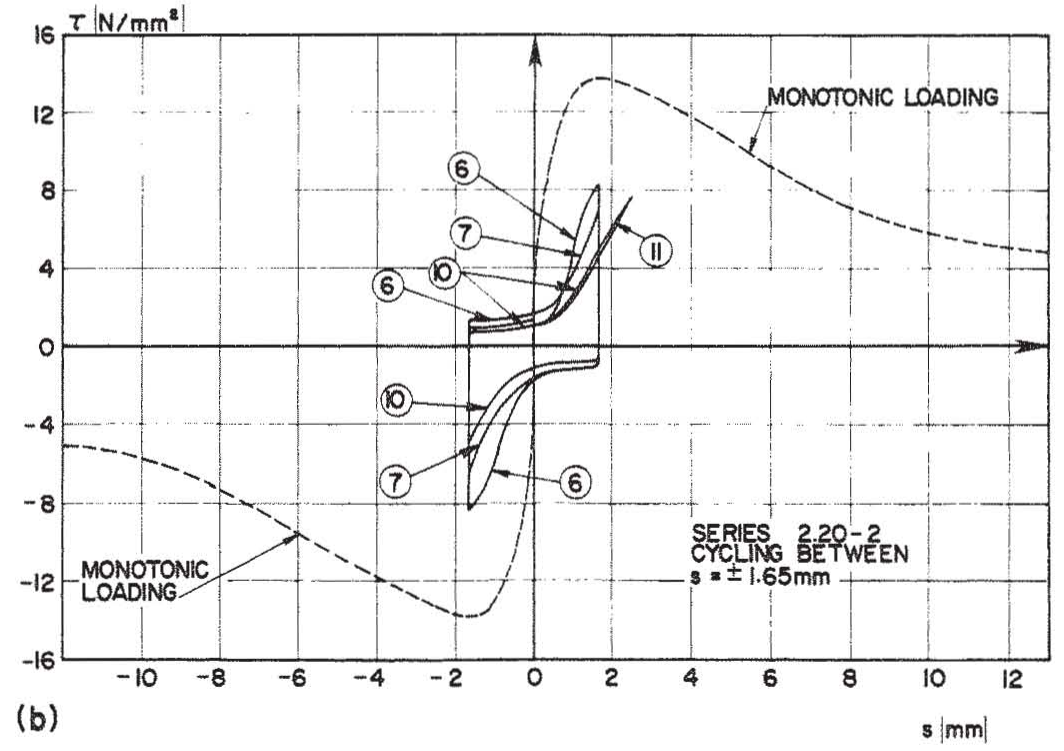

FIG. 4.40b BOND STRESS-SLIP RELATIONSHIP FOR CYCLIC LOADING, SERIES 2.20

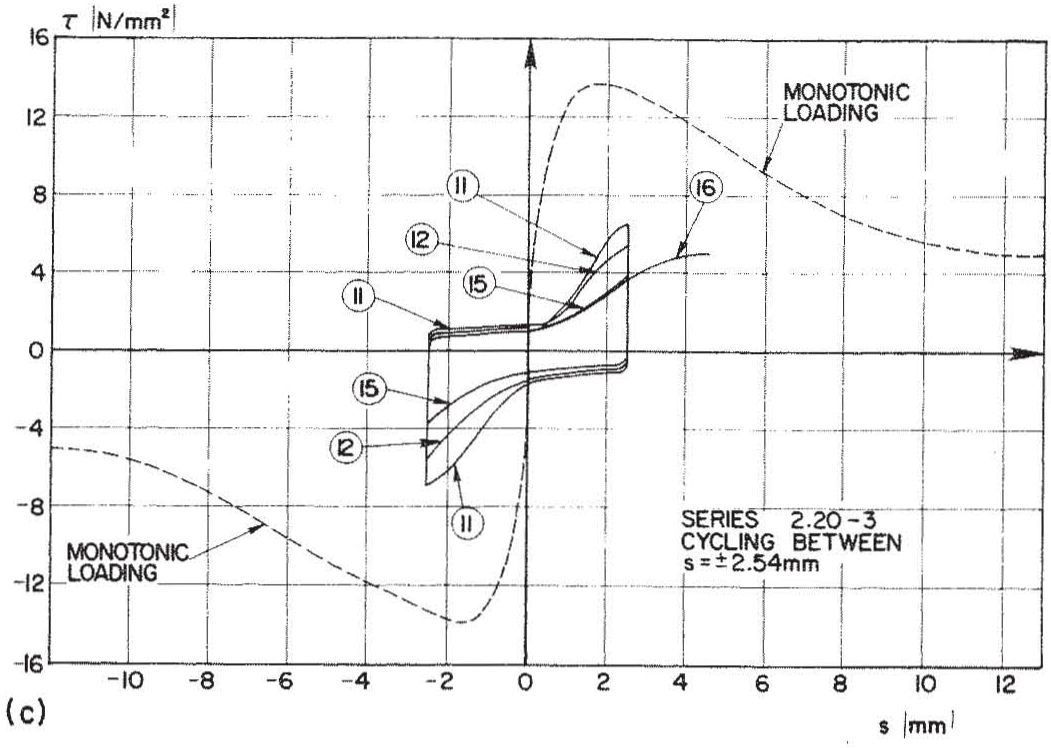

FIG. 4.40c BOND STRESS-SLIP RELATIONSHIP FOR CYCLIC LOADING, SERIES 2.20

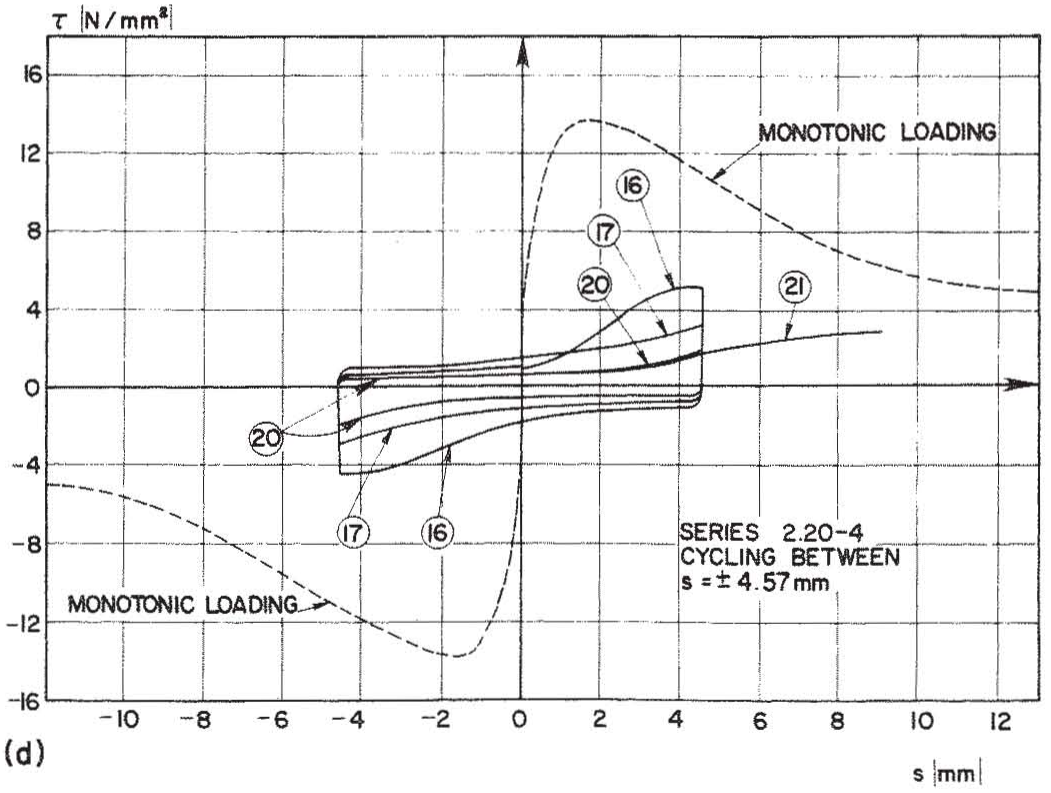

FIG. 4.40d BOND STRESS-SLIP RELATIONSHIP FOR CYCLIC LOADING, SERIES 2.20

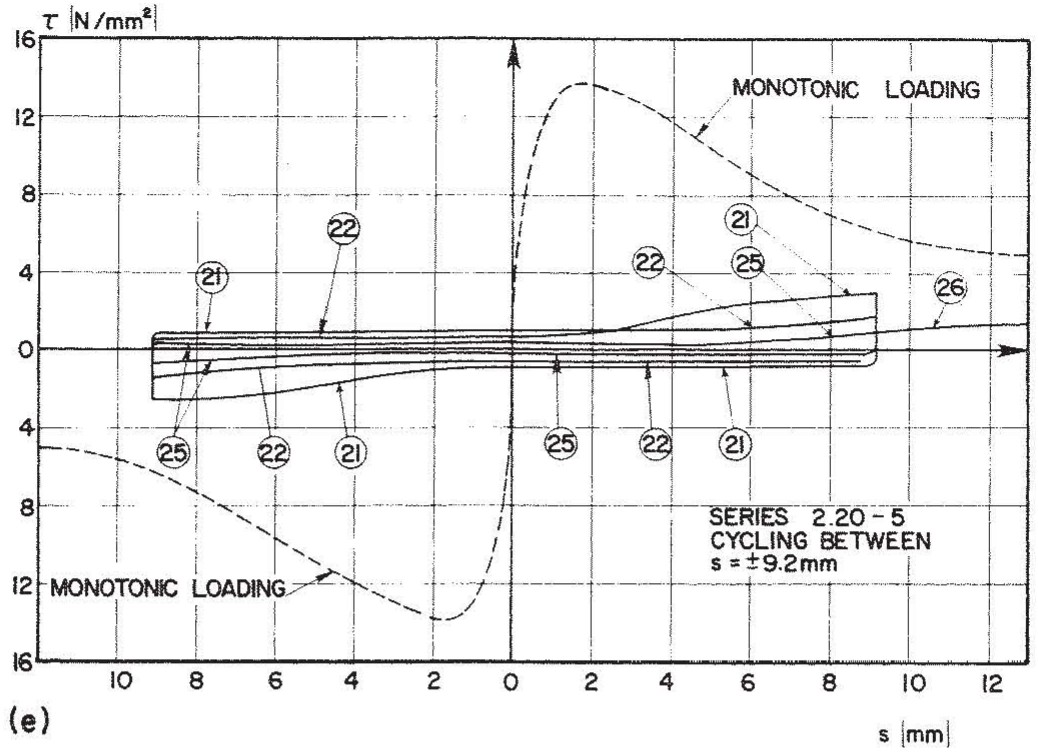

FIG. 4.40e BOND STRESS-SLIP RELATIONSHIP FOR CYCLIC LOADING, SERIES 2.20

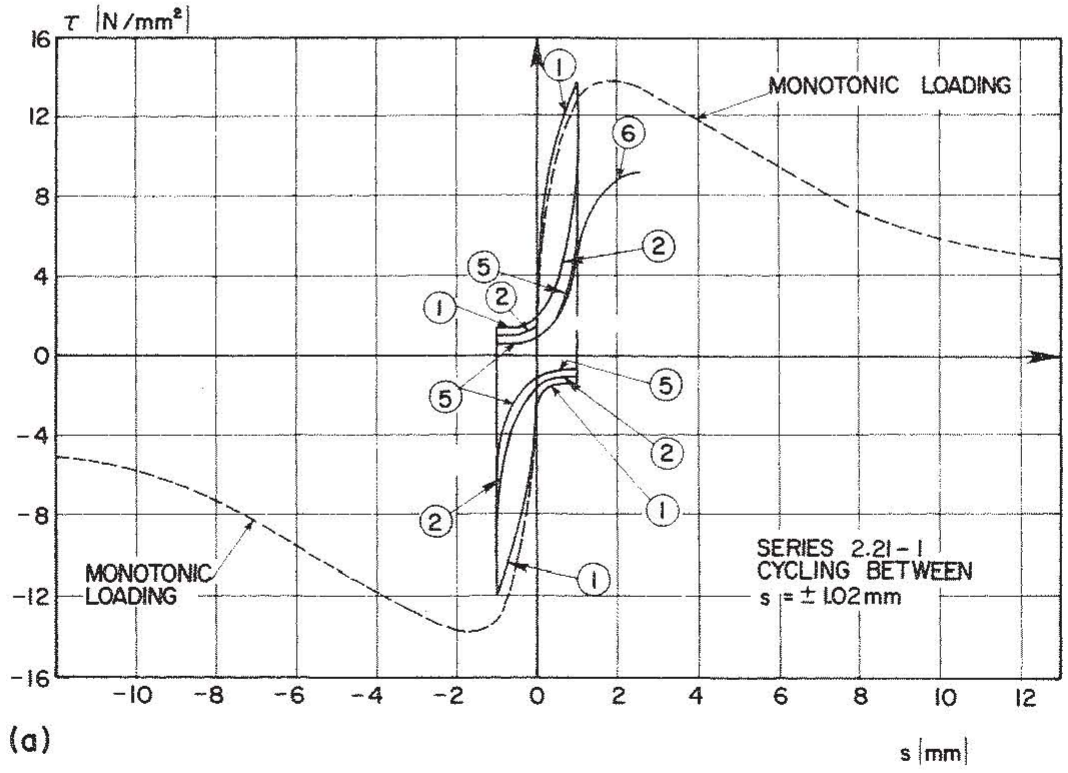

FIG. 4.41a BOND STRESS-SLIP RELATIONSHIP FOR CYCLIC LOADING, SERIES 2.21-1

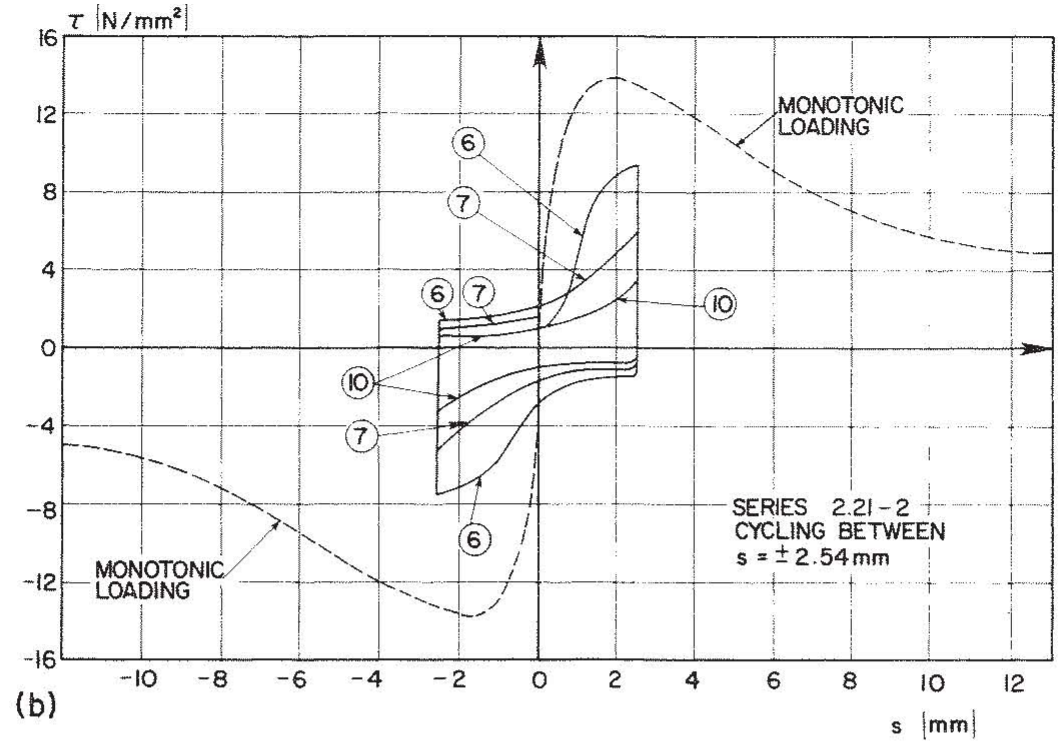

FIG. 4.41b BOND STRESS-SLIP RELATIONSHIP FOR CYCLIC LOADING, SERIES 2.21-2

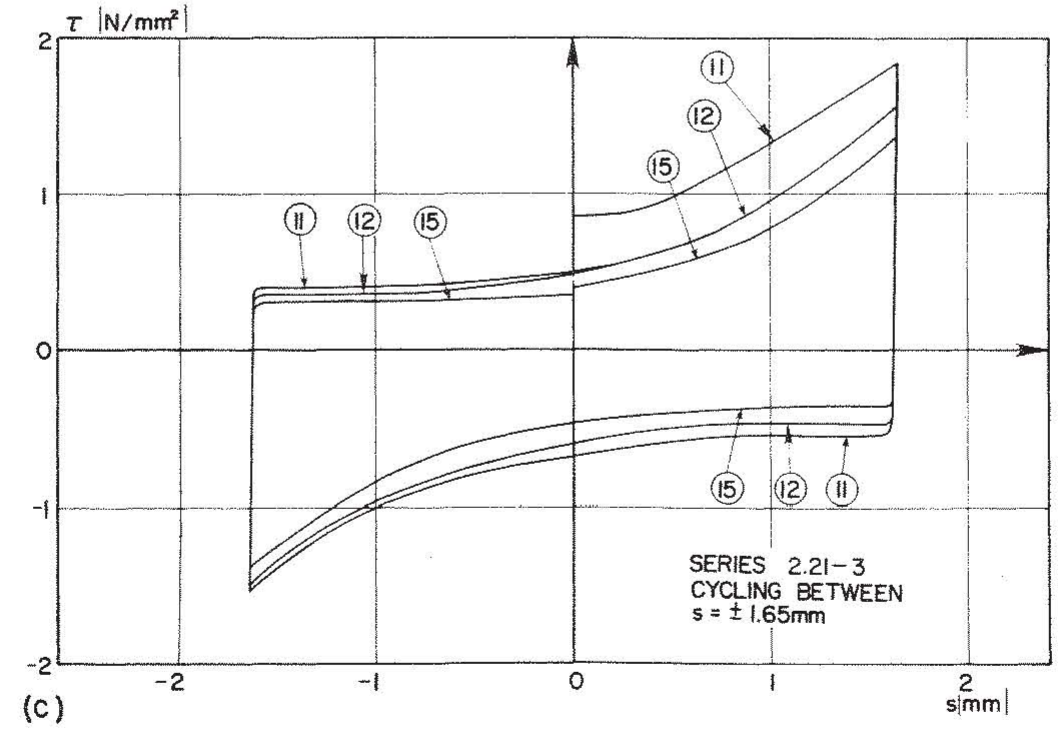

FIG. 4.41c BOND STRESS-SLIP RELATIONSHIP FOR CYCLIC LOADING, SERIES 2.21-3

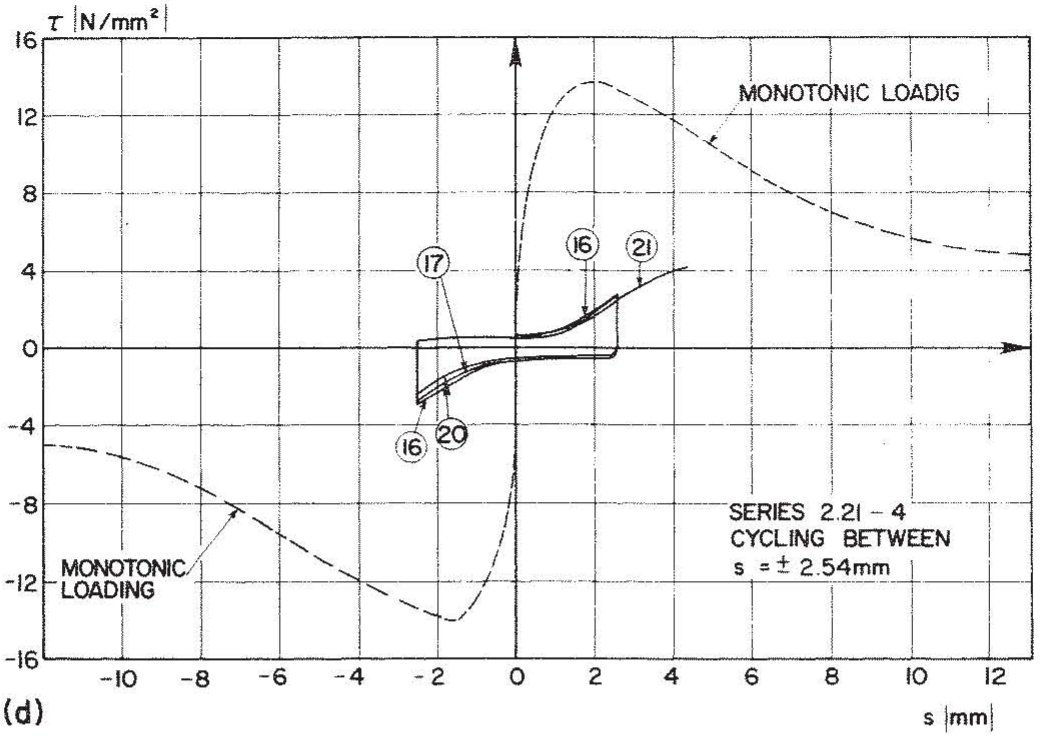

FIG. 4.41d BOND STRESS-SLIP RELATIONSHIP FOR CYCLIC LOADING, SERIES 2.21-4

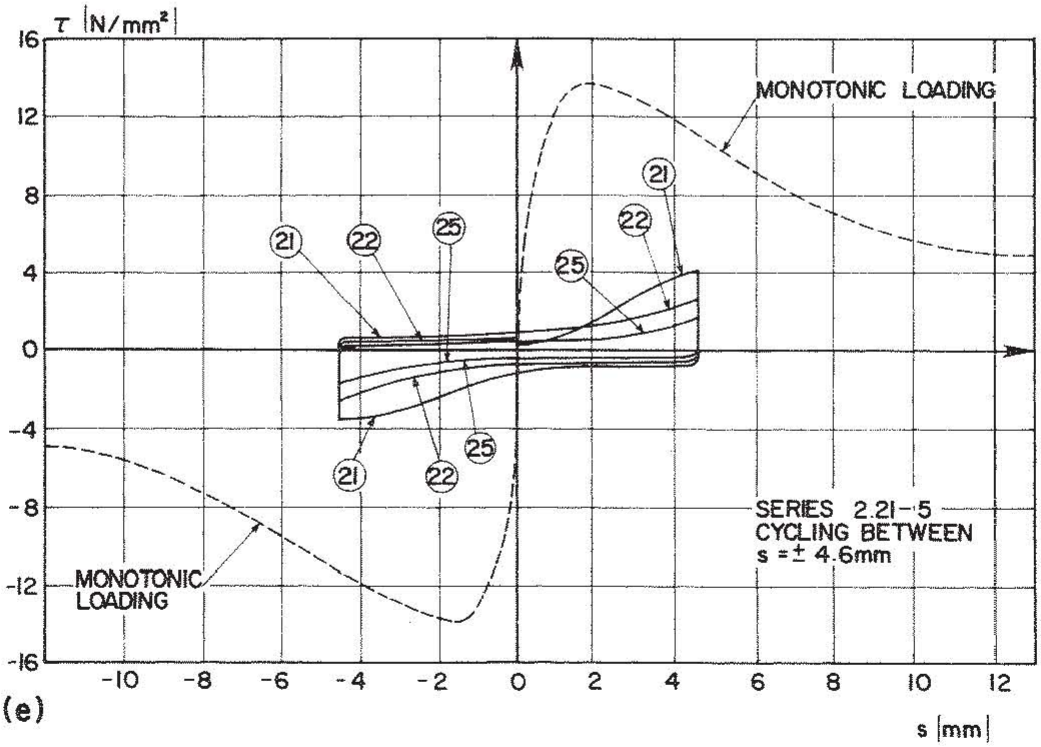

FIG. 4.41e BOND STRESS-SLIP RELATIONSHIP FOR CYCLIC LOADING, SERIES 2.21-5

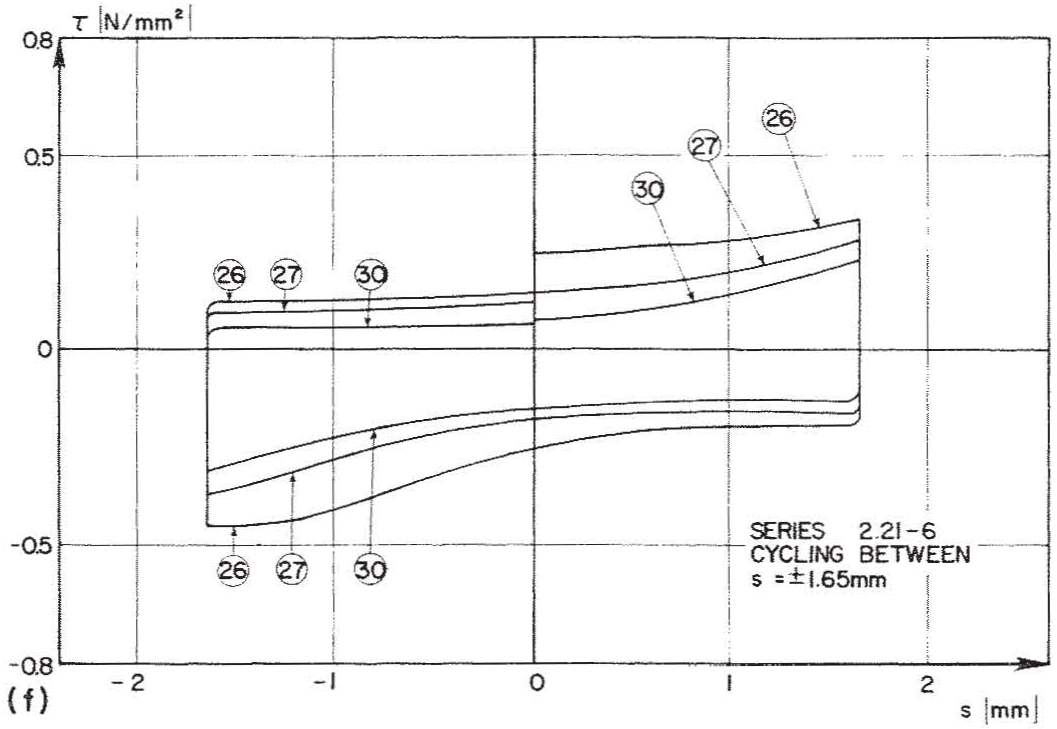

FIG. 4.41f BOND STRESS-SLIP RELATIONSHIP FOR CYCLIC LOADING, SERIES 2.21-6

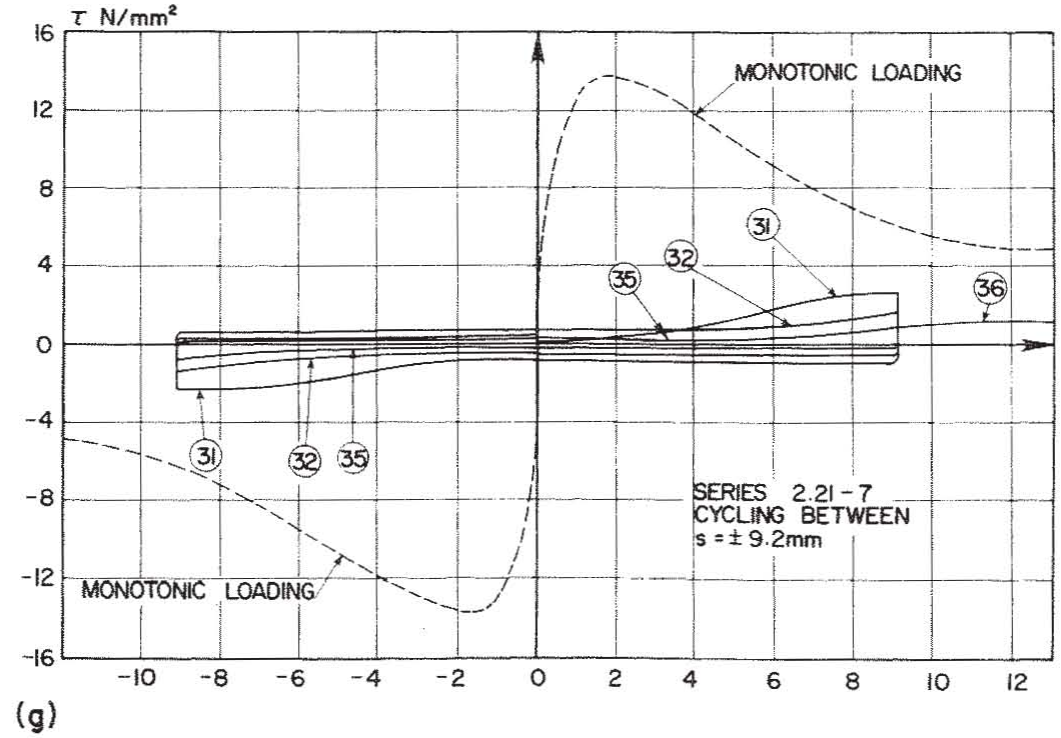

FIG. 4.41g BOND STRESS-SLIP RELATIONSHIP FOR CYCLIC LOADING, SERIES 2.21-7

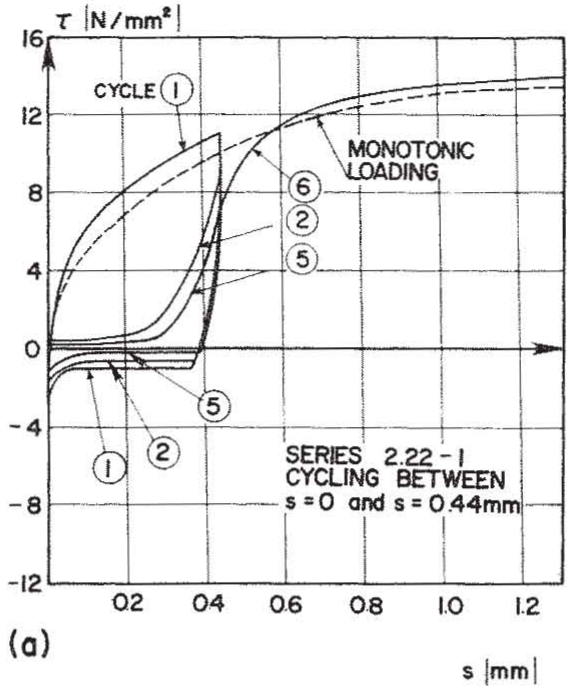

FIG. 4.42a BOND STRESS-SLIP RELATIONSHIP FOR CYCLIC LOADING, SERIES 2.22

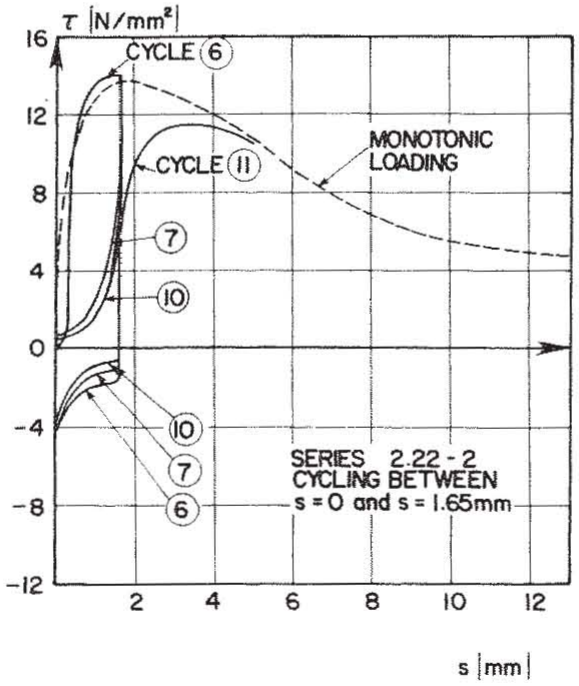

FIG. 4.42b BOND STRESS-SLIP RELATIONSHIP FOR CYCLIC LOADING, SERIES 2.22

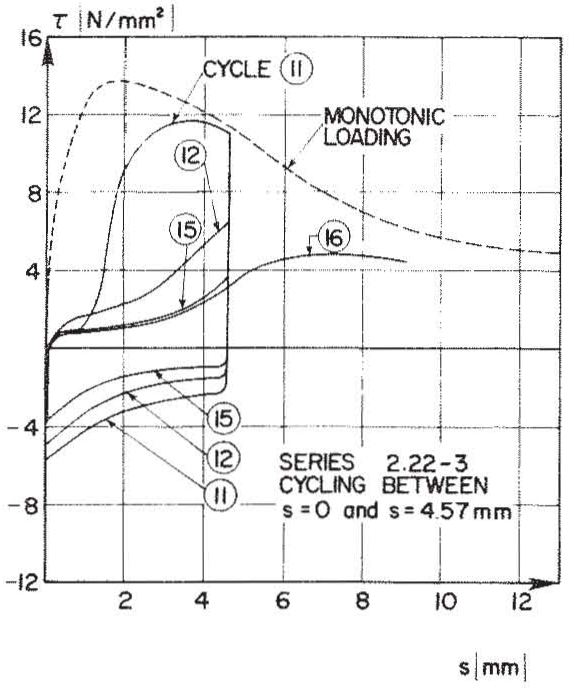

FIG. 4.42c BOND STRESS-SLIP RELATIONSHIP FOR CYCLIC LOADING, SERIES 2.22

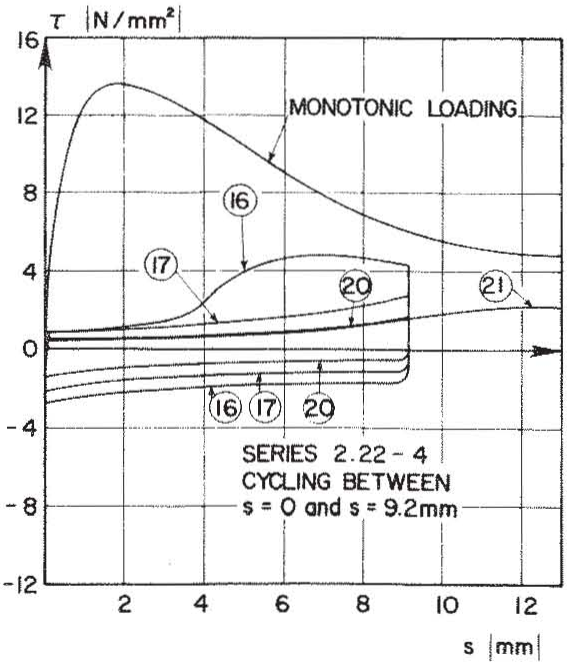

FIG. 4.42d BOND STRESS-SLIP RELATIONSHIP FOR CYCLIC LOADING, SERIES 2.22

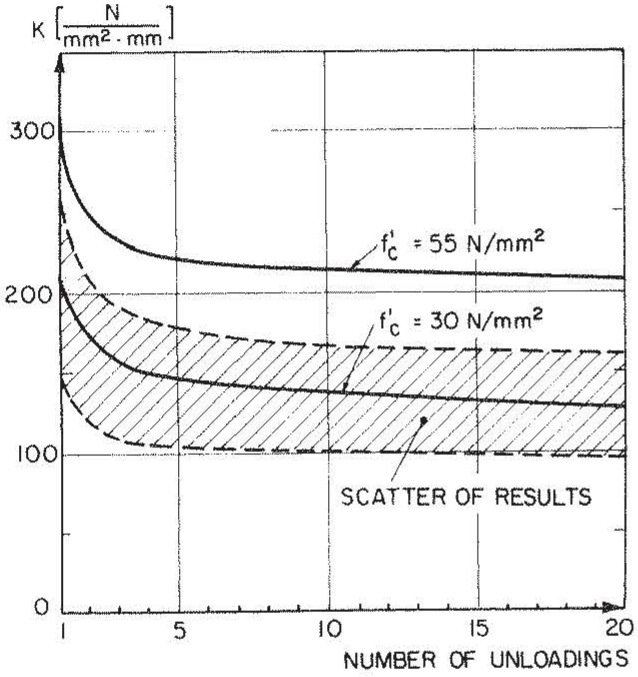

FIG. 4.43 STIFFNESS OF UNLOADING BRANCH AS A FUNCTION OF NUMBER OF UNLOADINGS

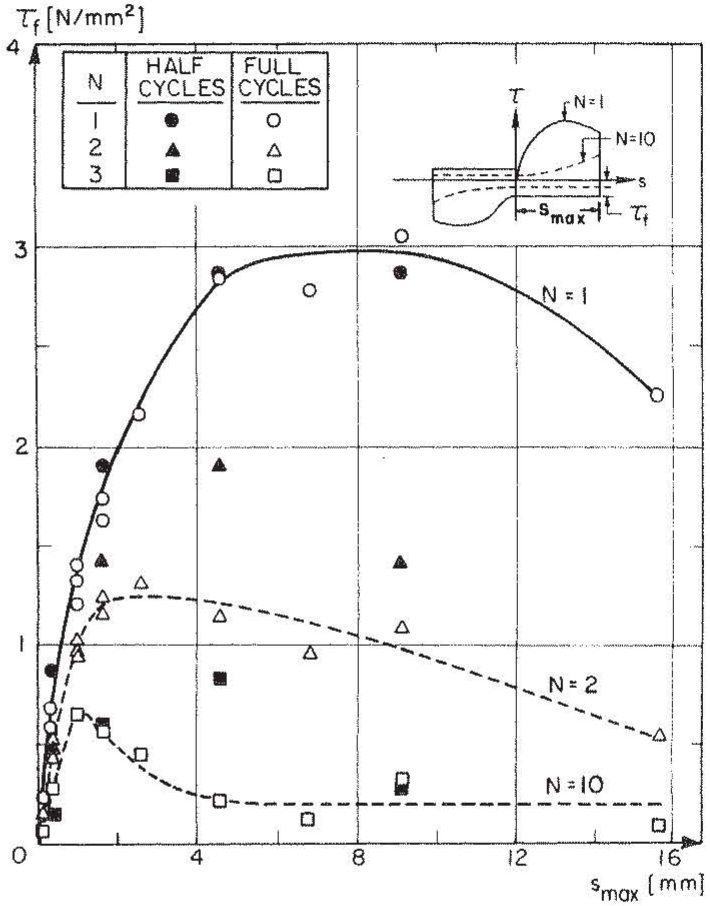

FIG. 4.44 FRICTIONAL BOND RESISTANCE DURING CYCLIC LOADING AS A FUNCTION OF PEAK SLIP s_{max}

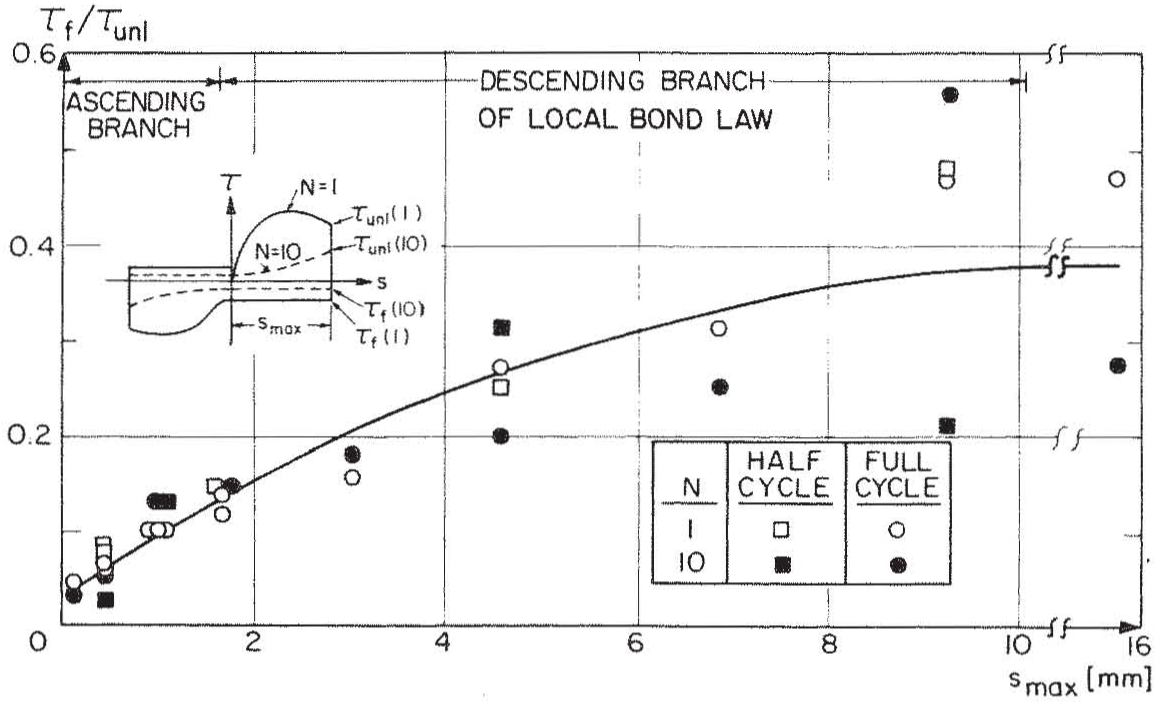

FIG. 4.45 RATIO BETWEEN FRICTIONAL BOND RESISTANCE DURING CYCLIC LOADING, τ_f, AND BOND RESISTANCE, τ_{unl}, FROM WHICH UNLOADING STARTS AS A FUNCTION OF PEAK SLIP s_{max}

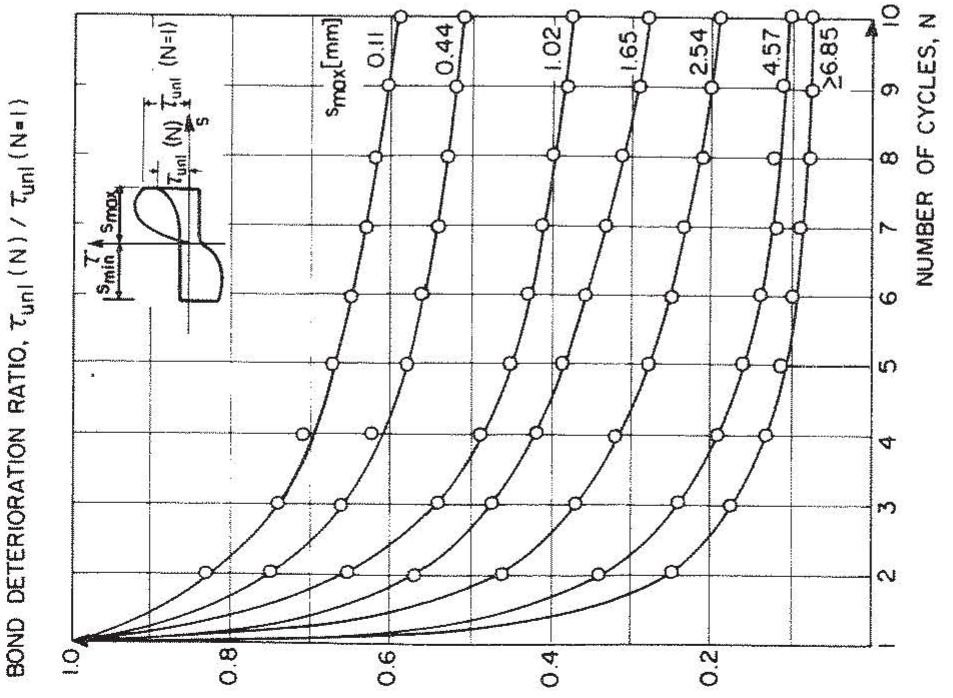

(a) CYCLES WITH FULL REVERSALS OF SLIP

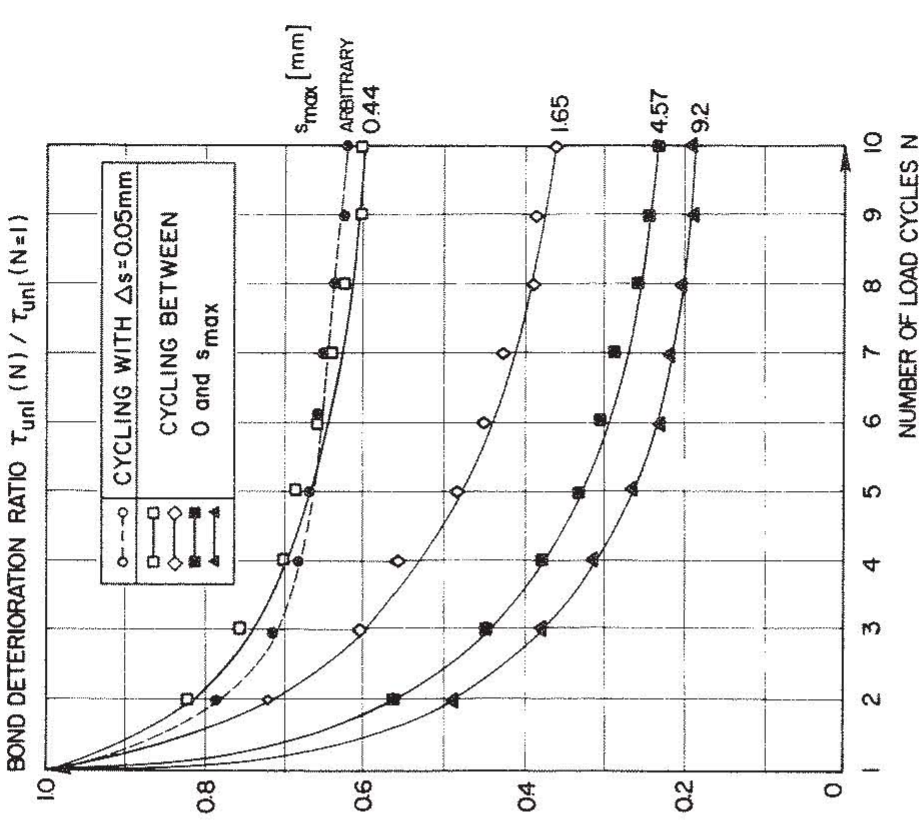

(b) CYCLES WITH Δs = 0.05 mm AND $\Delta s = s_{max}$ (HALF CYCLES)

FIG. 4.46 DETERIORATION OF BOND RESISTANCE AT PEAK SLIP AS A FUNCTION OF NUMBER OF CYCLES

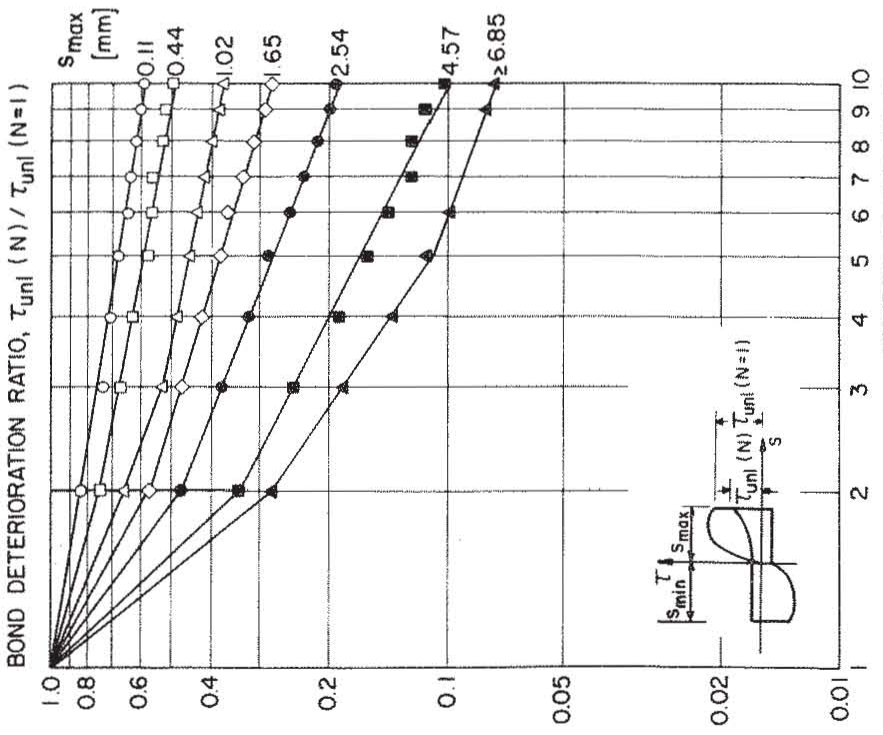

FIG. 4.47 DETERIORATION OF BOND RESISTANCE AT PEAK SLIP AS A FUNCTION OF NUMBER OF CYCLES, PLOTTED IN DOUBLE LOGARITHMIC SCALE

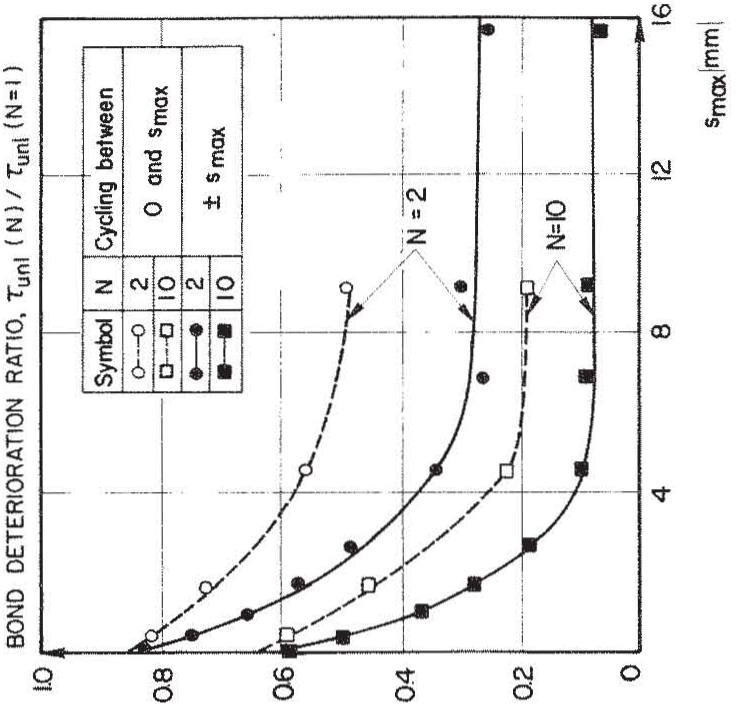

FIG. 4.48 DETERIORATION OF BOND RESISTANCE AT PEAK SLIP AS A FUNCTION OF THE PEAK VALUES OF SLIP s_{max}

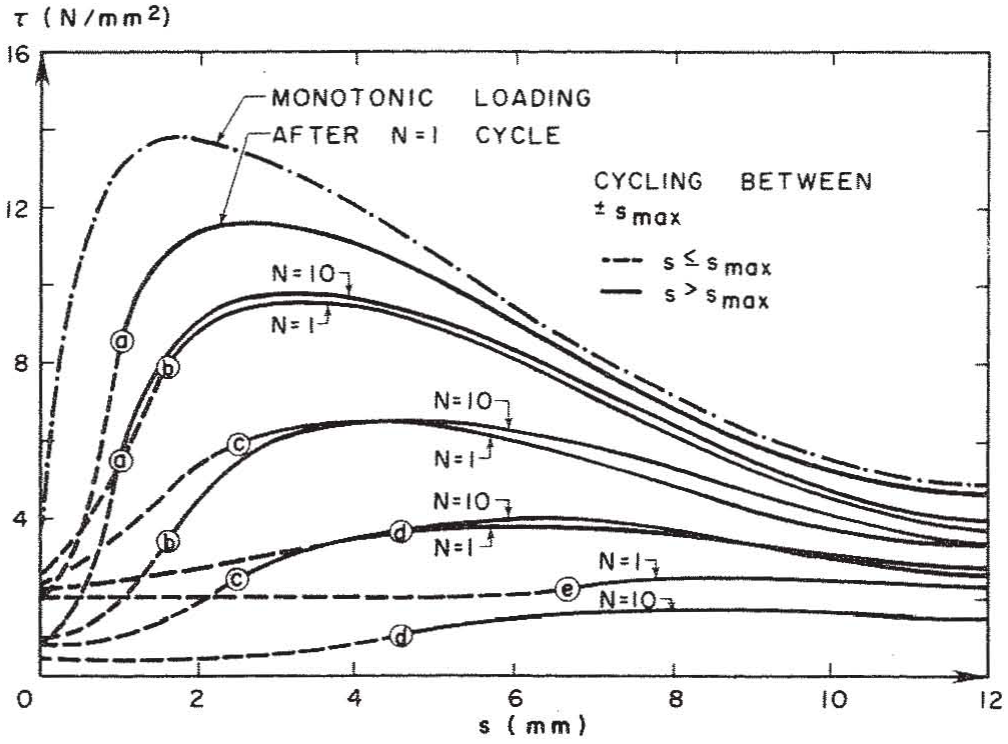

FIG. 4.49 EFFECTS OF NUMBER OF CYCLES AND OF THE PEAK VALUES OF SLIP s_{max} ON THE ENSUING BOND STRESS-SLIP RELATIONSHIP FOR $s > s_{max}$

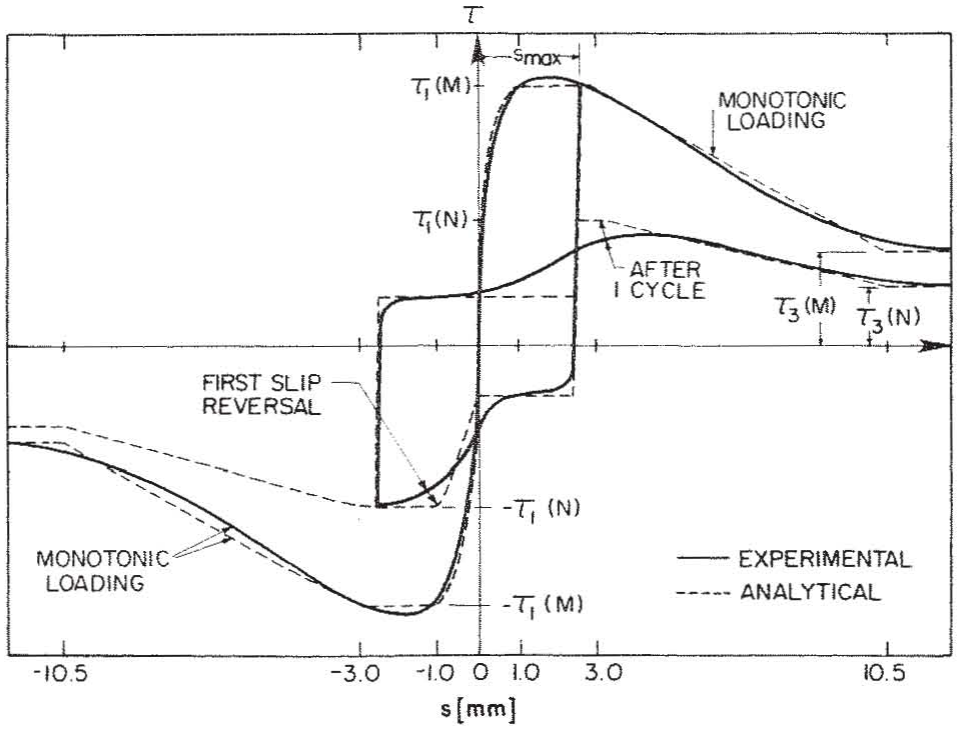

FIG. 4.50 IDEALIZATION OF BOND STRESS-SLIP RELATIONSHIP FOR CALCULATING THE CHARACTERISTIC VALUES OF THE REDUCED ENVELOPE.

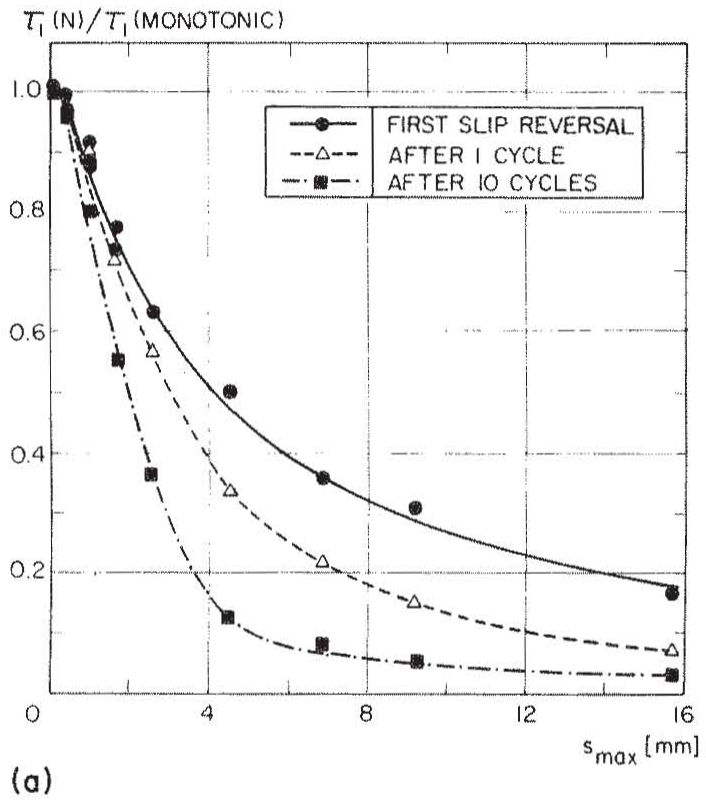

FIG. 4.51a REDUCTION OF MAXIMUM BOND RESISTANCE OF THE REDUCED ENVELOPE AS A FUNCTION OF THE PEAK VALUES OF SLIP AT WHICH CYCLING IS PERFORMED. TESTS WITH FULL REVERSALS OF SLIP.

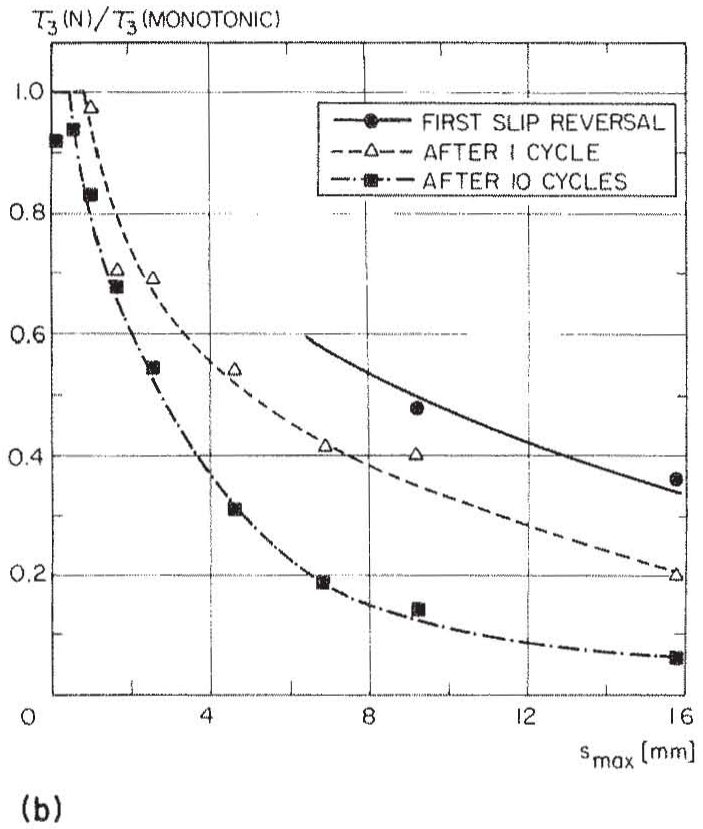

FIG. 4.51b REDUCTION OF ULTIMATE FRICTIONAL BOND RESISTANCE OF THE REDUCED ENVELOPE AS A FUNCTION OF THE PEAK VALUES OF SLIP AT WHICH CYCLING IS PERFORMED. TESTS WITH FULL REVERSALS OF SLIP.

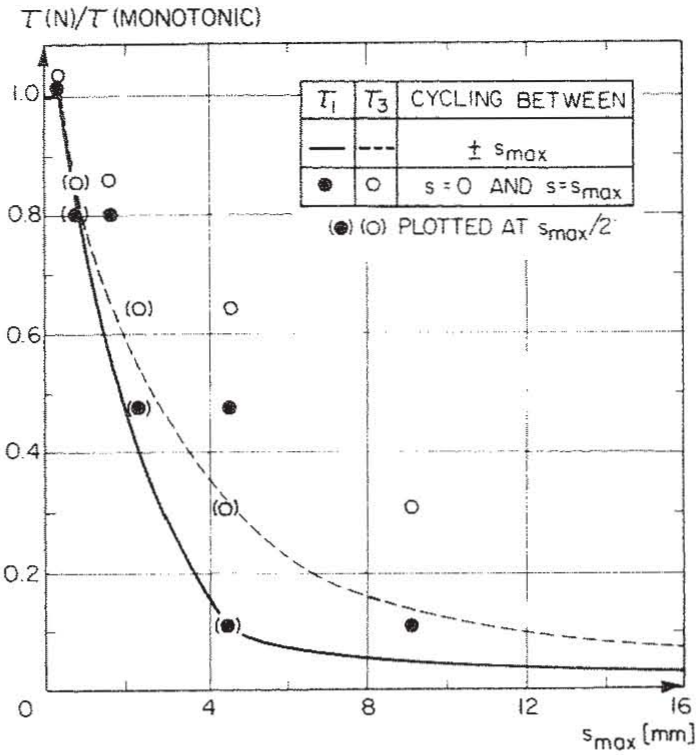

FIG. 4.52 REDUCTION OF BOND RESISTANCE OF THE REDUCED ENVELOPE AS A FUNCTION OF THE PEAK VALUES OF SLIP AT WHICH CYCLING IS PERFORMED. COMPARISON OF RESULTS OF TESTS WITH FULL AND HALF CYCLES.

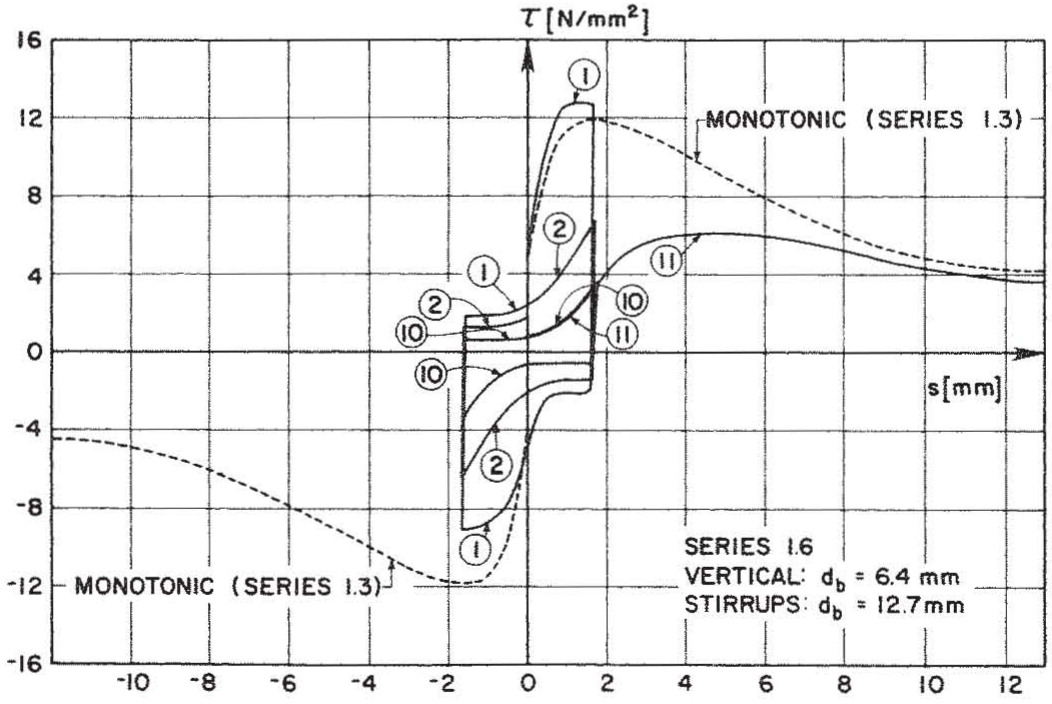

FIG. 4.53 BOND STRESS-SLIP RELATIONSHIP FOR CYCLIC LOADING, SERIES 1.6

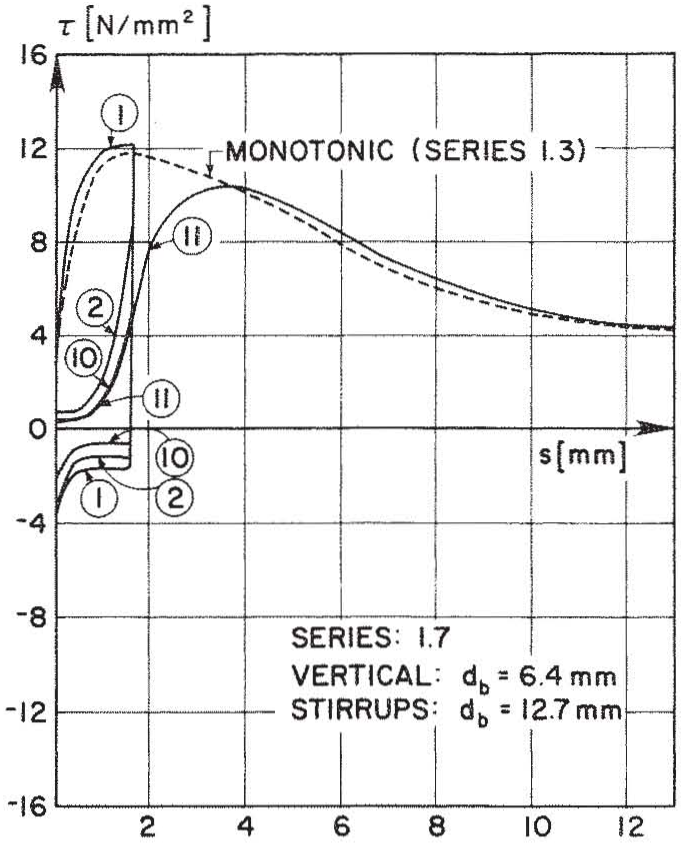

FIG. 4.54 BOND STRESS-SLIP RELATIONSHIP FOR CYCLIC LOADING, SERIES 1.7

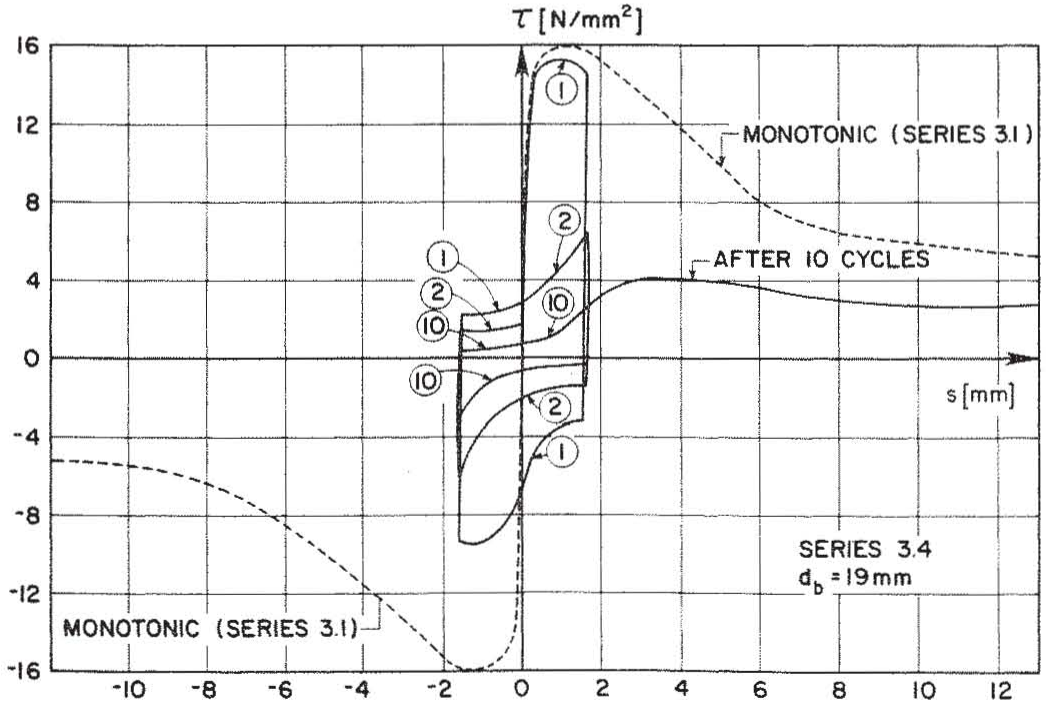

FIG. 4.55 BOND STRESS-SLIP RELATIONSHIP FOR CYCLIC LOADING, SERIES 3.4

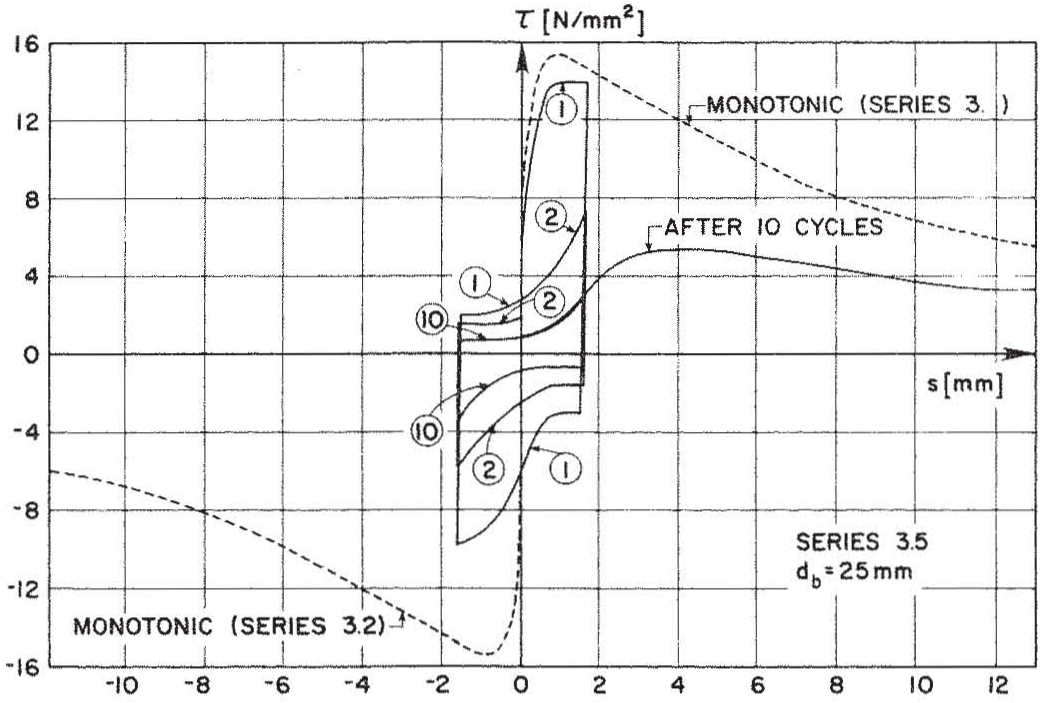

FIG. 4.56 BOND STRESS-SLIP RELATIONSHIP FOR CYCLIC LOADING, SERIES 3.5

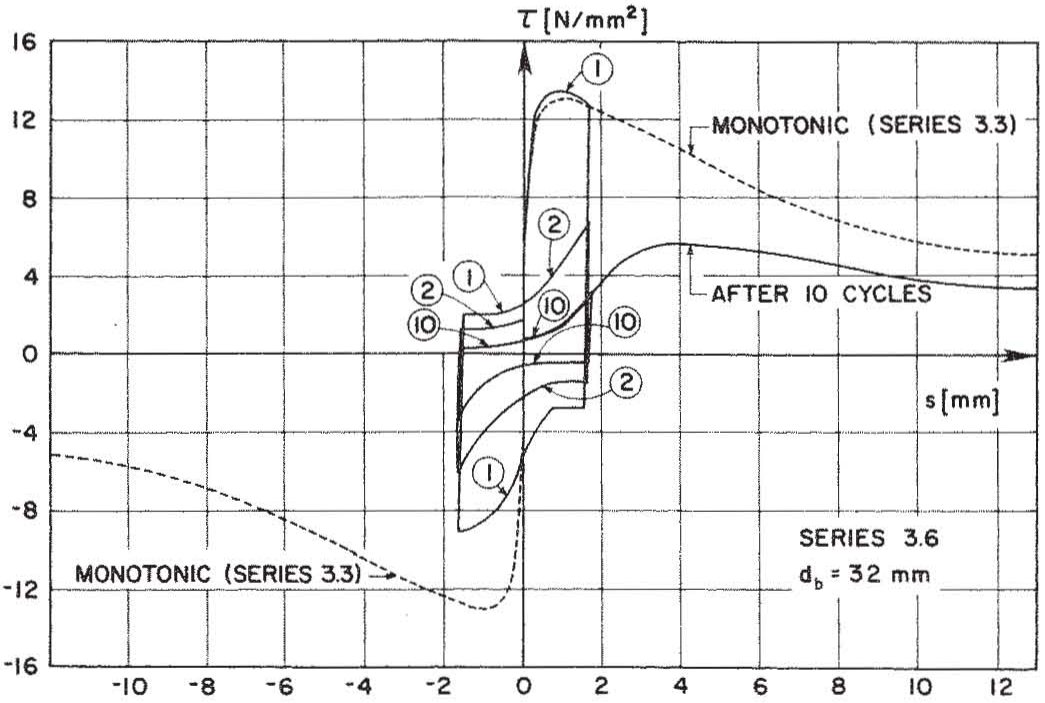

FIG. 4.57 BOND STRESS-SLIP RELATIONSHIP FOR CYCLIC LOADING, SERIES 3.6

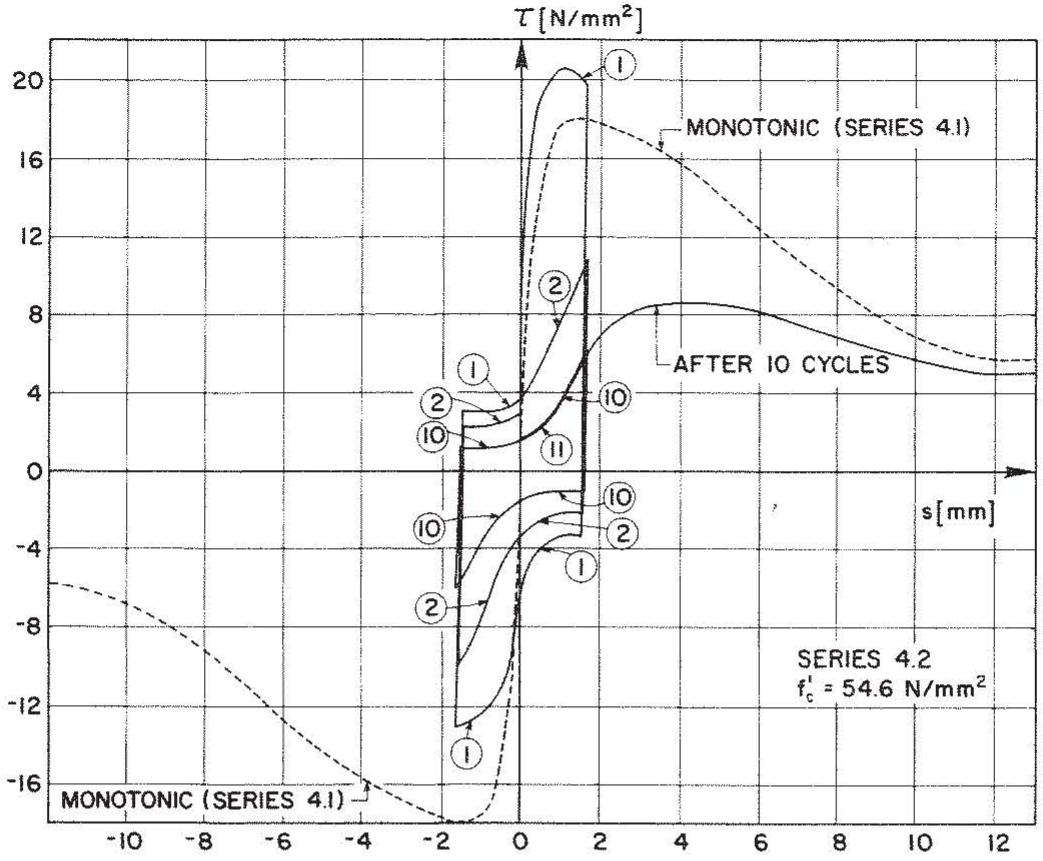

FIG. 4.58 BOND STRESS-SLIP RELATIONSHIP FOR CYCLIC LOADING, SERIES 4.2

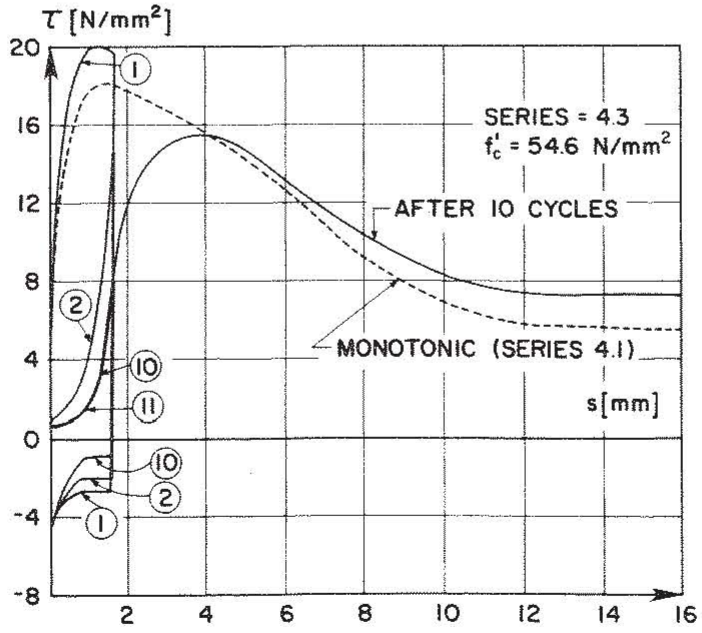

FIG. 4.59 BOND STRESS-SLIP RELATIONSHIP FOR CYCLIC LOADING, SERIES 4.3

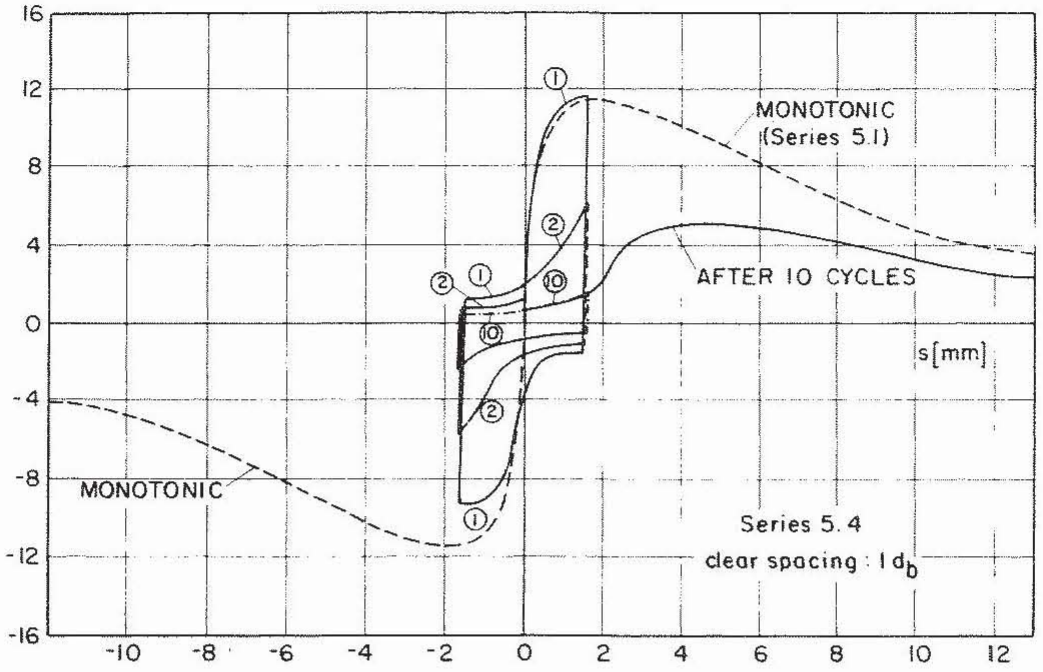

FIG. 4.60 BOND STRESS-SLIP RELATIONSHIP FOR CYCLIC LOADING, SERIES 5.4

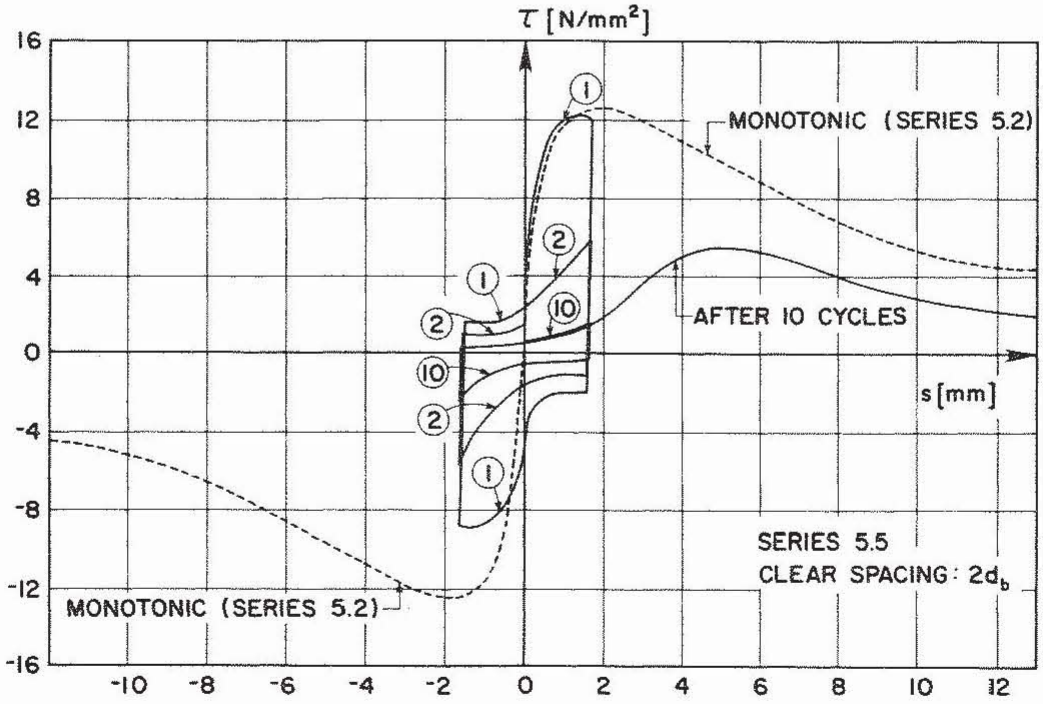

FIG. 4.61 BOND STRESS-SLIP RELATIONSHIP FOR CYCLIC LOADING, SERIES 5.5

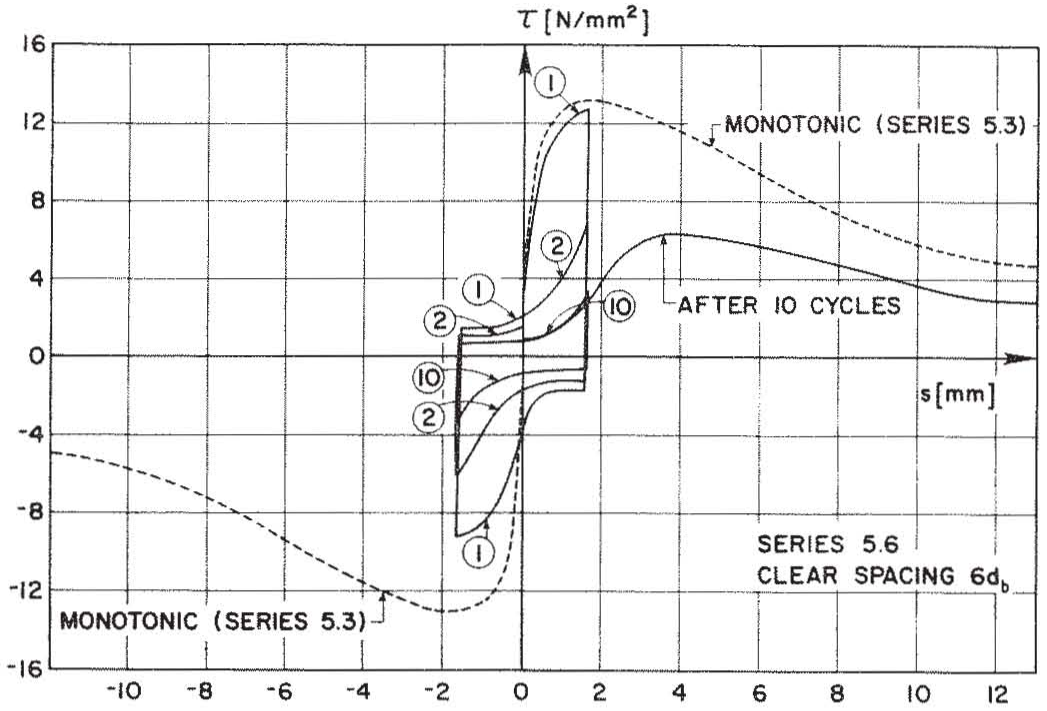

FIG. 4.62 BOND STRESS-SLIP RELATIONSHIP FOR CYCLIC LOADING, SERIES 5.6

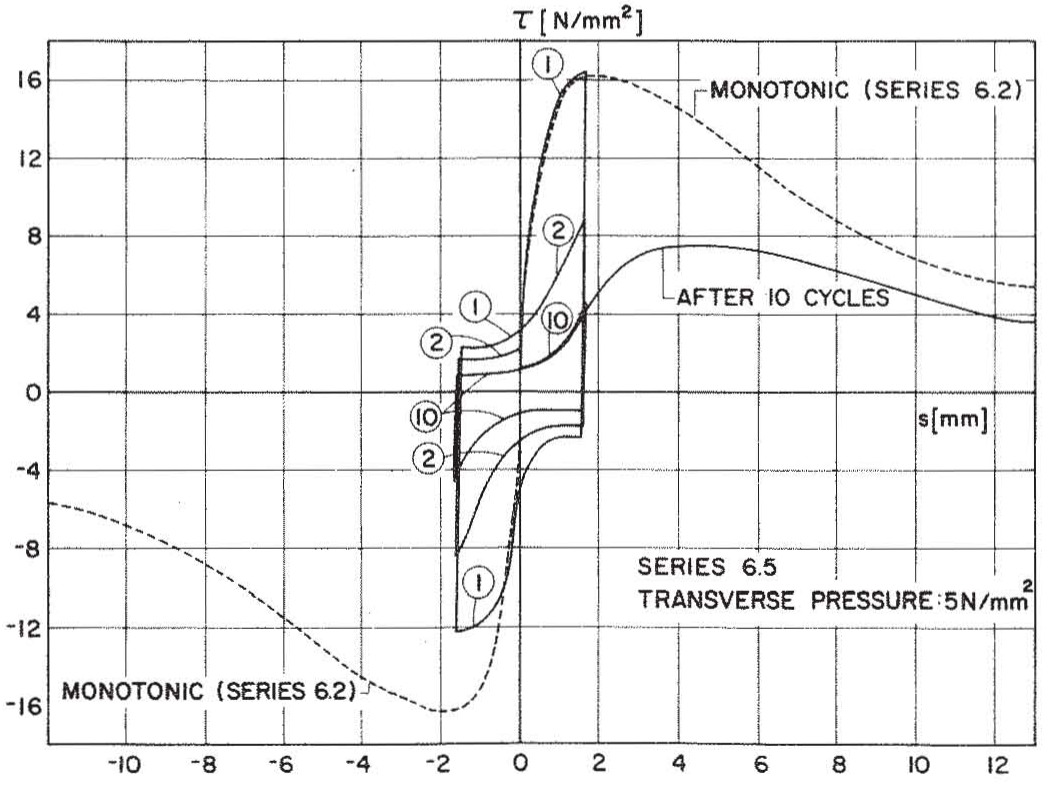

FIG. 4.63 BOND STRESS-SLIP RELATIONSHIP FOR CYCLIC LOADING, SERIES 6.5

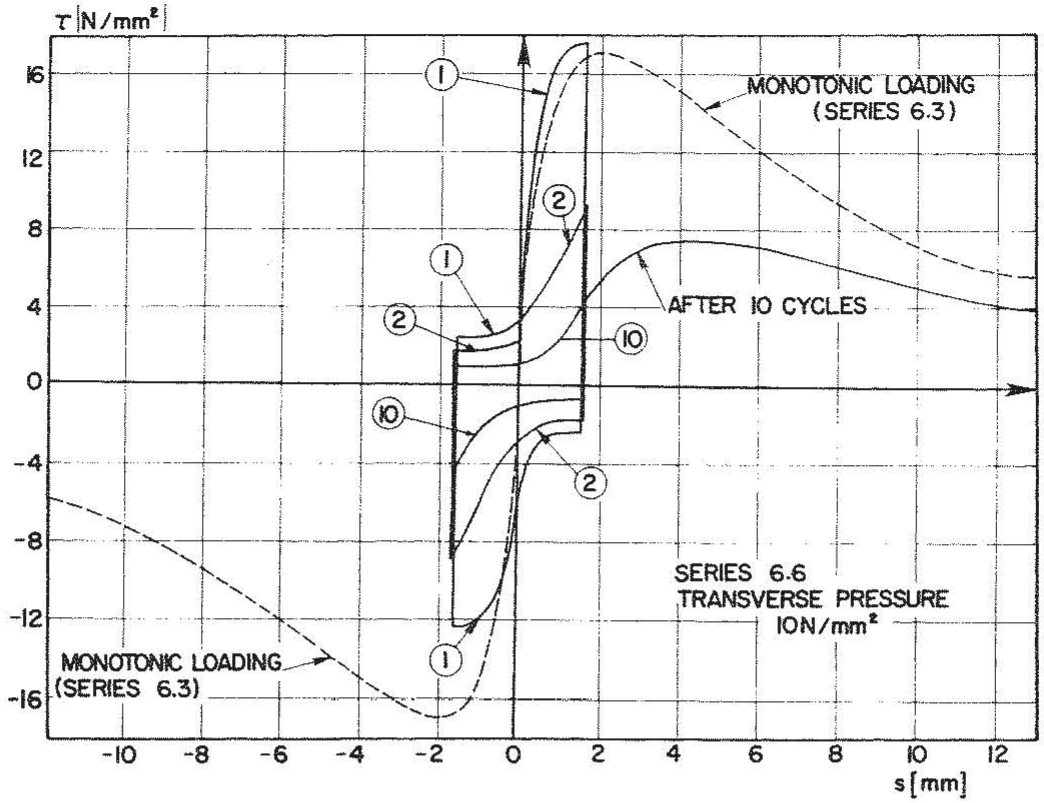

FIG. 4.64 BOND STRESS-SLIP RELATIONSHIP FOR CYCLIC LOADING, SERIES 6.6

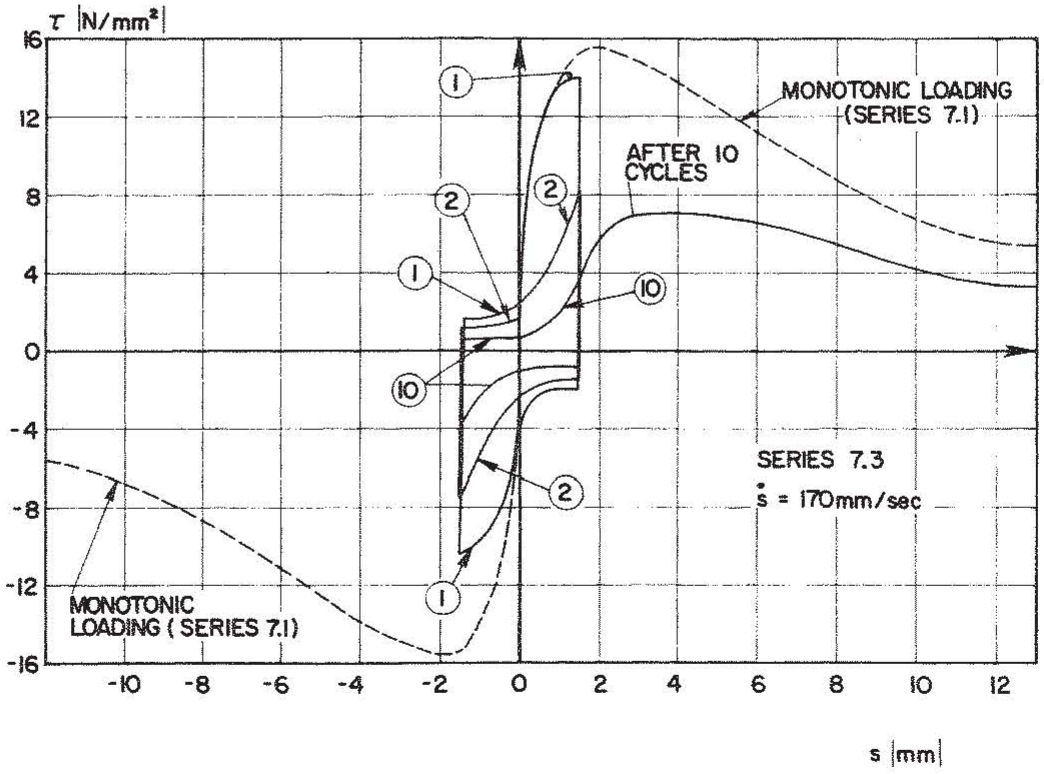

FIG. 4.65 BOND STRESS-SLIP RELATIONSHIP FOR CYCLIC LOADING, SERIES 7.3

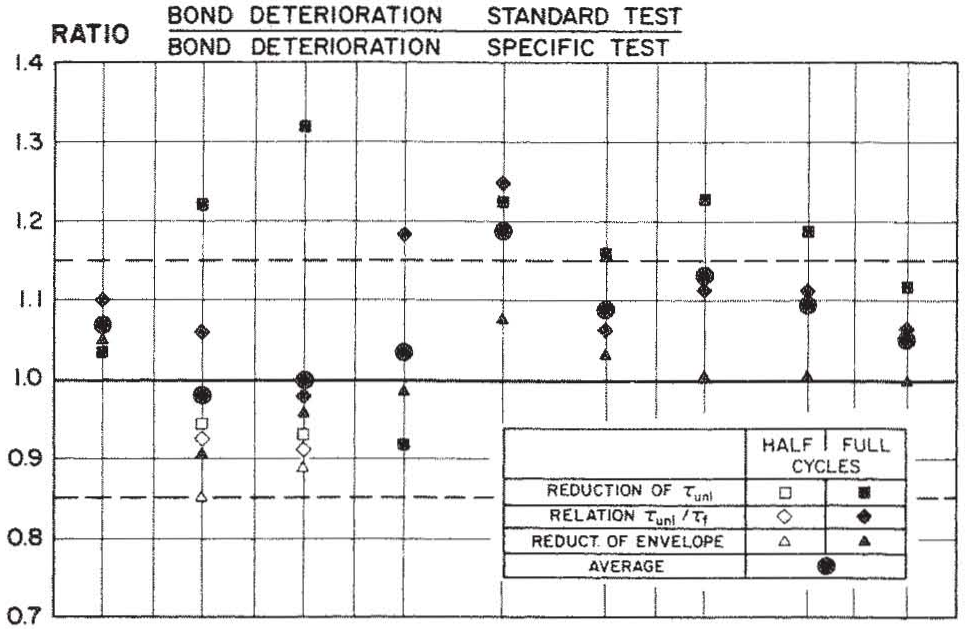

INVESTIGATED PARAMETER	COMPRES. LOADING	TRANSV. REINFORC.	CONCRETE STRENGTH	CLEAR BAR SPACING $1d_b$	$2d_b$	$6d_b$	TRANSV. PRESSURE 5 N/mm²	10 N/mm²	LOADING RATE
SERIES	2.6*	1.6+1.7	4.2+4.3	5.4	5.5	5.6	6.5	6.6	7.3

FIG. 4.66 INFLUENCE OF INVESTIGATED PARAMETERS (DIRECTION OF LOADING, CONCRETE STRENGTH, BAR SPACING, TRANSVERSE PRESSURE, RATE OF PULLOUT) ON BOND BEHAVIOR DURING CYCLIC LOADING.

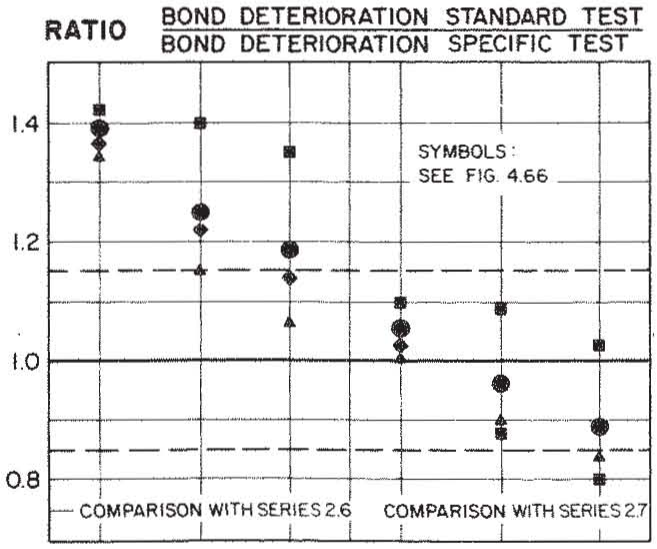

INVESTIGATED PARAMETER	BAR DIAMETER #6	#8	#10	#6	#8	#10
SERIES	3.4	3.5	3.6	3.4	3.5	3.6

FIG. 4.67 INFLUENCE OF BAR DIAMETER AND DEFORMATION PATTERN ON BOND BEHAVIOR DURING CYCLIC LOADING

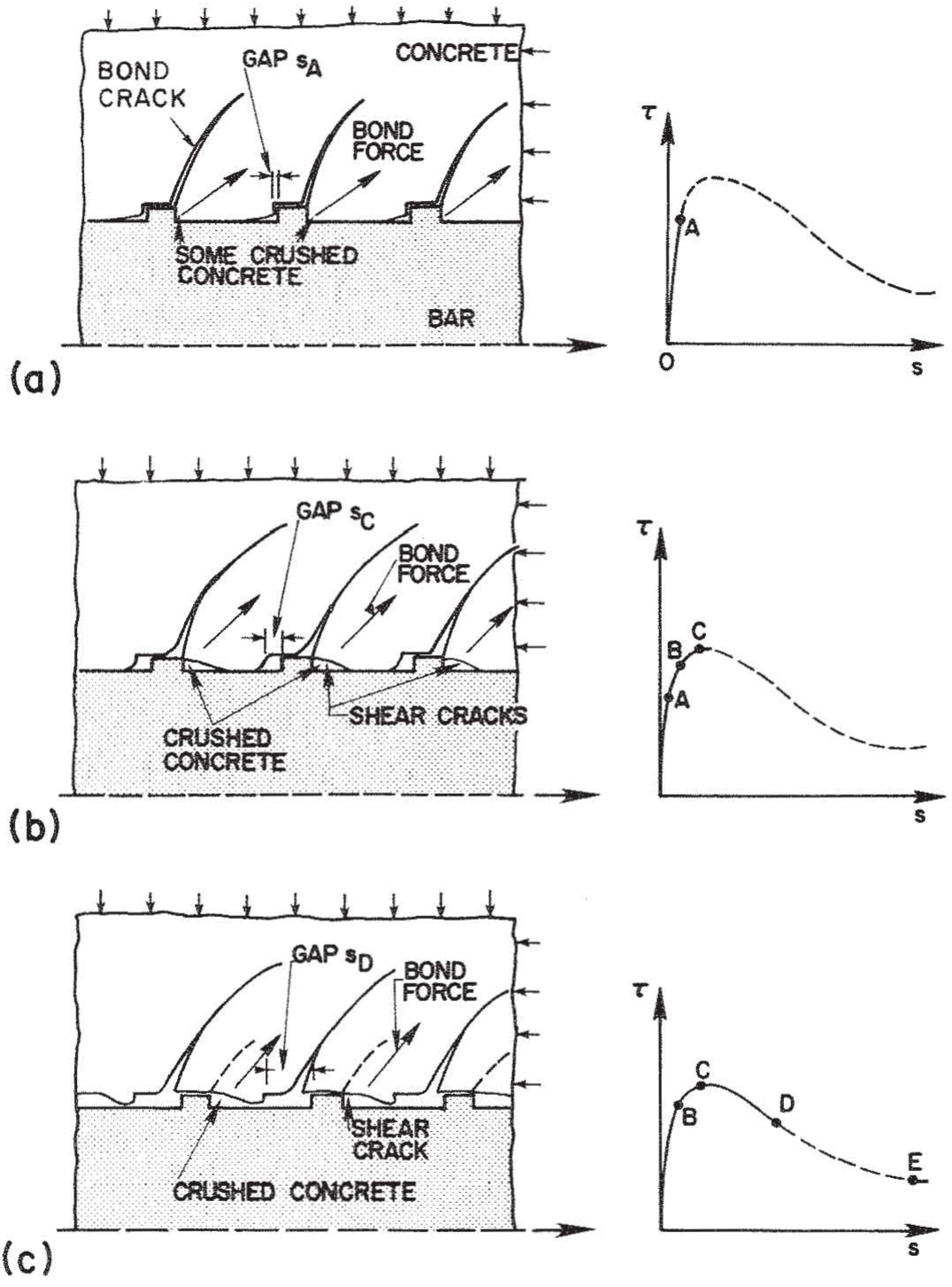

FIG. 5.1 MECHANISM OF BOND RESISTANCE, MONOTONIC LOADING

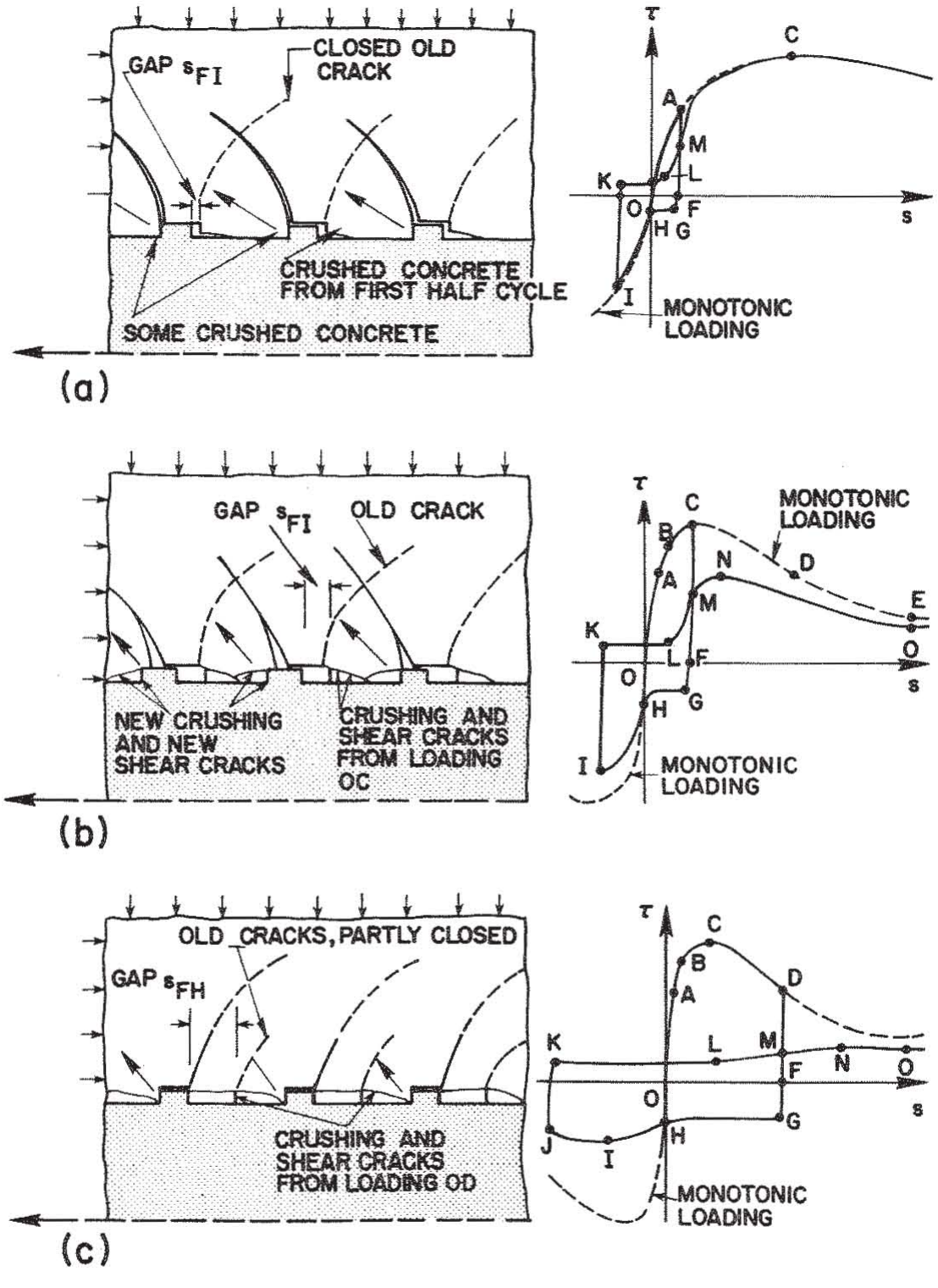

FIG. 5.2 MECHANISM OF BOND RESISTANCE, CYCLIC LOADING

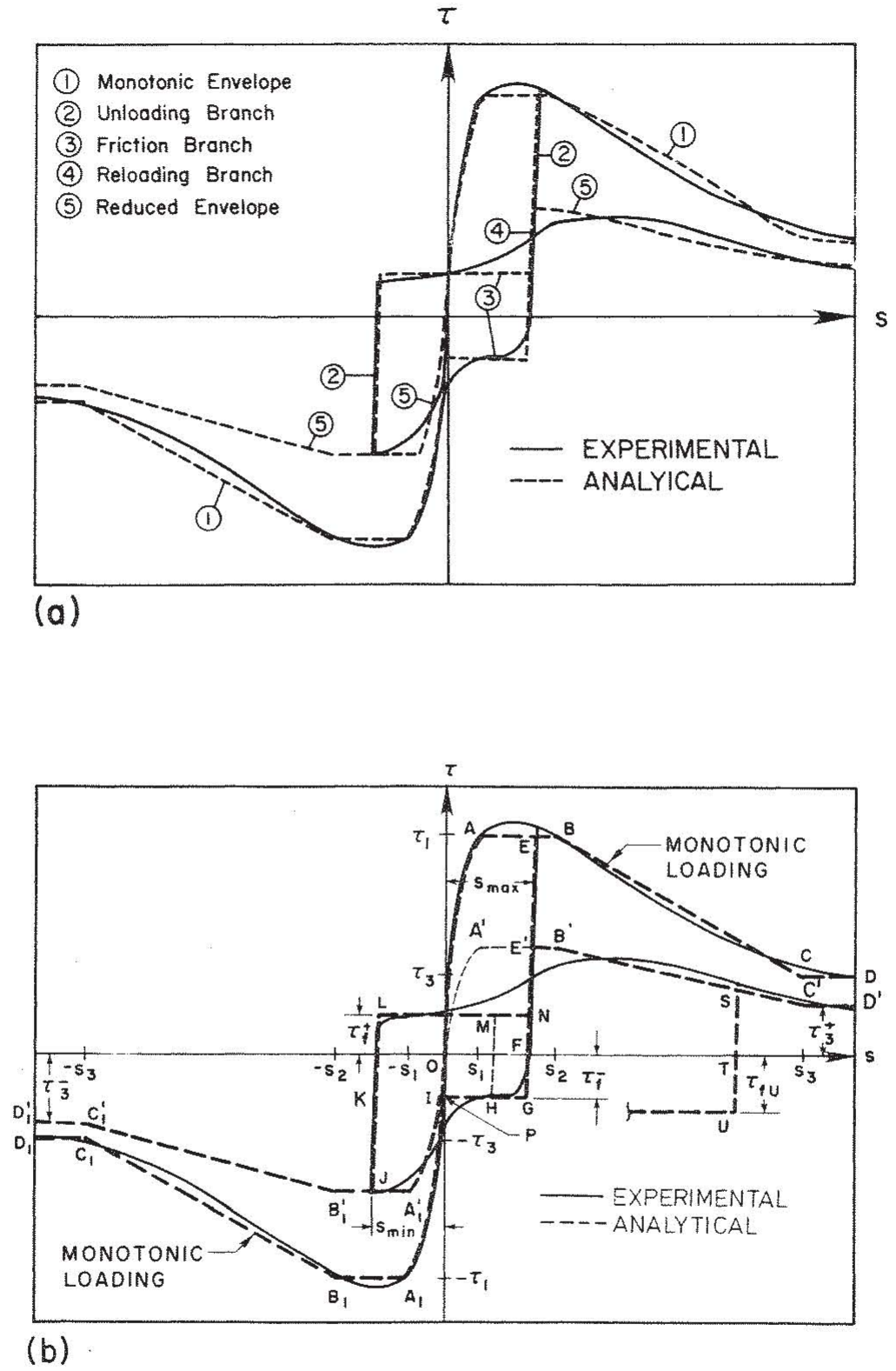

FIG. 5.3 PROPOSED ANALYTICAL MODEL FOR LOCAL BOND STRESS-SLIP RELATIONSHIP FOR CONFINED CONCRETE

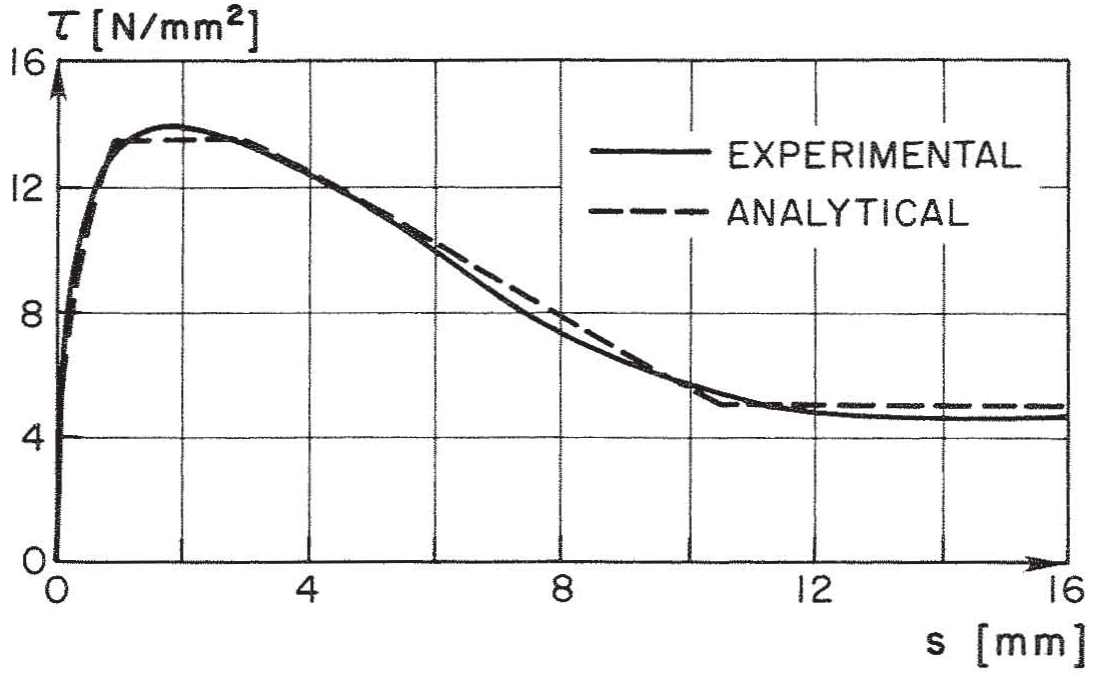

(a) FULL RANGE OF SLIP

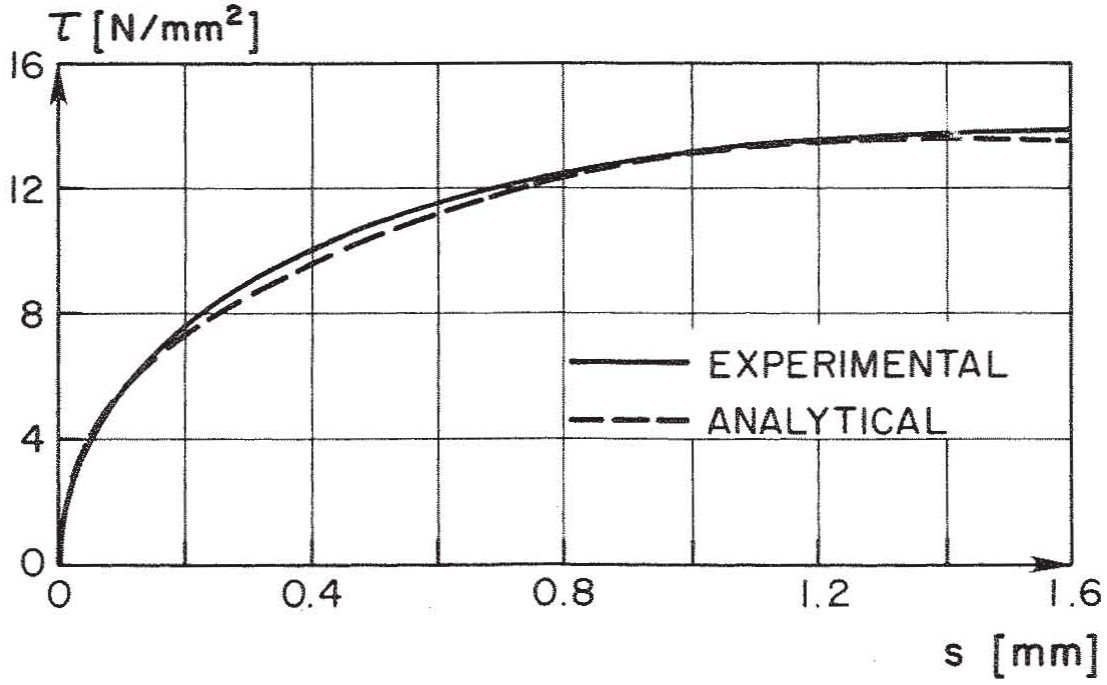

(b) ASCENDING BRANCH OF BOND STRESS-SLIP RELATIONSHIP

FIG. 5.4 COMPARISON OF EXPERIMENTAL AND ANALYTICAL RESULTS OF BOND STRESS-SLIP RELATIONSHIP UNDER MONOTONIC LOADING

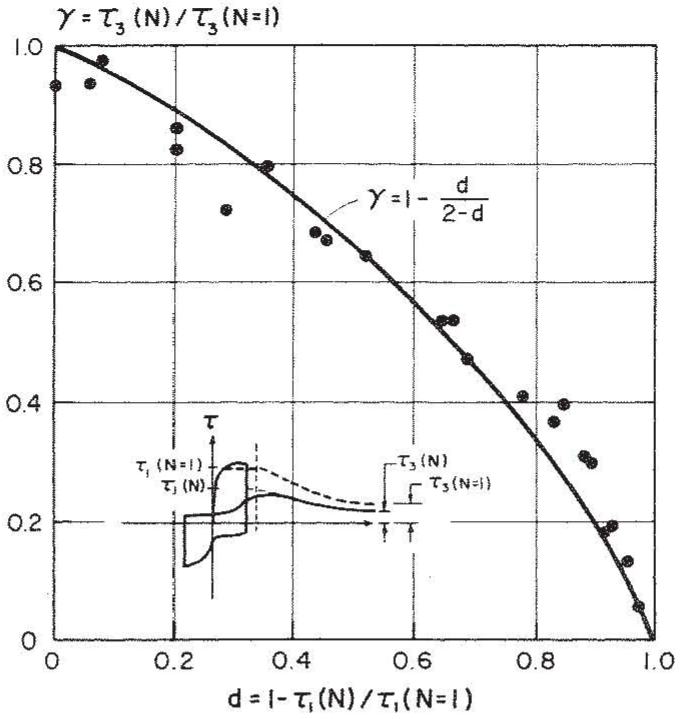

FIG. 5.5 RATIO BETWEEN ULTIMATE FRICTIONAL BOND RESISTANCE OF REDUCED ENVELOPE AND OF MONOTONIC ENVELOPE AS A FUNCTION OF THE DAMAGE FACTOR, d

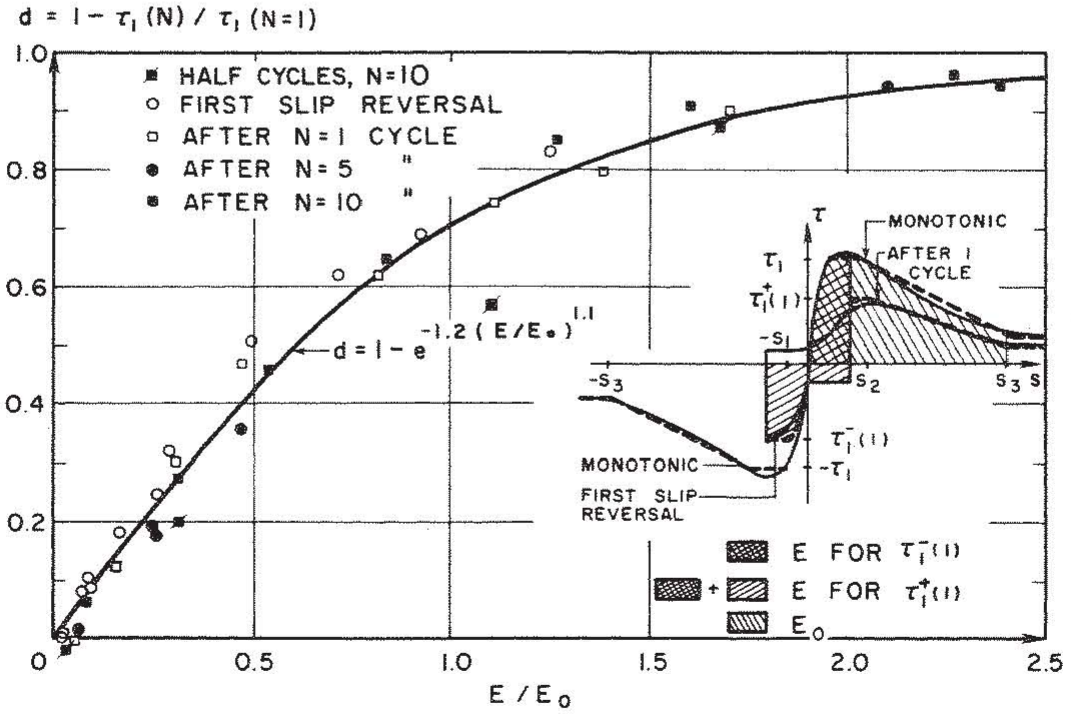

FIG. 5.6 DAMAGE FACTOR, d, FOR REDUCED ENVELOPE AS A FUNCTION OF THE DIMENSIONLESS ENERGY DISSIPATION E/E_0

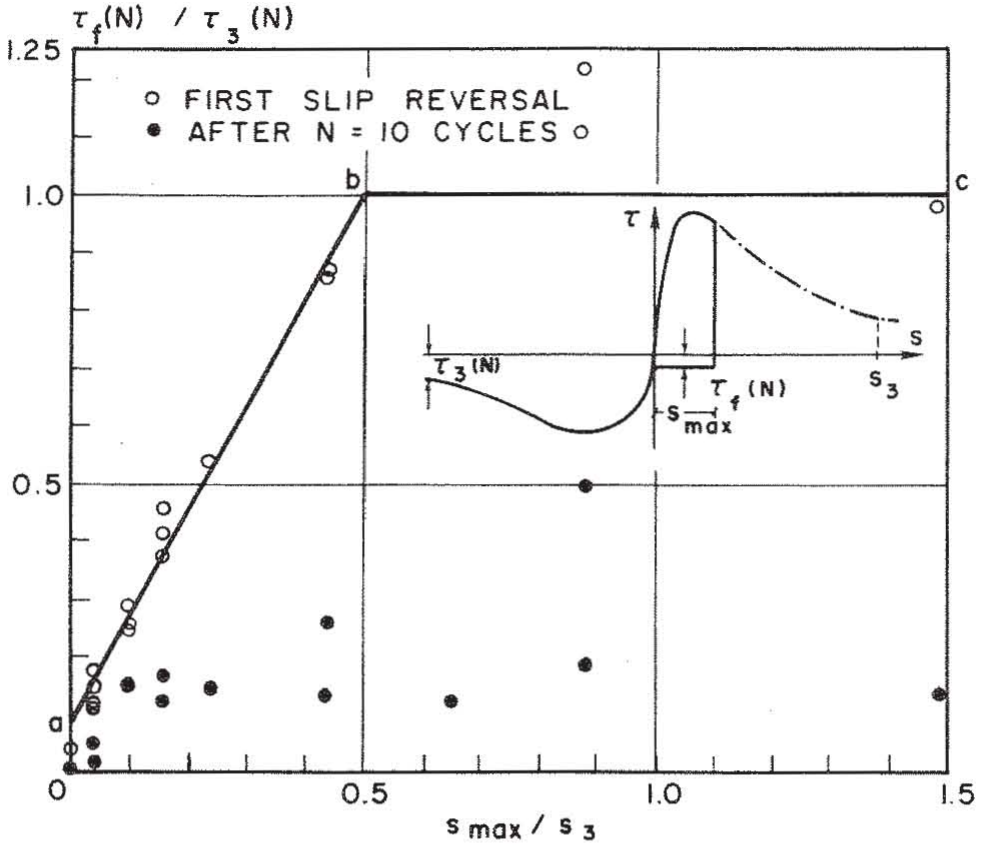

FIG. 5.7 RELATIONSHIP BETWEEN FRICTIONAL BOND RESISTANCE DURING CYCLING, $\tau_f(N)$, AND THE CORRESPONDING ULTIMATE FRICTIONAL BOND RESISTANCE $\tau_3(N)$

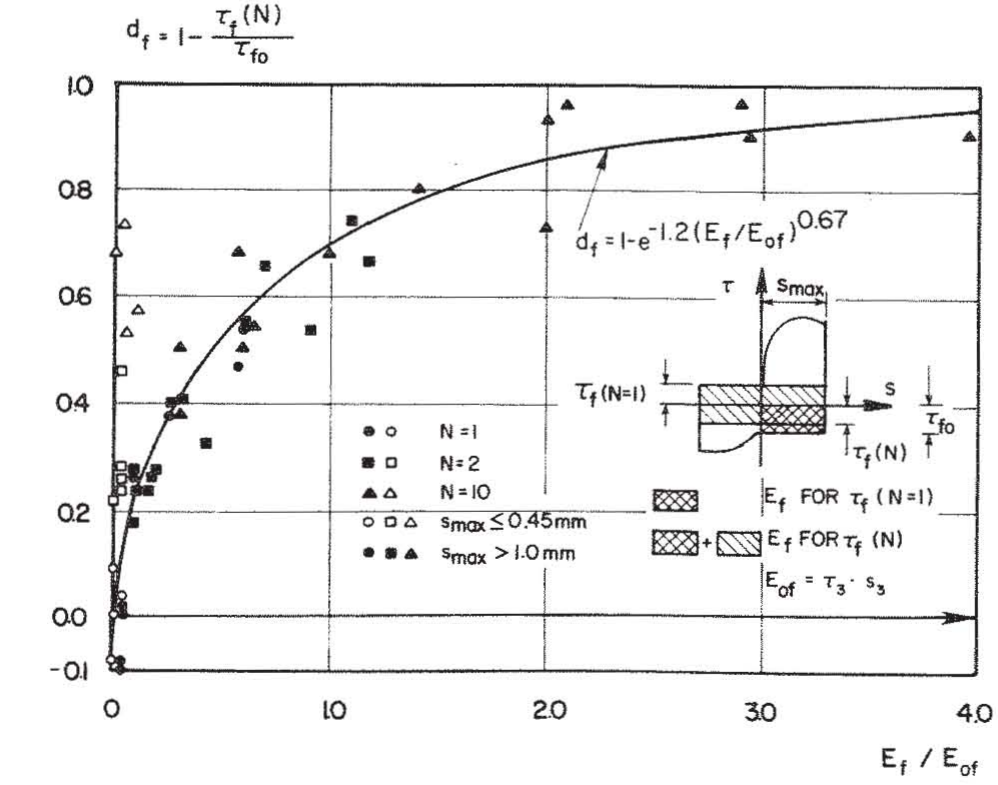

FIG. 5.8 DAMAGE FACTOR, d_f, FOR FRICTIONAL BOND RESISTANCE DURING CYCLING AS A FUNCTION OF THE DIMENSIONLESS ENERGY DISSIPATION E_f/E_{of}

$$\tau_{fo}(1) = \tau_f \text{ FOR FIRST SLIP REVERSAL}$$

$$\tau_f(1) = \tau_{fo}(1) \cdot (1 - d_f)$$

$$\tau_{fo}(2) = \tau_f(1) + K_1 (s_{max}(2) - s_{max}(1)) / s_3$$

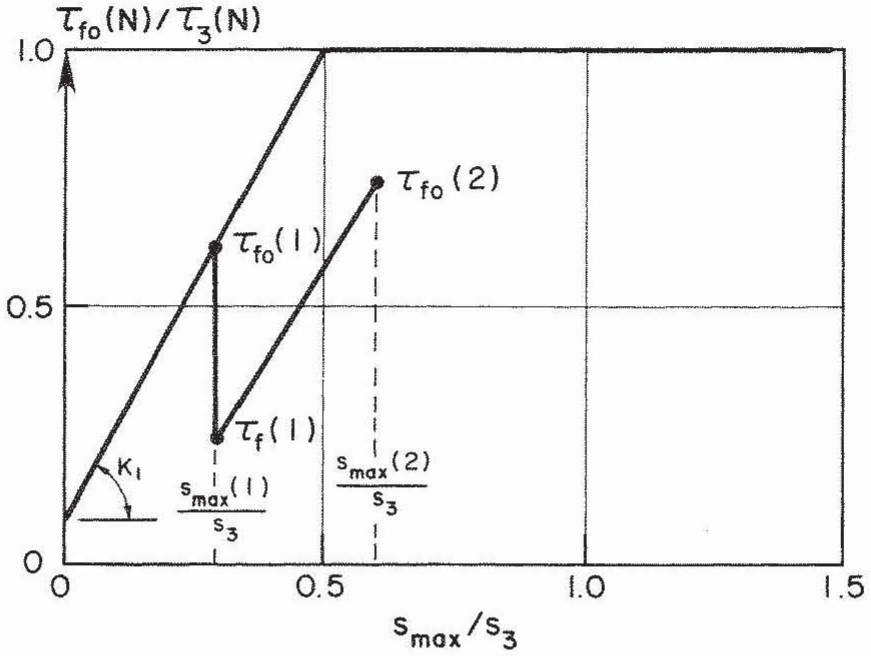

FIG. 5.9 CALCULATION OF ZERO INITIAL FRICTIONAL BOND RESISTANCE FOR UNLOADING FROM LARGER VALUE OF PEAK SLIP s_{max} THAN DURING PREVIOUS CYCLES

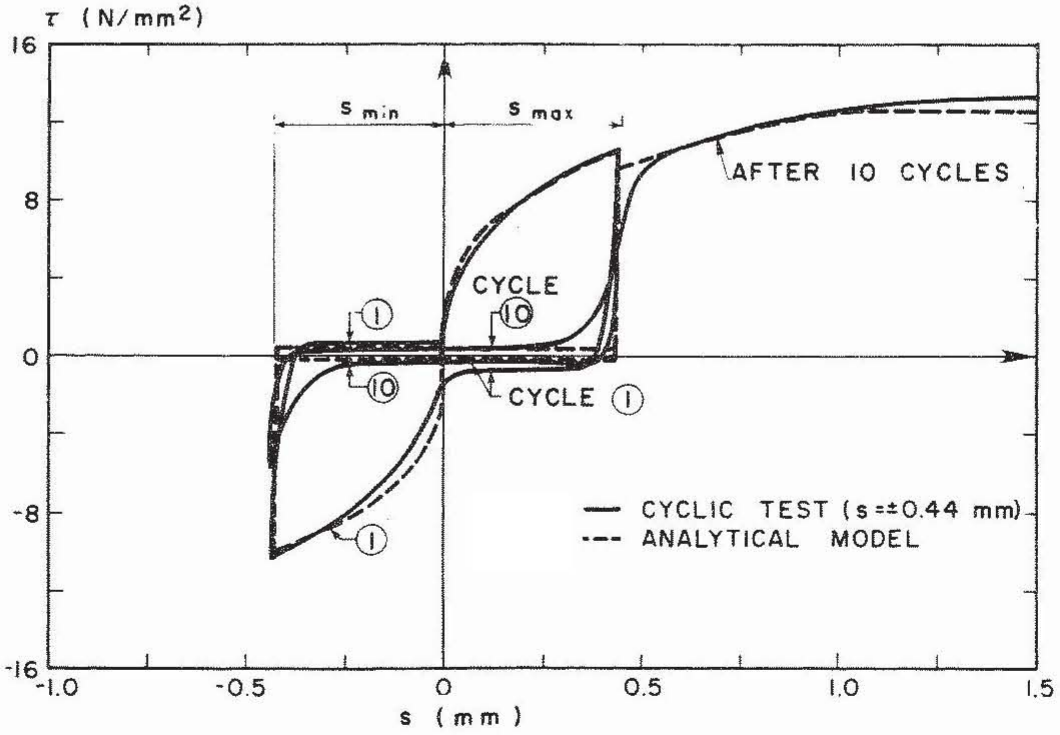

FIG. 5.10 COMPARISON OF EXPERIMENTAL AND ANALYTICAL RESULTS FOR BOND STRESS-SLIP RELATIONSHIPS FOR TEST SERIES 2.4

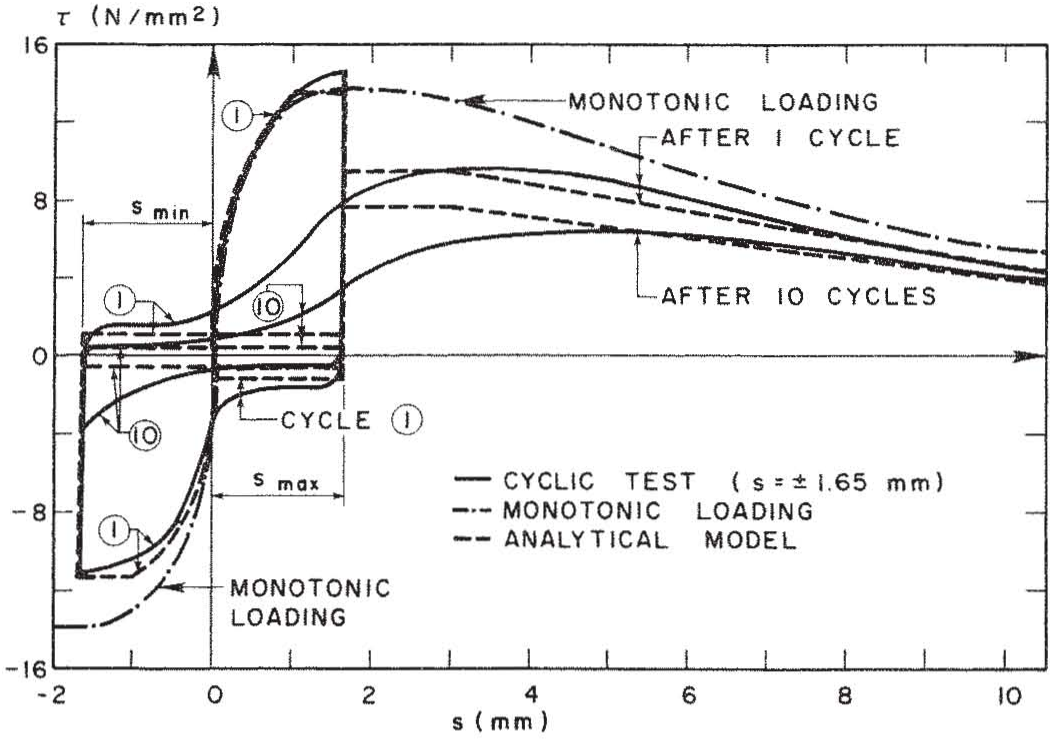

FIG. 5.11 COMPARISON OF EXPERIMENTAL AND ANALYTICAL RESULTS FOR BOND STRESS-SLIP RELATIONSHIPS FOR TEST SERIES 2.6

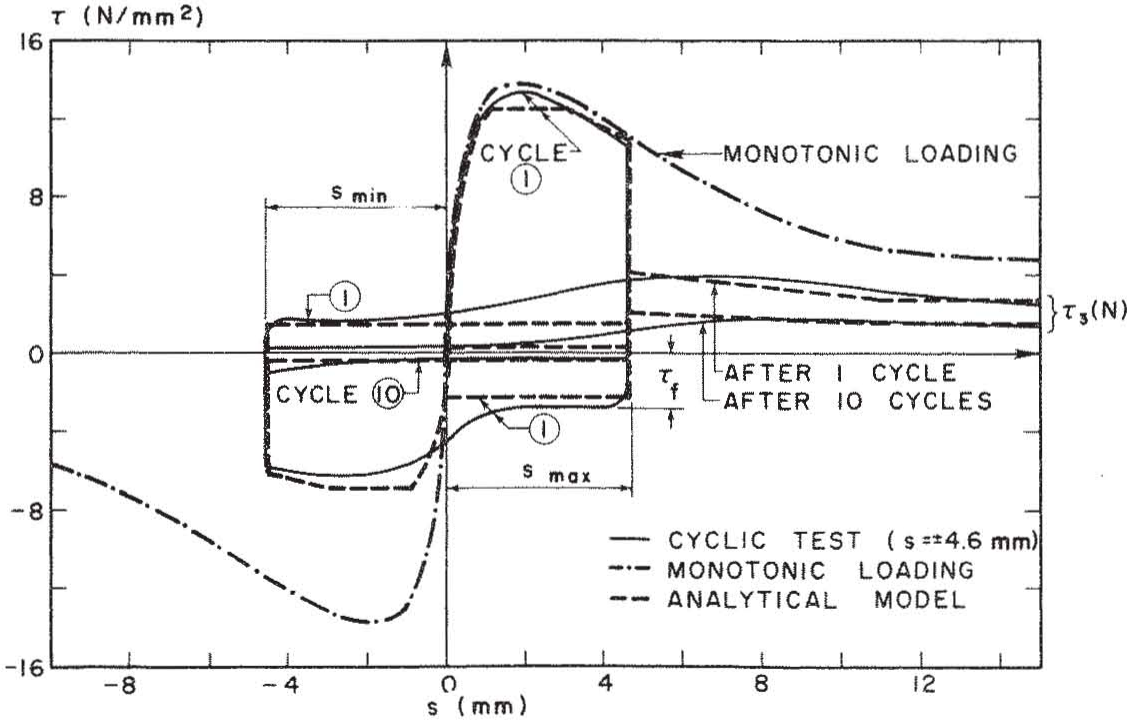

FIG. 5.12 COMPARISON OF EXPERIMENTAL AND ANALYTICAL RESULTS FOR BOND STRESS-SLIP RELATIONSHIPS FOR TEST SERIES 2.8

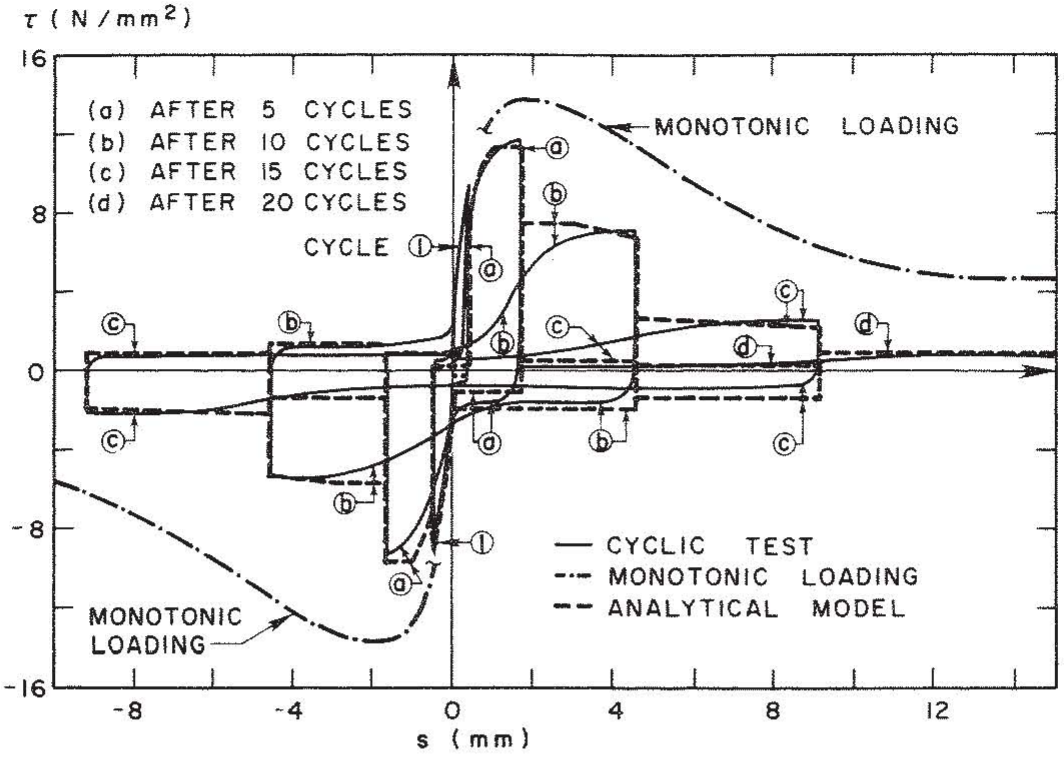

FIG. 5.13 COMPARISON OF EXPERIMENTAL AND ANALYTICAL RESULTS FOR BOND STRESS-SLIP RELATIONSHIPS FOR TEST SERIES 2.19

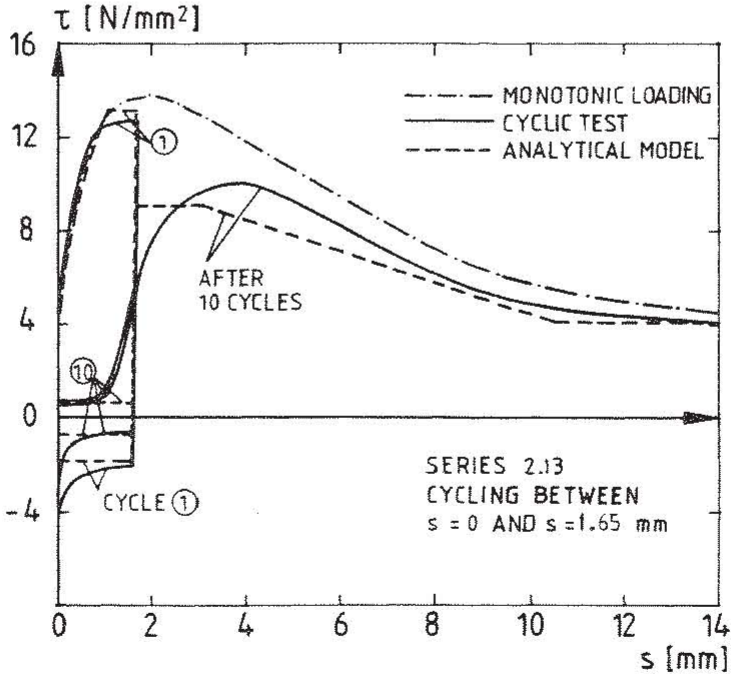

FIG. 5.14 COMPARISON OF EXPERIMENTAL AND ANALYTICAL RESULTS FOR BOND STRESS-SLIP RELATIONSHIPS FOR TEST SERIES 2.13

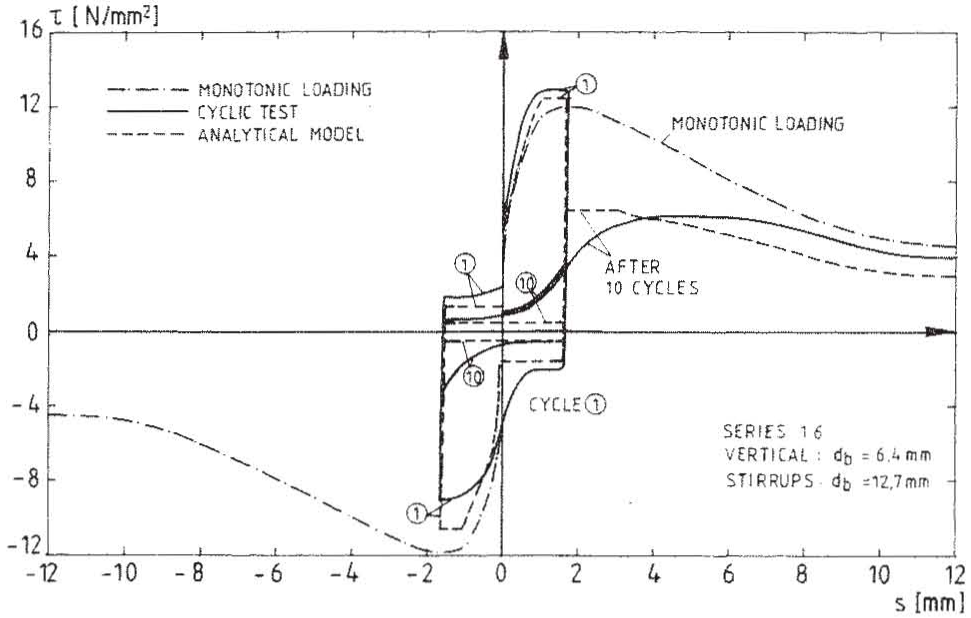

FIG. 5.15 COMPARISON OF EXPERIMENTAL AND ANALYTICAL RESULTS FOR BOND STRESS-SLIP RELATIONSHIPS FOR TEST SERIES 1.6 (#2 VERTICAL BARS)

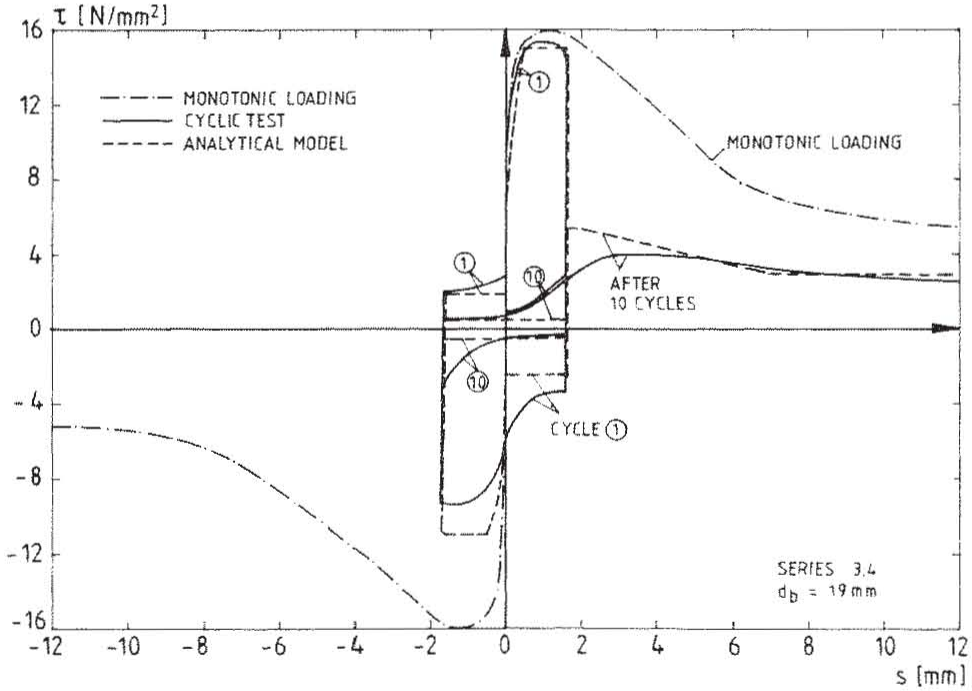

FIG. 5.16 COMPARISON OF EXPERIMENTAL AND ANALYTICAL RESULTS FOR BOND STRESS-SLIP RELATIONSHIPS FOR TEST SERIES 3.4 (#6 (19 mm) BAR)

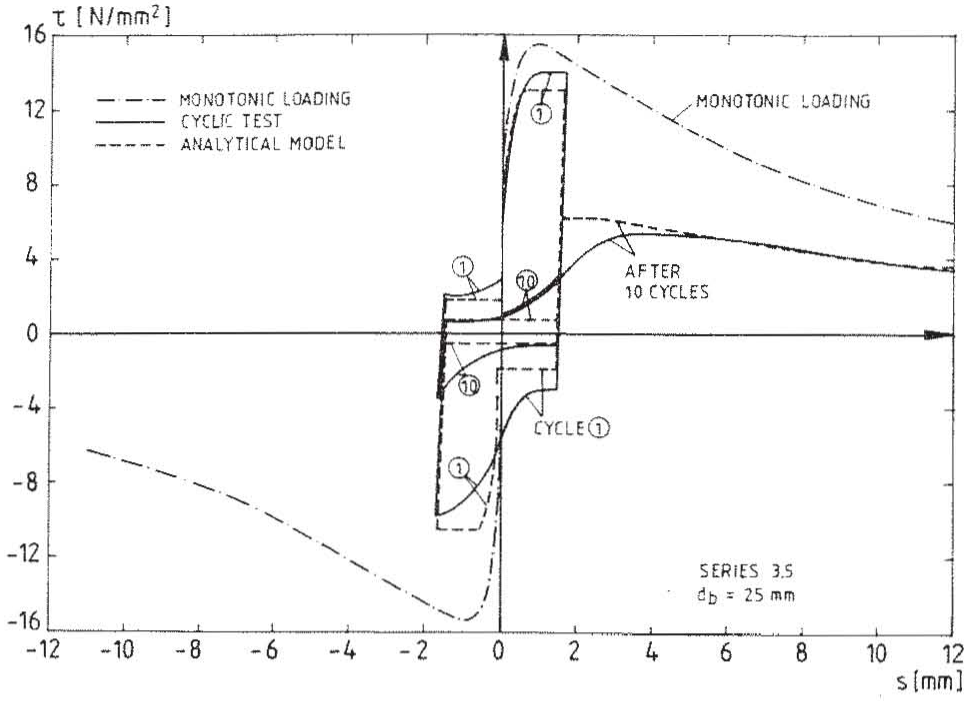

FIG. 5.17 COMPARISON OF EXPERIMENTAL AND ANALYTICAL RESULTS FOR BOND STRESS-SLIP RELATIONSHIPS FOR TEST SERIES 3.5 (#8 (25 mm) BAR)

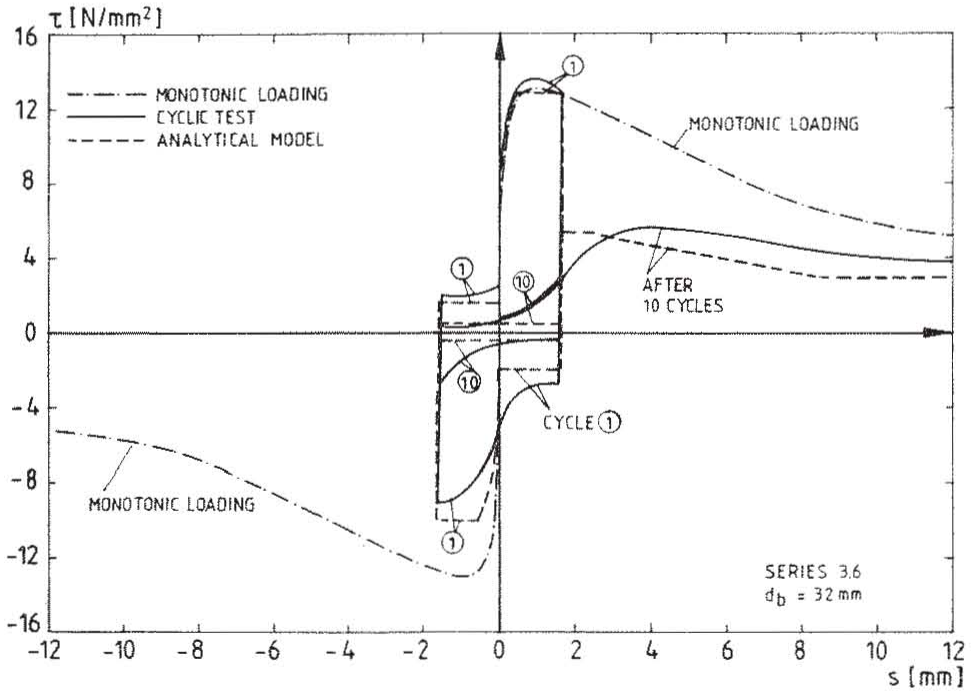

FIG. 5.18 COMPARISON OF EXPERIMENTAL AND ANALYTICAL RESULTS FOR BOND STRESS-SLIP RELATIONSHIPS FOR TEST SERIES 3.6 (#10 (32 mm) BAR)

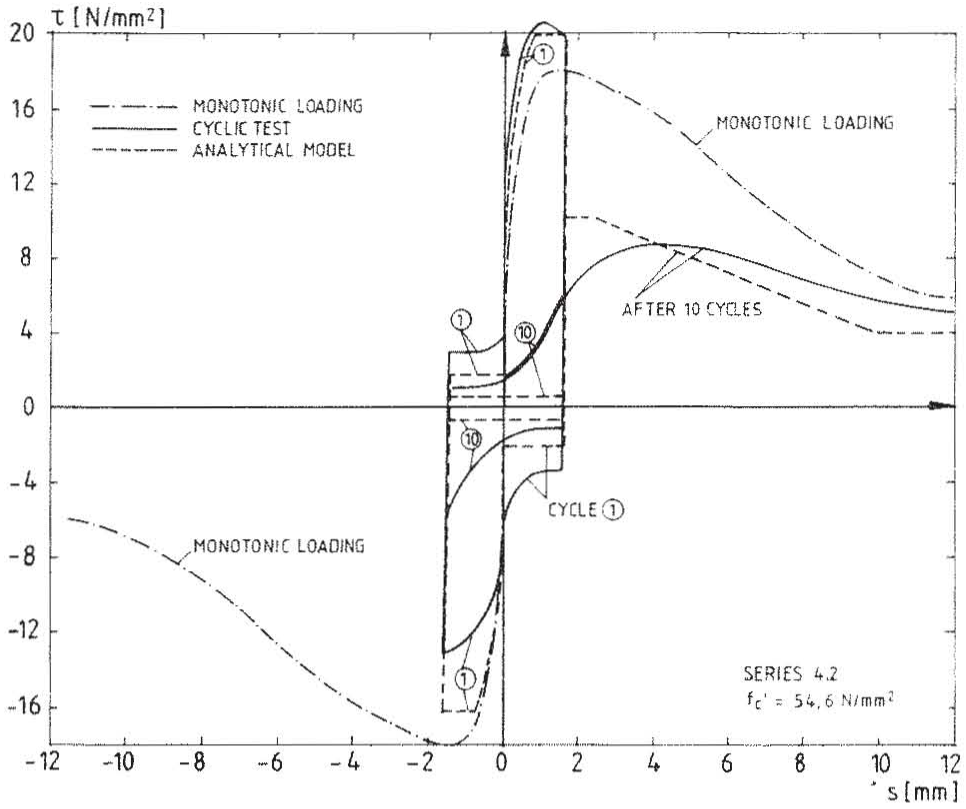

FIG. 5.19 COMPARISON OF EXPERIMENTAL AND ANALYTICAL RESULTS FOR BOND STRESS-SLIP RELATIONSHIPS FOR TEST SERIES 4.2 (f_c' = 54.6 N/mm²)

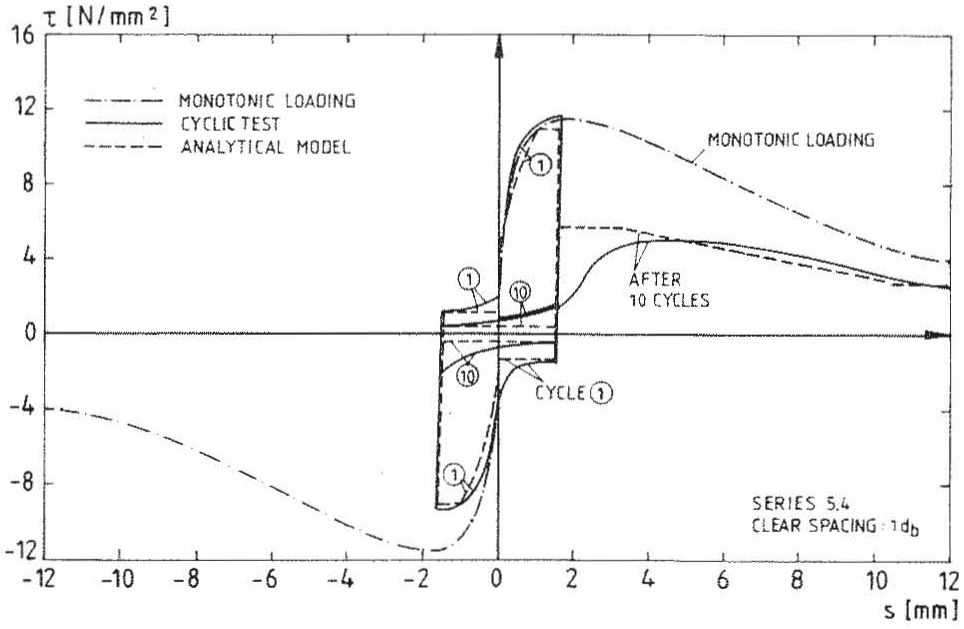

FIG. 5.20 COMPARISON OF EXPERIMENTAL AND ANALYTICAL RESULTS FOR BOND STRESS-SLIP RELATIONSHIPS FOR TEST SERIES 5.4 (CLEAR SPACING = 1 d_b)

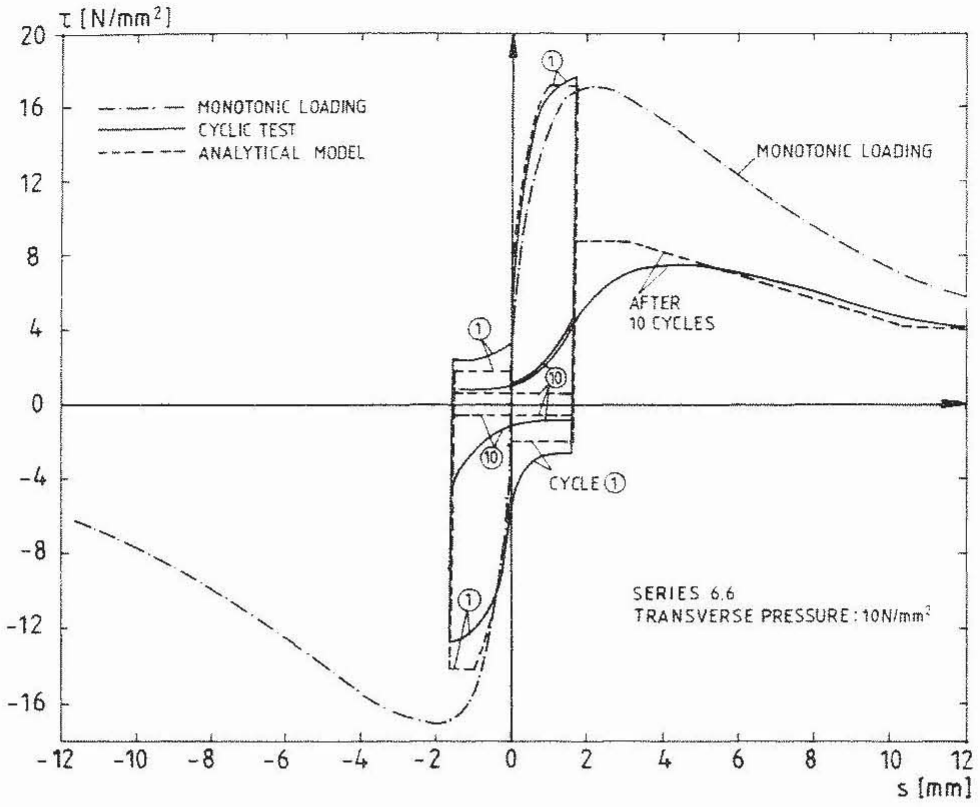

FIG. 5.21 COMPARISON OF EXPERIMENTAL AND ANALYTICAL RESULTS FOR BOND STRESS-SLIP RELATIONSHIPS FOR TEST SERIES 6.6 (p = 10 N/mm^2)

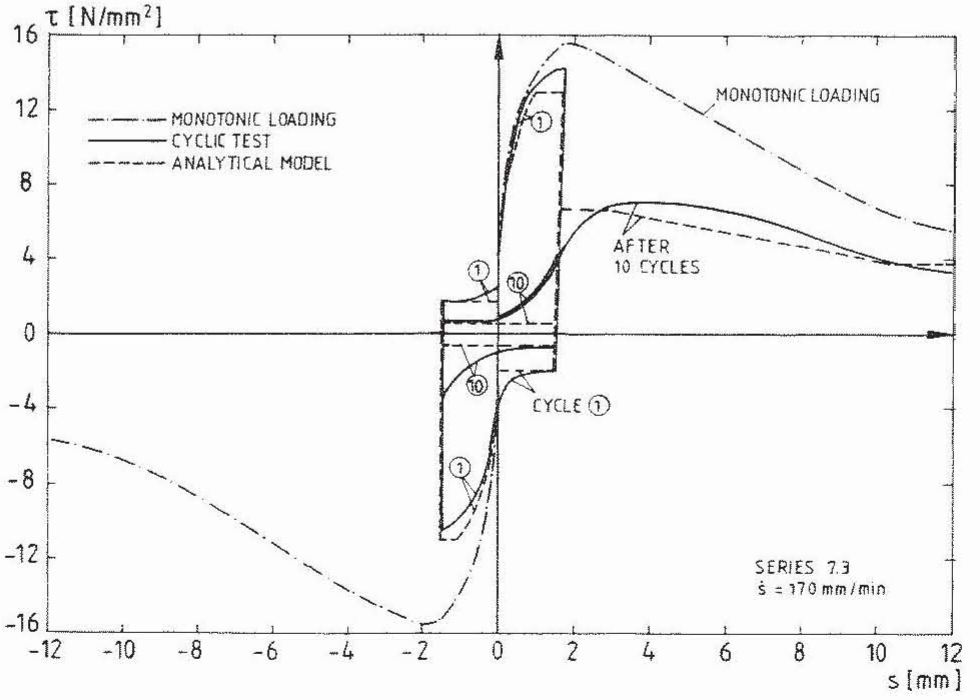

FIG. 5.22 COMPARISON OF EXPERIMENTAL AND ANALYTICAL RESULTS FOR BOND STRESS-SLIP RELATIONSHIPS FOR TEST SERIES 7.3 ($\dot{s}$ = 170 mm/min)

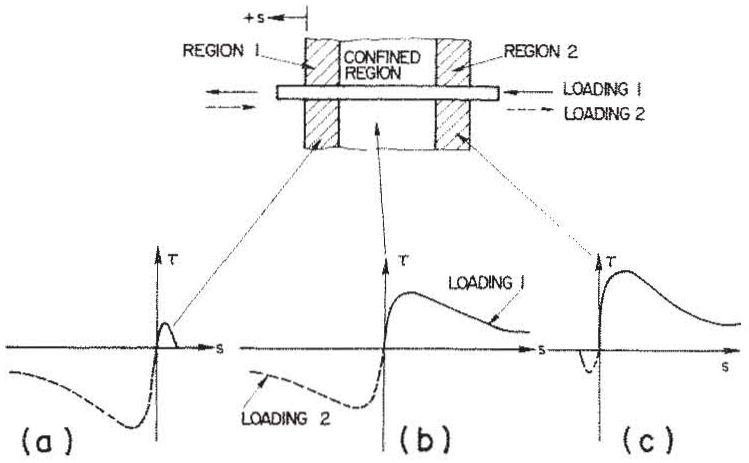

FIG. 5.23 BOND STRESS-SLIP RELATIONSHIPS UNDER MONOTONIC LOADING FOR DIFFERENT REGIONS IN A JOINT

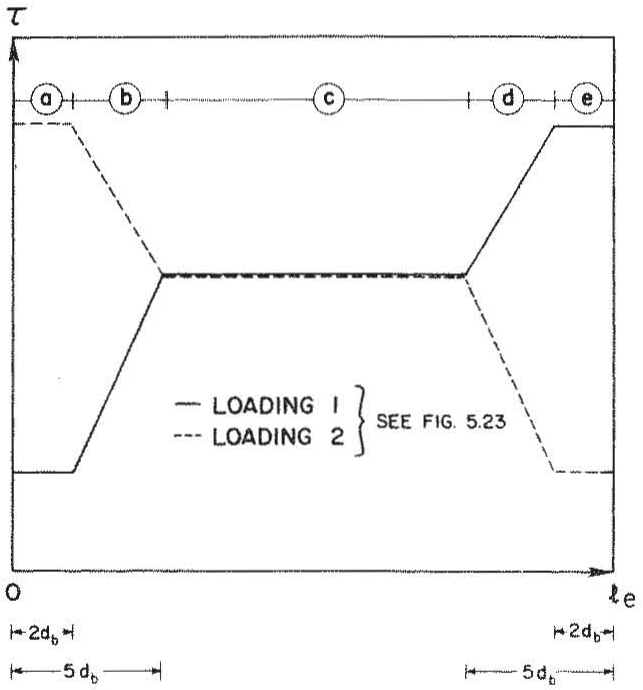

(a)	REGION 1	(Compare Fig. 5.23 a)
(c)	CONFINED CONCRETE	(Compare Fig. 5.23 b)
(e)	REGION 2	(Compare Fig. 5.23 c)
(b) (d)	TRANSIENT REGION	

FIG. 5.24 PROPOSED DISTRIBUTION OF CHARACTERISTIC VALUES OF BOND RESISTANCE AND SLIP ALONG THE ANCHORAGE LENGTH